A STUDY OF THE GALVOMAGNETIC AND RESISTIVITY PROPERTIES OF THIN BISMUTH FILMS.

A THESIS SUBMITTED FOR THE DEGREE OF DOCTOR OF PHILOSOPHY IN THE UNIVERSITY OF ASTON IN BIRMINGHAM.

ROBERT JAMES CRUICKSHANK, B.Sc.

Physics Department.

August, 1970.

ABSTRACT

The results of the measurements of the resistivity, Hall coefficient and magnetoresistance of thin bismuth films are presented. The films were prepared by thermal evaporation of 99.999 % bismuth at $< 5 \times 10^{-6}$ torr and shown to consist of oriented polycrystallites whose grain size was a function of the film thickness.

The range of thicknesses investigated was from 200 - 4500 Å and observations are reported at temperatures between 77°K and 300°K in transverse magnetic fields to 12 kilogauss. The longitudinal resistive and transverse Hall voltages were measured by a null method.

The resistivity of the films exceeded the bulk values and displayed a negative temperature coefficient. Surface scattering processes predominated at temperatures below approximately 160°K, the additional resistivity contribution being an oscillatory function of the film thickness. The thinnest films displayed a saturation in the resistivity resulting from the shape of the Fermi surfaces.

The Hall coefficient of bulk polycrystalline material was dominated by the negative coefficient, $R_{\perp}$, but increased crystallite orientation in the films displaced the curve to a positive ordinate. A field variation of the carrier density was demonstrated and mathematically analysed. The Hall coefficient was shown to be an oscillatory function of the film thickness.

The exponential-type increase in magnetoresistance at low temperatures occuring in bulk material was not observed in thin films, the limitations on the carrier path by the crystallite boundaries accounting for the greatly reduced magnetoresistance.

The carrier density and mobilities at various film thicknesses are presented as functions of temperature.

The carrier density and mobilities at various film

thicknesses are presented as functions of temperature.

The oscillatory nature in the thickness dependence of the resistivity, Hall coefficient, magnetoresistance and carrier mobility is attributed to a quantum size effect. A period of 400 $\mathring{A}$ was observed consistent with the theoretical predictions and gives a de Broglie wavelength of 800 $\mathring{A}$ for electrons and 200 $\mathring{A}$ for holes.

" We have a problem....."

Commander James Lovell, Apollo 13.

INDEX

CHAPTER 1.

THEORETICAL AND EXPERIMENTAL FOUNDATIONS

1.1. Introduction

A study of the electrical conducting properties of materials leads to a natural division of solids into three classes; metals, semiconductors and semi-metals. A metal has sufficient electrons to only partly fill its upper valence band, whereas in a semiconductor and semi-metal there are sufficient electrons to completely fill all bands up to a certain level. An energy gap separates the filled valence band from the neighbouring conduction band. In a semi-metal however, there may be no totally forbidden energy level, although a direct energy gap exists for any specified wave vector.

The effect of the anisotropy of the semi-metal band gap in k-space causes, even at the absolute zero of temperature, a spilling over of a number of electrons into the conduction band leaving an equal number of holes. It is this bridge between the electronic structures of metals and semi-conductors that has led to the pronounced interest in semi-metals.

The intense study of semiconductors in recent years has been concentrated on materials with energy gaps of one or more electron-volts as these form the basis of junction devices such as transistors. There are however, applications in which it is desirable to choose materials of much smaller energy-gap, for example, when constructing a photo-conductor for use in the far-infrared region of the spectrum, but the need for narrow gap materials for galvo-magnetic devices is brought out in a graph due to Wright [1], Fig. 1. A general trend is shown in a plot of the carrier mobility

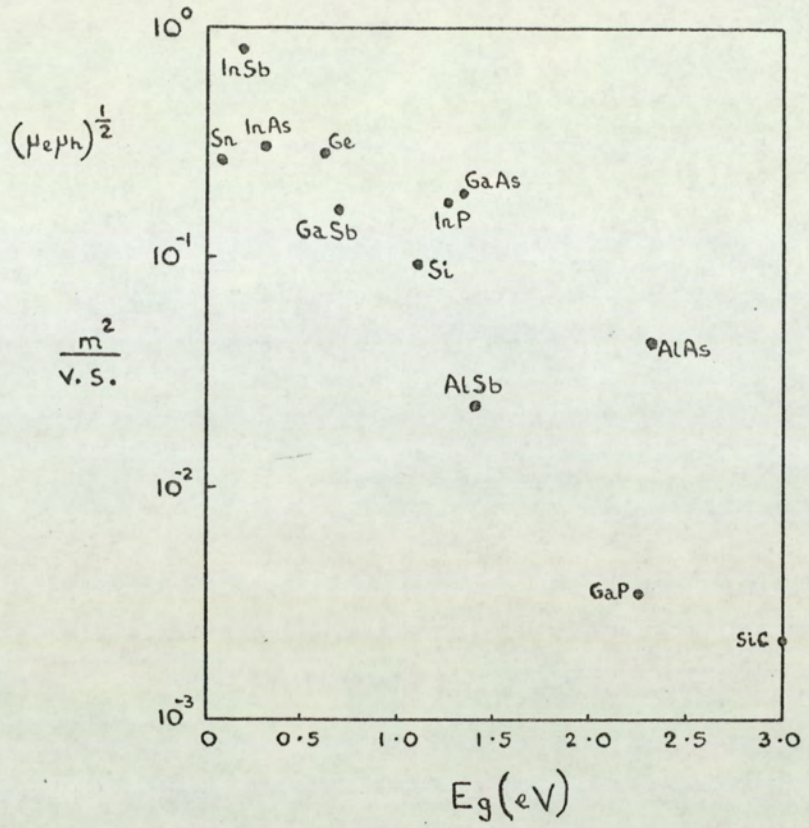

Fig 1. Energy gap vs. mean carrier mobility for a selection of elements and compounds (after Wright).

versus the energy gap for a selection of Group IV elements and III - V compounds in which the smaller gap materials show a higher mobility. The combination of a high mobility and high concentration of electrons and holes readily permits the observation of bipolar transport effects.

Amongst the elemental semi-metals bismuth has been the subject of the largest contribution to the literature, and was the material chosen for the present investigation. An immediate difficulty arising from the use of bismuth lies in obtaining specimens of high purity., With closely spaced bands and a high anisotropy, donor and acceptor impurities that are always present in any real material have a tendency to form impurity bands. As a result, one of two possibilities may occur,

(i) There may be an inequality in the number of electrons and holes producing an n - or p - type semiconductor

or

(ii) The essentially small activation energy required causes a blending together of the valency and conduction bands so that the material exhibits metallic behaviour.

The development of vacuum technology has made the use of thin films a powerful tool in the examination of the electrical properties of materials. Specimens may be prepared by thermal evaporation in an oil-free residual atmosphere to any desired profile. Commercially available equipment enables the specimen thickness to be predetermined from a few to many hundreds of Angstroms. By working within this range it is possible to examine the effect of reducing the size of the specimens from those in which bulk processes occur to those in which mean free path and quantum size effects become predominant. The long carrier wavelengths associated with a low effective mass enable surface phenomena such as specular reflectivity to be more readily observed in semi-metals than in a conventional metal.

To date the studies of thin bismuth films have in general been limited to analyses of galvomagnetic properties at $4.2^{\circ}K$, $77^{\circ}K$ and $300^{\circ}K$ [2-4], or to an occasional study of the effect on the d.c. conductivity of varying the temperature over the upper part of this range [5,6]. Moreover, investigations of the Hall effect and magnetoresistance have as a rule been reported separately, see for example [7-9]. In view of the strong influence of the impurities on the conductivities of solids at lower temperatures [10] accurate information on the relationship between the galvomagnetic effects can only be obtained through their concurrent investigation on the same specimen.

The scope of the present work is to investigate the d.c. conductivity, Hall effect and transverse magnetoresistance of thin bismuth films deposited on glass substrates as a function of their

temperature and thickness over a temperature range 77°K - 300°K. Additional information is sought with a view to contributing to the knowledge of the fundamental processes governing the electrical properties of solids.

1.2. Crystal structure of bismuth

The elements bismuth, antimony and arsenic, and the semi-metal compounds, bismuth and germanium telluride, possess the common space group R $\bar{3}$m. Bismuth has a trigonal (rhombohedral) structure in which the primitive cell has two atoms placed as shown in Fig 2. The lattice vectors a = 4.74 Å are mutually inclined at an angle α of 57° 23' (11). The atoms are situated at (u,u,u) and (-u,-u,-u) with respect to the lattice vectors, where u = 0.234. If u were in fact 0.250 and the angle α were 60° the system would reduce to simple cubic, and it is notable that the complex properties of bismuth derive from such a small difference.

The rhombohedral system can however be represented in terms of a hexagonal unit cell. It displays a disadvantage in that the projection of the cell shown in Fig.2 onto the hexagonal basal plane shows a six-fold symmetry about the trigonal axis whereas in fact only a three-fold symmetry exists. In certain applications, such as in the determination of crystallite orientations, it is more convenient to refer to the hexagonal system if one is dealing with a specimen in which the trigonal axes are aligned normal to the film surface. A table of transformations from the rhombohedral to the hexagonal lattice is readily available, (see for example Guinier (12)), but may be determined directly from Fig.2 if it is noted that the hexagonal lattice points are rotated by $\pi/6$ from the projections.

Boyle (13) suggested that it was possible that atoms in a layer perpendicular to the trigonal axis were held together mainly by covalent bonds but that the layers were only weakly held together by Van der Waals forces. This may account for the fact

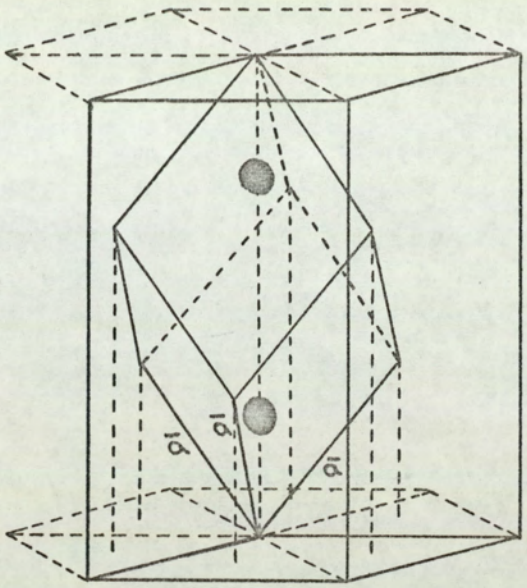

Fig. 2. The trigonal lattice unit cell and its relation to the complex hexagonal lattice.

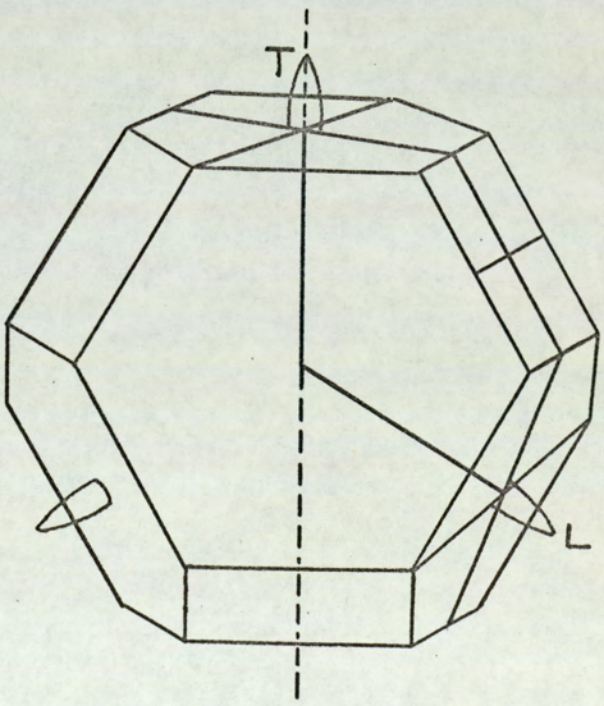

Fig. 3. Brillouin zone for bismuth. The relative magnitude of the carrier pockets has been enlarged for convenience.

that single crystals of bismuth cleave more easily in the hexagonal plane, and may explain why crystal growth takes place preferentially in a direction perpendicular to the trigonal axis. As a result of the one dimensional constraint imposed on a thin film it is expected that the trigonal axis will be perpendicular to the substrate.

1.3. Band structure of bismuth

It has long been recognised that the band structure of bismuth must derive from an almost filled Brillouin zone. Jones [14] constructed a zone, such as to accommodate exactly the five valency electrons, which was bounded by planes across which a small discontinuity in the energy surfaces should occur. He assumed that there was a small overlap in energy between this zone and the next such that small pockets of electrons and holes would be formed. Initially the evidence for the fact that one was dealing with a small number of electrons came from resistivity measurements in which it was found that the addition of minute ammounts of tetravelent tin changed the sign of the temperature coefficient of resistivity. Jones deduced that there would be less than 10^{-3} conduction electrons per atom.

By plotting the reciprocal lattice points for the rhombohedral crystal structure of bismuth, and by drawing the planes normal to the reciprocal lattice vectors the first Brillouin zone is obtained as shown in Fig.3. The two face-centred cubic lattices, of which the simple cubic is composed, are displaced relative to each other by a small amount in bismuth. Similarities exist between figure 3 and the regular zone for a face centred lattice shown in standard texts [15]. Only the two equivalent surfaces with 'T' as their centres are regular hexagons, the other six being somewhat distorted.

By symmetry arguments Jones showed that the Fermi surface for electrons in bismuth can be quite accurately described by a set of ellipsoids in momentum space, whose energy could be expressed as,

$$E = \frac{\hbar^2}{2m} (k_x^2 + k_y^2 + k_z^2) \qquad (1-1)$$

The exact number and location of the electron ellipsoids in the Brillouin zone have been the subject of much experimental and theoretical work, and a review is given by Jain and Koenig [16]. Oscillations periodic in the inverse magnetic field, such as the de Haas - van Alphen effect, yield directly the external cross-sectional area of the Fermi surface per ellipsoid normal to the applied magnetic field. Repeated readings over a wide range of geometries lead to the build up of a picture of the volume of the Fermi surface in momentum space, and hence give the number of electrons per ellipsoid, n. The total number of electrons, N, may be obtained from measurements such as the Hall effect, so that the number of ellipsoids may be obtained from the ratio N/n. Taking values of $n = 1.4 \times 10^{23}\ m^{-3}$, (Friedman and Koenig [17]) and $N = 3.9 \times 10^{23}\ m^{-3}$, (Boyle and Brailsford [18]) gives N/n close to three, indicating three electron ellipsoids.

It was not until 1960 that Brandt et al [19] observed the de Haas - van Alphen oscillations due to holes and found that p (defined similarly to n) was given by,

$$p = 3.4 \times 10^{23}\ m^{-3} = 0.87\ N.$$

The number of holes per ellipsoid is within 13% of the total electron concentration inferring that there can be but one hole ellipsoid, centred on the trigonal axis. The possibility of the remaining 13% being due to heavy holes has been suggested by Weiner [20], but Jain and Koenig do not rule out the possibility that experimental error could account for the difference.

The overlap of carriers across the Brillouin zone

boundaries result in pockets of holes and electrons as shown in Figure 3. The magnitude of the overlap is rather small and hence the pockets have been enlarged for convenience. The three electron ellipsoids (or six half-ellipsoids) are located at the points 'L' whilst the hole ellipsoid (as two half-ellipsoids) are at 'T'. The electron ellipsoids are not in fact exactly alligned on the three symmetry axes, but are displaced by some 5^{o}. As a result some of the cross-terms in the effective mass tensor are non-zero. It will be shown that for all the present observations, only those specimens with the magnetic field parallel to the trigonal axis will be considered, and hence the effective masses quoted by Kao [21] are applicable. Kao deduced the effective masses from cyclotron resonance measurements and compared the values with those of Aubrey [22] and of Galt et al [23] for a similar orientation. Table 1 summarises the observations.

Table 1

m^*/m_o by cyclotron resonance

H parallel to trigonal axis

Author	Electrons		Holes	
	$H_{\parallel}$	$H_{\perp}$	$H_{\parallel}$	$H_{\perp}$
Aubrey	0.06	0.009	0.04	0.15
Galt et al	0.08	0.0105	0.068	0.25
Kao	0.081	0.0107	0.067	0.23

The values of the mobility ratio μ_e/μ_h at 80°K and 300°K (Abelés and Meiboom) are such that only a very weak temperature dependence was observed. Gallo et al [24] assumed that the individual mobilities took the form,

$$\mu = c T^{-\frac{3}{2}} \qquad \text{——————} \quad (1-2).$$

and calculated the mobilities at intermediate temperatures. Applying the values obtained to the equations relating the electrical conductivity and carrier energy with the absolute Seebeck coefficient enabled Gallo to produce a graph of the electron and hole Fermi energies against temperature for bismuth single crystals. Fig 4. shows a schematic sketch of the overlapping bands of bismuth in which a direct energy gap is retained for a given k-vector. The electron and hole Fermi energies are measured from the maxima of their respective bands and the resulting overlap energy, E_o, is formed from the sum of the individual Fermi energies. By the usual sign convention of semiconductor technology E_o will be negative in the case of an overlap.

$$-E_o = E_F^e + E_F^h \qquad \text{——————} \quad (1-3).$$

Fig 5 shows the overlap energy, $-E_o$, as a function of the absolute temperature.

1.4. Background to the present research

1.4.1. Historical introduction

The classic work, and probably the earliest significant contribution on the properties of bismuth was undertaken by Kapitza in 1928. He investigated the galvanomagnetic properties of bismuth crystals in magnetic fields up to 3×10^5 gauss and at temperatures down to the boiling point of liquid nitrogen. At the turn of the decade Schubnikov and de Haas extended the work to liquid helium temperatures and noted an oscillation periodic in the inverse field

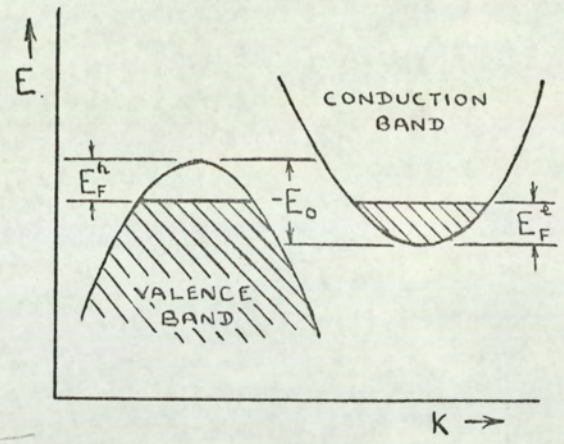

Fig.4. Schematic diagram of overlapping bands in bismuth.

superimposed on the magnetoresistance curves. The de Haas-van Alphen oscillations of the magnetic succeptability observable in most materials was a direct development of the work on bismuth.

Jones in 1935 investigated the band structure of bismuth and deduced a model based on an almost filled Brillouin zone. The foregoing work was re-analysed in the mid 1950's by Abelés and Meiboom and by Lifschitz in the light of modern theories of band structure. A review article by Boyle and Smith on bulk properties of bismuth was published in 1964.

The Fuchs - Sondheimer theory (1938) of metallic conduction in thin films has been applied to bismuth by several authors. Notable contributors to the problems concerning specimens with reduced dimensions

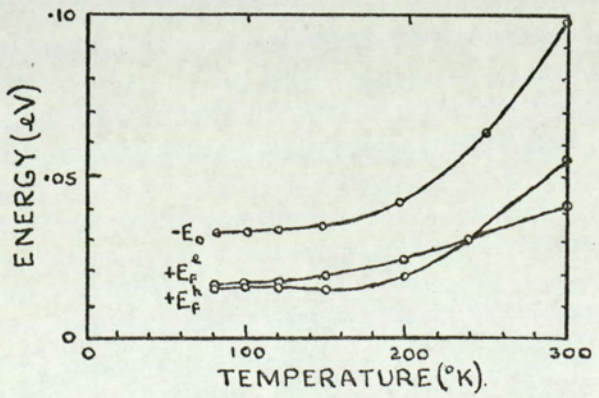

Fig.5. Fermi and overlap energies in bismuth vs. temperature (after Gallo).

have been Friedman and Koenig (1960), Price (1960) and more recently Cotti (1967). A series of papers by Palatnik (1958 - 1965) dealt with mechanisms of the condensation of bismuth vapour onto various substrates.

The majority of the investigations into the effects on the band structure of varying the thickness of films have been undertaken in the U.S.S.R. since 1966. The results display periodic oscillations of the electrical properties of bismuth as the thickness is reduced: Such properties are known as quantum size effects. The observations of Lutskii and of Ogrin are supplemented by the theory of Sandomirskii based on solutions of the Schroedinger equation. An alternative approach not reported in the literature gives a theory of the quantum size effect based on well established theories of electron diffraction and will be discussed in Chapter 2.

The relevant contributions to the literature on bismuth can be divided into three classes.

(i) Those dealing with the bulk properties of bismuth, its anisotropies and the effect of alloying.

(ii) Those dealing specifically with thin films of bismuth and related materials.

(iii) Those concerned with the technology, preparation and structure of specimens.

Many of the quoted parameters of bismuth for both films and bulk material vary between authors, possibly due to the presence of various degrees of impurities in the samples. To quote figures of high purity would in general refer to the metallic purity, and would not consider the effects of, for example, the take up of atmospheric oxygen as a doping material [25]. Further, the anisotropies of bismuth require the specimens to be of known orientation and in the case of bulk properties this would infer the use of single

crystals. For films, however, the need for single crystals is not stringent providing the orientation of the crystallites is known. Indeed it is shown later that for observations of quantum effects the presence of single crystal films is undesirable.

The bulk properties of bismuth are highly anisotropic and far from what one would expect from a near cubic lattice. The anisotropy arises from a lattice structure in which electrical conduction can take place more easily within the basal plane of the crystals than along the principal axis [26], a behaviour which is similar to that of graphite.

1.4.2. Resistivity of bismuth

The resistivity of bulk bismuth crystals shows a metallic behaviour in that it decreases almost linearily with decreasing temperature until impurity scattering dominates [27]. Unlike metals the number of carriers in bismuth increases with increasing temperature due to the thermal exitation of electrons from the valence to the conduction band. Galvomagnetic experiments of Abeles and Meiboom [28] have shown that the number of electrons increases from 0.46×10^{24} m^{-3} at $80^{\circ}K$ to 2.2×10^{24} m^{-3} at $300^{\circ}K$. The corresponding room temperature resistivity is $\rho_{\parallel} = 150$ $\mu\Omega$-cm for current parallel to the trigonal axis and $\rho_{\perp} = 120$ $\mu\Omega$-cm in the perpendicular direction. These values are at variance with those of Focke and Hill for the same orientation: $\rho_{\parallel} = 122$, $\rho_{\perp} = 100$. Gallo [24] reported room temperature values mid-way between these two and supplied values down to $77^{\circ}K$. It is not uncommon for the resistivity ratio $\rho_{4.2^{\circ}K}/\rho_{300^{\circ}K}$ to be of the order of 100 - 400 [22,29] and therefore the temperature coefficient of resistivity α for the two principal directions, Fig 7 (i) are

$\alpha_{\parallel} = 0.50$ $\mu\Omega$-cm $^{\circ}K^{-1}$, $\alpha_{\perp} = 0.40$ $\mu\Omega$-cm $^{\circ}K^{-1}$.

The length of the mean free path of the conduction electrons varies from about one hundred lattice spacings at room temperature to

the order of 1 m.m. at liquid helium temperatures [30]. In specimens whose dimensions approach that of the mean free path, boundary scattering occurs resulting in an enhanced resistivity. Measurements of Friedman and Koenig [17] indicated that this was specular rather than diffuse scattering, but it has been shown [31] that for a non-spherical Fermi-surface as in bismuth the effect will still occur due to the velocity and momentum of the carriers having different directions. The magnitude of the non-spherical effect should however reach a limiting value which is dependent on the shape of the constant energy surfaces. This saturation is in contrast to diffuse scattering for which the resistivity increases monotonically with decreasing sample thickness both for spherical and non-spherical surfaces.

Fig 6 shows the effect of the saturation taken from the observations of Friedman and Koenig [17] and of Aubrey et al [22] in which the bulk, film and saturated regions can be easily seen.

It is in many ways more practicable to maintain the thickness of the specimen constant and to lower its temperature in order to observe the effects of proportionately larger carrier wavelengths. Some authors however have chosen to vary the film thickness at fixed temperatures. One would not expect that the resistivity of even very thick films to reach those of single crystal bismuth due to the polycrystalline nature of the deposits, but the dimension quoted corresponding to a departure from a thickness independant value of the resistivity is by no means certain. A similar uncertainty shrouds the sign of the temperature coefficient of resistivity (T.C.R.). The account given below of the observations of various authors are summarised in Fig. 7 (ii-vi).

Kao [2] working on thick films up to 10 microns ($1\mu = 10^4 \text{Å}$) indicated an increase in resistivity for films less than 3μ in thickness and though a quantitative estimate of the T.C.R. is inaccurate from three temperature points, a negative value was

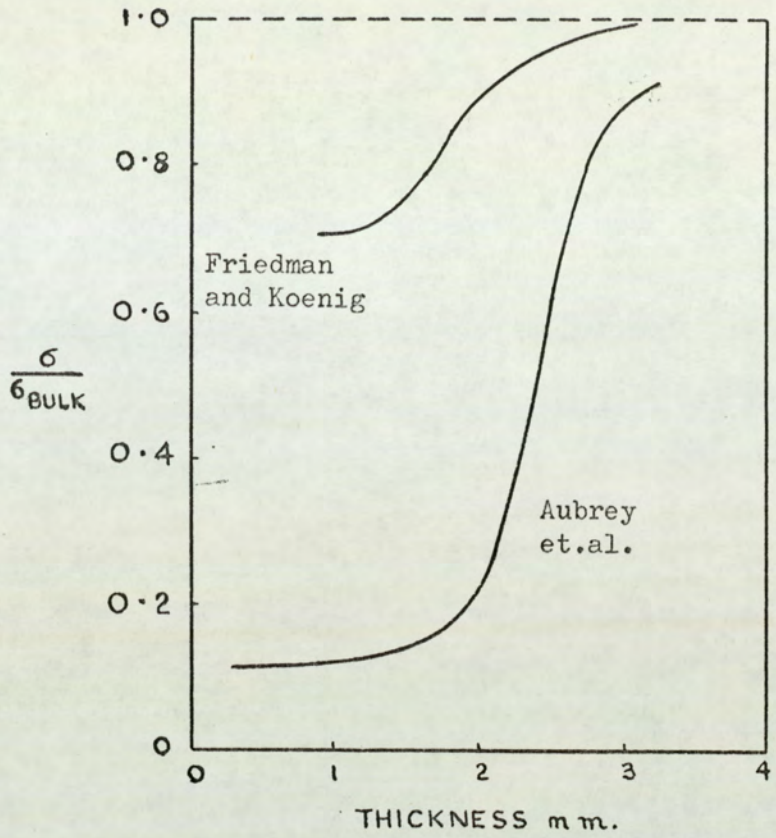

Fig.6. Variation of electrical conductivity of bismuth with sample thickness at 4.2°K.

indicated at all thicknesses. The room temperature resistivity in the thick limit was 200 $\mu\Omega$- cm. A similar observation by Duggal et al [32] indicated a sharp increment in the resistivity from a constant value of 150 $\mu\Omega$-cm at a thickness as low as 2000 Å. The interchange to a strongly negative T.C.R. occurred only below 1000 Å.

A comprehensive survey by Kioke [33] provided interesting results. A graph of resistivity against thickness containing some 150 points showed only a small variance from a thick limit value of resistivity of 180 $\mu\Omega$-cm, down to 4000 Å. Below this value there was an undoubtable trend towards increased resistivity as with other authors, but the scatter in the points spanned one order of magnitude. The corresponding graph of T.C.R. versus thickness, however, was linear with only an acceptable scatter in the points. The change to negative T.C.R. coincided with the onset of the region of uncertainty.

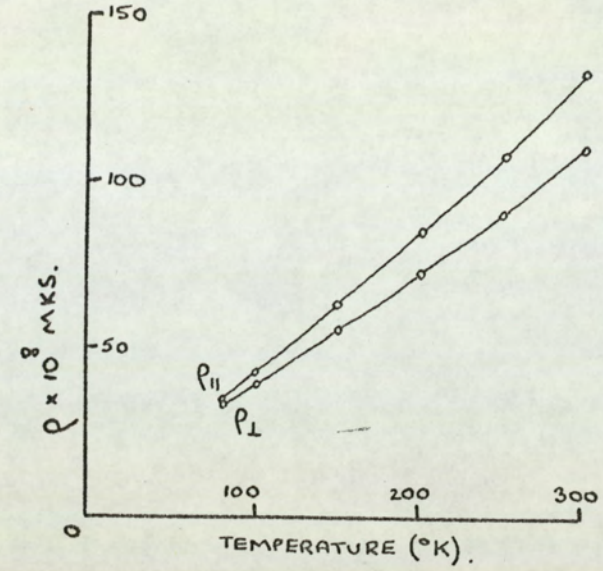

(i) ρ vs. T°K. Bi crystals (Gallo et al)

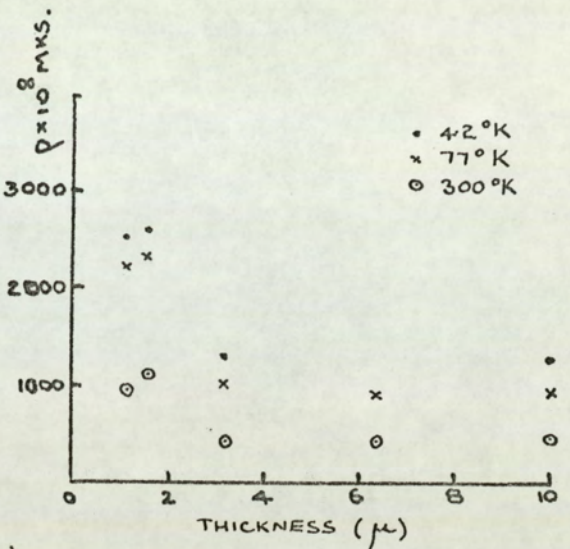

(ii) ρ vs. thickness (Kao)

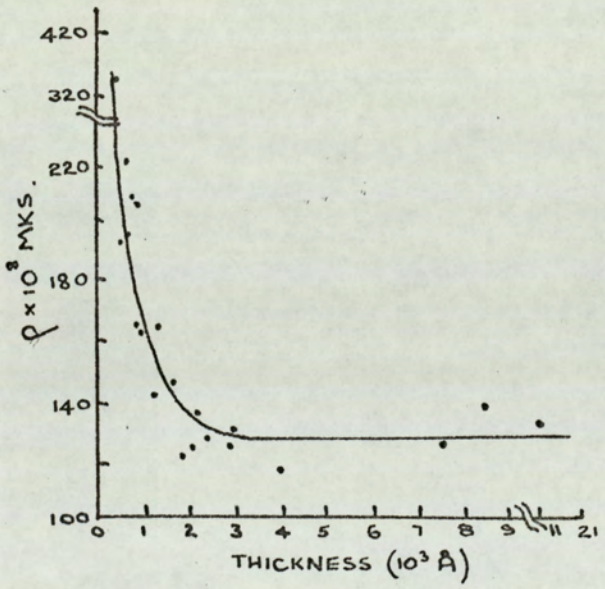

(iii) ρ vs. thickness (Duggal)

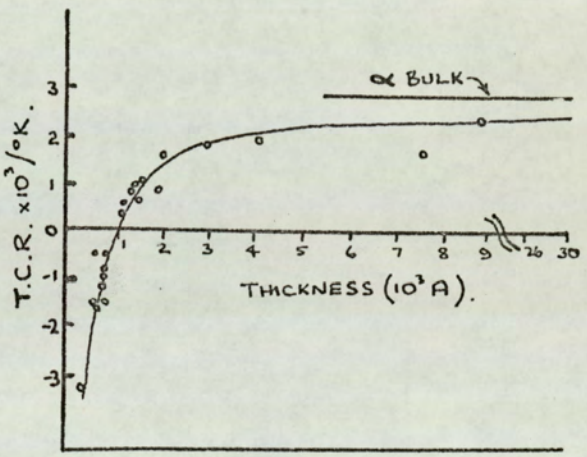

(iv) T.C.R. vs. thickness (Duggal).

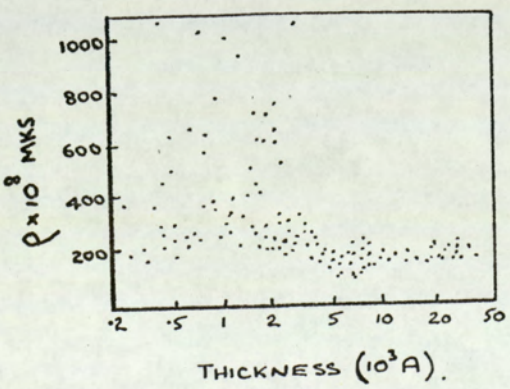

(v) ρ vs. thickness (Kioke)

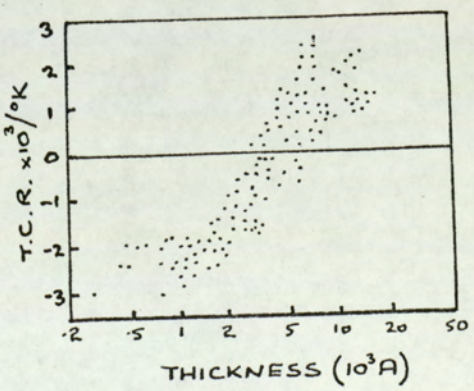

(vi) T.C.R. vs. thickness (Kioke).

Fig.7. Resistivity and temperature coefficient of resistivity for bismuth single crystals and films.

1.4.3. Magnetoresistance

Kapitza [34] investigated the change of resistance of many metals in magnetic fields up to 3×10^5 gauss. It was found that the intensity of the effect vastly increased with a reduction in temperature. At 2 - 4°K and fields of 10^4 gauss the resistance of many metals increased hundreds of times whereas for bulk bismuth the factor was millions [35]. The great increase in resistance is explained by a 10^3 - 10^4 - fold increase in the length of the meanfree path of the carriers in pure metals at these temperatures. Kohler [36] observed the variation of the magnetoresistance of many metals as a function of magnetic field and temperature and deduced that if, as an alternative to plotting $\Delta\rho/\rho$ against the magnetic field, H, one plotted $\Delta\rho/\rho$ against the ratio of H/ρ, the experimental data obtained at different temperatures fitted a common curve.

Fig.8 illustrates a Kohler-plot for magnesium over a range of temperatures. There is thus a direct relationship between the applied magnetic field and the mean free path of the electrons, an observation which led Borovik to suggest that the increase in mean free path caused by lowering the temperature was equivalent to a corresponding increase in the effective strength of the magnetic field. Consequently the true low temperature effects such as the Schubnikov - de Haas oscillations of the magnetoresistance can be separated from the observations in which a low temperature is only of secondary importance.

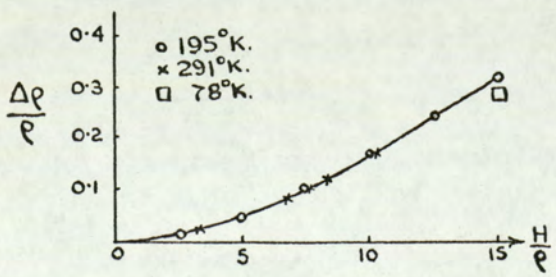

Fig.8. Kohler plot for magnesium (after Kohler).

The available experimental data on the resistive behaviour of metals at low temperatures permitted Justi [37] to divide metals into two classes.

(i) Those in which there is an unlimited increase of the resistance in magnetic fields, - bismuth, cadmium, magnesium, tungsten etc.

(ii) Those in which a saturation is observed. The resistance reaches a certain limiting value - aluminium, indium, sodium etc.

The differentiating factor between materials of the two groups lies in the process of conduction by two sets of carriers where the unlimited increase in resistance occurs in materials in which the electrons and holes are present in equal numbers. The Hall effect on the other hand is characterised by the alternative condition i.e. unlimited increase in resistance is associated with a saturation of the Hall voltage. In view of the strong influence of impurities on the conductivity of semi-metals and the inter-relation between the Hall effect and magnetoresistance accurate information can only be satisfactorily obtained through their concurrent investigation on the same specimen.

The majority of the magnetoresistance measurements reported in the literature have been undertaken on bulk single crystal specimens in high magnetic fields. The classic work on bismuth by Kapitza presented perhaps one of the most comprehensive treatments of the problem. Experimental data was given for various orientations of the orthogonally applied electric and magnetic fields with respect to the crystallographic axes. The present survey reports mainly those observations in which the electric field was perpendicular to the trigonal axis of the specimens.

Fig. 9 shows the ratio of the d.c. resistances with and

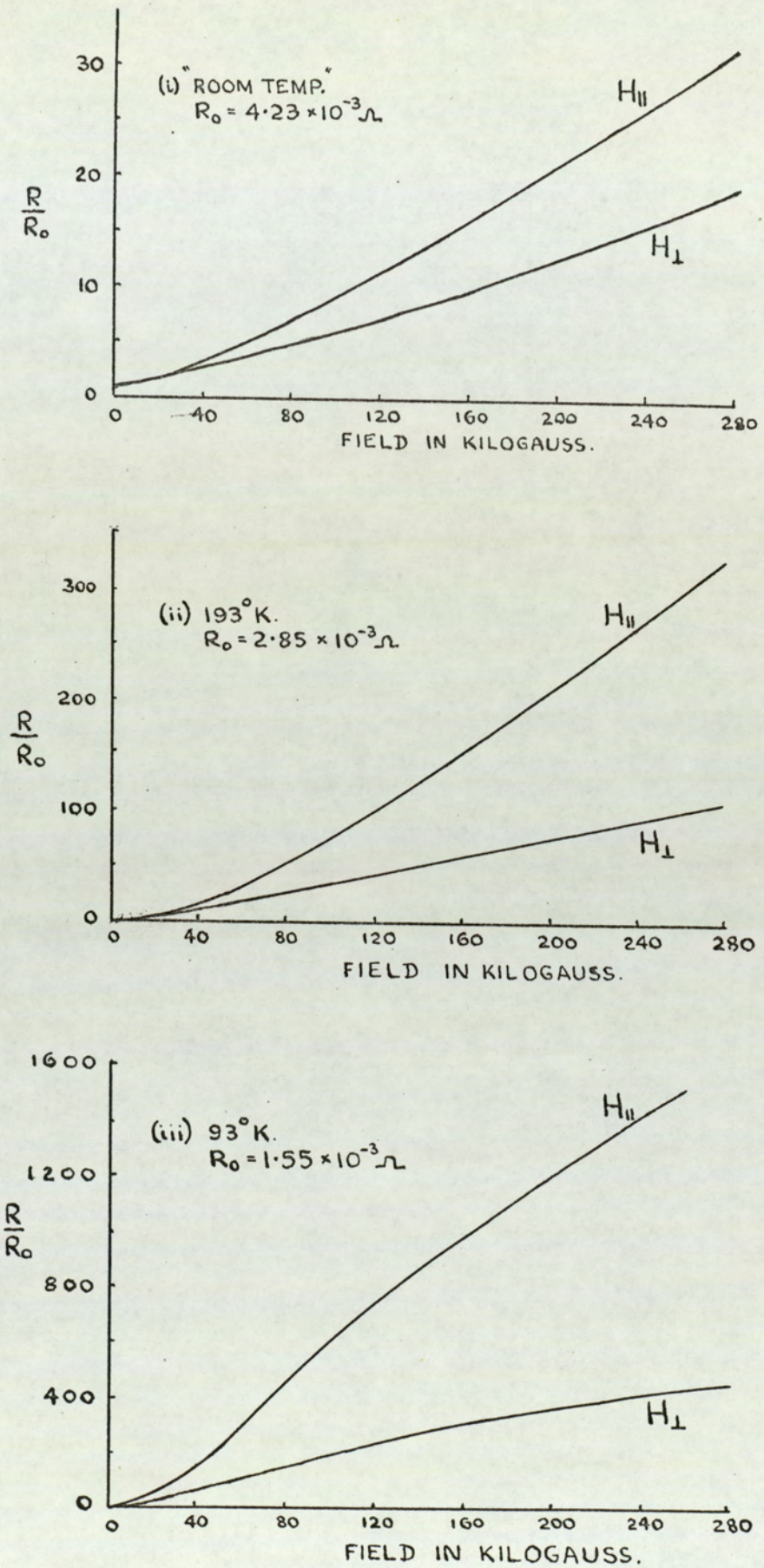

Fig.9. Magnetoresistance of single crystal bismuth with Field $\parallel$ and $\perp$ to trigonal axis (after Kapitza)

without the magnetic field against the magnetic field strength, up to 280 Kilogauss (Kg.). It will be seen that the general trend is such that the effect is enhanced by a lowering of the temperature, as would be indicated by a Kohler Plot. The magnitude of the magnetoresistance with the magnetic field parallel to the trigonal axis was a factor of between one and three greater than in the case where it was in the cleavage plane.

In the low field region (0 - 20 Kg) a quadratic dependence on magnetic field was observed, the effect reducing to a linear dependence at higher fields ($>$ 60 Kg.). Kapitza's relationships for the two regions were given as:

$$\frac{\Delta R}{R_o} = \beta H^2 \qquad \text{——————} \quad (1-4)$$

$$\frac{\Delta R}{R_o} = \gamma H \qquad \text{——————} \quad (1-5)$$

A slight indication of an ultimate region of saturation was observable at fields in excess of 200 Kg.

The critical field strength, H_k, at which the changeover from quadratic to linear dependence occurs was only weakly defined. At a given temperature the constant β was such that it's value was governed by the particular crystal orientation but γ was a characteristic of the specimen only. A summary of the values obtained is given in Table 2.

Table 2. Magnetoresistive Coeffients (after Kapitza)

Temperature ^{o}C	β (g^{-2})	γ (g^{-1})
"Room Temp"	1.24×10^{-9}	1.27×10^{-4}
- 80°C	1.0×10^{-8}	1.48×10^{-3}
- 180°C	0.88×10^{-7}	5.44×10^{-3}

From such few temperature points Kapitza was unable to deduce a definite law relating to the temperature coefficients of β and γ but suggested that it must vary inversely as the fourth or fifth power of the absolute temperature. He further surmised that the effect of lattice imperfections was to leave β and γ invariant but to reduce the value of the critical field, H_k.

Brandt [29] extended the observations to 450 Kg. at liquid helium temperatures and confirmed the foregoing data. At these higher fields it can be observed (Fig.10) that a saturation occurs in fields in excess of 200 Kg, at which point the value of the ratio ρ_H/ρ_o was approximately 6×10^5 for H parallel to the trigonal axis.

The value of H_k obtainable from other contributors is somewhat lower than that of Kapitza. Both Grenier et al [38] at 4.2°K and Gitsu and Ivanov [39] at room temperature show a departure to a linear dependence on the applied field at only 3 Kg as indicated in Fig.10. The latter graph shows clearly the superimposed Schubnikov - de Haas oscillations periodic in the inverse field strength. A log - log plot of Abelés and Meiboom [28] showed no departure from a square-law dependence for this orientation at their maximum magnetic field of 3 Kg.

Information relating specifically to the magnetoresistive properties of specimens with reduced dimensions is not so widely published. Friedman and Koenig [17] in a plot of magnetoresistance against squared field strength at 4.2°K show a value of β which reduces with size of specimen from 19×10^{-3} g^{-2} at 3mm. thickness to 9.1×10^{-3} g^{-2} at 1.8 mm. Kao [2] working in the micron range indicated a major fall of the magnetoresistive coefficient below 3μ corresponding to his point of enhanced resistivity.

Thin film observations by Huet and Colombani over a range

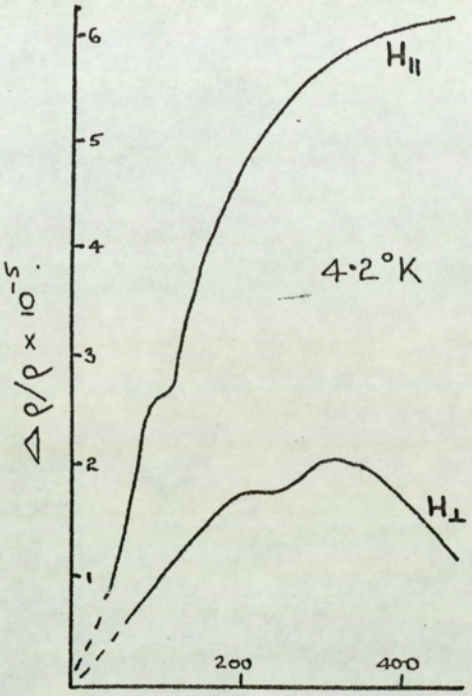

(i) after BRANDT et al.

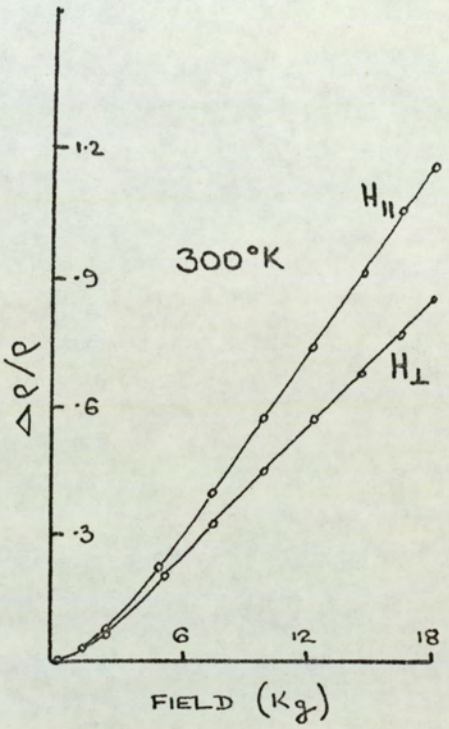

(ii) after GITSU and IVANOV.

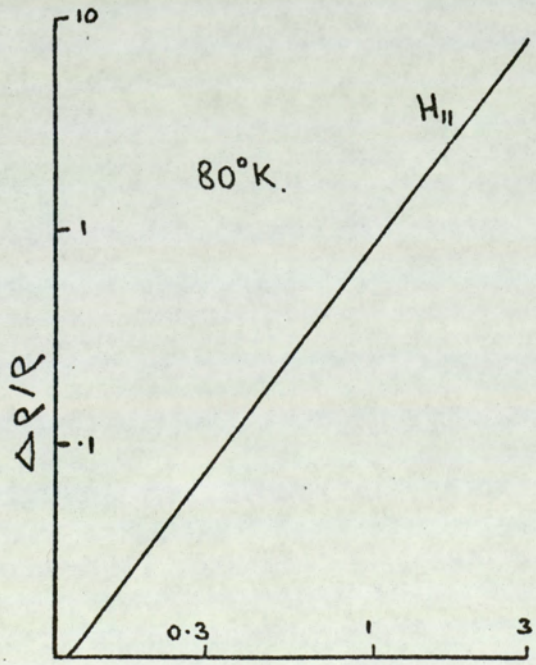

(iii) after ABELES and MEIBOOM.

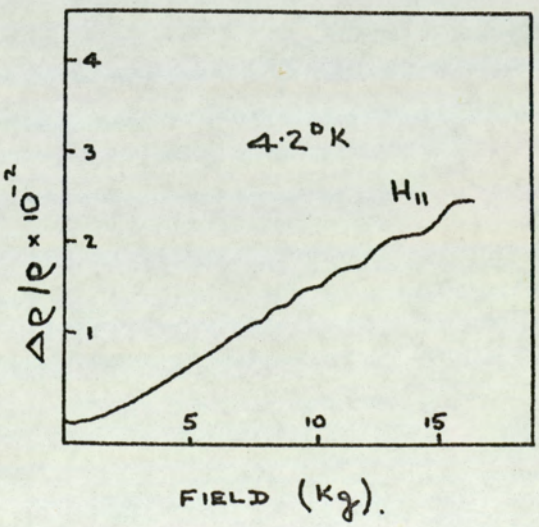

(iv) after GRENIER et al.

Fig. 10. The bulk magnetoresistive properties of bismuth.

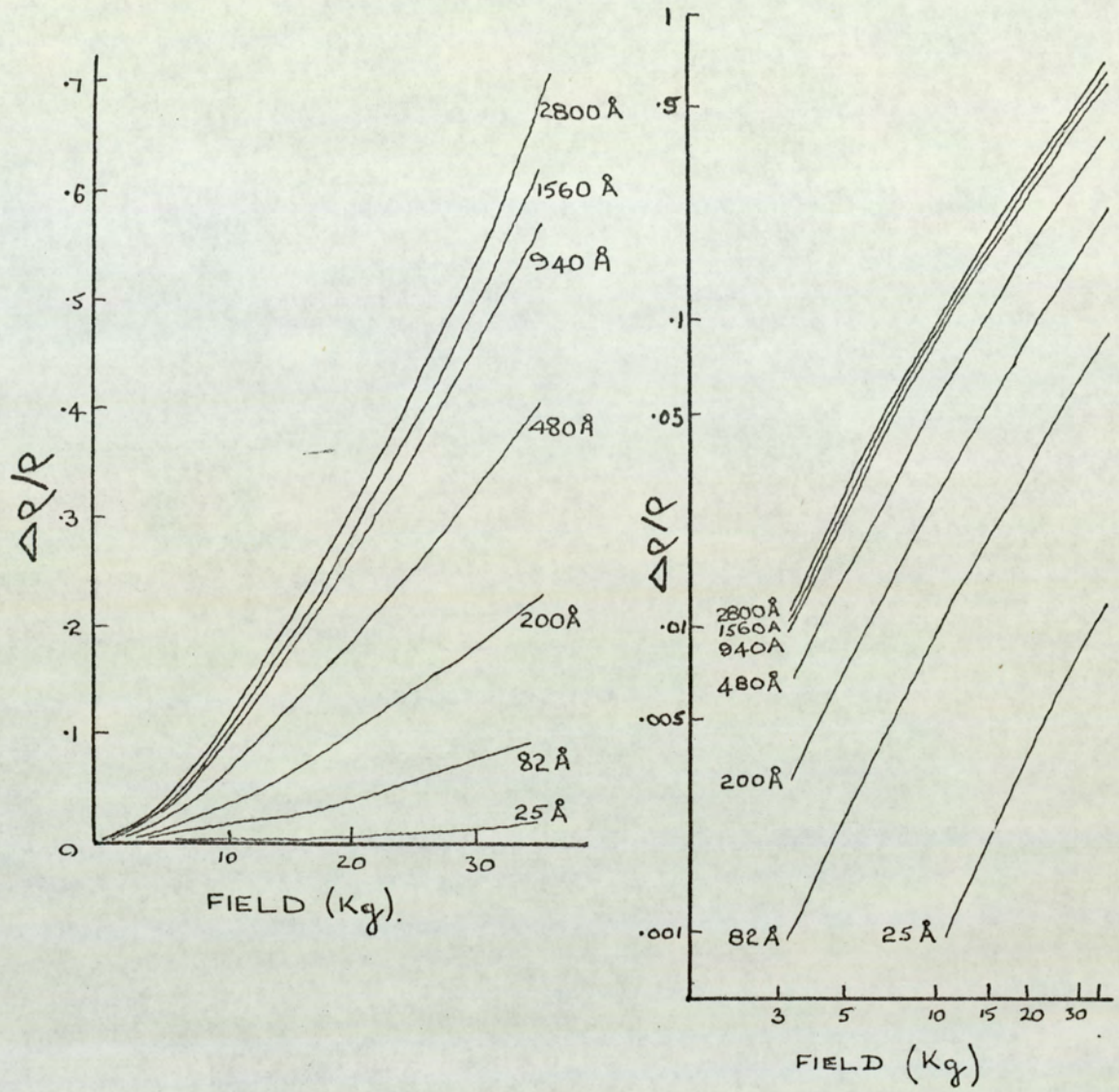

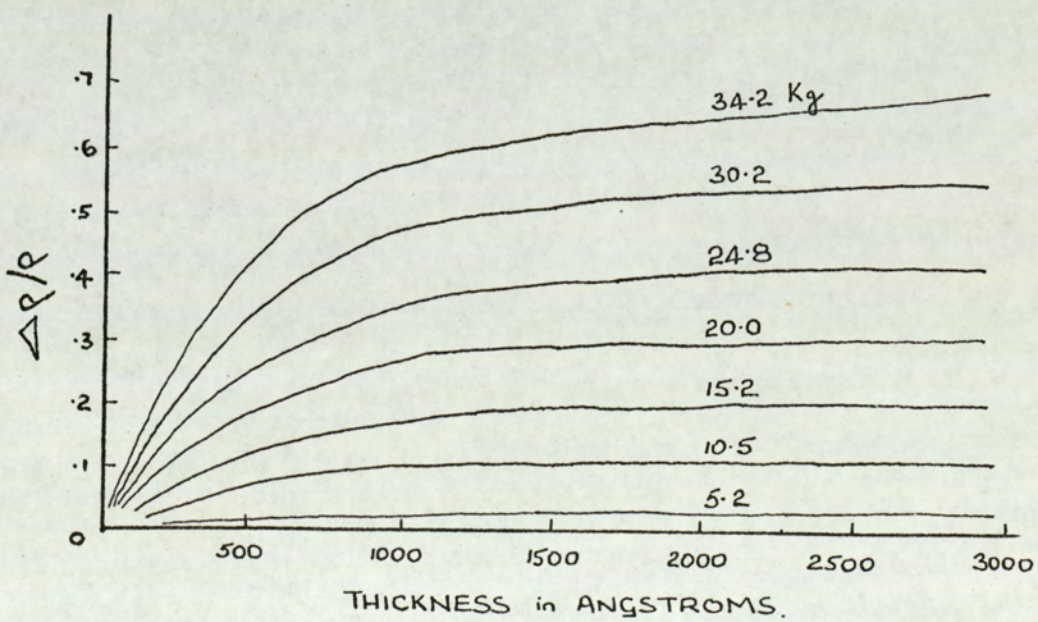

Fig.11. Thin film magnetoresistive properties of bismuth

(after Huet and Colombani)

of thicknesses from 25 - 2800 Å in thickness are shown in Fig.11. A power law dependence is readily shown by the gradient of a logarithmic plot and seen to be of a quadratic nature. For the thicker films at higher fields a trend towards a power dependence of $H^{1.5}$ is indicated. A final plot of $\Delta R/R$ against thickness for varying fields shows only a gradual increase in the magnetoresistance for thicknesses in excess of 1600 Å corresponding to an increase in resistivity of only 3% under conditions where it would be 150% in bulk material.

1.4.4. Hall effect

The Hall effect in a solid is a direct manifestation of the Lorentz force on moving charge carriers, and has long been recognised as a powerful tool for the direct observation of the charge and effective number of carriers in a material. The total force on a charged particle moving with a velocity v in an electric and magnetic field is given by the vector equation:-

$$F = e[E + v \wedge B] \qquad (1-6).$$

where F = force

e = particle charge

E = electric field strength

B = magnetic induction

If we consider a confined stream of particles in which the velocity is in the x - direction and the magnetic field is in the z - direction a deflection of the charged particle in the y - direction occurs. The nett unbalanced charge results in an electric field E_y. The Hall field causes a charge to be built up along the edges of the specimen until the force it exerts on the stream counteracts the Lorentz force. Subsequently particles of the same velocity are no longer deflected and a steady state exists.

The magnitude of the Hall coefficient is readily shown for a single type of carrier to be

$$R_H = \frac{E_y}{I_x B_z} = \frac{1}{ne} \qquad (1-7)$$

where I_x = current density

n = number of free carriers.

It is sufficient to say here that in the case of bismuth with n being small (compared to monovalent metals) and with R_H being the difference of two terms, the Hall coefficient is both large and sensitive to the presence of impurities. It is not unexpected therefore that a large diversity in the quoted values of the Hall coefficient exists. The analysis of Borovik [10] does however indicate, as mentioned earlier, that in solids of the bismuth type the unlimited increase in the magnetoresistance with magnetic field is coupled with a limited increase in R_H. As with the resistivity effects two principle independant Hall coefficients may be quoted — $R_{\parallel}$ in which the magnetic field is parallel to the trigonal axis, and $R_{\perp}$ in which the field lies in the cleavage plane.

The measurements of Jain [41] and of Jain and Koenig [16] on single crystal specimens of 99.998% purity (zone refined) show the value of R_H for both directions of magnetic field. For 'pure'

(i) Pure Bismuth

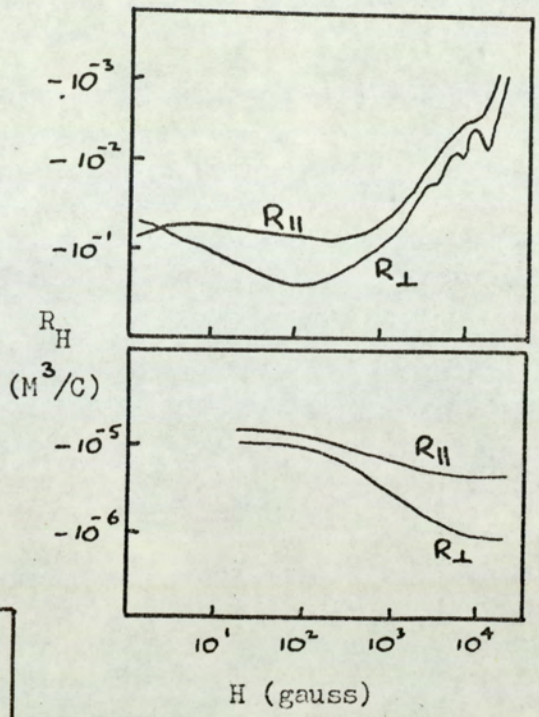

(ii) 14 p.p.m. Sn-doped bismuth.

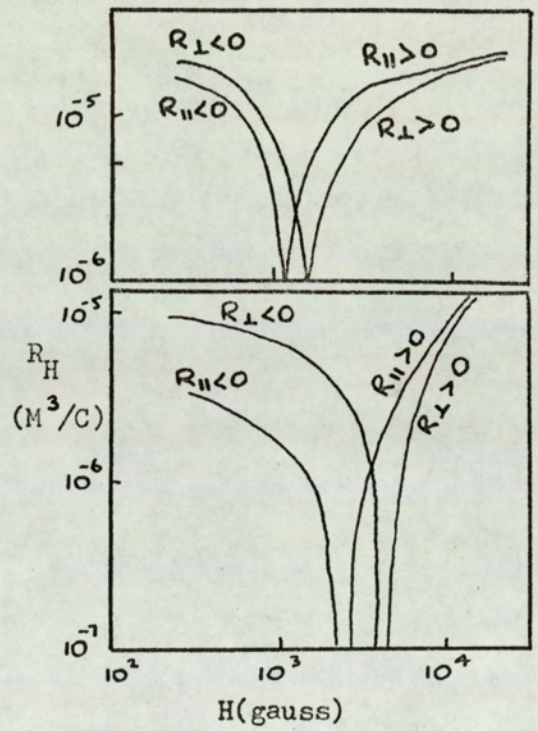

(iii) 17 p.p.m. Te - doped bismuth

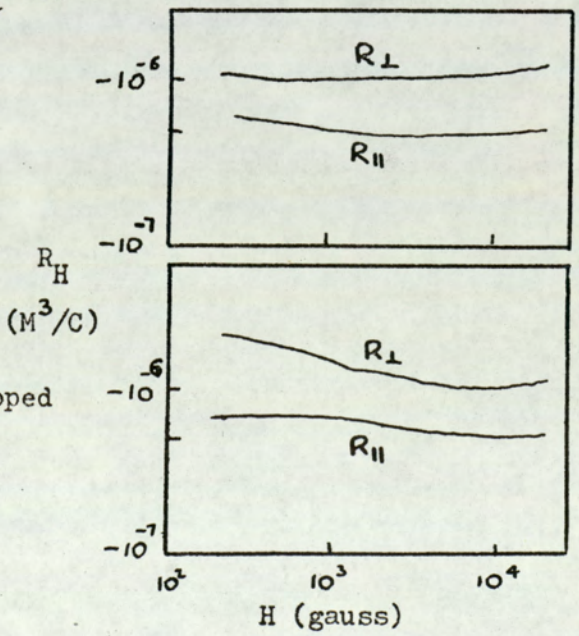

Fig. 13. Hall coefficient of bulk bismuth (after Suzuki)

bismuth and for alloys with less than 10% of added antimony, $R_{\parallel}$ is positive at all temperatures whilst $R_{\perp}$ is negative. The inverse temperature plot does not enable accurate extraction of data in the room temperature region, but values of the same sign are tabulated by Abeles and Meiboom [28] using crystals of 99.996% purity; $R_{\parallel,\perp}$ = 4.5, -135 x 10^{-7} MKS at 300°K; $R_{\parallel,\perp}$ = 27, -837 x 10^{-7} at 80°K.

An investigation by Suzuki [42] was performed using bismuth of ultra-high purity, 99.9999% and zone refined 20 times under vacuum. It is seen from Fig. 13 that for pure bismuth at both liquid nitrogen and liquid helium temperatures the sign of R_H is negative irrespective of the principal crystal orientation. The results of Suzuki are also shown in which the effects of impurity doping are observed. The addition of 17 parts per million (p.p.m) of tellurium lowered the magnitude of R_H somewhat, but retained the negative sign. 14 p.p.m. of tin however inverted the sign of R_H for both orientations below 2-5 x 10^3 gauss. The inference would be that the presence of traces of impurity and the use of fields up to 2 kilogauss in the specimens of Abeles and Meiboom were partially responsible for the inversion of the sign of R_H. For most practical purposes however the purity of samples is more likely to be such that the results of Abeles and Meiboom satisfactorily illustrate the properties of bulk material.

The earliest reported observations of the Hall coefficient measurements of bismuth films were those of Leverton and Dekker [43]. The single quoted value for the Hall coefficient at 300°K was + 0.89 x 10^{-7} MKS. Whilst an empirical relationship for the varation of R_H with magnetic field was given, the quoted values were averaged over the various film thicknesses from 0.2 - 1.3μ. Equation (1 - 8) may be re-arranged to express R_H only in terms of n and the ratio μ_1/μ_2. At a fixed temperature therefore R_H will be, to a first approximation,

insensitive to a size variation as long as the holes and electrons are scattered similarly at the film boundaries. Fig. 14 illustrates the observations of Kao [2] in the thick film region, and it is seen that R_H did in fact remain essentially invariant for all temperatures quoted. The condition still held at thicknesses below those in which the resistivity and magnetoresistance coefficients deviated from the size independent value. The coefficient R_H was, however, positive over the whole quoted thickness range of 1 - 10 μ. A similar graph by Duggal [32] showed a size dependence at thicknesses below 4000 Å although in this case the resistivity was still exhibiting the thick limit value.

It is reported that bismuth films prepared by thermal evaporation in vacuum display a preferred orientation in which the trigonal axis of the crystallites lies perpendicular to the surface of the film. The Hall effect of the thinner films has thus a positive coefficient in the plane of the film. As the film becomes thicker the crystallites grow, but this process cannot proceed indefinitely. It is not unexpected that for thicker films some orientation is lost, and a component of the much larger coefficient with the field perpendicular to the trigonal axis becomes predominant. It is difficult to imagine that the orientation that would be inferred by the results of Kao or Duggal was in fact present. Representative of the more typical observations was the contribution of Kioke [33]. Similar to his resistivity readings he observed a considerable spread of points with positive coefficients at thicknesses up to 1 μ above which a negative coefficient was observed (Fig. 14). The tabulated values of R_H at 294°K due to Harris and Piper [45] are also shown in Fig. 14. where it will be seen that the coefficient became negative at thicknesses above 4000 Å.

One of the reports of the gradual variation of R_H with

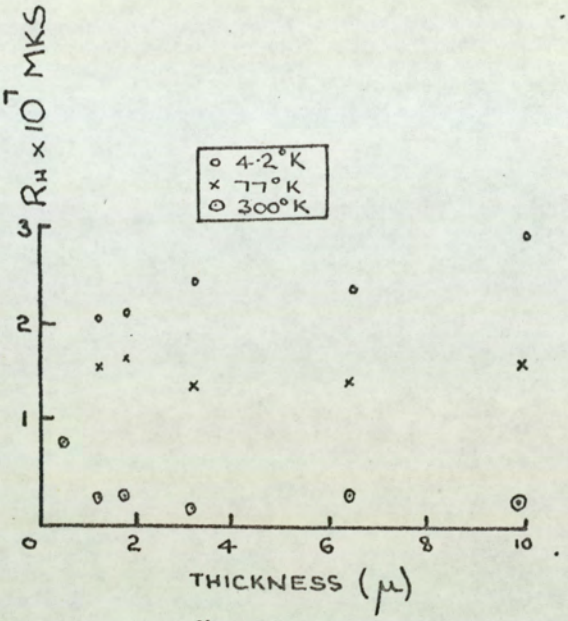

(i) after KAO

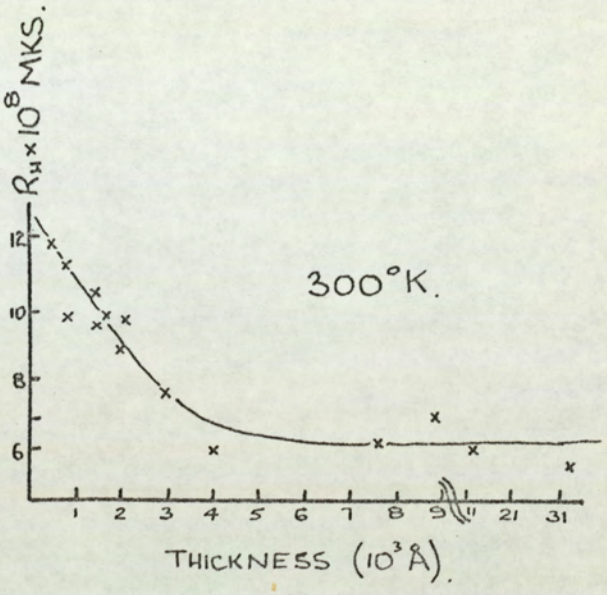

(ii) after DUGGAL et al.

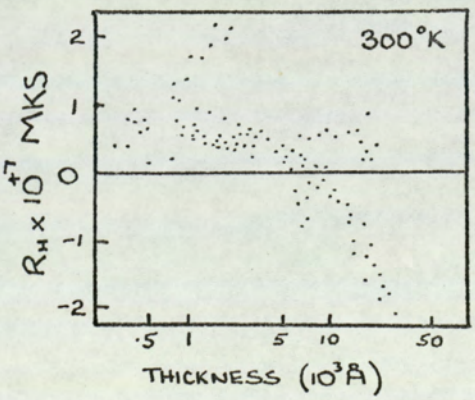

(iii) after KIOKE.

THICKNESS Å	$R_H \times 10^8$ MKS	$\rho \times 10^8$ Ω-M.
8960	−1·5	226
3760	+4·2	408
1660	+5·8	370
570	+7·3	526
220	+8·0	625

HALL COEFFICIENT AND RESISTIVITY vs. THICKNESS (294°K)

(iv) after HARRIS AND PIPER

Fig. 14. Hall Coefficient of thin bismuth films as a function of thickness.

temperature between 77°K and 300°K was due to Fritsche et al [6] whose graph is shown in Fig.15. The curve, for a 250 Å film, has been drawn so as to indicate a linear dependance of R_H on temperature below 220°K with a leveling off to a constant value at 300°K. At a temperature lower than 170°K the Hall coefficient became negative. Fritsche may have observed a maximum in their curve had a sufficiently high temperature been employed, as was suggested in the results of Ogrin et al [46] who chose to represent the graphs of R_H against temperature in a normalised form i.e. $R_H/R_{H\,max}$. The curves are basically that of Fritsche with a displacement towards the lower temperature region as the thickness was increased.

Several of the above authors have quoted the values of the Hall coefficient as being the extrapolation of R_H to zero magnetic field i.e. as $R_{H \to o}$ or more often R_{H_o}. The assumption that an extrapolation would result in such a value is felt to be an over-simplification. The fact that the Hall coefficient is so sensitive to the presence of impurities suggests that the perturbation due to the application of a magnetic field is likely to be complex and poses the question as to which of the transport variables gave rise to the effect. Colombani and Huet [47] in a plot of Hall voltage against magnetic field up to 3.5 Tesla showed a monotonic decrease in V_H as the thickness was increased, (Fig.16.). For a film in the region of thickness of 6000 Å it is seen that the Hall voltage changes from negative to positive. (The authors Colombani and Huet have been a little careless in presenting the graphical data. A negative Hall voltage must essentially give rise to a positive coefficient). The graph of Hall coefficient R_H against film thickness showed a maximum at around 700 Å, the value of the coefficient at all thicknesses increasing with decreasing magnetic field.

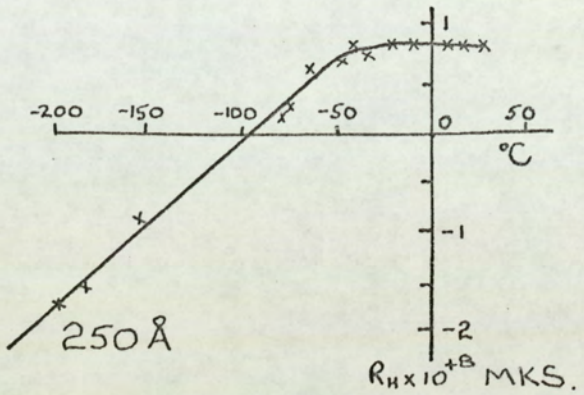

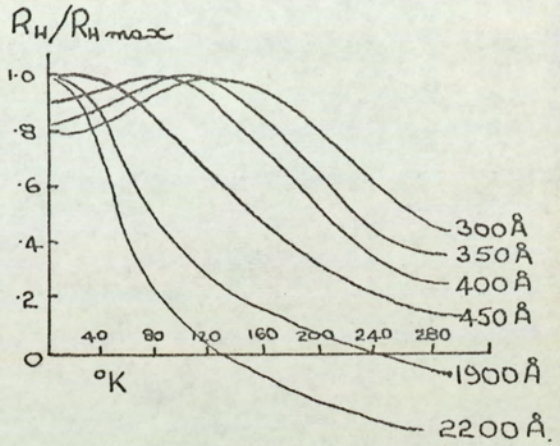

Fig 15(i) after FRITSCHE.

Fig 15(ii) after OGRIN et al.

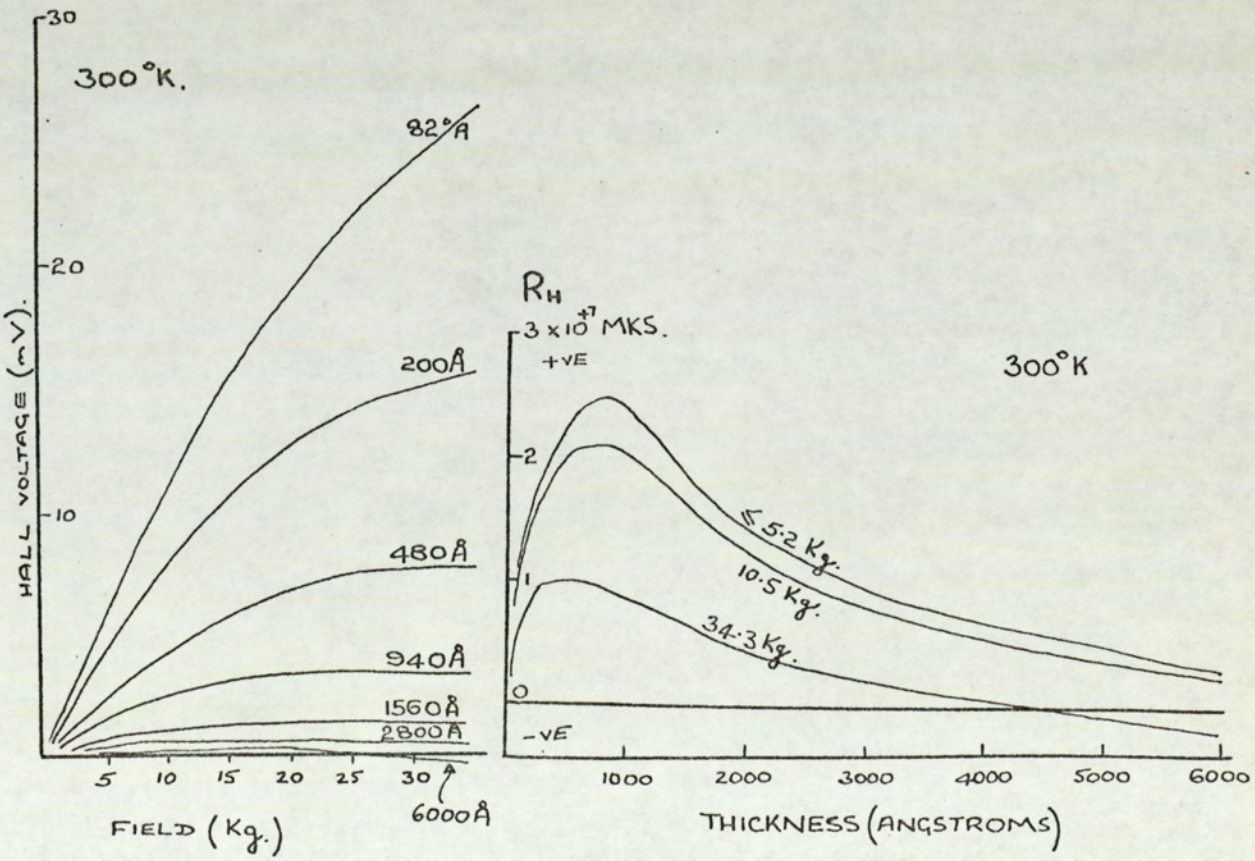

Fig 16(i) after COLOMBANI and HUET Fig 16(ii).

Fig.15 & 16. Hall Coefficient of thin bismuth films.

1.4.5. Crystallite size

The information in the present survey has so far quoted the thickness of a film as though it were a parameter fundamental to the evaluation of transport phenomena. There is however evidence to show that it is not the absolute thickness, but the mean grain size, which determines the electrical properties. The techniques of annealing films, which in general cause the crystallites to coalesce, will result in properties equivalent to those of a film of much greater thickness i.e. the properties will be closer to those of bulk material. The properties of a series of specimens of varying size are controlled directly by the internal crystalline make-up of the specimen. Though it may be deduced from the observations of Kioke (33) that the properties of the thinner films are not readily reproducible, they are by no means anomalous. The explanation of the reproducibility of annealed films stems from the fact that when the mean diameter of the crystallites exceeds about ten times the film thickness, electron scattering from the grain boundaries is superceded by a scattering process in which the accurately defined film thickness is the controlling factor.

Newman and Ko (48) performed experiments on bismuth films thermally evaporated in a vacuum of 10^{-7}mm.Hg. Fig.17 illustrates the plot of conductivity against film thickness, and it is seen that the scattering of the points is rather large. The microstrctures of the films were examined by transmission electron microscopy and a polycrystalline structure was observed. Newman measured the areas of the crystallites by comparing the areas on the micrographs with a series of known circles. A histogram was plotted, and the mode of the distribution taken as the crystallite area. The variance of the distribution was not quoted. A plot of conductivity against mean crystallite diameter resulted in a curve with much reduced scatter. These results seem reasonable if one considers the model of Ivanov and Papov (49) put forward for bulk polycrystalline bismuth. Since

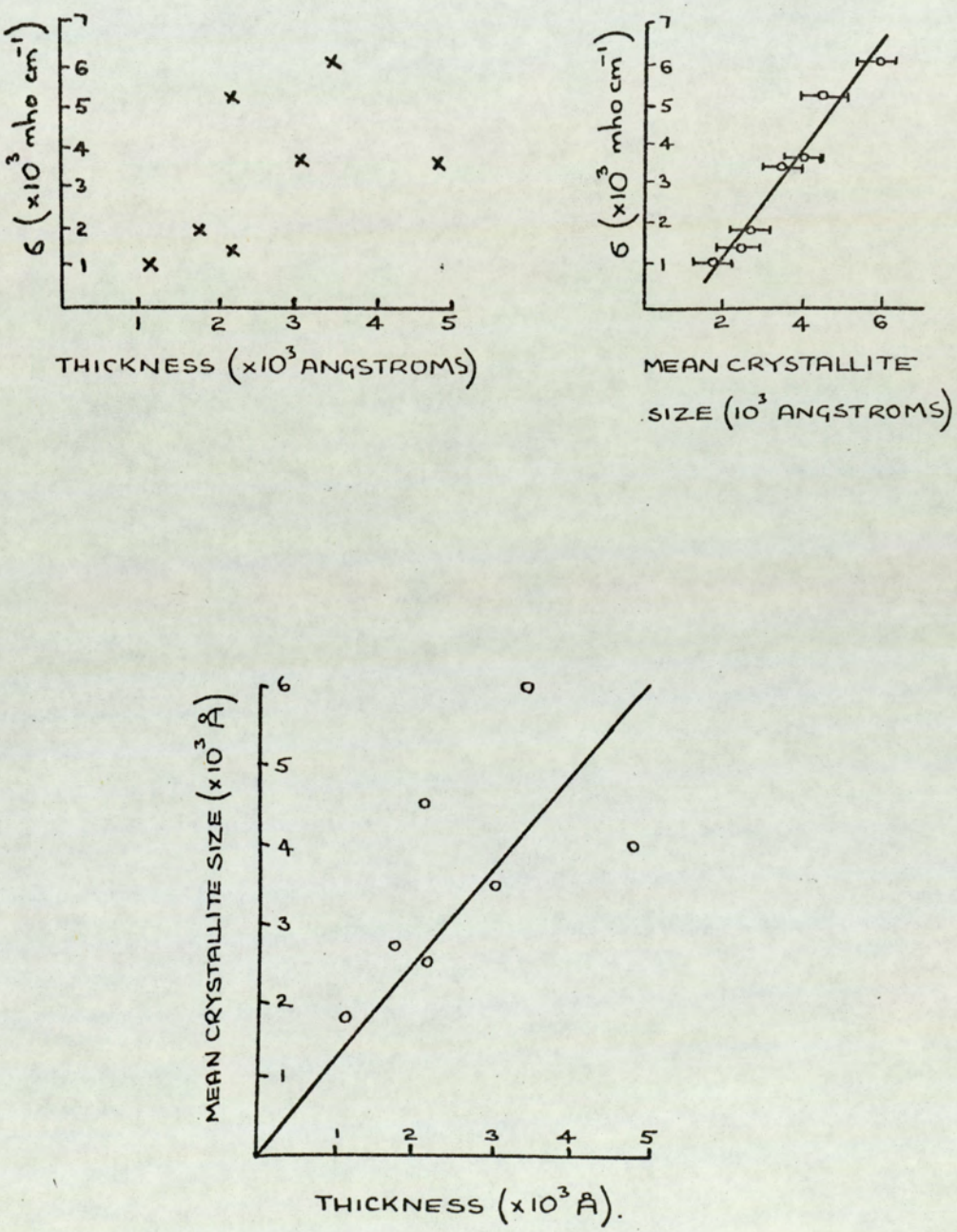

Fig.17. Relationship between film thickness and grain size for bismuth films (after Neuman and Ko).

the mean free path of carriers in bulk single crystal bismuth is of the order of a micron at room temperature [50] whilst the mean crystallite size in polycrystalline bulk specimen is an order of magnitude lower, the effective free path will be somewhat modified by the grain boundaries. It is therefore reasonable to expect that the conductivity will be proportional to the crystallite size. On the other hand, if the conductivity of polycrystalline bulk material is nominally that which one would expect from single crystals, there is an indication that the grain boundary scattering may be partially specular. The results of Newman indicated that the mean crystallite diameter in films exceeded that of the film thickness by approximately 30%.

A similar analysis by Chopra and Bahl [51] on films of copper, silver and gold indicated that for an unspecified film, annealing increased the size of crystallites from 400 Å to 1000 Å with a subsequent reduction in the thickness dependence. Epitaxially grown films exhibited an "as-grown" crystallite size of several microns, and an absence of thickness dependence was observed until the very thin region in which voids in the film provided additional scattering boundaries. Duggal and Rup [52] reported a thickness independent grain size of 1 - 3μ for epitaxially grown bismuth films on hot mica, whilst Harris and Piper [45] measured a grain size of 1000 - 4000 Å (the mode was 2000 Å) for 300 Å and 600 Å bismuth films on Al_2O_3 substrates. These results are in accordance with the observations that epitaxially grown films provide results more readily reproduced.

The most complete analysis of pre- and post- annealing effects was due to Clawson [53] who examined bismuth films on glass substrates before and after melting the films under controlled conditions. Using bismuth of 99.999% purity films were evaporated onto unheated glass substrates in a vacuum better than 10^{-5} torr. Film thicknesses

ranged from 5000 to 63000 Å. Initial attempts to re-crystallise the films resulted in the formation of droplets in the molten state, and it was found necessary to counteract surface tension forces in the molten metal by the formation of an oxide layer on the film surface. The thin oxide layer produced by heating to 200° Celsius at 1 torr for 5 minutes was thin enough not to obscure the structure determination of the re-crystallised film.

The re-crystallised films were shown to have large crystallites of approximately 0.02 x 0.2 mm.(20 x 200μ) compared with the evaporated film grain size diameter of 0.3μ . Fig 18 shows the results obtained for the various galvanomagnetic properties measured, the points 'E' referring to films 'as evaporated' and 'R' to 're-crystallised'. It can be seen that in the case of the resistivity the negative T.C.R. of the evaporated film gives way to a positive T.C.R. after re-crystallisation with values close to the bulk values of Abelés and Meiboom. The basic low field magnetoresistance relationship, $\Delta\rho/\rho_0 = \beta H^2$ was seen to be valid for both physical states of the film though the nitrogen point values of the re-crystallised film were two orders of magnitude larger. A separate graph, not produced by Clawson, shows the variation of the coefficient β . The Hall coefficient of evaporated films is characterised by a change in sign with a reduction in temperature. The re-crystallised films retained a positive coefficient similar to bulk single crystals of this orientation.

Similar observations of the resistivity of thin bismuth films were carried out by Colombani and Huet [47] who annealed films covering a wide range of thicknesses. Fig. 19 summarises the results of annealing on a thin (< 200 Å) and a thicker (> 2000 Å) film. Grain growth in the thicker film irreversabily changed the the temperature coefficient of resistivity from negative to positive,

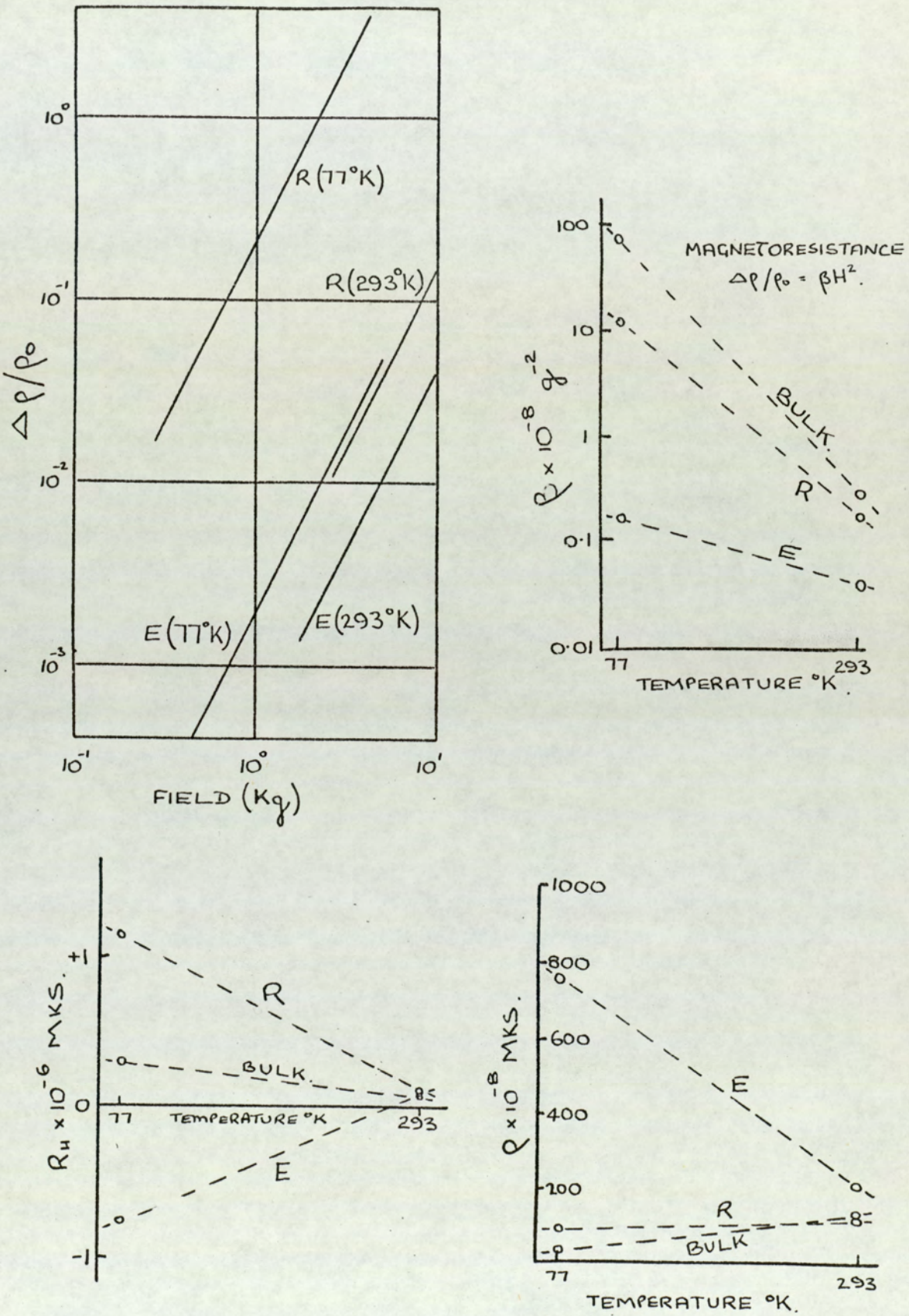

Fig.18. Effect of recrystallisation on the galvanomagnetic properties of bismuth thin films (after Clawson) (dashed lines arbitarily link similar points).

and at the same time reduced the absolute value of the resistivity. This observation is consistant with the appearance of larger grains. The thin film however retained a negative T.C.R. after annealing and displayed enhanced resistivity. The post-nucleation growth process discussed shortly provides a ready explanation in terms of surface mobility of the adatom islands. At 200 Å the film, whilst electrically continuous, consists of a series of irregular islands having many voids, the effective density of which increases as the islands are allowed to take a more circular shape.

The conclusions to be drawn from the combined results of Newman and Ko and of Clawson suggest that the pseudo-anomalous results obtained with evaporated films are in fact small grain effects rather than thin film effects. Only when the grains become large is it true to assume that surface contributes significantly to the conduction processes. Further, in considering the effects of the mean free path of the carriers much useful information may be obtained from one film by varying the temperature so that uncertainties in the

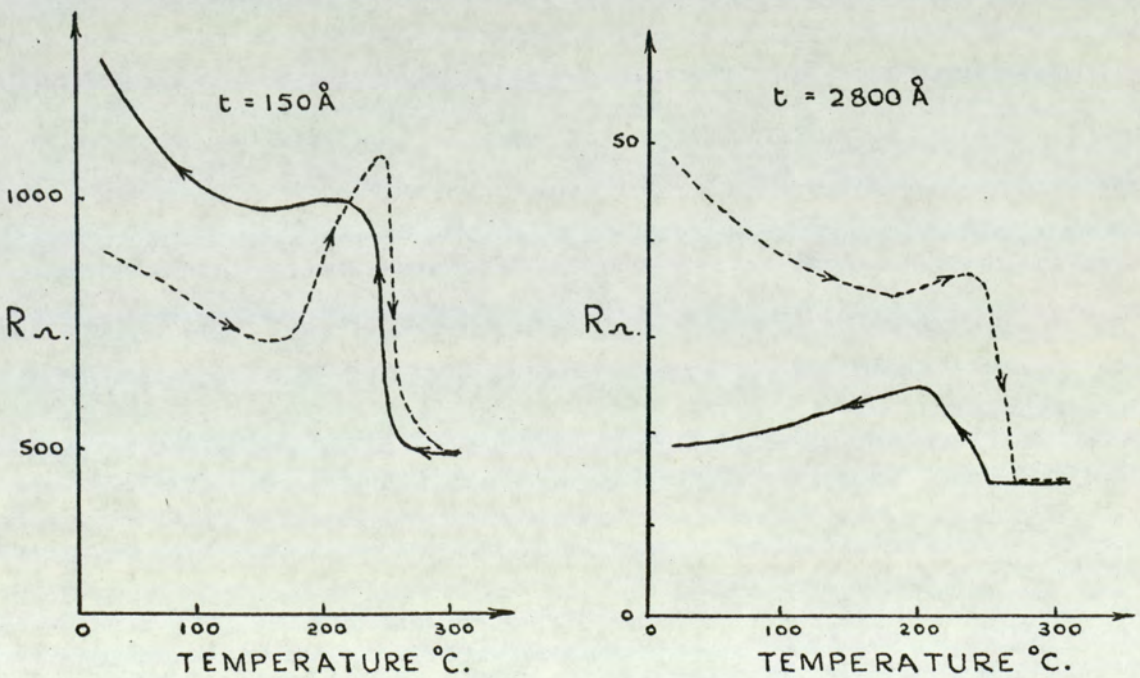

Fig.19. To show the effect on T.C.R. of annealing a thick and thin bismuth film (after Colombani and Huet).

variation of grain size are minimised.

1.4.6. Nucleation and growth processes

A comprehensive analysis of the properties of thin films would be incomplete without an understanding of the fundamental processes occuring in the embryonic stages of specimen preparation. The ever increasing use of films in devices and thin film research dictates that there be a clear understanding of the role of the various parameters in determining the structure, growth and properties of films. A brief review of the nucleation and post-nucleation stages of deposition is outlined.

The basic idea of a condensation process by nucleation was due to Frenkel [54] and has since been the subject for discussion by many authors. According to McCarrol and Ehrlich [55] an adatom arriving at a surface can lose an appreciable amount of kinetic energy by collisions with the host lattice enabling it to condense. Thereafter it moves over the surface of the substrate with its parallel component of velocity. The adatom has a finite lifetime before it re-evaporates. During this time there is a finite possibility of a collision with other vapour atoms to form a nucleus of more than one atom, certain groups having a minimum "surface energy" when in contact with each other. Three atoms triangularily located are known to form such a nucleus and therefore a nucleus of two atoms becomes a "critical cluster" [56] - an adatom will preferentially adhere to such a nucleus. The second critical cluster contains six atoms, as a group of seven consisting of one in the centre and six round its perifery is very stable. It becomes clear that above a certain size of nucleus the surface energy becomes moderately insensitive to the nucleonic size and therefore additional adatoms just tack onto the edges. Recent attempts to explain the condensation mechanism suggest that the process of traversing the surface of the substrate is by a series of hops [57]. At 2000°K an atom has a kinetic energy

of 0.3 eV., and it is possible that it loses some 50% of its energy on each hop. After ten hops the energy is much reduced so that after the average surface lifetime of 10^3 hops the atom can retain no knowledge of its initial energy. Using arguments of this nature one can justify the observation that the nucleation stage of film growth is independent of the kinetic energy of the vapour, i.e. the temperature of the source and hence the rate of evaporation. This is an oversimplification ignoring the following factors,

(i) The rate of arrival of atoms compared with those of residual gas atoms

(ii) The effects of micro-damage to the substrate caused by too large an initial impact energy of an adatom.

(iii) The possibility of 'lumps' of evaporant being ejected by the source.

The energy imparted to a cluster by a sticking atom enables it to possess surface mobility. A high surface mobility enables a nucleus to continually re-arrange itself into a minimum energy shape. The freehand sketches (Fig.20) show the shape of a typical island at various residual pressures when it will be readily

Fig. 20. The relation between residual pressure and surface mobility

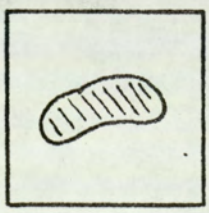

1×10^{-11} torr
smooth island.

1×10^{-9} torr
irregular
perimeter.

10^{-6} torr
poor surface
mobility.

seen that the lower residual pressures produce higher surface mobilities. The surface density of nuclei obviously determines whether adatom joins an established cluster or forms a new one, but basically the post-nucleation growth process concerns the motion of the nuclii themselves. The work of Pashley et al [58] has dealt extensively with this problem. Two adjacant nuclii which enlarge until they touch run together in a form of liquid-like coalescence. A form of mass transfer takes place brought about by surface diffusion. The series of sketches, Fig. 21, are taken from a cinefilm of a film grown in an electron microscope, in which

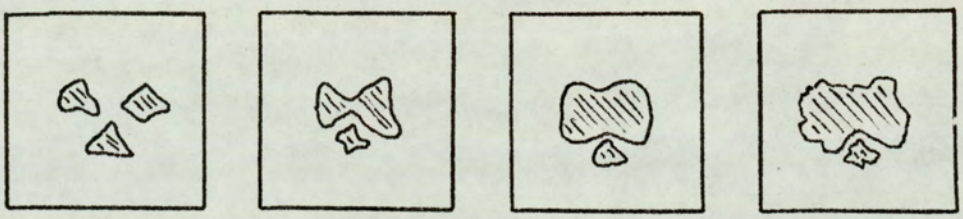

Fig. 21. Coalescence of nuclei.

the evaporant is cut off at a time t = o. No further energy was being supplied to the deposit and thus the coalescence was due only to surface diffusion. In a theoretical treatment of this complex subject Pashley [59] has shown that the force on the biconcave neck formed at coalescence,

Fig. 22. Pictorial model of coalescence

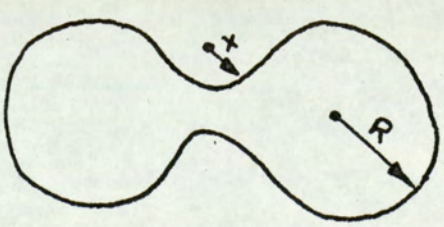

is such that 'r' will tend to increase in a way that is inversely related to the magnitude of 'r'. The rate of coalescence drops with larger nuclei as a result of this. It is fundamental to the condensation process that any parameter which encourages surface mobility and diffusion will lead to enhanced agglomeration. Several are mentioned here,

(i) An increased substrate temperature results in a lower proportion of the adatom energy being shared on each hop.

(ii) The use of an ultrasonically agitated substrate produces the same effects as an elevated substrate temperature [60], but has the advantage of being able to be switched on and off.

(iii) Oblique incidence of the evaporant vapour gives the adatoms an additional velocity component parallel to the plane of the film.

As a result of increased agglomeration the film is more free from strains and dislocations but as is seen from the micrographs of any typical work (Chopra and Randlett [61]) the thickness at which the film becomes electrically continuous is essentially increased. A possible exception to this rule is a film produced in the presence of an electric field or electrostatic charge [62]. The charges cause not only agglomeration, but also a joining together of islands to produce a continuous film having numerous voids. This may be the ultimate source of pinholing in films as reported by Jorgenson [63]. If we consider two small spheres of radii r_1 and r_2 carrying charges q_1 and q_2 separated by a distance d then taking into account image charges the nett force is,

$$F = \frac{q_1 q_2}{d^2} - \frac{q_1^2 r_2 d}{(r_1^2 - d^2)} - \frac{q_2^2 r_1 d}{(r_2^2 - d^2)^2} \qquad (1-9)$$

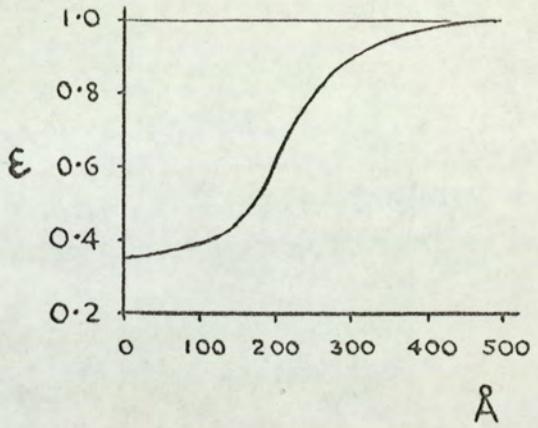

Fig. 23. The sticking coefficient, ε, for gold on rocksalt against deposition thickness (after Chopra)

It is interesting to note that if either charge is much larger than the other, or if the radii are nearly equal to d then the force is attractive irrespective of their sign. To get an idea of the order of magnitude, if $r_1 = 100$ Å, $q_1 = 100$ unit charges, $r_2 = 20$ Å, $q_2 = 1$ unit charge, $d = 200$ Å the attractive force is 10^{-4} dynes. The shear stress on the small particle is 10^{10} dynes cm^{-2} (approximately 10^4 atmos.) and is of a high enough order to qualitatively explain the island coalescence. Chopra concluded that the influence of the applied field was a secondary parameter which served to accelerate the redistribution of charges on coalescence.

As a result of the foregoing discussion a practical point arises in the determination of film thicknesses in the thin limit by inference of the amount of material removed from the source. The possibility of the re-evaporation of an adatom from the substrate surface in the ultrathin region leads to the concept of a sticking coefficient, ε. Fig. 23 shows a typical sticking coefficient curve for gold evaporated on rocksalt single crystals at room temperature and indicates that for films of a final thickness of 400 Angstroms, less than 50% of the incident beam adhered to the substrate.

In the evaporation of deposits onto glass substrates no difference was found by Chopra [64] between the use of pyrex

and soda glass though there is disagreement about the possible use of a final in-situ cleaning procedure prior to the evaporation. Isler and Bullis [65] investigated the effectiveness of both a.c. and d.c. glow discharge over a range of pressures and measured the

Fig. 24. Surface protrusions after ion bombardment (after Stewart and Thompson)

effectiveness in terms of the temperature increment caused by it. Stewart and Thompson [66] on the other hand have analysed the microtopography of materials under ion bombardment by means of a scanning electron microscope. A striking feature of their pictorial results is the presence of conical protrustions sketched in Fig. 24, in which cones with a base diamter of about 4μ were observed. The origin of the cones is attributed to the presence of impurities near the surface which shield the underlying material. Cones were not observed with high purity zone refined materials. Bearing in mind the magnitude of thickness of thin films and the increased boundary length caused by the protrusions one is led to question the advisability of using glow discharge cleaning techniques.

1.4.7. The structure of thin films

The orientation produced in thin films as a function of substrate temperature has been reported by Hopkins and Dobson [67] for a range of materials which did not include bismuth. Table 3 summarises their results. It will be seen that an elevated substrate temperature enhanced the degree of preferred orientation to an extent

	Material	Melting Point °K	Orientations at various substrate temperatures °K				Texture
			Random	Slight	Moderate	Strong	
F.C.C.	Pt	2042	300-450	—	—	—	-
	Ni	1726	300-500	700	—	—	111
	Au	1336	—	300	500	700	111
	Ag	1234	—	300	—	700	111
	Al	933	—	—	300	—	111
	Pb	600	—	—	—	300	111
B.C.C.	W	3653	300-750	—	—	—	-
	Mo	2893	300-750	—	—	—	-
	Fe	1812	300-500	700	—	—	110

Table 3. The relationship between preferred orientation and substrate temperature (after Hopkins and Dobson)

which depended on the melting point of the material. Both F.C.C. and B.C.C. lattices displayed a similar temperature dependence, although the texture was different. Assuming that the observations may be extended to trigonal bismuth, melting points 544.3 ^{o}K [68] a strong orientation should exist at 300 ^{o}K. Hopkins observed no structural difference between evaporations at 1×10^{-6} and 1×10^{-10} torr. A contribution by Wojtczak [69], dealing with the reduction of the melting point of films of a reduced number of atoms normal to the substrate was felt to be insignificant in the present investigation.

A series of investigations of the condensation mechanism of bismuth vapour onto neutral substrates have been performed by Palatnik et al and Komnik et al [70-74]. A polished annular ring heated at one end and cooled at the other resulted in a substrate having a linear variation of temperature. There existed two critical temperatures T_{c_1} and T_{c_2}, $(T_{c_2} > T_{c_1})$, at which distinct changes in the nature of the deposit were observed:-

(i) $T > T_{c_2}$. The adatom energy and surface lifetime are such that no stable nuclei will form and a deposit will not be observed.

(ii) $T < T_{c_1}$. Condensation of the evaporant vapour occurs by sublimation direct from the vapours to the solid phase. In many cases this can lead to a condensate of an homogeneous crystalline aggregate.

(iii) $T_{c_1} < T < T_{c_2}$. An intermediate liquid phase is formed which remains until a drop of some 100 Å builds up at which time the usual liquid - solid transformation occurs. It is believed that this liquid phase enables the nuclei to attain a state of order and thus produce the characteristic crystalline structure with the basal planes parallel to the substrate.

It is thus necessary to obtain a knowledge of the critical condensation temperatures in order to lay down a film displaying a preferred orientation. For all materials these are independent of the crystal structure of the material and depend only on the melting point. T_{C_1} was observed to be 2/3 of the melting point i.e. 366 ^{o}K for bismuth, Whilst T_{C_2} was around the melting point of the material.

Within the liquid phase region Palatnik observed that for condensates thicker than 100 $\overset{o}{A}$ a transformation occured from a two dimensional "colloidal" to a texture produced by recrystallisation processes. For thicker deposits the structure showed the presence of columnar polyhedrons growing from the basically flat surface of the film.

An investigation by Kooy and Nieuwenhuizen [75] described the structural effects in thin films by examining their cross-section in an electron microscope. An aluminium film was traversed by a razor blade in such a way that the atomic layers close to the cut crumbled away to give a true sectional profile. The step was overlayed and the replica removed in the usual way. The series of photographs shown by Kooy illustrate that the aluminium film displayed a columner growth of crystallites extending from the bottom to the top of the film. A distinctive feature of the pictures is the presence of a much finer grain size towards the base

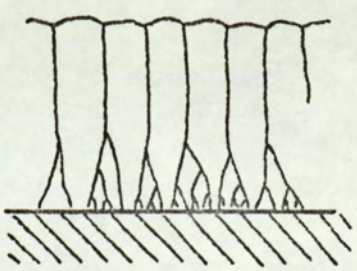

Fig. 25.
Selected grain growth
in aluminium films
(after Kooy et al)

of the film which gives way to a selection process so that the fibre texture of larger grains exists in the bulk of the film (Fig. 25). Kooy observed that the grain size changed from the 50 Å diameter nucleation size to some 5000 Å in the thicker films. Whilst the foregoing analysis referred specifically to aluminium, there are reasonable grounds (as will be shown later) for applying the argument to the growth of bismuth films.

The temperature of the substrate as measured by a thermocouple is generally quoted in reporting thin film observations. However, the heat of condensation of the adatoms, the low thermal capacity of the film and the insulating nature of the substrate lead to the conclusion that the mean temperature of the film may exceed that of the substrate. Observations of Belovs and Wayman [76] and of Namba [77] reported the temperature rise, but differ in the measured size of the effect by more than an order of magnitude. Belovs constructed a set of nickel-gold thermocouples in series and Fig. 26 shows that for substrate temperatures between 100 °K and 400 °K the film temperature exceeded this by 300 - 400 °K.

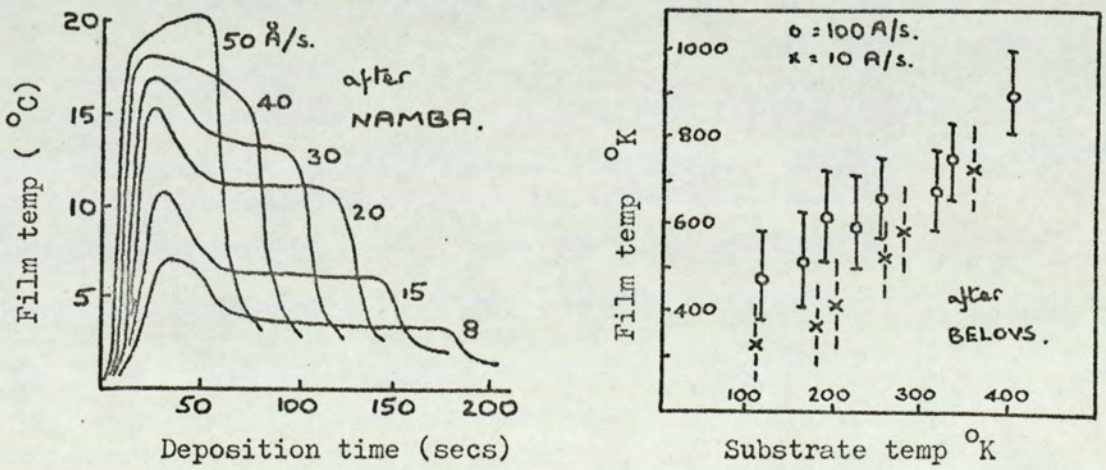

Fig. 26. Film surface temperature during deposition

Namba evaporated a nickel-gold pair of thermocouple arms but left a wide gap between them. During the experiment the evaporation of gold simultaneously formed the thermocouple and

enabled measurements to be made. The maximum temperature rise detained was 20° Celsius (at 50 Å.s.$^{-1}$). The difference between the observations is large and neither method would stand extensive criticism. A way of resolving some of the difficulties would be to resort to the method of Belous, but to sputter onto the thermocouples a thin (250 Å) layer of glass. The thermocouple would then be shielded from the electrical effects of the evaporant and would indicate the temperature of the film only at the intersection of the thermocouple arms. It is expected the the true temperature rise is somewhere between these two values.

1.4.8. Summary

The diversity of values quoted in the literature led to the conclusions that a meaningful analysis of the electrical conducting problems of thin films would only result from the careful control of the deposition variables. The considerations governing the proposed programme are suggested below.

(i) An evaporator was required with which to prepare thin coherent bismuth layers of high purity bounded by smooth parallel surfaces. Films must be capable of being prepared over a range of thicknesses up to several thousand angstroms. A controlled deposition rate was essential and the thickness of the films was required to be measured with high accuracy.

(ii) Bismuth of 99.999 % purity and an evaporation residual pressure of 1 x 10^{-6} mm. Hg. were considered sufficient for specimens in which the galvomagnetic properties were measured external to the evaporator.

(iii) In order to attain a reproducible structure for a given film thickness the evaporations were required to be carried out at a temperature around the lower critical point for bismuth. A heater which raised the

substrate temperature to 60 °K above ambient would suffice.

(iv) For an amorphous substrate, soda glass was chosen and would be subject to the following cleaning procedure. The substrates would be boiled in detergent and distilled water followed by five minutes agitation in an ultrasonic bath. After a distilled water rinse the slides would be boiled in isopropyl alcohol and finally given a vapour clean. It was not proposed to further clean the surfaces in vacuo by ion bombardment.

(v) An attempt would be made to eliminate irreversable changes of resistivity of the films due to self-annealing processes, whilst still retaining the intrinsic "as grown" structure.

(vi) Above all, sets of data at one thickness would be considered for computation only if the entire programme of readings proposed was taken consecutively on one specimen.

It was proposed to examine the resistivity, magneto-resistance and Hall effect of bismuth films of thicknesses up to several thousand Angstroms, in magnetic fields to 12 Kilogauss and at temperatures between 77 °K and 300 °K.

CHAPTER 2

THEORY

2.1. Resistivity

A theory of metallic conduction postulating the existance of a gas of free electrons was first introduced by Drude in 1900. A more detailed analysis of the behaviour of electrons was subsequently made by Lorentz in 1905 who introduced a simplified model for the collisions between electrons and atoms in the lattice. The theory predicted the Wiedemann-Franz relationship connecting the electrical and thermal conductivities, but the assumption of a Maxwell-Boltzmann distribution of velocities later introduced some difficulties when applied to specific heats. With the introduction of quantum mechanics Somerfeld and Pauli in 1928 recalculated the conductivity along the lines of the Lorentz theory, but replaced classical with Fermi-Dirac statistics.

The electrical conductivity σ derived from the Sommerfeld theory is,

$$\sigma = \frac{ne^2\lambda}{mv_F}$$

where n = no. of free electrons per unit volume.

e,m = electronic charge, mass.

λ = mean free path of the electrons

v_F = velocity of an electron at the surface of the Fermi distribution.

It was necessary to assume that λ was of the order of a hundred or so atomic distances at ambient temperatures and that it

increased rapidly with reduction in temperature.

The idea of long mean free paths was difficult to explain on the classical theory, but became more clear following the initial work of Bloch who analysed quantum mechanically the motion of electrons in a crystal lattice. The electrons were regarded as being distributed over a number of energy bands, filling most of them completely. All the electrons were free to move in the crystal lattice, but only those which are contained in incomplete energy bands could contribute to electrical conduction. Such electrons became known as free electrons and their density as the effective number of electrons per unit volume, n_{eff}.

The relationship for the temperature dependence of the electrical conductivity of a metal, after simplifications concerning the interaction between the electrons and the lattice vibrations, was deduced by Wilson [78] as being,

$$\frac{1}{\sigma} = \frac{mv}{ne^2\lambda} + \left[\frac{m}{2}\right]^{\frac{1}{2}} \frac{9\pi h^2 C^2}{8n\Delta eMk\Theta E_F^{3/2}} \left[\frac{T}{\Theta}\right]^5 \int_0^{\frac{\Theta}{T}} \frac{z^5 dz}{(e^z-1)(1-e^{-z})} \quad \ldots (2.2)$$

where k = Boltzmann constant

E_F = Fermi energy

Θ = Debye temperature

M = mass of a lattice atom

Δ = volume of unit cell of the lattice

C = characteristic quantity relating to the electron-phonon interaction and has a value close to the Fermi energy.

The expression is in good agreement with observation and leads to an ideal resistance proportional to T at temperatures above the Debye temperatures and to T^5 at temperatures very much less than the Debye temperature.

The Debye temperature for bismuth has been determined by Keesom and van den Ende [79] by three different methods and their results are summarised as follows;

Method	Θ_D
Sp.Ht. at low temp.	100°K
Electrical conductivity	62°K
Compressibility	110°K

The important conclusion to be drawn from the quantum mechanical theory is that the simple Sommerfeld treatment remains correct within certain limits. In the Sommerfeld theory the electrons are perfectly free and their energy is proportional to the square of the velocity. In multivalent metals however in which the electrons occupy more than one band the model may still be used to give a semi-quantitative picture by letting "n" be the number of free electrons in a band and "m" be an effective mass of the electron written as m^*.

A concept introduced into the Sommerfeld theory is that of a relaxation time τ. If a Fermi-Dirac distribution function f describes a system under the influence of external forces which in equilibrium would be represented by f_o then the rate of approach to equilibrium on removal of the external forces due to the influence of collisions alone is given by

$$\left[\frac{\partial f}{\partial t}\right]_{\text{collisions}} = -\frac{(f-f_o)}{\tau} \quad \ldots \quad (2.3)$$

If v_F is the velocity of the electrons to which τ refers then the corresponding mean free path is defined by

$$\lambda = v_F \tau_F \quad \ldots\ldots\ldots\ldots \quad (2.4)$$

The relaxation time is in general dependent on the energy E of the conduction electrons and can be calculated at temperatures higher than the Debye characteristic temperature Θ_D in terms of a relation due to Wilson, 1953 (80).

$$\tau = \frac{2\hbar}{\sqrt{\tfrac{1}{2} m^*}} \frac{\Lambda}{D} \frac{\Theta_D}{T} E^{3/2} \qquad T > \Theta_D \quad \ldots (2.5)$$

where

$$\Lambda = \left[\frac{4\pi}{3}\right]^{1/3} \frac{4Ma}{3h^2} \frac{k\Theta_D}{C^2} \; ; \qquad D = \frac{(6\pi^2)^{2/3} \hbar^2}{4m^* a^2}$$

k,C,M as in equation (2.2), a = lattice constant.

The contributions to the conductivity are additive for a metal in which the electrons are shared between two bands.

$$\sigma = \frac{n_1 e^2 \tau_1}{m_1^*} + \frac{n_2 e^2 \tau_2}{m_2^*} \quad \ldots\ldots (2.6)$$

In the case of an equal number of electrons and holes as with bismuth equation (2.6) can be reduced to:

$$= n e^2 \left[\frac{\tau_e}{m_e^*} + \frac{\tau_h}{m_h^*}\right] \quad \ldots\ldots\ldots (2.7)$$

In many investigations particularly at higher temperatures it is not possible to obtain direct information to enable either τ_i or m_i^* to be determined separately and it is often convenient to reduce the conductivity term to one containing the carrier mobilility as defined by:

$$\mu_i = \frac{e\tau_i}{m_i^*} \quad \ldots\ldots\ldots (2.8)$$

thus $\sigma = ne(\mu_e + \mu_h) \quad \ldots\ldots\ldots\ldots (2.9)$

In a perfect and rigid lattice there would be no resistance to electron flow, but a finite free path is provided at temperatures above the absolute zero by the thermal vibrations of the lattice. As the temperature is lowered the conductivity will increase, but tends towards a value limited by the static lattice imperfections such as impurity atoms, vacancies and dislocations. Provided the number of static imperfections is small then the contributions to the resistivity may be treated additively as expressed in Matthieson's Rule,

$$\rho_o = \rho_L + \rho_I \quad \ldots\ldots\ldots\ldots\ldots (2.10)$$

ρ_L is the scattering due to lattice vibrations and will be temperature dependent. ρ_I is the contribution of the imperfections and will, neglecting reversible annealing effects, be temperature independent.

The temperature dependence of ρ_L depends on the magnitude of the temperature with respect to the Debye characteristic temperature Θ_D. As ρ_L only fails to be proportional to the absolute temperature at temperatures considerably below Θ_D it would suggest that at a minimum temperature of around the normal boiling point of liquid nitrogen there should be negligible deviation from the linear condition in bismuth. On differentiating (2.10) therefore it follows that the temperature dependence of the measured resistivity is independent of the lattice imperfections and that the coefficient α is constant.

$$\frac{\partial \rho_o}{\partial T} = \frac{\partial \rho_L}{\partial T} = \alpha \quad \ldots\ldots (2.11)$$

By diminishing one, two or even three of the dimensions of a sample to such an extent that the mean free path becomes comparable in magnitude with this dimension, for example the thickness

of a thin film, the resistivity will be increased by the artificial limitation of the mean free path by the boundaries. Such effects are known as 'mean free path effects', or often 'size effects'. In the case of thin films a further term ρ_S can be added to the Matthieson equation representing the contribution to the resistivity of the boundary scattering:

$$\rho_o = \rho_L + \rho_I + \rho_S \quad \ldots\ldots\ldots \quad (2.12)$$

As the temperature is reduced, and thus the mean free path of the carriers increased, the proportion of carriers undergoing boundary scattering increases and temperature dependence of ρ_S is essentially negative

$$\frac{\partial \rho_o}{\partial T} = \frac{\partial \rho_L}{\partial T} + \frac{\partial \rho_S}{\partial T} = \alpha + \alpha' \ldots \quad (2.13)$$

The actual temperature dependence of ρ_S depends on the mechanism of scattering from the surface of the films. The two extreme processes by which surface scattering can take place are as follows:

1) Diffuse scattering as is the more usual case in metals. The free path of a conduction electron is terminated at the surface of the films, the distribution of the electrons leaving the surface being independent of direction. The electron retains no memory of the pre-collision period. By introducing a scattering centre for the electrons at a point earlier than would have been the case in a bulk specimen the effect is such that a reduction in the conductivity results.

2) Specular reflection is the process by which an electron is reflected from the surface of a film in such a way that

the angles of incidence and reflection obey the laws of elementary optics. The path of the electron is not in fact terminated by the boundary, but merely reflected back towards the lattice scattering centres. As a result total specular reflection would, to a first approximation, have no effect on the conductivity of the film and the temperature dependence of ρ_s should be zero. The film resistivity would not display a classical size effect.

An analysis of the conductivity of a thin metallic film in which the scattering was entirely diffuse has been given by Fuchs [81] and was later extended by Sondheimer [82] to cover the case of partially specular reflection. Fuchs postulated that in the size effect there would be a deviation from the equilibrium of the electronic distribution function dependent on the position in the metal. The distribution can be written as:

$$f(\bar{v}, \bar{r}) = f_o(\bar{v}) + f_1(\bar{v},\bar{r}) \quad \ldots\ldots (2.14)$$

where $f_o(\bar{v})$ is the equilibrium distribution and $f_1(\bar{v},\bar{r})$ is the deviation of the distribution from equilibrium. In a thin film of thickness t in which the surfaces form two planes having a common normal and in which the electric field, E_x, is perpendicular to this normal, then the distribution $f(\bar{v},\bar{r})$ must be independent of the x ,y - directions. The function reduces to $f(\bar{v},z)$. The effective film conductivity in the x - direction as derived by Fuchs and quoted in standard texts [82] is given by:

$$\sigma = \sigma_o \left[1 - \frac{3}{2t} \int_0^{\frac{\pi}{2}} \sin^3\theta \cos\theta \left\{ 1 - \exp\left(- \frac{t}{\lambda \cos\theta}\right)\right\} d\theta \right] \quad \ldots (2.15)$$

σ_o = conductivity in the bulk material

λ = bulk mean free path at the surface of the Fermi distribution.

A convenient parameter of use in the evaluation of size effect problems is that of the ratio of the film thickness to bulk mean free path,

$$k = \frac{t}{\lambda} \qquad \ldots\ldots\ldots\ldots (2.16)$$

Equation (2.15) may be more usefully be written in terms of k and it is usual to express this as the ratio of the film to bulk resistivity:

$$\frac{\rho}{\rho_o} = \frac{\sigma_o}{\sigma} = \frac{\Phi(k)}{k} \qquad \ldots\ldots\ldots\ldots (2.17)$$

where,

$$\frac{1}{\Phi(k)} = \frac{1}{k} - \frac{3}{8k^2} + \frac{3}{2k^2}\int_1^\infty \left(\frac{1}{a^3} - \frac{1}{a^5}\right) e^{-ka}\, da \qquad (2.18)$$

In the limiting form if k is large (thick films),

$$\frac{\rho}{\rho_o} = 1 + \frac{3}{8K} \qquad (k \gg 1) \qquad \ldots\ldots\ldots (2.19)$$

and for very thin films,

$$\frac{\rho}{\rho_o} = \frac{4}{3K \log \frac{1}{k}} \qquad (k \ll 1) \qquad \ldots\ldots\ldots (2.20)$$

A somewhat more general theory by Sondheimer was derived in which a fraction p of the electrons is scattered elastically at the surface with a reversal of the velocity component v_2 whilst the rest are scattered diffusely with complete loss of their drift velocity. The specular reflection coefficient p was assumed

constant and independent of the direction of motion of the electrons. The resistivity was evaluated as before and resulted in a slightly different expression for the Φ-function:

$$\frac{1}{\Phi_p^{(k)}} = \frac{1}{k} - \frac{3}{2k^2}(1-p)\int_1^\infty \left(\frac{1}{a^3} - \frac{1}{a^5}\right)\frac{1 - e^{-ka}}{1 - pe^{-ka}}\,da \qquad (2.21)$$

from which is derived the approximations,

$$\frac{\rho}{\rho_o} = \frac{1}{k} + \frac{3}{8k}(1-p) \text{ - - - - - } (k \gg 1) \ldots . \qquad (2.22)$$

$$\frac{\rho}{\rho_o} = \frac{4}{3}\frac{(1-p)}{(1+p)}\frac{1}{k \log 1/k} \text{ - - - - } (k \ll 1) \ldots \qquad (2.23)$$

As a result of the approximations applied in the derivation of (2.23) the equation can be used only in the region where $(1-p) > k$.

Table 4 shows values of the ratio ρ/ρ_o for diffuse and partially diffuse scattering for various values of k.

Table 4. ρ/ρ_o for various k

k, $\frac{\text{thickness}}{\text{mean free path}}$	ρ/ρ_o	
	p = o	p = ½
0.001	182	73.5
0.01	26.5	11.8
0.1	4.72	2.62
1	1.462	1.206
10	1.039	1.019
100	1.004	1.002

A neat treatment given recently by Cottey [83] assumed that in the case of materials of the bismuth type whose surface

specular coefficient is higher than about 0.8, the effective path of the electrons could be separated into two isolated components. It was then only necessary to consider the contribution to the conductivity caused by those few carriers which were scattered at

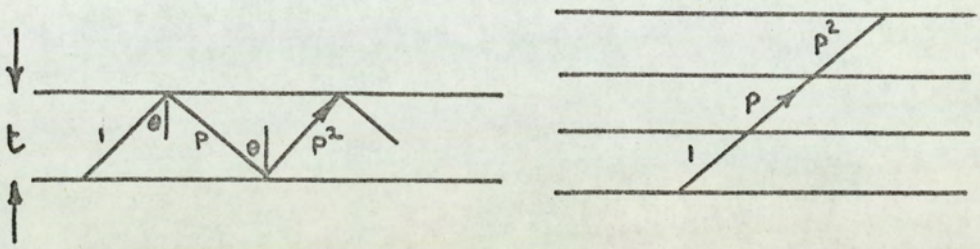

Fig. 27. Layer model of a thin film (after Cottey).

the boundary. Fig. 27 shows Cottey's layer model in which the number of electrons unscattered after a time t falls off as an infinite geometric progression. By writing:

$$p\left[\frac{l}{t/\cos\theta}\right] = \exp\left[-\lambda_s(\theta)\, l\right]$$

one can obtain an overall mean free path of:

$$\frac{1}{\lambda_F} = \frac{1}{\lambda_S(\theta)} + \frac{1}{\lambda_{bulk}}$$

Substituting λ_F in the equations normally associated with bulk derivations leads to the results of equations (2.19) and (2.20).

The units of resistivity employed in the present work will be the S.I. unit of Ω - M with use of the subdivision, $\mu\Omega$-M.

2.2. Galvomagnetic properties

2.2.1. Introduction

The existence of the Hall effect in a material is a direct manifestation of the action of the Lorentz force on a moving charged carrier in a magnetic field. It is a powerful tool for studying the electronic properties of metals and semi-conductors in that it is available for experimental observations at any temperature. A carrier is deflected in the crossed electric and magnetic fields until in a finite specimen a charge builds up along its edges to supress the deflection of further carriers.

The quantitative Hall expressions are quite straight forward in a conventional metal in which there are usually free conduction electrons, whose energies are all around the Fermi energy and whose energy surfaces are spherical. Further simplifications occur if the applied magnetic field is small so that the tangent of the angle of deflection, Θ , of a carrier may be approximated to Θ.

Under the influence of an equilibrium Hall field the path of an electron in metallic conduction is unmodified as the Hall field exactly balances the Lorentz force. No change in conductivity should occur, and indeed no magnetoresistance effect is observed in most simple metals. In the case of a two-carrier system however the Hall field is able to counteract only carriers whose velocity arises from the mean of the electron and hole mobilities. In general the Lorentz force will exceed the Hall field for one set of carriers, and be less than the Hall field for the other set. Though the resultant transverse current is still zero, the change from the equilibrium distribution results in an increased resistivity, and gives rise to the magnetoresistance effect. An analysis of the problem in bismuth is complicated by the

existence of elliptical Fermi-surfaces, a strong anisotropy and a polycrystalline structure. Careful specimen control was shown to remove some of the anisotropy and a theory is developed which is in reasonable agreement with the experimental observations.

In the following treatment, rectangular Cartesian co-ordinates will be used in which the applied electric field, E_x, lies along the x-axis and the applied magnetic field, B_z, along the z-axis. The Hall field, E_y, is developed along the y-axis.

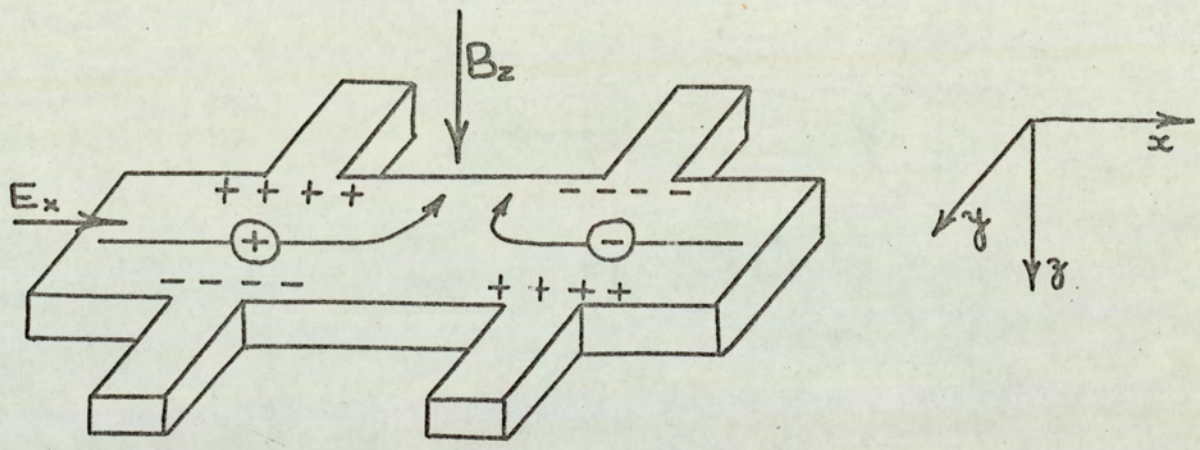

Fig. 28. The Lorentz force on electrons and holes.

The Lorentz equation for a particle of charge + e travelling along the x-positive axis is given by:

$$F = e\left[E_x + v \wedge B_z\right] \quad \ldots\ldots (2.24)$$

The deflection of carriers of two types are shown in Fig. 28 in which electrons and holes are deflected to the same side of the specimen. The force exerted on a hole is observed to be in a direction opposing the Hall field and thus E_y is

negative. A positive value of E_y arises for electrons in which the deflection is along the Hall field.

2.2.2. Magnetoresistance

The theory of the magnetoresistance in bismuth may be developed for any magnitude of magnetic field by the solution of the equations of motion of an electron. The equations arise from the perpendicular components of the Lorentz equation. The trajectories will be averaged over all possible collision times to obtain two orthogonal components of the electric current. Under the influence of the Hall field the Hall current is reduced to zero from which the expression for the conductivity in the presence of a magnetic field may be deduced. This will then be extended to cover the two carrier case. An expression for the ratio of the increase in resistivity to that of the zero field resistivity will be developed.

The orthogonal components of the acceleration of an electron under the influence of the Lorentz force with applied fields as in Fig. 28, are given by:

$$\begin{aligned} m_e^* \dot{v}_x &= -eE_x - ev_y B_z \\ m_e^* \dot{v}_y &= -eE_y + ev_x B_z \end{aligned} \qquad \ldots\ldots\ldots \quad (2.25)$$

Introducing the cyloctron frequency ω defined by:

$$\omega = \frac{eB}{m_e^*}$$

results in the expressions:

$$\begin{aligned} \dot{v}_x &= -(e/m_e^*) E_x - \omega v_y \\ \dot{v}_y &= -(e/m_e^*) E_y + \omega v_x \end{aligned} \qquad \ldots\ldots\ldots \quad (2.26)$$

These are the well-known equations for the motion of electrons in crossed electric and magnetic fields. A convenient solution arises out of the use of the complex variables $Z=v_x+iv_y$ and $z = x + iy$ and so equation (2.26) may be written in the form:

$$\dot{Z} - i\omega Z = - (e/m_e^*)(E_x + iE_y) \quad \ldots\ldots\ldots \quad (2.27)$$

The general solution of the equation is:

$$Z = Z_o + (e/m_e^*)(E_x + iE_y)(1 - e^{i\omega t}) / i\omega$$

where $Z_o = v_{xo} + iv_{yo}$ and is the isotropic distribution of velocities at $t = o$. Averaging the value of Z over all possible collision times and putting $\bar{Z}_o = 0$, results in an expression for the complex mean velocity,

$$\bar{Z} = \bar{v}_x + i\bar{v}_y = \frac{1}{\tau} \int_o^\infty Z \exp(-t/\tau)\, dt \quad \ldots\ldots \quad (2.28)$$

$$= (-e/m_e^*)(E_x + E_y)\tau/(1 - i\omega\tau) \quad \ldots\ldots\ldots\ldots \quad (2.29)$$

Taking the real and imaginary parts of (2.29) and substituting $J_j = - ne\bar{v}_j$ we obtain two perpendicular components of the electron current:

$$J_x = \frac{ne^2}{m_e^*}\left[\frac{\tau E_x}{1+\omega^2\tau^2} - \frac{\omega\tau^2 E_y}{1+\omega^2\tau^2}\right] \ldots\ldots \quad (2.30)$$

$$J_y = \frac{ne^2}{m_e^*}\left[\frac{\tau E_y}{1+\omega^2\tau^2} + \frac{\omega\tau^2 E_x}{1+\omega^2\tau^2}\right] \ldots\ldots \quad (2.31)$$

The Hall field results in the supression of J_y to zero, under which condition it can be seen that:

$$E_y/E_x = -\omega\tau \quad (= \mu B = \phi) \quad \ldots\ldots\ldots \quad (2.32)$$

Substituting into the numerator of (2.30) and re-arranging gives the conductivity in the presence of a magnetic field for a one carrier system as:

$$\sigma_H = \frac{J_x}{E_x} = \frac{\frac{ne^2\gamma}{m_e^*}}{1 + \phi_e^2} \left[1 + \left(\frac{E_y}{E_x} \right)^2 \right]$$

$$= \frac{\sigma_e}{1 + \phi_e^2} \left[1 + \left(\frac{E_y}{E_x} \right)^2 \right] \quad \ldots\ldots (2.33)$$

For one carrier this is just the ordinary zero field expression, and verifies that the magnetoresistance is zero. The addition of a similar term relating to hole conduction results in current components of:

$$J_x = (A_e + A_h) E_x - (C_e + C_h) E_y \quad \ldots\ldots\ldots (2.34)$$

$$J_y = (A_e + A_h) E_y + (C_e + C_h) E_x \quad \ldots\ldots\ldots (2.35)$$

where A and C are the appropriate constant terms of equation (2.30). The overall conductivity for equal numbers of electrons and holes is given by:

$$\sigma_H = \left[\frac{\sigma_e}{(1 + \phi_e^2)} + \frac{\sigma_h}{(1 + \phi_h^2)} \right] \left[1 + \left(\frac{E_y}{E_x} \right)^2 \right] \quad (2.36)$$

which will not in general reduce to the zero field expression. A similar re-arrangement of (2.31) results in an expression for the Hall field of:

$$\frac{E_y}{E_x} = \frac{\dfrac{n_h \phi_h^2}{1+\phi_h^2} - \dfrac{n_e \phi_e^2}{1+\phi_e^2}}{\dfrac{n_h \phi_h}{1+\phi_h^2} + \dfrac{n_e \phi_e}{1+\phi_e^2}} = \frac{\phi_h - \phi_e}{1 + \phi_h \phi_e} \quad \ldots (2.37)$$

The magnetoresistance ratio is given by the expression,

$$\frac{\Delta\rho}{\rho} = \frac{\rho_H - \rho_0}{\rho_0} = \frac{\sigma_0}{\sigma_H} - 1$$

Substituting equation (2.37) into equation (2.36) gives the ratio as:

$$\frac{\Delta\rho}{\rho} = \frac{\sigma_h + \sigma_e}{\left[\dfrac{\sigma_h}{1+\phi_h^2} \dfrac{\sigma_e}{1+\phi_e^2}\right]\left[1+\dfrac{(\phi_h - \phi_e)^2}{(1+\phi_h\phi_e)^2}\right]} - 1 \quad (2.38)$$

Expansion and re-arrangement of terms, and substituting the transformation:

$$\sigma_i = n e \mu_i = \frac{ne\phi_i}{B_z}$$

enables the expression to be reduced without approximation to:

$$\frac{\Delta\rho}{\rho} = \phi_h \phi_e = \mu_h \mu_e B_z^2$$

In diamagnetic bismuth the relative permeability, μ_r, is only a few parts in 10^4 less than unity, and thus for calculation purposes free interchange between B, the magnetic flux and H, the field is permissable. The magnetoresistance coefficient, traditionally quoted as B, is defined as:

$$B = \mu_h \mu_e = \frac{\Delta\rho}{\rho H^2} \quad \ldots\ldots\ldots\ldots \quad (2.39)$$

and has units of inverse square field, $(W/M^2)^{-2}$.

In the following chapters, to avoid ambiguity, the symbol B will be reserved for the magnetoresistance coefficient whilst H is used for the magnetic field strength.

Many problems are associated with a theory of thin film magnetoresistance when derived specifically for simple metals. A consideration of the variables of thickness, magnetic field, grain size, multiple energy bands and specular reflectivity make even the most approximate of analyses unsuitable for bismuth films. It is possible for simple monovalent metal films to display a thin film effect even though no magnetoresistance exists in the bulk material. As discussed by Sondheimer[82] it is not immediately obvious by simple physical arguments how the presence of a magnetic field affects the film conductivity at all in this case. An effect is predicted however by a formal analysis using the generalised solutions of the Boltzmann equation in crossed fields. A solution identical to equations 2.18 and 2.21 are obtained for the cases of diffuse and partially specular reflection, but in which Φ is a function of a complex variable, s,

$$\frac{\sigma_o}{\sigma_H} = \frac{\Phi(s)}{k} \quad \ldots\ldots\ldots\ldots \quad (2.40)$$

where $s = k + i\beta$

β is a further dimensionless quantity t/r_o where r_o is the cyclotron radius of the carrier. $k = t/\lambda$ as before. The graph of σ_o/σ_H against β shows a curve which is oscillatory in β for values of β around unity, but having a monotonic component independent of β. The value of the predicted magnetoresistance effect increases with decrease in k. It is felt that the theory

as presented is so far removed from that which could be applied directly to bismuth films, that further discussion at this stage would not add to the qualitative picture.

2.2.3. Hall Coefficient

The Hall expression for a two carrier system may be developed by considering the transverse field developed in the presence of crossed electron and magnetic fields. The Hall coefficient is defined by the relationship:

$$R_H = \frac{E_y}{J_x B_z} \quad \ldots\ldots\ldots\ldots\ldots\ldots (2.41)$$

where E_y = transverse electric field

J_x = longitudinal current

B_z = magnetic induction.

The transverse currents arising from the action of the Lorentz force on both holes and electrons are given by:

$$J_e = \sigma_e \left[E_y + v_e \wedge B \right] \quad \ldots\ldots\ldots (2.42)$$

$$J_h = \sigma_h \left[E_y - v_h \wedge B \right] \quad \ldots\ldots\ldots (2.43)$$

The resultant transverse current is the sum of the two components:

$$J_y = J_e + J_h = \sigma_e \left[E_y + v_e \times B_z \right] + \sigma_h \left[E_y - v_h \times B_z \right] \ldots (2.44)$$

In the presence of an equilibrium Hall field, equation 2.44 becomes zero, and thus on dividing throughout by $B_z J_x$:

$$0 = \sigma_h \left[\frac{E_y}{B_z J_x} - \frac{v_h}{J_x} \right] + \sigma_e \left[\frac{E_y}{B_z J_x} + \frac{v_e}{J_x} \right]$$

$$= \sigma_h \left[R_H - \frac{v_h}{J_x} \right] + \sigma_e \left[R_H + \frac{v_e}{J_x} \right] \ldots\ldots (2.45)$$

Under the transformation $v_i = E_x e \tau_i / m_i^*$ and putting $J_x = (\sigma_e + \sigma_h) E_x$ equation 2.45 can be re-arranged to produce the expession:

$$R_H = e \left[\frac{\tau_h \sigma_h / M_h^* - \tau_e \sigma_e / M_e^*}{(\sigma_h + \sigma_e)^2} \right]$$

Introducing $\sigma_i = ne\mu_i$, and allowing for equal numbers of electrons and holes, the Hall coefficient in terms of the electron and hole mobilities is:

$$R_H = \frac{1}{Ne} \left[\frac{\mu_h - \mu_e}{\mu_h + \mu_e} \right] \quad \ldots\ldots\ldots\ldots (2.46)$$

The units of R_H taken from equation 2.41 and derived from the measured quantities of E in volts per metre, J in amperes per metre^2 and magnetic induction in webers per metre^2 result in an S.I. unit of metre^3/coulomb. Few quantities in common use are quoted in such a multiplicity of units as is the Hall coefficient, and justifies a brief mention at this stage to allow comparison with other authors. Apart from the S.I. system, the two more common units in the literature are those of cm^3/coulomb (S.I. x 10^6) and volt-cm/ampere-gauss (S.I. x 10^{-2}). The c.g.s. unit is infrequently quoted, possibly due to the practical nature of the Hall experiment.

As with the magnetoresistance size effect, the corresponding Hall size effect derivation is unlikely to be anything more than qualitatively applicable to bismuth films. In the idealised case presented previously it can be shown that the Hall size effect arises from the imaginary part of the Boltzmann solution, namely:

$$\frac{R_H}{R_{HO}} = \oint \left\{ \frac{\Phi(S)}{\beta} \right\} \quad \ldots\ldots\ldots\ldots (2.42)$$

Few approximations are available for equation 2.42.

For very thin films ($K \ll 1$)

$$\frac{R_H}{R_{HO}} = \frac{4}{3} \quad \frac{1 - P}{1 + P} \quad \frac{1}{K\left\{\log(1/K)\right\}^2} \quad \ldots \quad (2.43)$$

The film value is always greater than that of bulk material but the ratio tends slowly to unity with an increase in P or K.

Again, further pursuit of this idealised model is unprofitable at this stage.

2.2.4. Inter-relationship between the galvomagnetic coefficients

The expressions developed for the Hall and magnetoresistance coefficients are not totally complete as will be shown later. It is known that the magnetic field changes the effective number of carriers. However, within the limits of the deviation an inter-relationship between the two coefficients exists which enables metals for which $n_e = n_h$ (Bi, Zn, Be etc.) to be uniquely separated from those in which there is an inequality (In, Al). In bismuth it can be seen from equation (2.37) that in weak magnetic fields ($\phi \ll 1$) that the Hall field is proportional to H whilst the magnetoresistance varies on the square of the field. The Hall coefficient is thus constant. In strong fields ($\phi \gg 1$) the Hall field becomes proportional to H^{-1} resulting in an ultimate saturation value. The magnetoresistance ratio continues to increase without limit.

For $n_e \neq n_h$ there is little difference in the low field behaviour but at high fields equation (2.37) results in a Hall field proportional to H with unlimited growth, whereas the magnetoresistance ratio tends to a limiting value. A resumé of observations on the classification of metals by this means is given by Borovik[10].

2.3. Simultaneous solution of the coefficients of ϱ, B, R_H

Expressions, in terms of the effective number of carriers

and the separate mobilities of electrons and holes, have been derived for the coefficients of resistivity, magnetoresistance and Hall effect. They may be summarised as:

$$\rho = \frac{1}{Ne(\mu_h + \mu_e)} \quad \ldots\ldots\ldots\ldots \quad (2.9)$$

$$B = \mu_e \mu_h \quad \ldots\ldots\ldots\ldots \quad (2.39)$$

$$R_H = \frac{1}{N e} \left[\frac{\mu_h - \mu_e}{\mu_h + \mu_e}\right] \quad \ldots\ldots\ldots \quad (2.46)$$

In order to solve the three equations separately for the unknown quantities a series of assumptions are required:

(i) that the Hall mobilities do not differ significantly from those arising in the conductivity expression

(ii) that the mobilities are invariant to changes in the magnetic field

(iii) that the change in the number of carriers in the magnetic field is capable of separate elimination prior to obtaining a solution.

A re-arrangement of the equations results in the expressions for the effective number of carriers N, and the hole and electron mobilities:

$$N = \frac{1}{e\sqrt{R_H^2 + 4B\rho^2}}$$

$$\mu_h = \frac{1}{2\rho}\left[\sqrt{R_H^2 + 4B\rho^2} + R_H\right] \quad \ldots\ldots\ldots (2.46)$$

$$\mu_e = \frac{1}{2\rho}\left[\sqrt{R_H^2 + 4B\rho^2} - R_H\right]$$

To assess the sensitivity of the parameters to variations of the coefficients, and to obtain an order of magnitude, a typical

set of readings taken on a film of 504 ^{o}A at 290 ^{o}K is analysed.

$$B = 5.184 \times 10^{-3}\ M^{4}W^{-2}$$
$$\rho = 4.66 \times 10^{-6}\ \Omega\text{-M}$$
$$R_H = +0.854 \times 10^{-7}\ M^{3}C^{-1}$$
$$e = 1.6 \times 10^{-19}\ C$$

$$\therefore N = 9.24 \times 10^{24}\ M^{-3}$$

A comparison of this figure with the number of atoms per cubic metre of 2.825×10^{28} gives a ratio of 3.25×10^{-4}, a figure which is within the limits of values reported in the literature.

$$\mu_h = 8.22 \times 10^{-2}\ M^{2}W^{-1}$$
$$\mu_e = 6.39 \times 10^{-2}\ M^{2}W^{-1}$$

It is observed that R_H^2 is very much less than $4B\rho^2$ and thus the sensitivity of N to errors in the three coefficients is such that it is inversely proportional to both ρ and $B^{1/2}$. The value of the mobility is however sensitive only to $B^{1/2}$. This reliance of the parameters on the magnetoresistance coefficient is somewhat disadvantageous as this is the least accurate of the measured quantities.

2.4. The origins of quantum oscillations in bismuth films

2.4.1. Introduction

The quantum size effect is defined as the dependence of the electrical properties of solids on their characteristic geometric dimensions and arises when the latter become comparable with the de-Broglie wavelength of the carriers. In bulk material the separation of the lower energy levels is small, about 10^{-6} eV, and thus the distribution of carrier energies becomes continuous for most practical purposes. The Eigen values of the carrier energy are, however, an inverse function of the

specimen size and thus for a polycrystalline thin film the separation of the energy levels may be sufficient to produce a perturbing effect on the electrical properties. It is further known that bismuth thin films display semi-conductor properties at very small thicknesses which could only arise by a modification of the band structure.

The de-Broglie wavelength of electrons is long and the momentum small compared with similar properties of X-rays. Though the resulting diffraction from crystal planes becomes insignificant, diffraction from both geometrical and grain boundaries is however possible. It is only in semi-metal films, in which the effective masses are usually small, that the minimum physical dimensions required to observe electron diffraction can be obtained in a film which is electrically continuous. A picture develops of a semi-metal film in which the film and grain boundaries form a "super-lattice" whose dimensions are comparable with the wavelength of the carriers.

The theory of the quantum size effect may be developed in terms of the modifications to the available energy levels of the carriers resulting from the small dimensions. These arise out of solutions of the Schröedinger equation. The fact that the conduction is along the large dimension of the specimen is of no consequence as the conduction direction defines only the direction of the Bloch wave. The overall conduction picture is one of crossed waves travelling in a wave guide.

2.4.2. Wave mechanical basis for a quantum size effect.

A wave mechanical treatment of the properties of a material as complex as bismuth must eventually be undertaken in the presence of many simplifying assumptions. The present elementary treatment assumes that the electrons and holes are independent 'particles' moving within the confines of a flat bottomed potential wall with infinite walls. It is further assumed that the effective masses of the carriers are independent of the size of the specimen.

Consider the time-independent Schröedinger wave equation

for an electron in a conservative system:

$$\nabla^2\psi + \frac{2m}{\hbar^2}(E-V)\psi = 0$$

If the film is considered to be large in the y- and z-directions and have a thickness 'a' along the x-direction, then for the case of electrons the normalized wave functions are given by:

$$\psi = \left[\frac{8}{aL_yL_z}\right]^{\frac{1}{2}} \sin\frac{n\pi x}{a} \exp\left[\frac{2\pi i n_y}{L_y} + \frac{2\pi i n_z}{L_z}\right] \quad \ldots\ldots \quad (2.47)$$

where L_y and L_z are the lengths of the sides of the normalisation rectangle, n = 1,2,3 .....

The Eigen-values of the energy spectrum are given by:

$$E_n = \frac{\hbar^2\pi^2 n^2}{2m_e a^2} + \frac{\hbar^2\pi^2}{2m_e}\left[\left(\frac{2n_y}{L_y}\right)^2 + \left(\frac{2n_z}{L_z}\right)^2\right] \quad \ldots \quad (2.48)$$

For a film of large area the second term of equation 2.48 becomes insignificant and thus the quantized energy levels are given by:

$$E_n = \frac{\hbar^2\pi^2 n^2}{2m_e a^2} \quad \ldots\ldots\ldots\ldots \quad (2.49)$$

The effect of a reduction in one of the principal dimensions has thus been to quantize the available energy levels of the electrons or holes. As will be discussed in section 6.7 the low carrier density in bismuth resulted in a small number of these sub-bands being populated and thus the conduction carriers exist within close proximity to the Fermi level and have energies close to E_F. Conduction will therefore be important under the conditons such that the Fermi-energy corresponds to an energy level permitted by the Eigen-values of the Schröedinger equation. Equation 2.49 was solved therefore under the assumption of the following values; E_F = 0.022 eV, the value determined by Weiner [20] and an effective electronic mass $m_e = 0.01\ m_o$, Kao [21]:

$$\frac{a}{n} = 413\ \text{Å} \quad \ldots\ldots\ldots \quad (2.50)$$

The only available energy level for which conduction can readily take place is fixed at the Fermi energy. As the thickness varies Eigen-functions of equation 2.47 are satisfied whenever $a/n = 413$ Å, i.e. multiples of 413 Å as the quantum number, n, increases discretely. Fig. 29 illustrates the practical significance of the effect in terms of the resultant standing waves. Whilst solutions are available for

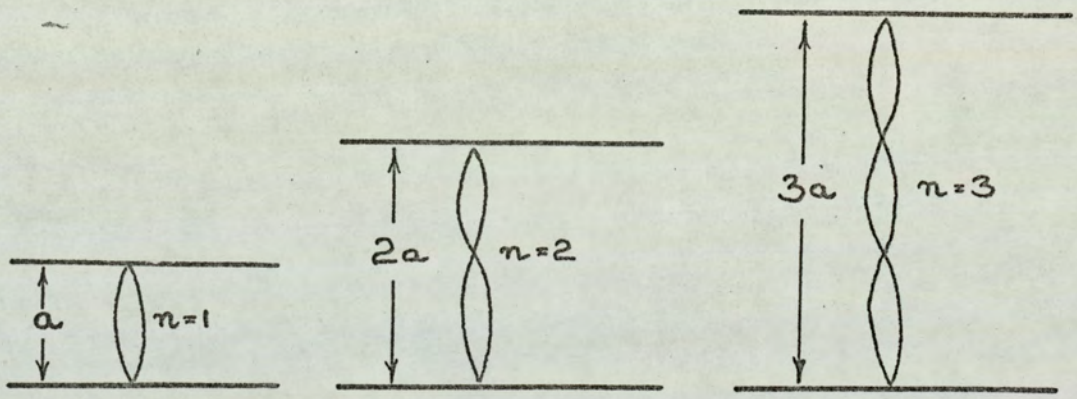

Fig. 29. Standing waves of the conduction electrons in a thin film.

all thicknesses it is those for which this critical thickness occurs that are of interest in the present work. Under the conditions of standing waves the impedance of the film is ideally infinite and thus a minimum in the conductivity arises. The practical shape of the experimental curve is however expected to be more of a sinusoidal nature due to the influence of kT vibrations within the carrier sub-band.

The above derivation was calculated for electrons whereas a significant contribution in the thin film limit arises from holes. A far heavier mass of $0.15\ m_o$ is quoted by Kao[21], resulting in a period of 107 Å. It could possibly result that this small period is not resolved under experimental conditions and therefore conduction by holes not only continues at all thicknesses but contributes to

the masking of the depressions in conductivity due to the electrons.

It does not follow from the above argument that the carrier density would oscillate with thickness, but an appreciable modification to the mobility is certain. An oscillatory behaviour in the measurements against thickness of the Hall and magnetoresistance coefficients would be expected as a result of this.

An additional interpretation of the analysis is given by Sandomirskii (85) who discussed the relative motion of the conduction and valence bands in the presence of a size quantisation of the energy levels. Figure 30 shows the overlapping bands condensed to a common k-vector. A reduction in film thickness causes a relative separation of the two bands (at a constant value of E_F) such that the standing wave

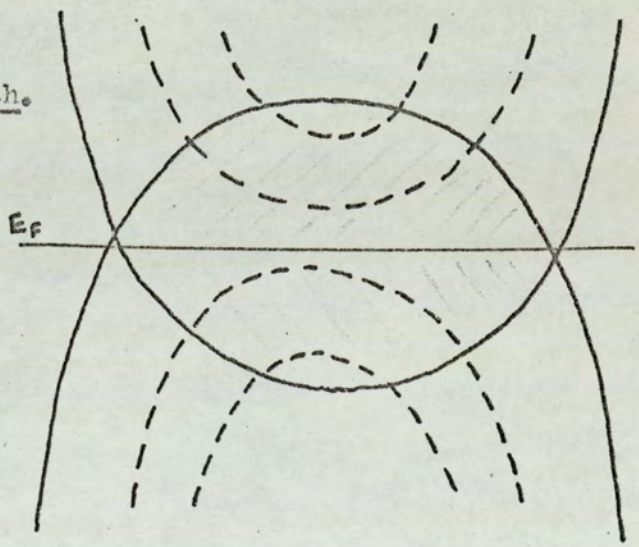

Fig. 30. Band structure of bismuth. The dashed lines represent the film condition; the shading is that of the bulk semi-metal. (after Sandomirskii).

condition occurs periodically with thickness. At a thickness corresponding to n = 1 the two band edges are coincident giving the final minima in conductivity. At lower thicknesses the bands separate completely to result in a material displaying true semi-conductor properties. It is not concluded that the associated increase in resistivity is entirely due to this source as under these conditions doubts as to the continuity of the film structure begin to arise.

CHAPTER 3

Experimental Apparatus

3.1. Evaporation assembly

3.1.1. Introduction

A vacuum coating assembly suitable for the production of thin films having reproducable purities and structures should have the following basic requirements:

1) A low residual pressure.

2) A minimal oil contamination of the substrate surface.

3) It should be demountable.

4) The turn round time should be short.

The pumping speed of the proposed system was limited by the Edwards E02 2" oil diffusion pump available and thus it was preferable to minimise the chamber volume. A short cycle time would produce the additional advantage that ancillary evaporations, such as the laying down of contact areas for thermal bonding of electrical contacts to the films, could readily be performed under equally clean vacuum conditions.

The basic vacuum coating assembly was in the early stages of design when the present work was started. The proposed system included a water-cooled oil diffusion pump surmounted by a chevron baffle and liquid nitrogen cooled trap, acting directly onto the chamber. It was intended originally to interpose a butterfly valve between the trap and chamber so that the latter could be returned to atmospheric pressure with the nitrogen trap still charged, as suggested in the manufacturer's literature. Unfortunately, this arrangement suffered from the fact that a second pump-down resulted in the condensation onto all surfaces of the trap of chamber

residuals which would otherwise be pumped away. Overnight discharging would then release the condensate from the upper parts of the trap into the chamber producing undesirable contamination of the substrates. The same consequence arises as with the overfilling of traps from room temperature in which only the lower few centimeters of trap should be allowed to do the trapping. The remainder of the trap, filled thirty minutes later, acts solely as a reservoir.

On test it was verified that the butterfly valve close to the chamber yielded films whose adherence to their substrates was only mediocre and it was concluded that the trap had to be emptied after each evaporation. If,however , trap emptying was a necessity then it would be advantageous to situate the nitrogen trap in close proximity to the chamber consistant with U.H.V. practice. This latter modification was adopted.

The backing line in the first instance consisted of an Edwards E.S. 35 (35 $l.s.^{-1}$) single stage rotary pump, pumping through a zeolite trap from either the pump or chamber. It was soon apparent that the conductivity of the trap was less then might be expected and was unable to reduce the chamber pressure adequately. The zeolite powder produced by thermal cycling caused rapid deterioration of the pump and hand valve seats dispite the use of the recommended glass wool baffles.

Following the preliminary tests the pumping system finally adopted is illustrated in Fig. 31.

3.1.2. Backing line

The ½" backing line to the diffusion pump outlet was pumped using an Edwards ED 250 twin stage non gas ballast rotary pump. Suitably trapped,the pump would readily achieve 40 - 50 μHg. at the diffusion pump outlet, but despite the trapping, the ultimate performance was erratic due to condensed vapour in the pump oil which could not be readily removed. Haller[87] described an

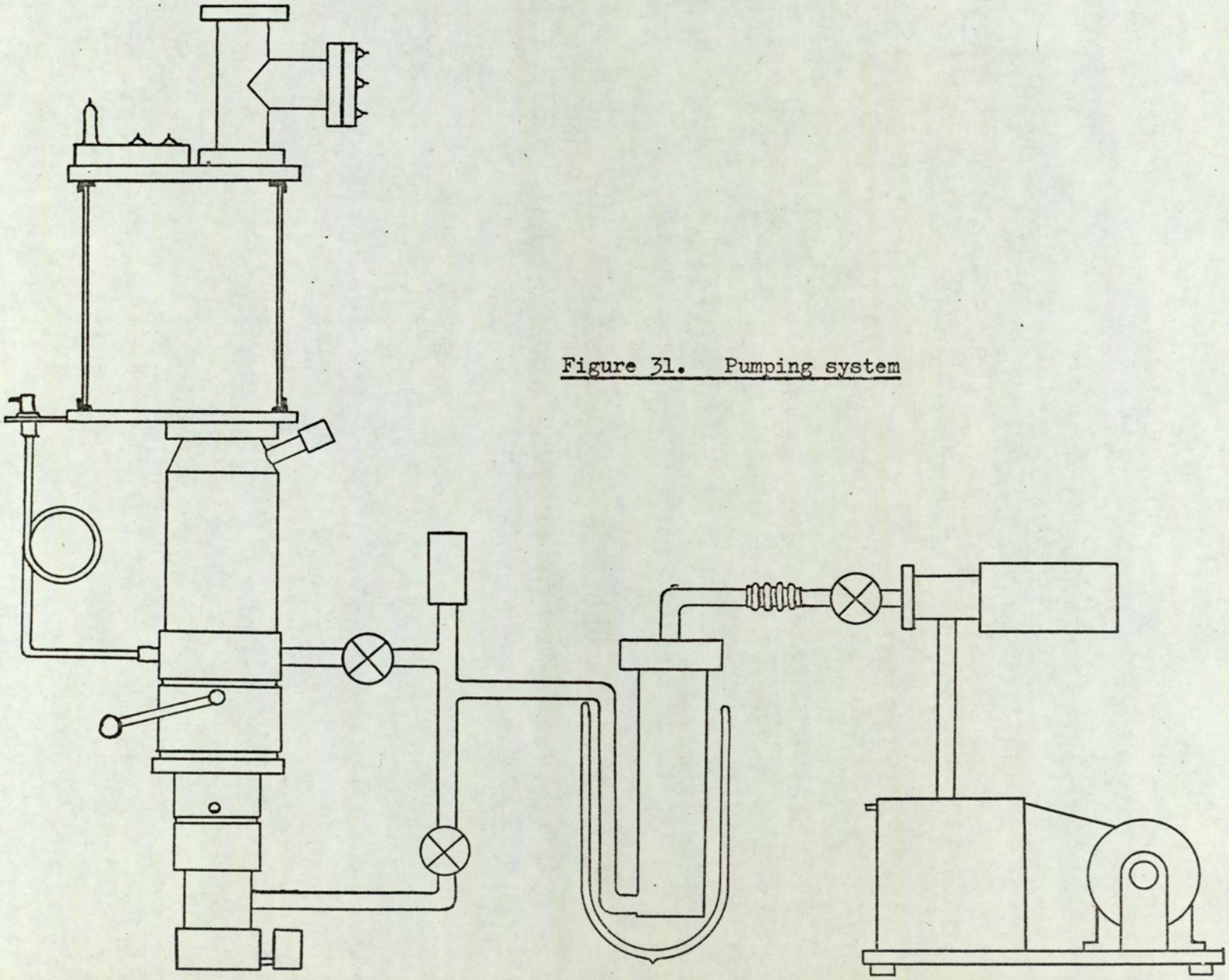

Figure 31. Pumping system

all glass sorption trap using porous glass discs within a convoluted glass envelope. The use of glass in this system being avoided where possible a sorption pump was constructed having a stainless steel tubular outer case of 0.009" wall. By free standing a selection of stainless steel tubes in open dewars of liquid nitrogen it was determined that in equilibrium the frost ring above the liquid level occupied about 3 cms. and the dew band a further 0.5 cms. above this. Thus in designing a trap use could be made by hand tightened couplings with nitrile 'O' rings provided they are located four centimeters above the top of the dewar. A series of 10 discs, 50 mm. diamter x 3 mm. thick in porous glass were obtained in the British equivalent of Corning type 7930 whose specification is quoted as having a mean pore size of 40 $\mathring{A}$ and an internal surface area of 200 $m^2.g^{-1}$. This figure is ¼ that of zeolite. A segment of approximately 15% of the area was ground from each of the discs prior to placing them inside the stainless tube. Aluminium spacers held the discs at 1.5 cm. intervals with the segments so arranged in antiphase to eliminate the direct optical path through the assembly. The inlet to the pump was via a ½" stainless steel tube let into the base cap, and a 2" Edwards brass hand coupling formed the upper outlet and access to the discs. A sketch of the assembly is shown in Fig. 32.

By roughing the system to 50 μ with the rotary pump the action of filling the dewar with liquid nitrogen brought the backing pressure to below 1 μ (the limit of the pirani gauge) within seconds. It appeared to be of no detriment to the performance of the sorbpump to repeat the roughing procedure on a later run with the nitrogen trap already filled. Occasionally the backing line alone would be allowed to pump at room temperature overnight to clear accumulated water condensed on the porous glass. Baking was avoided in order to leave the condensed oil in situ, this being removed by occasionally dismantling the trap.

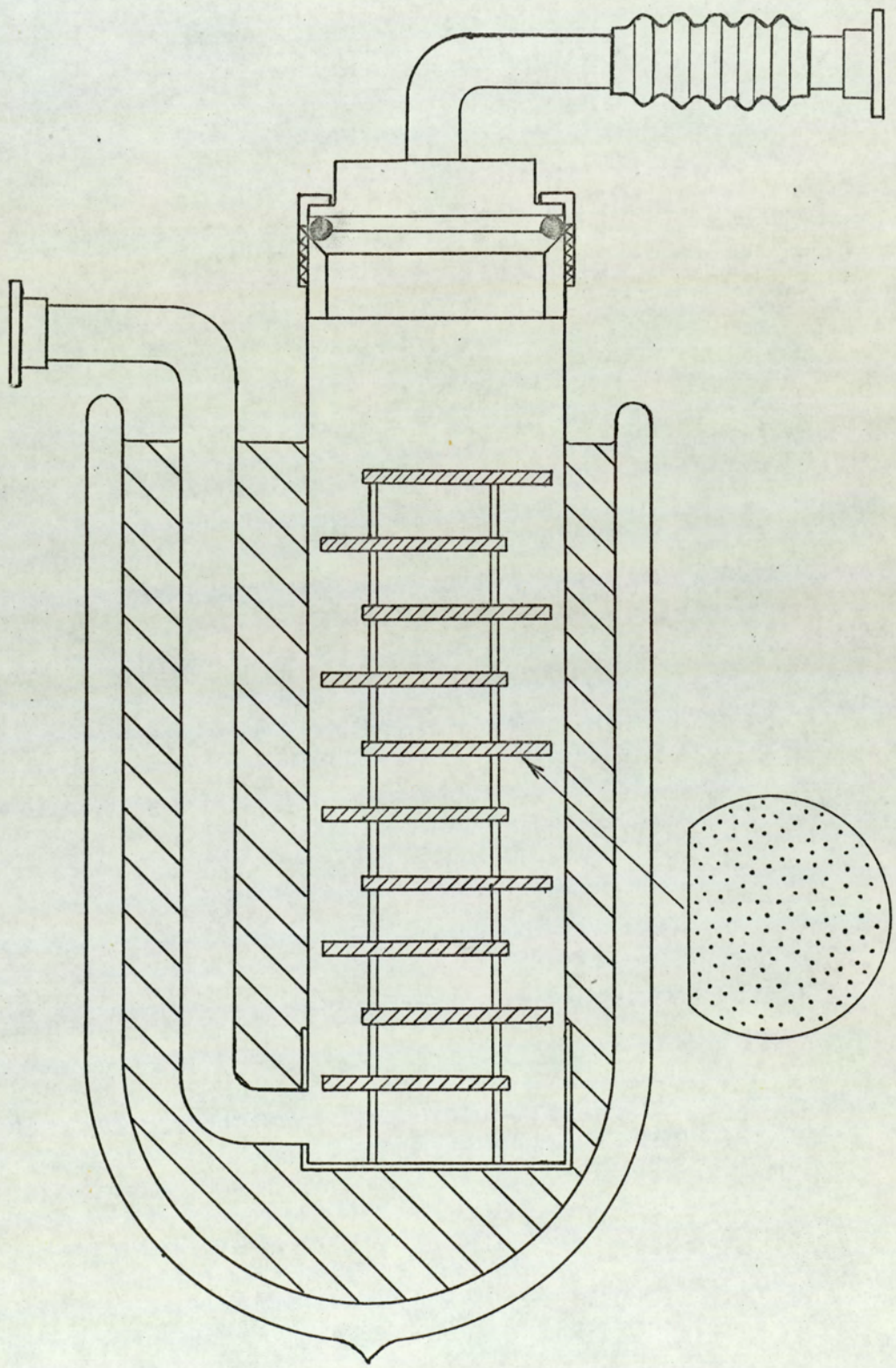

Fig. 32 . Backing line sorb-pump.

The backing line was protected by a magnetic mains isolation valve, and a series of hand valves enabled the roughing procedure to be performed whilst the diffusion pump was operational. The backing pressure in the region of the diffusion pump outlet was monitored using a pirani gauge.

3.1.3. Fore-pump system

The fore-pump was an Edwards E02 water-cooled oil diffusion pump charged with Silicone 704 oil and having a throat speed of 150 ℓs^{-1}. Backstreaming vapour from the pump was reduced by a water-cooled baffle and the pump isolated from the chamber region with a quarter swing butterfly valve fitted with a Viton 'O' ring. To enable the liquid nitrogen trap to remain as close as possible to the chamber the spacer ring carrying the service ports was placed immediately above the butterfly valve. Ports were used for vacuum roughing and for the admittance through a needle valve of dry gases. Ports were also available during commissioning for a penning gauge and further pirani gauge. For testing purposes a 6½"diameter borosilicate glass bell jar was used as a working chamber sealed to the baseplate by a Viton 'L' gasket, and having a Baynard-Alpert gauge on a limb extended from the top of the jar.

The conductances of the accesories used are given in Table 5 , together with an estimate of the effective pumping speed.

Table 5 . Foreline Conductances

Accessory	Edwards type no.	Air Conductance $\ell . s^{-1}$.
Baffle	CB02	95
Butterfly valve	QSB2	220
Spacer	-	> 600
N_2 trap	NTM2	60

$$\frac{1}{C_{total}} = \sum \frac{1}{C_{individual}} = \frac{1}{150} + \frac{1}{95} + \frac{1}{220} + \frac{1}{600} + \frac{1}{60}$$

$$C = 25\ l.\ s^{-1}$$

It was hoped that a pumping speed of this magnitude would be available to pump the chamber volume of three litres to give a clean vacuum of around 10^{-7} torr.

3.1.4. Chamber Furniture

The baseplate was manufactured from an EN58B stainless steel blank 8" diameter and ⅜" thick, and finished in a high polish. The workshop drawing is shown in Fig. 33 and contains the following main features:

i) The major pumping port with suitable bolting facilities.

ii) Four large ports to accommodate interchangably high current lead-throughs, rotary shafts or an eight way lead- through.

iii) Two small ports to accommodate high voltage electrodes.

iv) The equilaterally spaced holes to hold the pilars from which to mount the chamber furniture.

Live leadthroughs rated at 400 amps were placed on either side of one support pillar whilst a flat stainless steel strip of 10 gauge metal joined the other two pillars to form a common earth return. The plate and tops of the two electrodes were drilled with a series of 2 B.A. holes so that "V" clamps could hold in position any profile of filament. A thin stainless steel shield anchored to the earth return plate constrained the evaporant beam from being either deposited downwards towards the pump or cross-wise to the other filament.

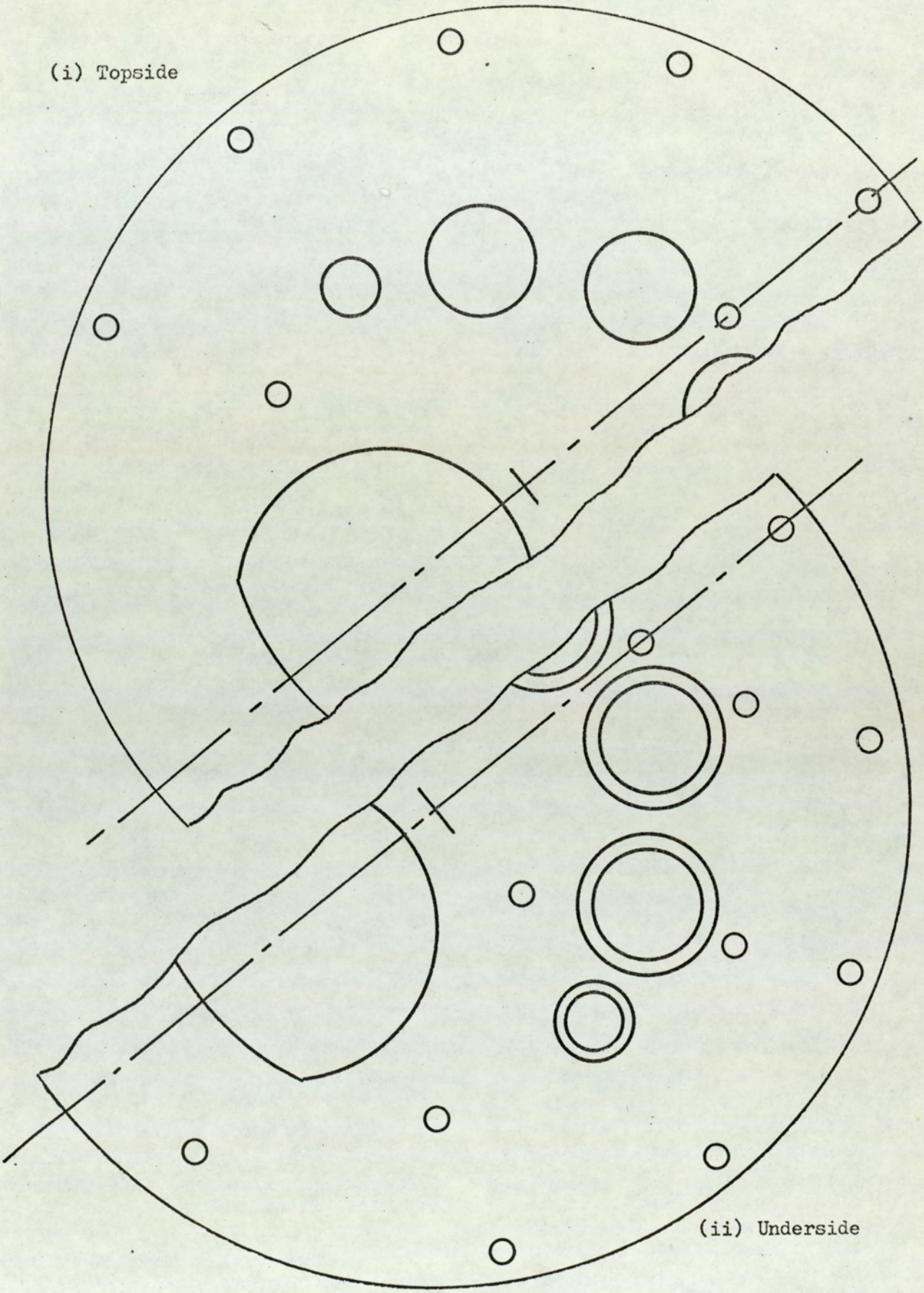

Fig. 33 . Plan view of the baseplate, $\frac{3}{4}$ full scale

Whilst the surface tension of bismuth is such that it is not possible to evaporate from tungsten filaments, a molybdenum basket can be used with some success. In the case of a basket with 4π evaporation geometry the material charge required to evaporate thick films over a distance of 15 cms. would render this technique impracticable. Proprietory molybdenum boats are of low cost and an attempt was made to make direct use of these. Under clean vacuum conditions however excessive wetting of the boat surface resulted in a drop in evaporation current, and a loss of the "point source" approximation.

The extremely high price of tungsten boats did not appear to be justified when considering the relative price of the raw materials. A simple technology developed by Archer-Hall[88] enabled these items to be rapidly produced on a small spot welding assembly for one fifteenth of the purchase price.

Tungsten strips 12" x ½" x 0.006" were cut to 2" lengths and placed within the recess in a copper former as shown in Fig. 34 A copper dolly was mated with a depression in the recess. By experimenting with variations in the welding current and pulse duration time the depression formed tended to show a maximum in depth after which it became weak around the perifery and eventually broke into a hole. The arbitrary settings which produced the maximum depression resulted in a boat free from thinning effects, but with a blue oxide band around the depression. A comprehensive cleaning procedure for tungsten as given by Kohl[89] was used. The boat formed the anode in a N/10 solution of sodium hydroxide etched at a current density of 0.045 $A.cm^{-2}$ (i.e. 600 mA). The matt finish of clean tungsten achieved after 15 - 25 minutes was followed by the usual high temperature clean in vacuo.

'V' - shaped tungsten filaments were found to be suitable

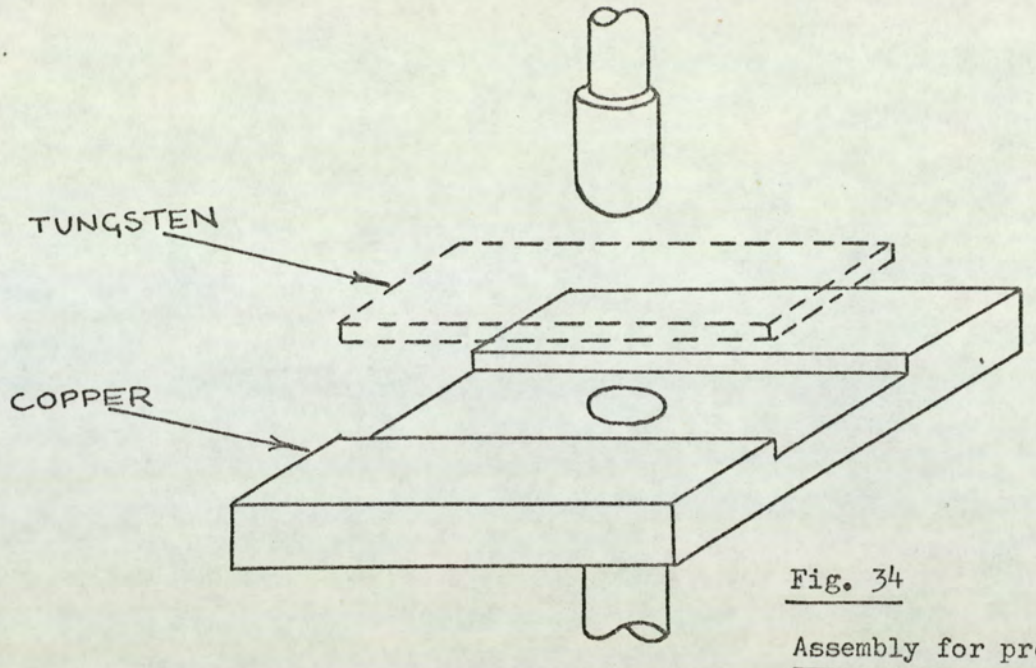

Fig. 34

Assembly for preparation of tungsten boats.

for the evaporation of aluminium or copper used to prepare the bismuth film borders. To maintain the bead of aluminium or copper evaporant at roughly the same horizontal level as the bismuth a more complex filament shape was developed hindered only by the brittle fibrous nature of tungsten. Two filaments together with a sub-assembly within the chamber are shown in the photograph, Fig.35. The a.c. power to the filaments was supplied from a transformer capable of delivering a maximum of 200 amps at 20 volts or 400 amps at 10 volts. The primary to the transformer was controlled by a 20 amps autotransformer and was capable of being switched 'on load' by a suitable isolating unit.

The required substrate/mask assembly was such that it would be possible in one evacuation to evaporate both the experimental film and its associated border with a very fine locational tolerance. Indeed the standing voltage compensating arms each of 0.5 mm. wide and having a similar interspacing required to be overlayed with a similar deposit to give at least 90% of common

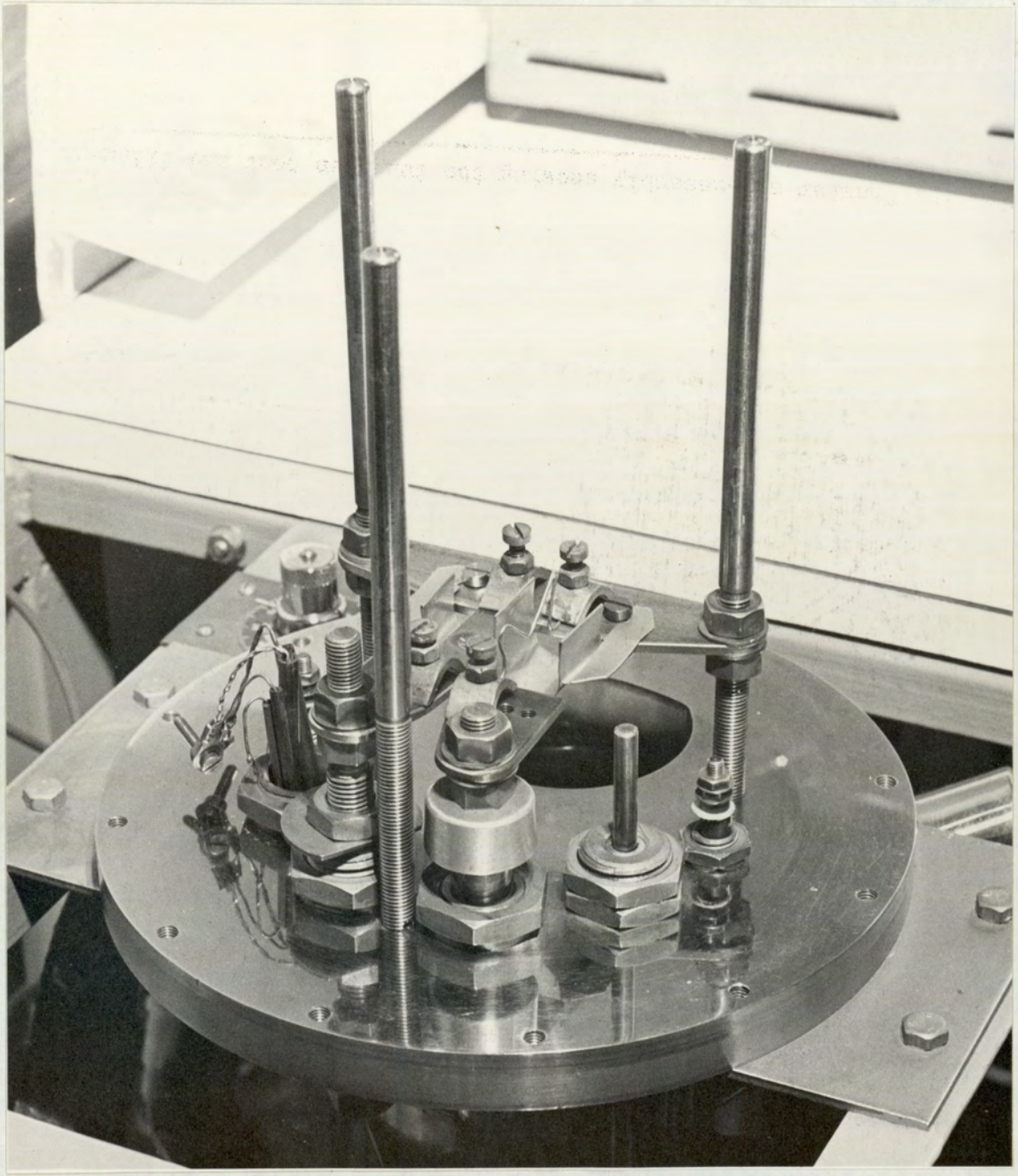

Fig. 35. Chamber sub-assembly showing the tungsten boat and filament.

coverage, i.e. to within 0.05 mm. A mechanism yielding such precision resulted in a mask holder carrying two masks and keyed to the rotary shaft through the baseplate. The holder would be located in the proximity of the substrate by means of microdowels. To allow for precision alignment of the substrate holder dowels with respect to the mask holder, a separate substrate holder plate was machined and held proud of the main backing plate. The backing plate had three tack welded bosses to locate it close to the top of the furniture pillars and a further three half bosses to space the substrate holder from the plate, Fig. 36. From a smaller diameter piece of 10 gauge sheet, an annular portion of about 70% of the plate thickness was turned away and a further diametrical path milled out, to leave two segmental islands from which the pointed microdowels protruded. Thin clamps with two small claws held the substrate firmly in a centralised position with minimal surface contact. It was thus hoped to bring either mask over the dowels to rest parallel to, and less than 0.5 mm. from the substrate. A 10 B.A. countersunk screw in the centre of the substrate area provided, from the rear, an anchorage for both a thermocouple and a copper thermal sink. Six holes were drilled in the central recess to lead away electrical contacts from films in which in situ measurements were required. The substrate holder and backing plate were connected by three loose fitting screws which would allow a degree of lateral relative motion prior to final clamping.

The mask holder illustrated in Fig. 36 was designed to fulfil a three-fold duty. From a remote position outside the vacuum chamber the holder should:

i) Be capable of blanking off the substrate while outgassing the evaporant.

ii) Move into position a mask through which to evaporate

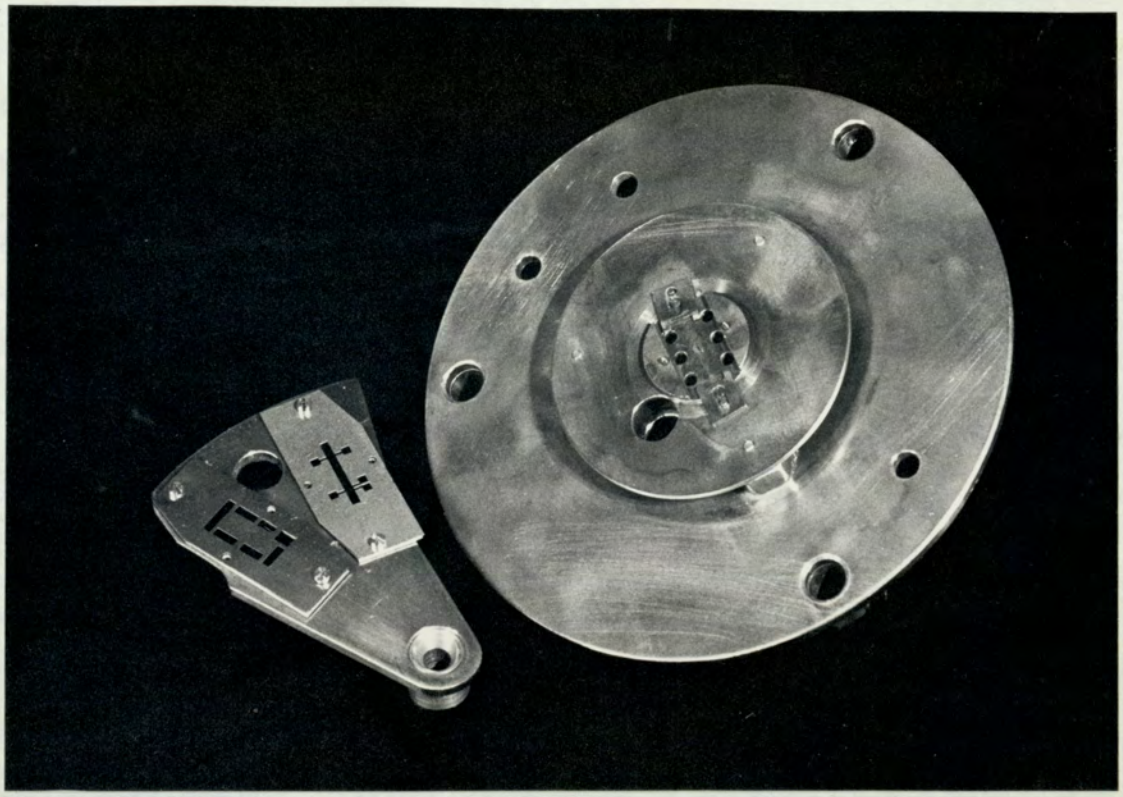

Fig. 36. Substrate holder plate and mask holder showing the film and border masks.

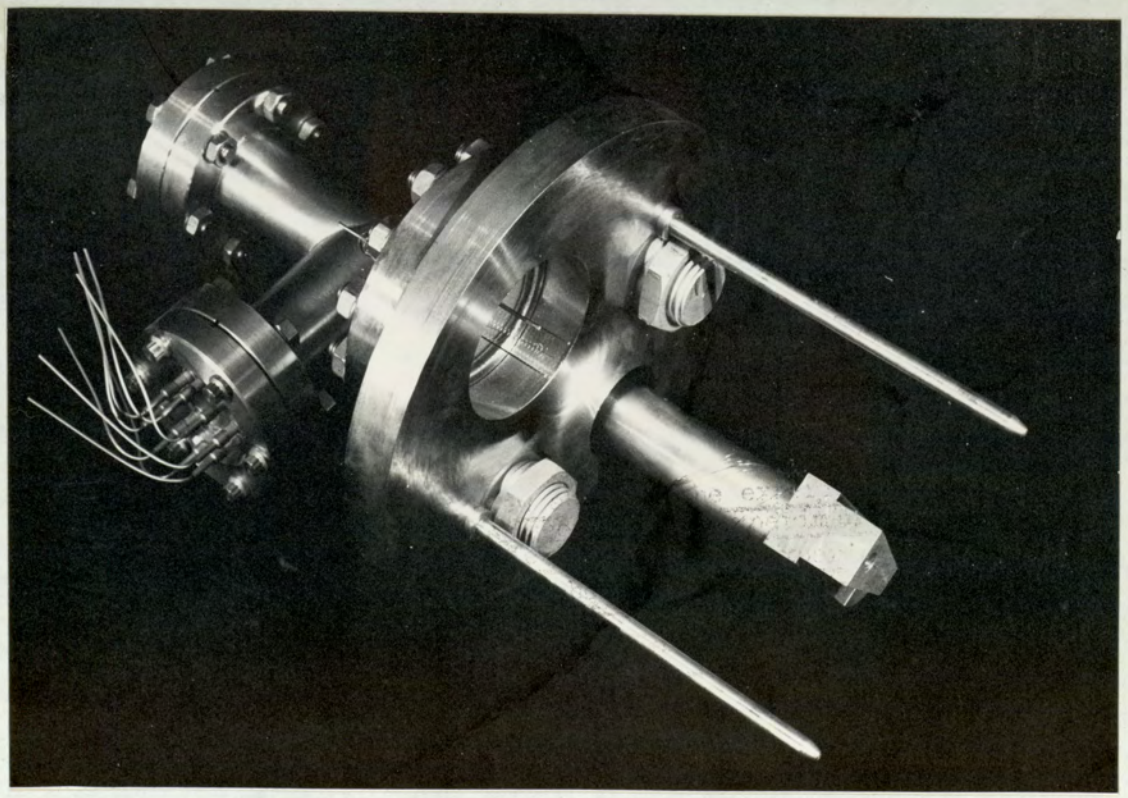

Fig. 38. Top plate showing the re-entrant cold finger and copper heat sink.

the film borders.

(iii) Move into position a mask through which to evaporate the film.

A fourth facility was incorporated to enable the holder to move completely clear of the substrate for high voltage cleaning, so as to retain a multi-purpose nature to the assembly.

In order to obtain the necessary rigidity stainless steel masks 0.003" in thickness were produced by the chemical etching technique "Etchineering"[90]. The series of masks prepared provided a wide range of film and associated border profiles and were etched complete with bolt and dowel holes to avoid the need for further machining. By etching from one side only in order to further reduce shadowing a cross-section of the mask could be obtained as in Fig. 37.

Fig. 37. etched profile of film mask.

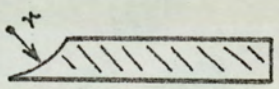

Two masks were fastened radially onto a sectored plate pivoted about a rotary leadthrough, each having a support plate. The loose fitting of the bolt holes provided a free movement of either mask of about 0.025" so that when offered to position the only restrictions to its final position were the tapered dowels and island of the substrate holder. A four positioned radius arm operating outside the chamber within a cranked guide indicated approximate locating positions for the holder and at the same time prevented the dowels from penetrating the mask whilst traversing from one position to another. On the underside of the mask holder a central triangular area provided a location for a reference substrate

for interferometric thickness measurements. A small 32 - gauge mask having five x 1/16" slots milled across it served to clamp the reference substrate in position. A plain mask enabled an overlay to be deposited. The interferometric picture obtained this way would be characterised by a battlement shape and thus dismiss the not uncommon doubts about whether the measured step was indeed the correct one. A small fixed shield prevented evaporation onto the reference substrate whilst the mask holder was in the position for evaporation of film borders.

The deposition rate was controlled with the aid of a commercially available oscillating quartz crystal film thickness monitor whose crystal was required to be situated such that it was subject to only a minimum amount of direct radiation from the filament. An attempt to mount the crystal beneath the mask holder failed despite a degree of radiation shielding. It was remounted above the substrate assembly on an upraised platform designed to give rigidity to the crystal holder whilst having a minimal thermal connection to more bulky components. A succession of holes in the substrate holder, backing plate and mask holder acted as radiation baffles and besides improving the features mentioned, the ultimate range of the instrument was increased by an order of magnitude due to the increased distance from the source.

The top plate of the chamber housed a nude IOG 13 Baynard-Alpert gauge and a U.H.V. tee-piece through which a re-entrant thimble was located and terminated in a large copper heat sink. The block formed a sliding fit coupling to the rear of the substrate enabling its temperature to be maintained over a wide range of values. The side arm of the tee held an eight-way U.H.V. leadthrough from which 40 gauge copper wires led down the thimble and were available to monitor the film electrically in situ.

The photograph, Fig. 38 , shows the top plate. A borosilicate glass cylinder formed the chamber wall and was sealed to both end plates with Viton 'L' - section gaskets.

Due to the thermal inertia of such a stainless steel system, bake-out from the exterior was beset by many disadvantages not the least of which was the limit imposed on the internal temperature by the viton seals and Wilson-type rotary seal. An internal oven was located in the region below the substrate assembly. It consisted of an annular plate having a periferal skirt and a set of tubular ceramic insulators around which was wound a double tier of bright Nichrome[91] wire. The oven once initially outgassed proved to be extremely reliable. An elementary treatment of radiation losses indicated that with the ½ kW. dissipation available from the heater the oven surface was capable of being raised in temperature to about 300°C which would not thermally stress the weaker components. Provision was in fact made in the base plate perifery for the attachment of a radiation cooling water jacket but this was not needed. A state of equilibrium in which the glass rose to about 110°Celsius with the interior stainless steel at about 200° Celsius was achieved with a current of 3 amperes in the heater corresponding to a dissipation of about 300 watts.

The final refinement to the chamber interior was the inclusion of a 70 mm. diameter glass sleeve 70 mm long which stood on the filament holders and terminated close to the central hole of the oven. Its purpose was to confine the evaporant to a cylindrical region thus preventing deposition onto components which were tricky to clean (electrodes etc.). Such was the success of the method that no trace of evaporant was found on the chamber wall and thus gas inclusion by unwanted deposits was reduced to a minimum. A further advantage came from the ability to observe, first directly

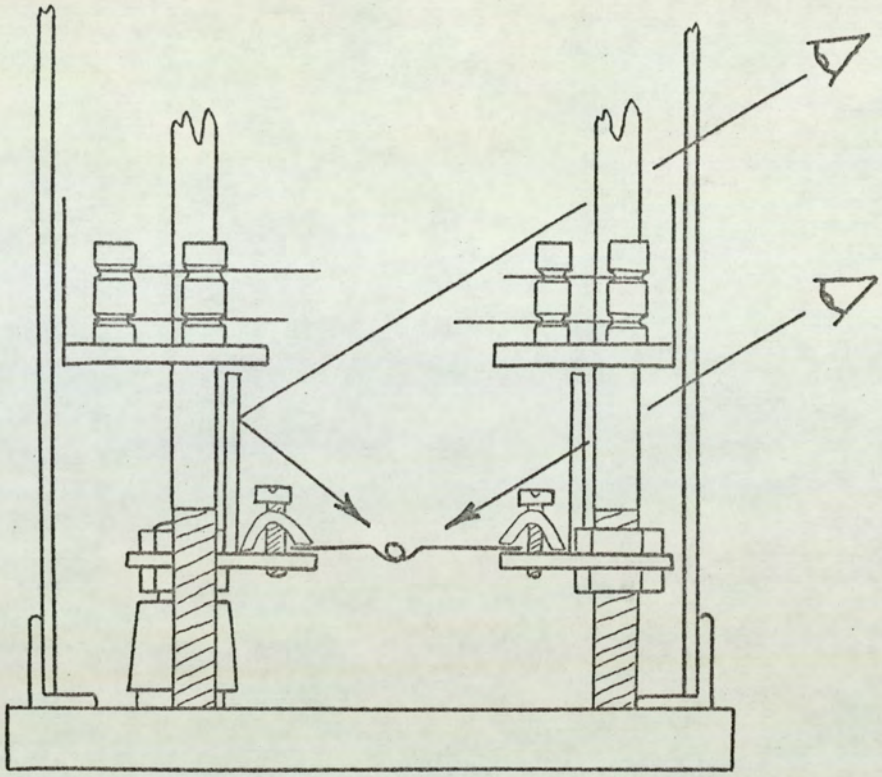

Fig. 39. View of evaporation chamber showing observation cylinder.

and then by reflection, the source itself at all stages of the evaporation as shown in the sketch Fig.39.

A series of photographs showing the chamber and an overall laboratory view are shown in Figures 40 - 42.

3.1.5. Evacuation performance test

The evacuation assembly was tested to establish both the ultimate vacuum attainable, and the pressure which could reasonably be expected during a typical evaporation. The materials in common use for gaskets are never fully outgassed and thus the commencement of filament heating, even with a de-gassed source material, results in a rise in pressure of approximately half an order of magnitude at the lower pressures.

Whilst a detailed description of the standard evaporation procedure is not described, Fig.43 illustrates the pumping performance of the assembly in which the effect of the various

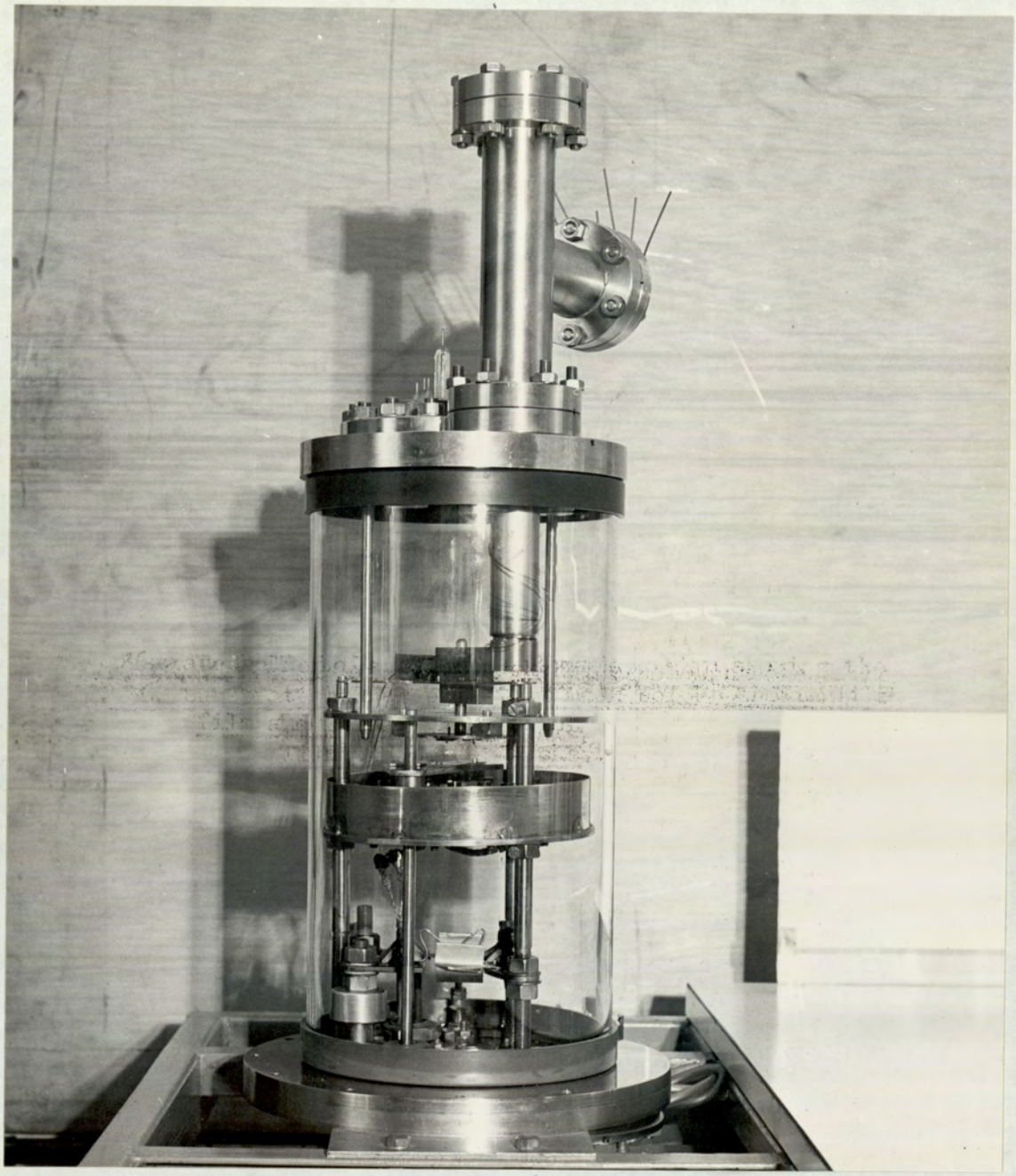

Fig. 40. Assembled evaporation chamber showing the internal bake-out oven.

Fig. 41. Evaporation trolley showing the foreline sysyem and control units.

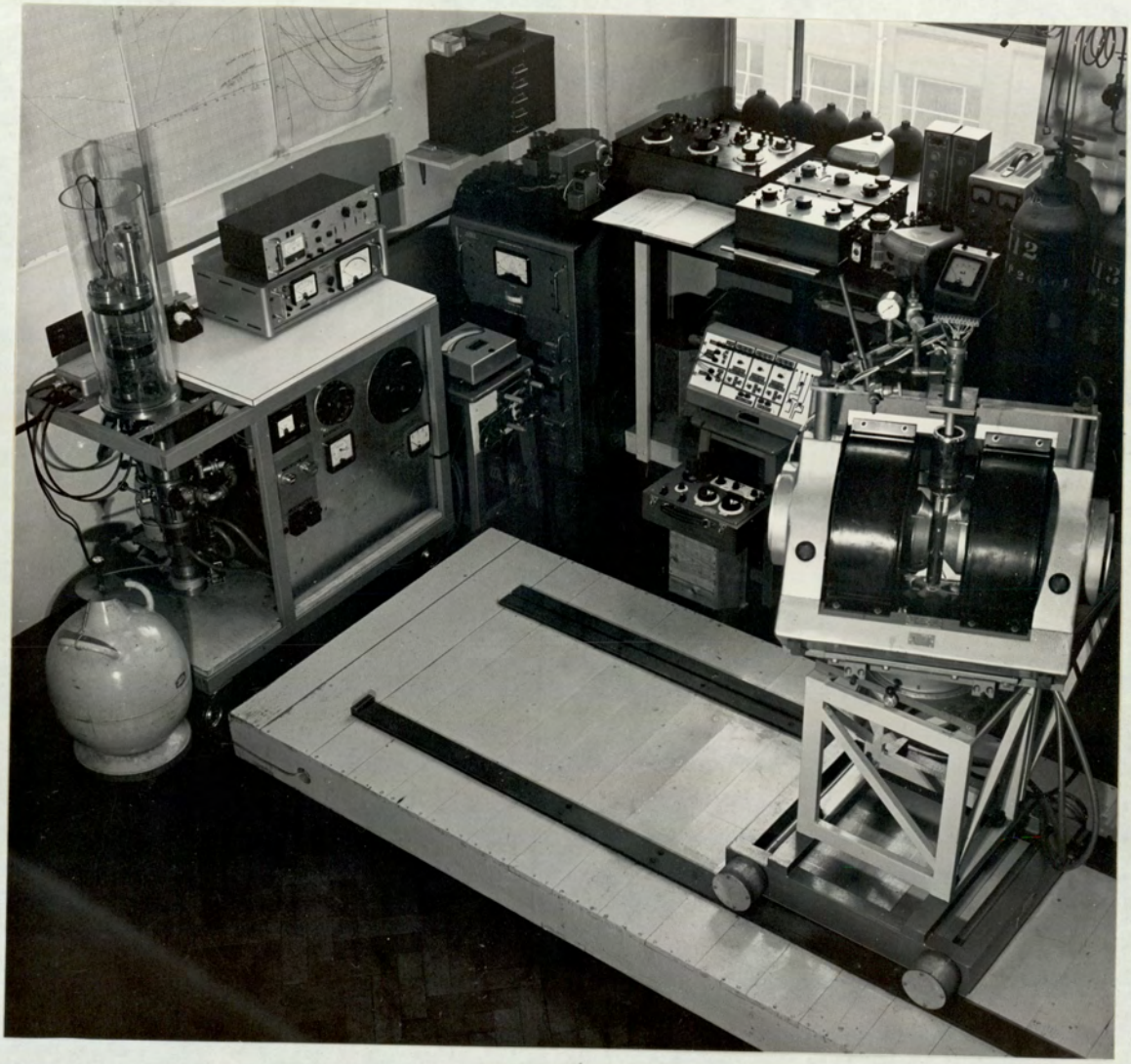

Fig. 42. An overall laboratory view showing the experimental layout.

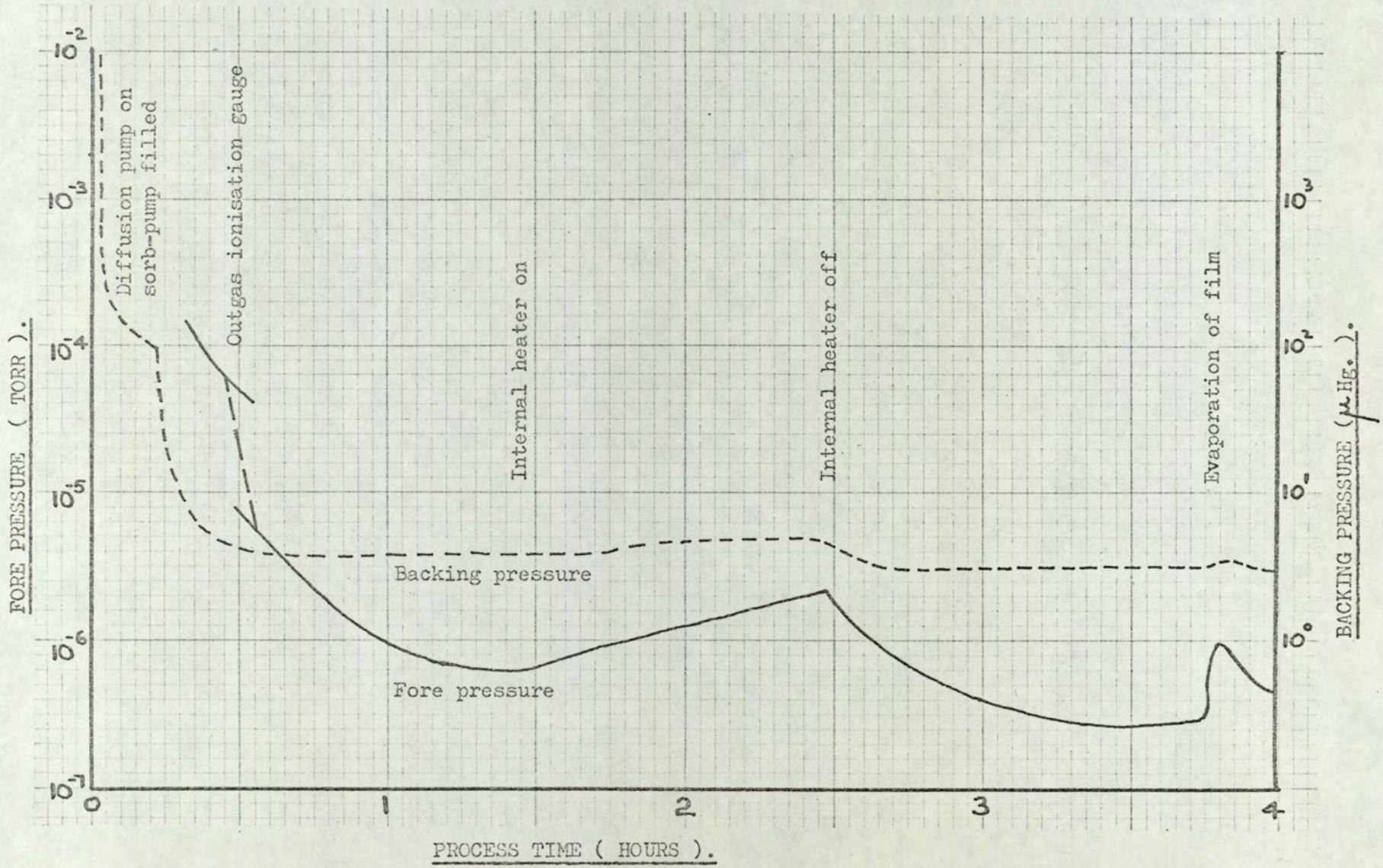

Fig. 43. Pumping performance of evaporation assembly.

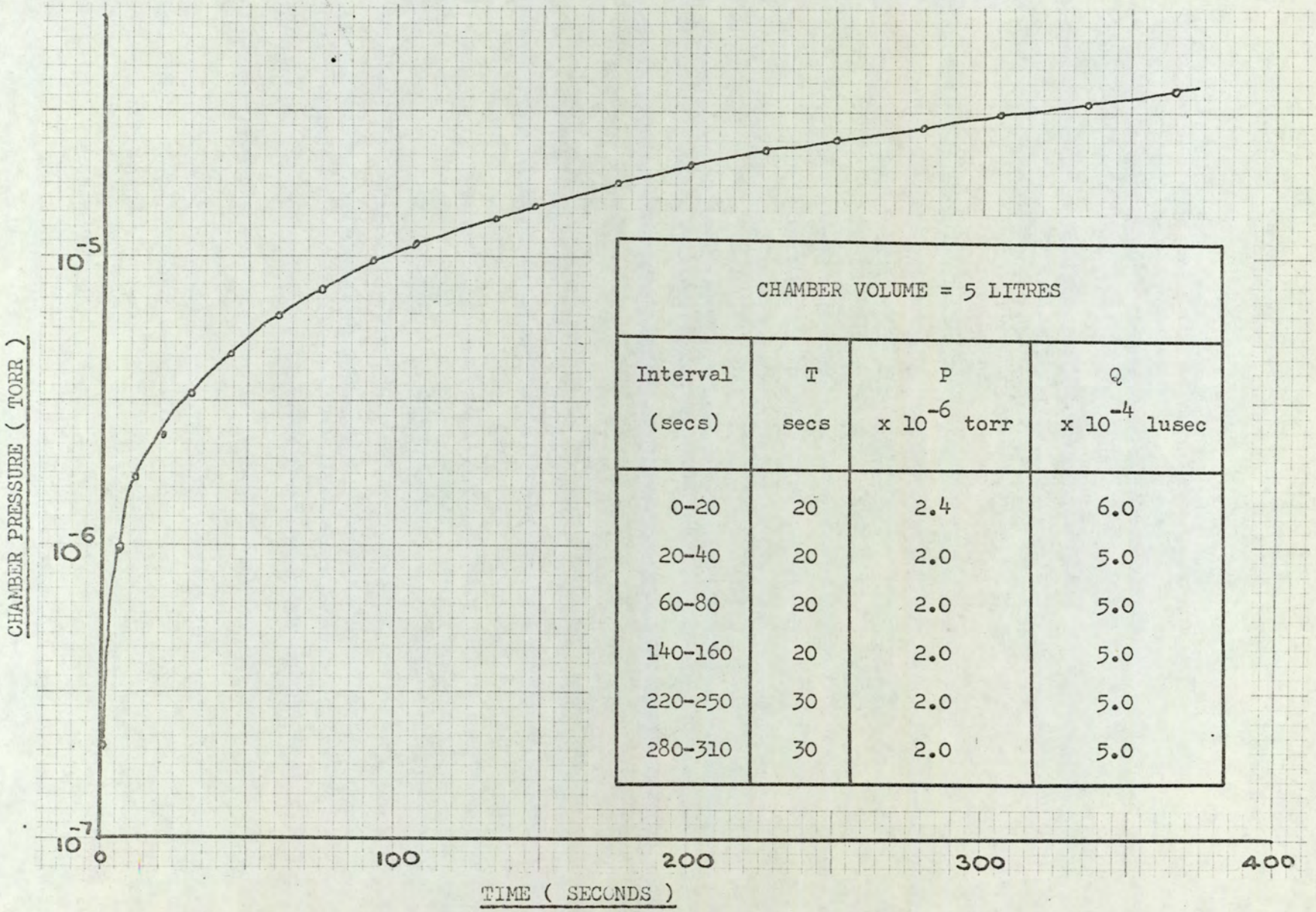

CHAMBER VOLUME = 5 LITRES			
Interval (secs)	T secs	P x 10^{-6} torr	Q x 10^{-4} lusec
0-20	20	2.4	6.0
20-40	20	2.0	5.0
60-80	20	2.0	5.0
140-160	20	2.0	5.0
220-250	30	2.0	5.0
280-310	30	2.0	5.0

Fig. 44. Leak rate investigation.

stages of control may be observed. The ultimate practical pressure employed before evaporation in the present work was 2×10^{-7} torr although a pressure of 7×10^{-8} torr was possible under idealised conditions. During an evaporation the pressure rose to $1 - 1.5 \times 10^{-6}$ torr after which equilibrium was quickly restored.

Under isolation a plot was made of the rise in pressure within the chamber and accessories, a total volume of 5 litres, in order to assess the total leak rate for the system,

$$Q = \frac{(p_2 - p_1) \times V}{t}$$

where p = chamber pressure in microns Hg.

V = chamber volume in litres

t = time in seconds for the pressure to rise from p_1 to p_2

Q = leak rate in litre microns per second (lusecs)

Fig.44 illustrates the pressure rise with time and indicates a leak rate of 5×10^{-4} lusecs which is near the ultimate for gasket sealed systems.

3.2. Specimen Design

Evaporation through masks prepared by modern techniques enabled films of a precise geometrical shape to be prepared, thus the need to resort to the van der Pauw method[92] for randomly shaped specimens did not arise. A strip specimen having a pair of current contacts at the extremities together with a pair of longitudinal and transverse contacts would enable the resistance and Hall measurements to be performed on one film. The basic film shape and principal dimensions are given in Fig.45 and represents a modification to the usual "six-probe" technique. The voltage

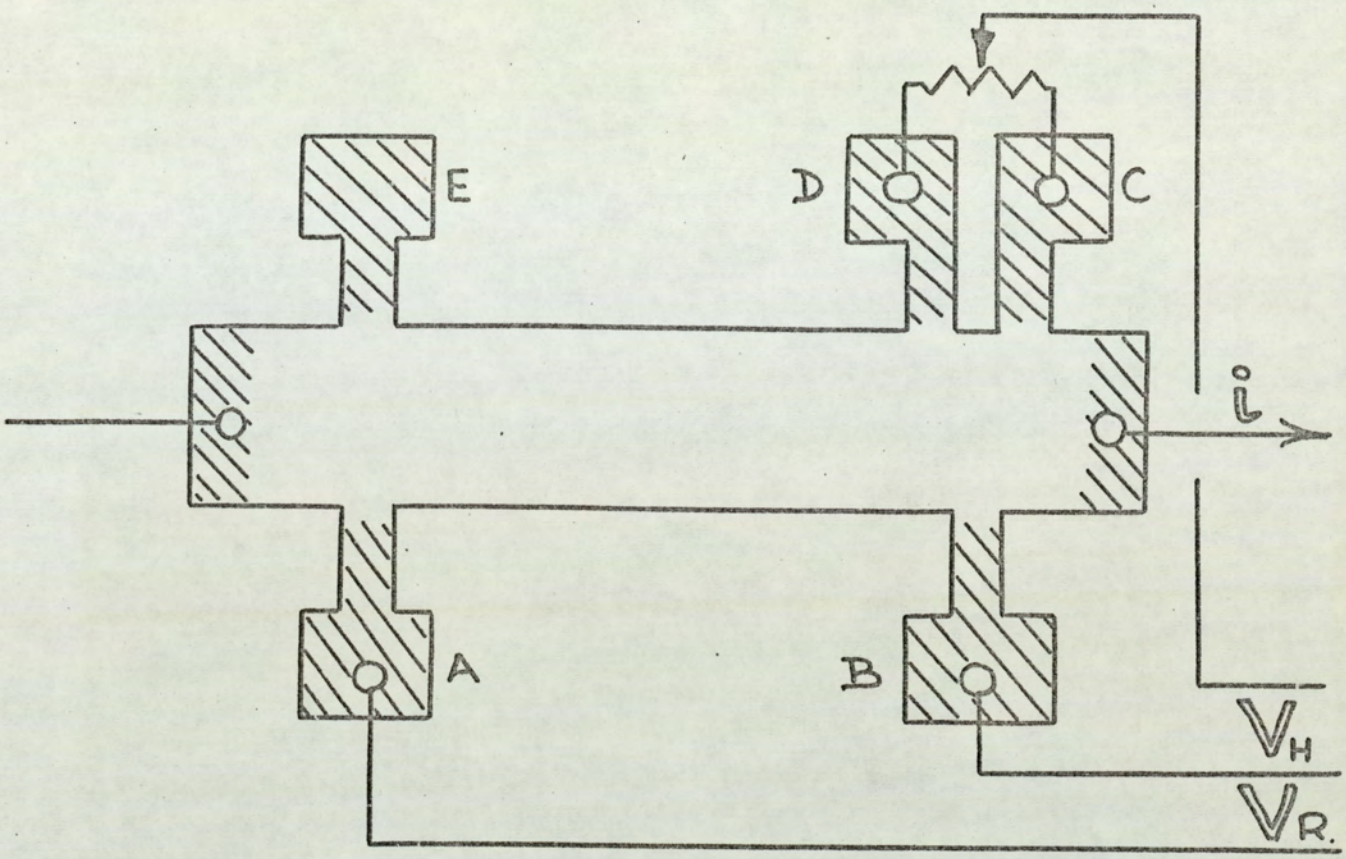

Mean film width = 0.216 $\pm$ 0.001 cm.

Mid-probe length A-B = 1.109 cm.

Mid-probe length E-D = 1.055 cm.

Mid-probe length E-C = 1.157 cm.

Probe widths A,B,C,D,E = 62, 62, 55, 54, 65 x 10^{-3} cms.

Interprobe gap C-D = 0.048 cms.

Shaded regions indicate the areas thickened by a second evaporation to reduce side arm and contact resistance.

Fig. 45 Specimen design and principal dimensions.

measuring probes were evaporated in the form of side arms in order to minimise the perturbation of the electron flow.

In the measurements of the Hall voltage, V_H, in thin films there will in general be a standing voltage, V_S, superimposed on V_H arising from the mal-alignment of the Hall potential probes. In high resistivity semi-metals the magnitude of V_S may be of sufficient magnitude to move the combined measured voltage into a lower sensitivity range thus detracting from the accuracy of V_H.

A current of 1 mA through a 1000 Å bismuth film 2 mm. wide resulted in a voltage drop along the film of 1 volt/cm at 77 °K and 0.5 volts/cm at 300 °K. At 77 °K this amounted to 10^3 μV for every 10^{-3} cm. of Hall probe mal-alignment. In a magnetic field of 2 kilogauss the corresponding Hall voltage was only 8.8 μV. If we consider a potentiometer capable of detecting 10^{-1} μV one would have to forfeit the final figure should $V_H + V_S$ exceed 10^4 μV i.e. the mal-alignment had to be considerably less than 10^{-2} cm in high fields.

The intensional offset in the probes C and D resulted in an alternate V_S sign when each is measured with respect to the fixed probe. The wiper of the variable potentiometer simulated a virtual Hall probe and enabled V_S to be "backed off" to a satisfactory value (or even reduced to zero) prior to observations. As a matter of course with bismuth films a second evaporation was used to thicken the side arms. The value of the variable resistance needed only to be about 25 - 50 Ω since the side arms had considerable resistance, and avoided loss of sensitivity. The constant film current necessary was obtained by introducing a large series resistance R.

Although the double probe technique was useful, only one end of the film was so modified because of the occasional erratic nature of the electrical contacts. Compared with the resistance of the film the contact resistance was found to be quite high. For example on a typical film, potentiometric measurements indicated a

film resistance of 200Ω whereas an 'Avometer' reading indicated 2000Ω. With a changing temperature and an associated differential expansion the contact resistance tended to change by discrete jumps. This would not affect a potentiometric balance point on a conventional Hall pair of probes but when occuring on one of the twin probes would appear as a pseudo-movement of the virtual probe. The applied technique was in fact to use the twin probes on occasions when contact resistance was stable, but to switch to the conventional pair in the presence of spasmodic readings . The introduction of the probe 'E' also descreased the probability of total film failure. To ensure parallel carrier flow through the specimen at the measuring points the probes were spaced at least a few mean free paths from the incoming current electrodes. The ratio of the specimen length to width was a factor of seven. A special film having a central set of Hall probes verified that the spacings of the experimental probes from the ends of the film was sufficient over the range of temperatures available.

3.3. Electrical contacts to films

The problems associated with making reliable electrical contacts to thin films are as old as the technology itself. The method finally adopted is often limited by the application for which the films are to be used. It would be pointless for example to make use of a bulky pressure contact assembly in space research where films were only used by virtue of their mass. On the other hand restrictions within a laboratory may not be as stringent allowing more freedom of choice. The types of contact in common use fall into three categories:

i) Those relying for connection on a self-adhering process, such as the thermal bonding of gold wires.

ii) Those using an intermediate material bonding to

both the wire and the film. Air drying metallic paints, tin, indium or Woods metal solders are typical.

iii) Those whose contact is governed by the action of an applied force such as spring loaded pins and phosphor-bronze strips.

For systems requiring a high bake-out temperature thermal bonding will suffice, but differential contraction on rapid cooling to cryogenic temperatures often leads to contact failure. Some of the methods having the advantage that contacts may be made to any film material without the need for additional borders. Three separate methods were employed at various stages of the present investigation as indicated.

i Thermal bonding of gold wires

The thermal bonding of gold wires directly to bismuth was not possible due to oxidation and low melting point effects. Bonding will occur to clean aluminium requiring the ancillary evaporation of aluminium borders 1000 $\overset{o}{A}$ thick. The substrate was removed from the vacuum and heated to 300 ^{o} Celcius on a hot-plate. A 0.003" diameter gold wire protruding from a capillary tube was flamed across its

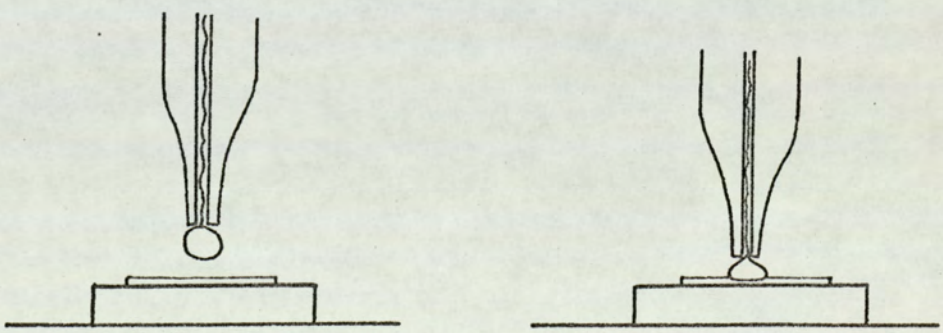

Fig. 46. The thermal bonding process

end to form a small sphere which was retracted onto the

end of the tube as in Fig. 46 . By lowering to the substrate and applying pressure, plastic deformation of the sphere takes place, and a degree of bonding occurs. The process took fifteen minutes to adhere seven contacts to the borders during which time oxidisation occurred. Recently a development utilising a heated capillary head on a cool film offset many of the oxidisation difficulties.

The substrate complete with contact wires was replaced in the vacuum chamber and the bismuth film evaporated. Several times,on early runs,the oxidation of the aluminium was such that the overlaid bismuth deposit did not make electrical contact with the borders. To overcome this, 100 Å of aluminium were evaporated over the original borders. The higher temperature of the evaporant was sufficient to break down the oxide layer leaving an atomically clean surface upon which to deposit the bismuth film. Contacts which became detached subsequently were re-adhered to the side arms using air drying conducting silver paint.

ii) Soft Solder Methods

Some techniques available for making contacts to film borders become possible only when the evaporations were carried out under clean vacuum conditions. Copper borders of 2000 Å thick on glass substrates may be tinned directly with multicore solder enabling 40 s.w.g. enamelled copper wires to be attached. The surplus flux was removed by immersing in warm ethyl alcohol. The strength of these contacts often exceeded the tensile strength of the wire itself.

iii) Pressure Contact Assembly

The concept of a pressure contact assembly arose

from the need to minimise the voltages resulting from the Ettinghausen effect. The substrate mounted in the conventional way with the film uppermost did not exclude the possibility of one side of the film heating up with respect to the other due to the energetic formation and recombination of electron-hole pairs. A method of reducing the magnitude of the resultant thermal voltage was to apply a thermal shunt across the extremes of the film. Electrical contact would of course need to be avoided.

The brass backing plate to which the substrate was clamped face downwards (as described in a later section) formed a useful heat shunt. A thin layer of P.T.F.E. tape acted as an electrical insulator. The pressure contact assembly described is illustrated in a later figure (Fig. 60). It can be seen that the assembly was mounted on the adjacent side of the backing plate in order to establish contact with the film. Seven small brass pins were mounted within recesses in an insulating block. The springs each of three turns were mounted such that the pins were biased towards the film. 40 s.w.g. enamelled copper wires held the assembly together. The contact ends of the pins were guided through the backing plate by small insulating bushes and protruded 0.05 cm. above the level of the P.T.F.E. tape.

The substrate was held firmly in position by two clamps onto which were soldered a copper and a constantin wire. The resultant thermocouple having a split junction gave a most accurate average of the film surface temperature.

iv) Summary

Thermally bonded contacts were used for films deposited

during the commissioning period but a change was made to the use of pressure contacts prior to the commencement of the main experimental investigation. Electrical conductivity measurements on films made in situ immediately after deposition were carried out using soft soldered wires on copper borders.

The galvanometer sensitivity was dependent on the appropriate circuit resistance when balancing the various voltages. As the films, and hence their side arms, became thinner, it was difficult to accurately determine a null point. However, using a system in which precise alignment of masks was a reality it was thought possible to first lay down about 1000 Å of bismuth through a mask having only the contact areas and side arms exposed. Measurements on the superimposed thin film would not then suffer from the effects of reduced sensitivity.

In practice it was found that the side arms had such a sharp profile that the overlayed film became discontinuous at the step, possibly due to a micro-shadowing effect. The problem was overcome by laying down the thin film prior to thickening up the side arms.

Thick contact areas had the additional advantage of reducing the local current density at the point of contact with the pins.

CHAPTER 4

Preparative Techniques

4.1. Quartz crystal film thickness monitor

The thickness and rate of deposition of the films were monitored by means of a commercially available quartz crystal film thickness monitor.

A 6.5. MHz. AT-cut quartz crystal was mounted within the evaporation chamber so that it received a deposit of material concurrently with the test substrate. A sealed reference crystal of 6.0 MHz. was mounted in close proximity outside the chamber. The beat frequency of 500 KHz. provided the input to the main unit where it was mixed with the output from a variable oscillator giving a final difference in frequency of between zero and 150 KHz. The signal was fed to a monostable circuit producing a d.c. output proportional to the incoming frequency and actuated the frequency shift meter. Deposition of a mass of material onto the monitor crystal reduced the natural resonant frequency, and hence increased the differential with respect to the reference frequency. The difference resulted in a displacement of the frequency shift meter. The shift signal was also fed into an R-C circuit whose output monitored the rate of traverse of the shift meter in terms of scale divisions per second, and gave a direct reading of the rate of deposition.

Following an evaporation the thickness meter was re-set to zero to await a further deposit. Each crystal was capable of being used repeatedly up to a maximum deposit equivalent to some 40,000 Å of aluminium prior to being cleaned, though crystal failure was not uncommon if deposits were allowed to approach these thicknesses.

The double beating technique used to produce the final signal required the "zero" to which the meters were set to be 10% of full scale deflection to prevent a degree of frequency "locking" between the various oscillators.

The treatment of the fundamental equations of first harmonic propagation in crystals is given by Cady[93] and applied by Lawson[94] to the film thickness monitor. The fundamental equation is given by:

$$f = \frac{A(\rho q)^{\frac{1}{2}}}{2M} \qquad \ldots\ldots\ldots \quad (4.1)$$

where M = mass of vibrating area

q = stiffness factor dependent on the cut of the crystal.

ρ = crystal density

A = vibrating area.

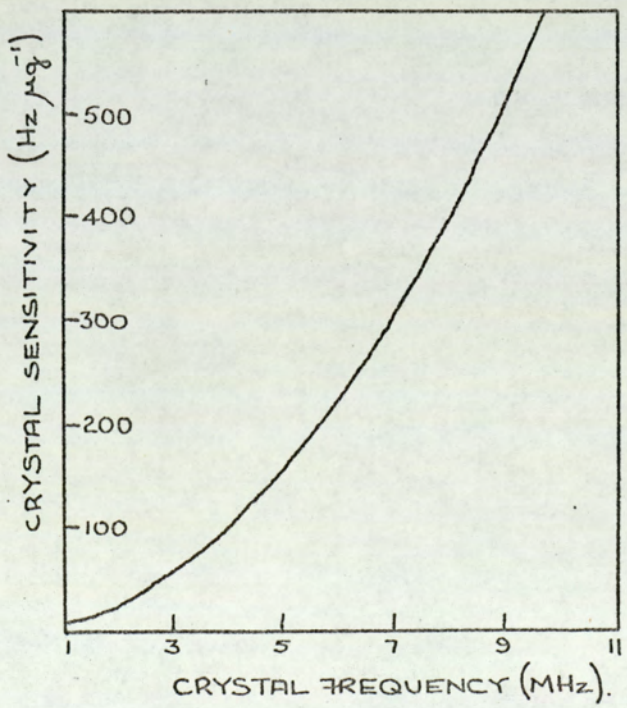

Fig. 47. Sensitivity of AT-cut crystal VS frequency (after Cady)

Differentiating with respect to M

$$\frac{df}{dM} = \frac{-A\,(\rho_q)^{\frac{1}{2}}}{2M} = \frac{-f}{M} \quad \ldots\ldots \quad (4.2)$$

The change in resonant frequency is proportional to dM, the mass deposited, and the ratio is called the mass sensitivity, S. Writing the crystal mass as $A\rho t$, where t is the thickness, equation 4.2 becomes:

$$S = \frac{-f}{A\rho t} = \frac{-f}{A\rho H} \quad \ldots\ldots\ldots \quad (4.3)$$

where the product ft is the wave constant H and is characteristic of the crystal cut. The sensitivity was therefore proportional to the square of the frequency. A graph of crystal sensitivity against frequency for a particular commercial crystal is shown in Fig. 47. The device was of course sensitive to an inverse square law of distance from the source and to the area of crystal onto which the deposit was allowed to fall. An AT-cut crystal vibrating in this mode has a stationary point on the temperature coefficient curve at 28° Celsius either side of which the maximum uncertainty due to thermal drift is less than 9 Hz. $^{\circ}C^{-1}$. With careful design an error arising from this course should be negligible. An error also occurs due to effective density figures for ultrathin films [95], but this range of film thicknesses was not examined in the present investigation, and bulk density figures were employed in calculating film thicknesses.

The ease of cleaning a crystal without damaging the contacts depends upon the deposit material, but the difficulty can be readily overcome by pre-evaporating approximately 1000 Å of aluminium onto the crystal face to cover a larger area than would be used for film monitoring. The removal of the aluminium with sodium hydroxide solution will thus completely remove all additional deposits.

The relative thickness of deposits on the crystal (c), substrate (f) and reference slide (R) were connected by the simple inverse square relationship:

$$\frac{t_c}{d_c^2} = \frac{t_f}{d_f^2} = \frac{t_R}{d_R^2} \quad \ldots\ldots (4.4)$$

where d_i is the distance to the source. An error of p% in each measurement resulted in a 4p % uncertainty in the film thickness. However, as the design of the chamber allowed no relative movement between any of these three components a considerable reduction in the total error could be achieved. The top of the furniture pillars formed a datum from which each dimension was determined using surface plate techniques (Fig.48.). It was thus necessary on each change of filament to measure only the datum distance, D, to the source using a suitable depth gauge. A fourth term was introduced into equation 4.4 to which the following simple transformation was applied:

$$\alpha_i = D - d_i \quad ;$$

$$\alpha_c = 1.525 \; ; \alpha_f = 2.350 \; ; \alpha_R = 2.880 \text{ cms.}$$

The two alternative expressions for the film thickness with respect to the thicknesses measured at the crystal and at the reference substrate were derived from equation 4.4;

$$t_f = \frac{(D - \alpha_f)}{(D - \alpha_c)} t_c \qquad \ldots\ldots (4.5)$$

$$t_f = \frac{(D - \alpha_f)}{(D - \alpha_R)} t_R$$

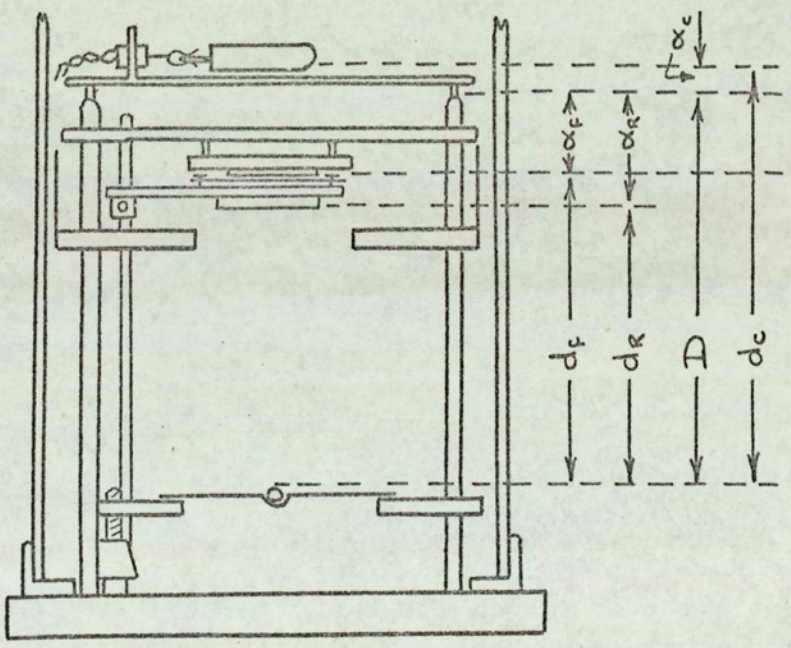

Fig. 48. To show the chamber geometry with respect to the datum distance D.

D exceeded α_i by a factor of eight or so and the expression became moderately insensitive to the accuracy of D as can be seen from Table 6 in which the crystal and reference thicknesses are quoted as a percentage of the substrate thickness.

Table 6 . Relative thicknesses within the chamber

D cms.	d_c cms.	d_f cms.	d_R cms.	t_c as % of t_f	t_R as % of t_f
13.2	14.72	10.85	10.32	183.6	90.0
13.4	14.92	11.05	10.52	182.8	90.6
13.6	15.12	11.25	10.72	180.5	90.9
13.8	15.32	11.45	10.92	178.6	90.8
14.0	15.52	11.65	11.12	177.5	91.1
14.2	15.72	11.85	11.32	176.3	91.4
14.4	15.92	12.05	11.52	174.2	91.6
14.6	16.12	12.25	11.72	173.3	91.3

The errors in t_f caused by a 1% error in D were 0.65% and 0.14% when referred to t_c and t_R respectively, as opposed to 4% by separate measurements to the surface of a diminishing source.

4.1.1. Monitoring film thicknesses

The procedure adopted to deposit a film of a given thickness on the test substrate (e.g. 1000 Å) was as follows. The crystal sensitivity at 6.5 MHz. taken from Fig. 47 was used to determine the frequency shift required, the crystal being arranged to receive a deposit of ¾" diameter. Let the datum distance to the source D be 14.0 cms.

Mass sensitivity = 271 Hz. μg^{-1}

Substrate thickness required = 1000 $\overset{o}{A}$

Deposition thickness required on crystal = $\frac{1000}{1.775}$ = 564 $\overset{o}{A}$ (From Table)

Bulk density = 9.8 g. cm^{-3}

∴ Mass of bismuth deposited = 17.4 μg.

Frequency shift, $\triangle f$ = 17.4 x 271 = 4720 Hz.

4.1.2. Deposition rate

In all experiments the deposition rate was kept constant at nominally 10 $\overset{o}{A}\ s^{-1}$. For the above film the instrument would be set on the 10 KHz. range and by controlling the rate of evaporation at 0.5 divisions per second the true rate became:

$$1000 \times \frac{0.5}{47.2} = 10.6 \ \overset{o}{A}\ s^{-1}$$

Whilst the oscillating quartz crystal method of determining film thicknesses was not an absolute one, it was considered an essential feature of a coating assembly as a method of controlling the rate of evaporation.

4.2. Multiple beam interferometry

The calibration of the quartz crystal monitor was carried out on the reference slide using multiple beam interferometry. The reference stripes of evaporant were overlaid with an opaque layer of aluminium and placed beneath a partially silvered flat. On illumination of the assembly with white light the reflected beam was shown to be deficient in a series of lines within an otherwise continuous spectrum. The fringes have been named by Tolansky[96] "Fringes of equal chromatic order".

Consider an overlaid film beneath a half silvered flat such that a small parallel air gap exists (Fig. 49). There

will exist in the incident beam of white light a frequency such that m (not necessarily integral) wavelengths are contained within the double path length $2y_1$

$$2y_1 = m\lambda + \frac{\delta}{\pi}\lambda \quad \ldots\ldots\ldots \quad (4.6)$$

where m = order of the fringe

δ = phase change on reflection

A shorter wavelength λ' also exists such that (m+1) wavelengths are contained therein.

$$2y_1 = (m+1)\lambda' + \frac{\delta}{\pi}\lambda' \quad \ldots\ldots\ldots \quad (4.7)$$

If we neglect the phase term for a moment, then an integral number of wavelengths within the gap will result in destructive interference and thus produce a fringe. From 4.6 and 4.7;

$$m = \frac{\lambda'}{\lambda - \lambda'} \quad \ldots\ldots\ldots \quad (4.8)$$

In a region y_2 in which the path length is slightly different to y_1 there will be a slightly different wavelength such that a fringe of the same order m is produced.

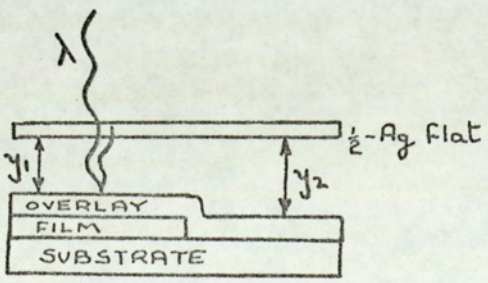

Fig.49 Fringe formation

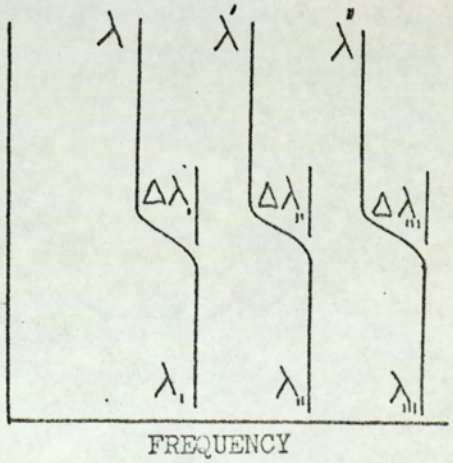

Fig. 50. Fringe profile

$$2y_2 = m\lambda_1 \quad \ldots\ldots\ldots\ldots\ldots \quad (4.9)$$

The thickness of the film is given from 4.6 and 4.9.

$$t = y_2 - y_1 = \frac{m}{2}(\lambda_1 - \lambda) = \frac{m}{2}\Delta\lambda \quad \ldots\ldots (4.10)$$

The image in the spectrometer would thus be a continuous spectrum with a series of stepped fringes superimposed as in Fig.50 By measuring the wavelengths λ^i the order for a number of fringes could be determined and should increase as consecutive integers towards the violet end of the spectrum. A similar measurement of λ_i will yield $\Delta\lambda$ and hence the film thickness.

The phase parameter in 4.6 will in general be a function of the wavelength but Koehler [97] has shown this to be nearly constant at 0.97 in the visible spectrum for silver deposits over 80% reflectivity. Shultz [98] indicated a similar dependence for aluminium. If δ was independent of λ it follows from equations 4.6 and 4.7 that:

$$\left(m - \frac{\delta}{\pi}\right) = \frac{\lambda'}{\lambda - \lambda'} \quad \ldots\ldots\ldots\ldots (4.11)$$

$$\text{and} \quad t = \left(m - \frac{\delta}{\pi}\right)\frac{\Delta\lambda}{2}.$$

The order derived from the elementary theory was therefore almost one less than that from Koehler's treatment. For a true order of two the measured order would be 1.03 which would be interpreted as unity on the elementary theory. An error of 3% thus arises. In order to obtain a measurable $\Delta\lambda$ it is only with ultrathin films that there is a need to resort to such low order fringes. For films in the 10^3 Angstrom region orders of 12 - 25

are more practicable, and in such circumstances the possible error reduces to 0.15%. The practical convenience of the elementary theory however does not detract from the academic value of the more advanced theory.

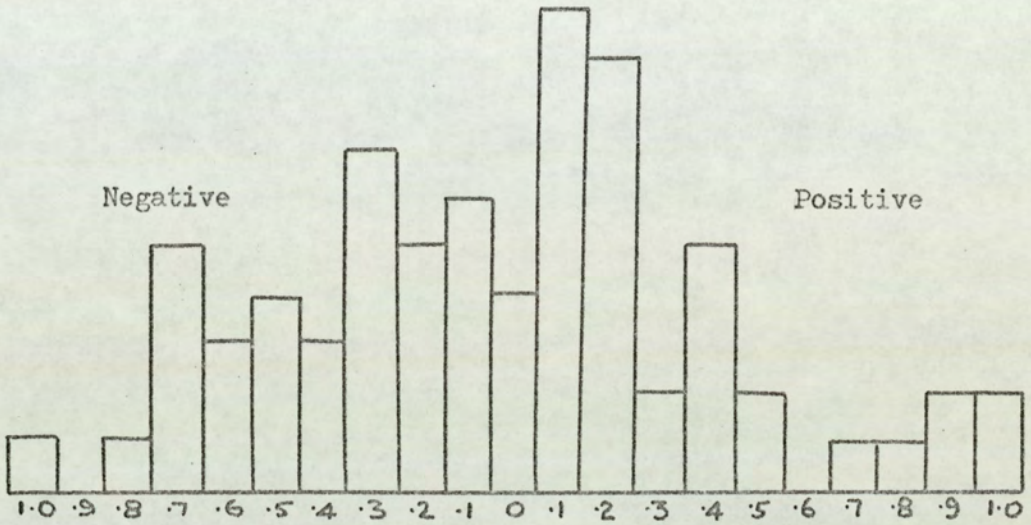

Fig.51 Fractional order by which m_{expt} exceeds $m_{integral}$.

A hystogram was plotted of the differences between the experimental and integral values of the orders covering 100 readings from 15 films (Fig. 51.). The mode of the distribution lay at 0.1 and 0.2 above the integral value assuming an elementary theory. Using Koehler's interpretation one could suggest that the phase change on reflection was thus 0.8 - 0.9 for $\frac{\delta}{\pi}$ which is consistant with the observations of Shultz.

The experimental apparatus for the production of fringes of equal chromatic order consisted of a jig to hold the reference substrate to the part silvered flat, and an optical arrangement to project the frings onto a spectrometer slit. Fig.52. illustrates these.

The body of the jig consisted of a top plate supported on four rigid pillars. From a bush in the centre of the base a

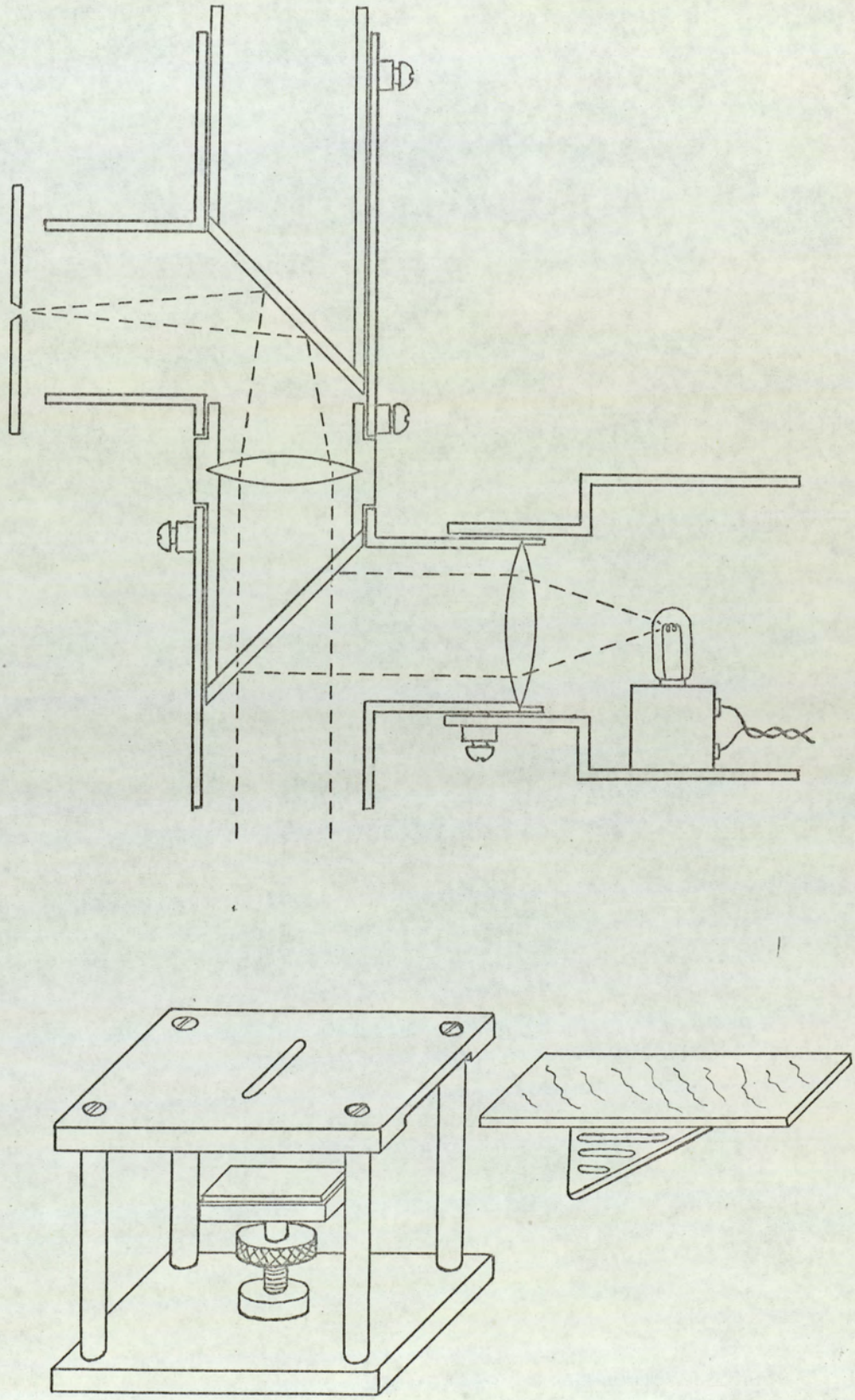

Fig. 52. Experimental arrangement for observing fringes

screw with a knurled nut and surmounted by a rubber pad served to compress the reference substrate and flat onto the underside of the top plate. A narrow central slit in the plate restricted the field of view of the substrate, and by reducing distortion of the flat produced fringes of a better quality. A transverse channel in the underside of the plate prevented the rotation of the flat whilst tightening the nut.

. The optical arrangement was manufactured from a pair of 1" gun-metal water tees having full and half silvered mirrors inclined at 45^{o} together with a 5 cm. focal length microscope objective as shown. The position of a 12 volts quartz iodide lamp was adjustable with respect to a fixed lens of 10 cm. focal length. The lamp was placed at the focus of the lens in order to project a beam of parallel light down onto the jig. The image of the surface was reflected back and focused on the slit of a Hilger Constant Deviation Spectrometer.

The part silvered flat in the interferometer jig was found to result in the sharpest fringes when the thickness of the layer appeared blue-grey in the daylight transmission (about 400 $\mathring{A}$).

Scott et al[99] found that the fringe width produced with commercial microscope cover slides were a quarter of the width of those with optical flats, possibly because the fire polished slides were smoother over a short range than the ground finish of the flats. The quoted short range flatness is in fact $\lambda/150$, amounting to some 30 $\mathring{A}$.

A typical set of results is given in Table. 7. for a film whose thickness as determined by the quartz crystal oscillator was 942 $\mathring{A}$. A discrepancy between the crystal and optical methods of 1.5% exists in this instance. The scatter about the integral values of the observed orders can be appreciated following a short

λ -undisplaced Fringe	6627	6369	6128	5903	5701	5509	5327	5160	5001	4853	4716	4583
λ' -displaced Fringe	6539	6282	6042	5823	5622	5433	5256	5090	4936	4791	4650	-
$\lambda - \lambda'$ Fringe spacing	258	241	225	202	192	182	167	159	148	137	133	-
$m_{observed}$	24.7	25.4	26.2	28.2	28.7	29.3	30.9	31.4	32.8	34.4	34.5	-
m_{actual}	25	26	27	28	29	30	31	32	33	34	35	-
thickness Å	1100	1130	1160	1120	1145	1140	1100	1120	1073	1055	1155	-

Table .7. Typical set of interferometer readings

Mean thickness by interferometry = 1014 $\pm$ 50 Å

Film thickness at substrate = 926 Å (from Table. 6)

Film thickness with reference to quartz crystal = 942 Å

treatment of errors.

$$\text{Let } m = \frac{\lambda'}{\lambda^\circ - \lambda'} \qquad \ldots\ldots\ldots\ldots\ldots (4.12)$$

and let λ' be measured correctly. Consider the effect of an error $\delta\lambda$ in λ°,

$$\bar{m} = \frac{\lambda'}{(\lambda^\circ + \delta\lambda) - \lambda'} \qquad \ldots\ldots\ldots\ldots\ldots (4.13)$$

Consider the error in $\delta\lambda$ necessary to render m incorrect by one complete order.

$$m - \bar{m} = 1 \qquad \ldots\ldots\ldots\ldots\ldots\ldots (4.14)$$

and therefore:

$$\delta\lambda = \frac{(\lambda^\circ - \lambda')^2}{2\lambda' - \lambda^\circ} \qquad \ldots\ldots\ldots\ldots\ldots (4.15)$$

For a typical order of 30 and $\lambda' = 5000$ $\overset{\circ}{A}$, equation 4.12 gives λ° as 5167 and hence a value of $\delta\lambda$ of 5.8 $\overset{\circ}{A}$. Similarily if an error $\delta\lambda$ exists in opposition in both λ° and λ' then

$$\delta\lambda = \frac{(\lambda^\circ - \lambda')^2}{3\lambda' - \lambda^\circ} = 2.8 \overset{\circ}{A}$$

Readings to 1 $\overset{\circ}{A}$ are thus necessary for accurate results inferring the use of sharp, fine fringes and a high resolution spectrometer. Following extensive calibration it was determined that within the limits of experimental error the thickness indicated by the oscillating quartz crystal method agreed with the results

obtained by multiple beam interferometry.

4.3. Structure of evaporated bismuth films.

4.3.1. X-ray analysis of bismuth films

It is known that bismuth films deposited on glass substrates display under certain conditions a preferred orientation. The orientation has been noted by several authors [100] and in general the structure depends both on the condensation mechanism and the surface mobility of the adatoms. Palatnik [74] has shown that independent of the material and crystal lattice types there exist two critical condensation temperatures T_1 and T_2 related to the melting point of the material. Within the range of temperatures $T_2 < T < T_1$ preferred orientation is predominant, and those prepared for the present investigation were evaporated at about 60° Celsius. Each evaporated film was subjected to an X-ray analysis.

The A.S.T.M. crystallographic index uses the hexagonal lattice system to describe bismuth in which the princpal Bragg reflection occurs for the [102] set of planes having a d-spacing of 3.28 Å. In the presence of an orientation in which the trigonal axis is normal to the plane of the film there will be a proportionately stronger reflection from the basal [003] plane. The [003] d-spacing is 3.95 Å.

For a randomly orientated deposit the relative diffracted intensities are related by,

$$\frac{I_{[002]}}{I_{[003]}} = \frac{100}{9} \quad \ldots\ldots\ldots\ldots \quad (4.16)$$

Any deviation from this condition would be an indication of a preferred basal orientation. Applying the Bragg relationship to chromium $K\alpha$ radiation the reflecting conditions are given by:

$$2d \sin\theta = n\lambda$$

$$\lambda_{Cr} = 2.29 \text{ Å}$$

$$\therefore \theta = \sin^{-1} \frac{2.29}{2d}$$

For $[102]$ planes,

$$\theta = 20^\circ 26' ; \quad 2\theta = 40^\circ 52'$$

For $[003]$ planes,

$$\theta = 16^\circ 51' ; \quad 2\theta = 33^\circ 42'$$

Using a Bragg diffractometer (Fig. 53) the substrate and detector were linked in such a way as to receive only a diffracted beam from crystal planes lying in the plane of the film within a range 2θ from 29° to 43°.

Figure 55(i) taken on a film of 2045 Å thick was typical of the graphs obtained and gives an indication of the degree of orientation existing in the films. A true quantitative estimate of the percentage of trigonal axes residing normal to the surface was impracticable as any attempt to reduce the $[003]$ peak to below full scale deflection caused the $[102]$ peak to be lost in the background count. An estimate of the areas contained under the two peaks indicated a ratio of about 100: 1. Combined with the inverse ratio of 100: 9 for a randomly oriented specimen this indicated almost total preferred orientation. On many other films the degree of orientation was such that the $[102]$ peak could not be distinguished from the background.

A bulk specimen, prepared by vacuum casting, showed a random orientation (Fig. 55ii) as would be expected, whilst the ribbon specimen showed a preferentially orientated $[102]$ peak possibly caused by the rolling process in manufacture.

The simple Bragg diffractometer, whilst providing a rapid check on each film as it was produced was unable to give

FIG.53

BRAGG DIFFRACTOMETER

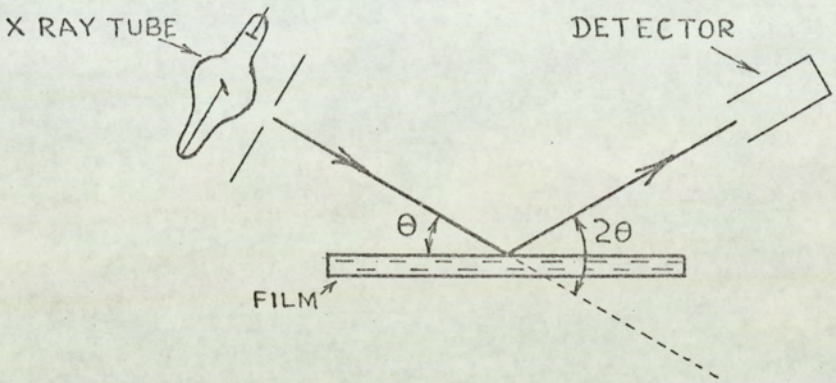

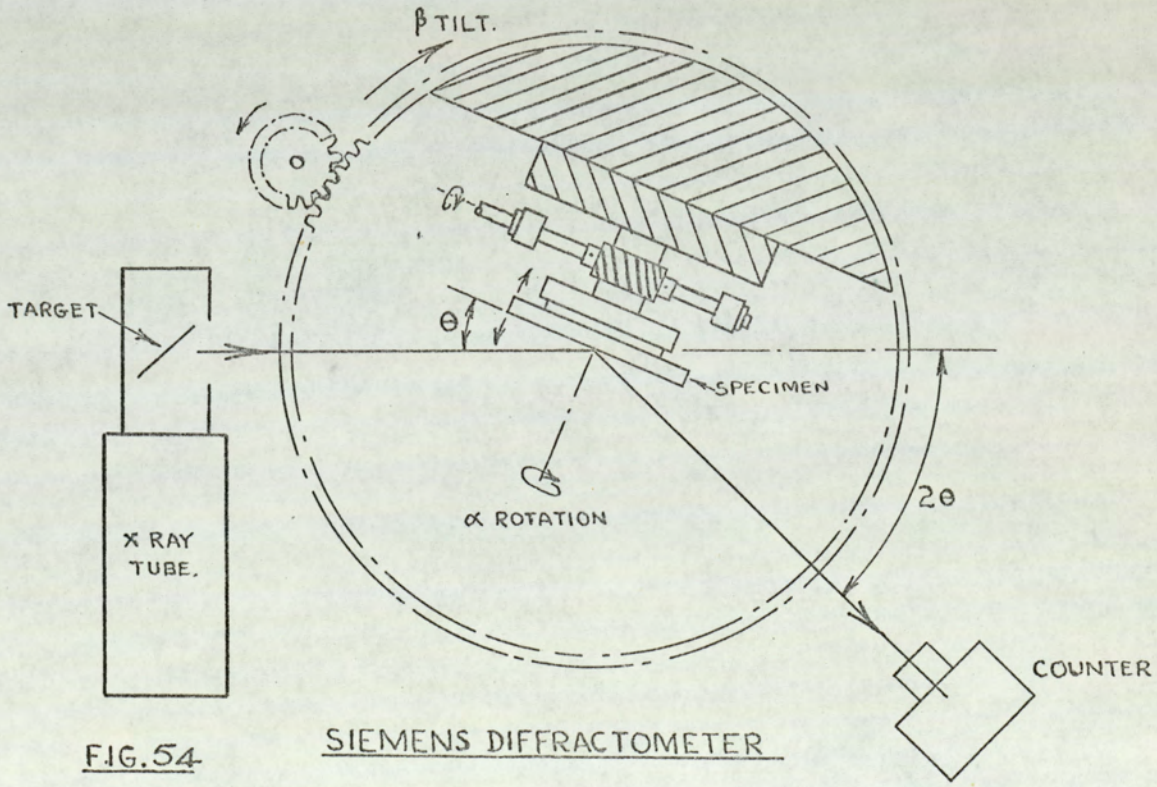

FIG.54

SIEMENS DIFFRACTOMETER

SHOWING THE GREAT CIRCLE AND RECIPROCATING TABLE.
THE ARROWS INDICATE THE POSSIBLE MOTIONS OF THE TABLE.

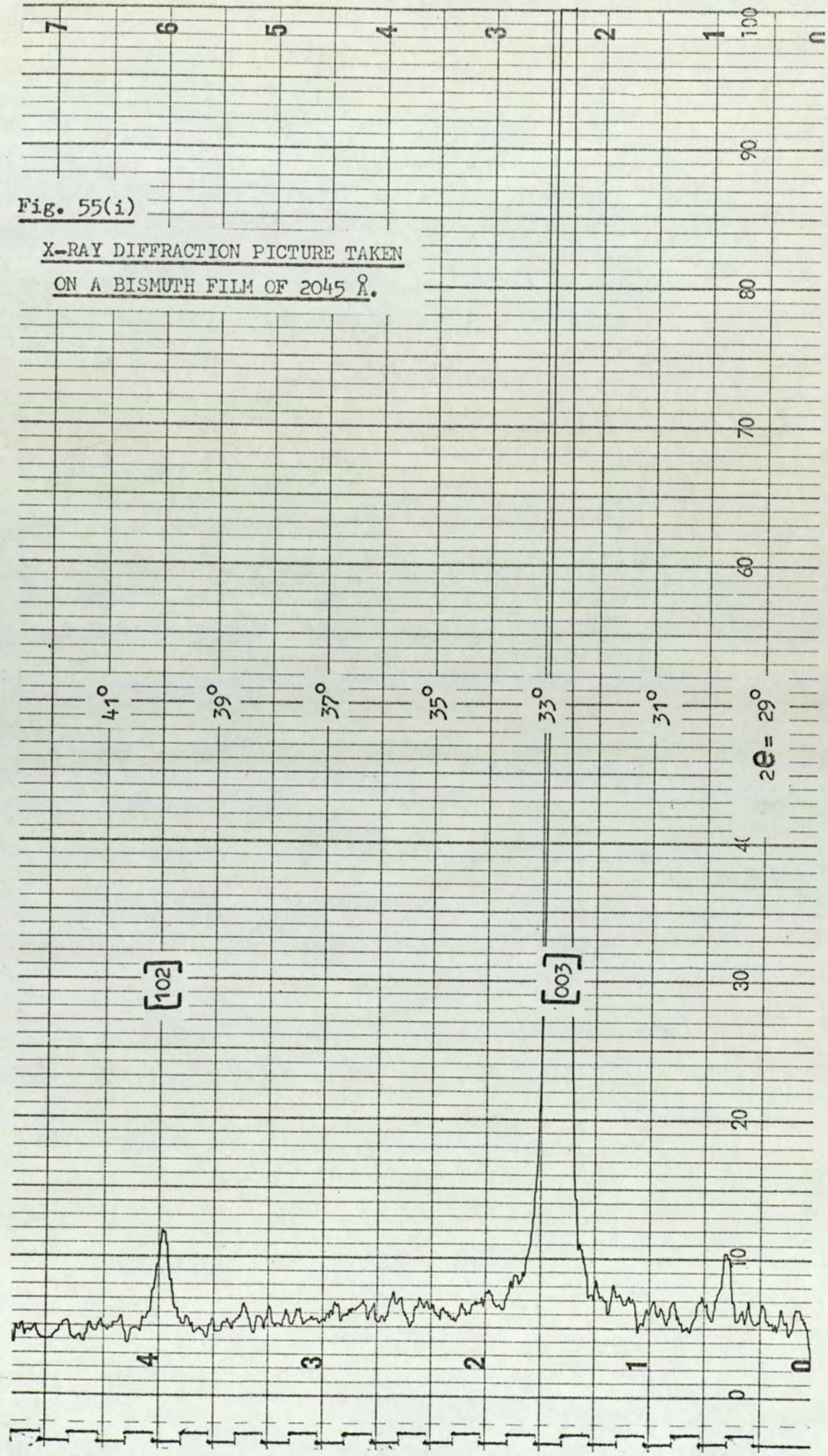

Fig. 55(i)

X-RAY DIFFRACTION PICTURE TAKEN ON A BISMUTH FILM OF 2045 Å.

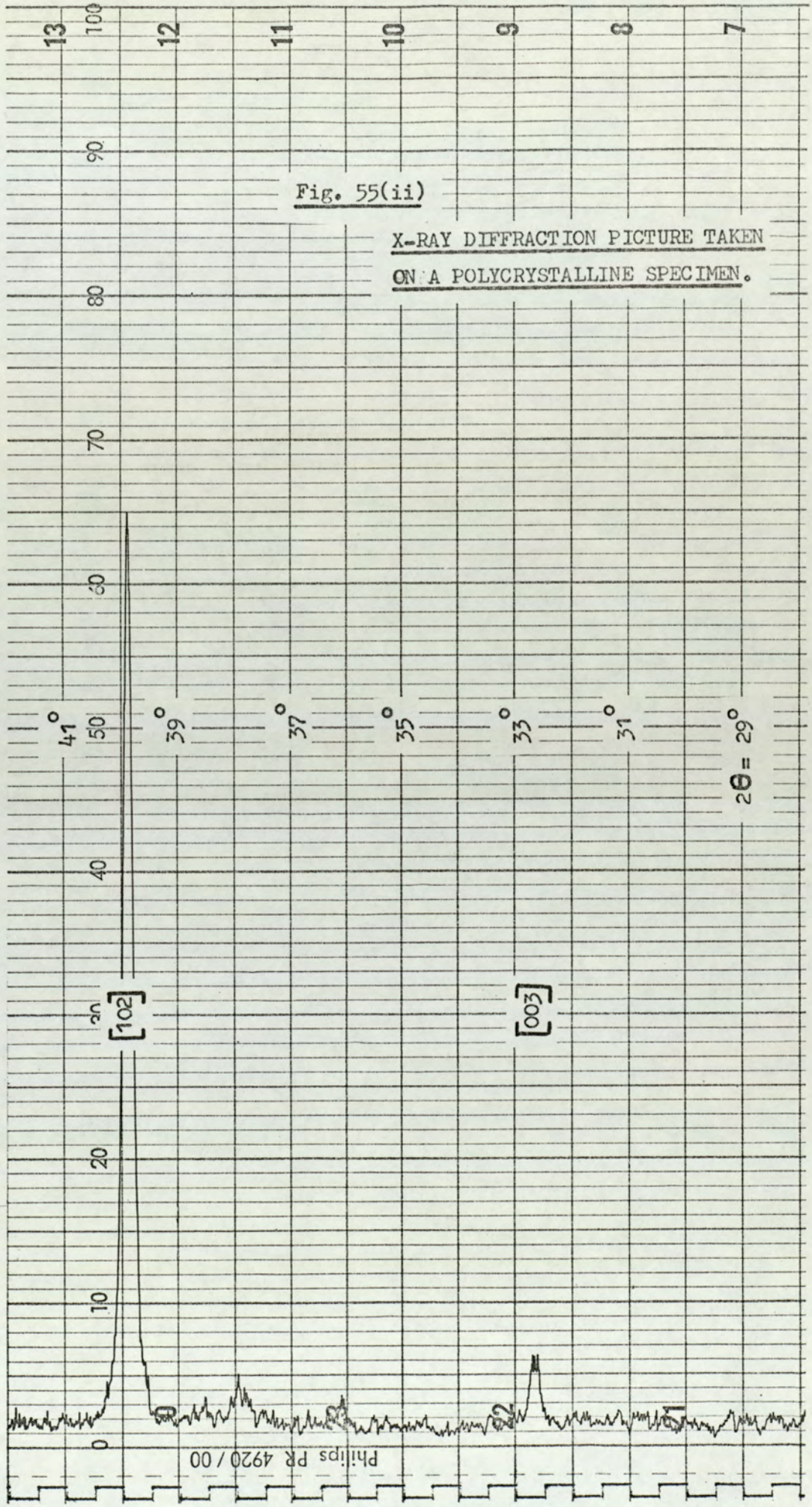

Fig. 55(ii)

X-RAY DIFFRACTION PICTURE TAKEN ON A POLYCRYSTALLINE SPECIMEN.

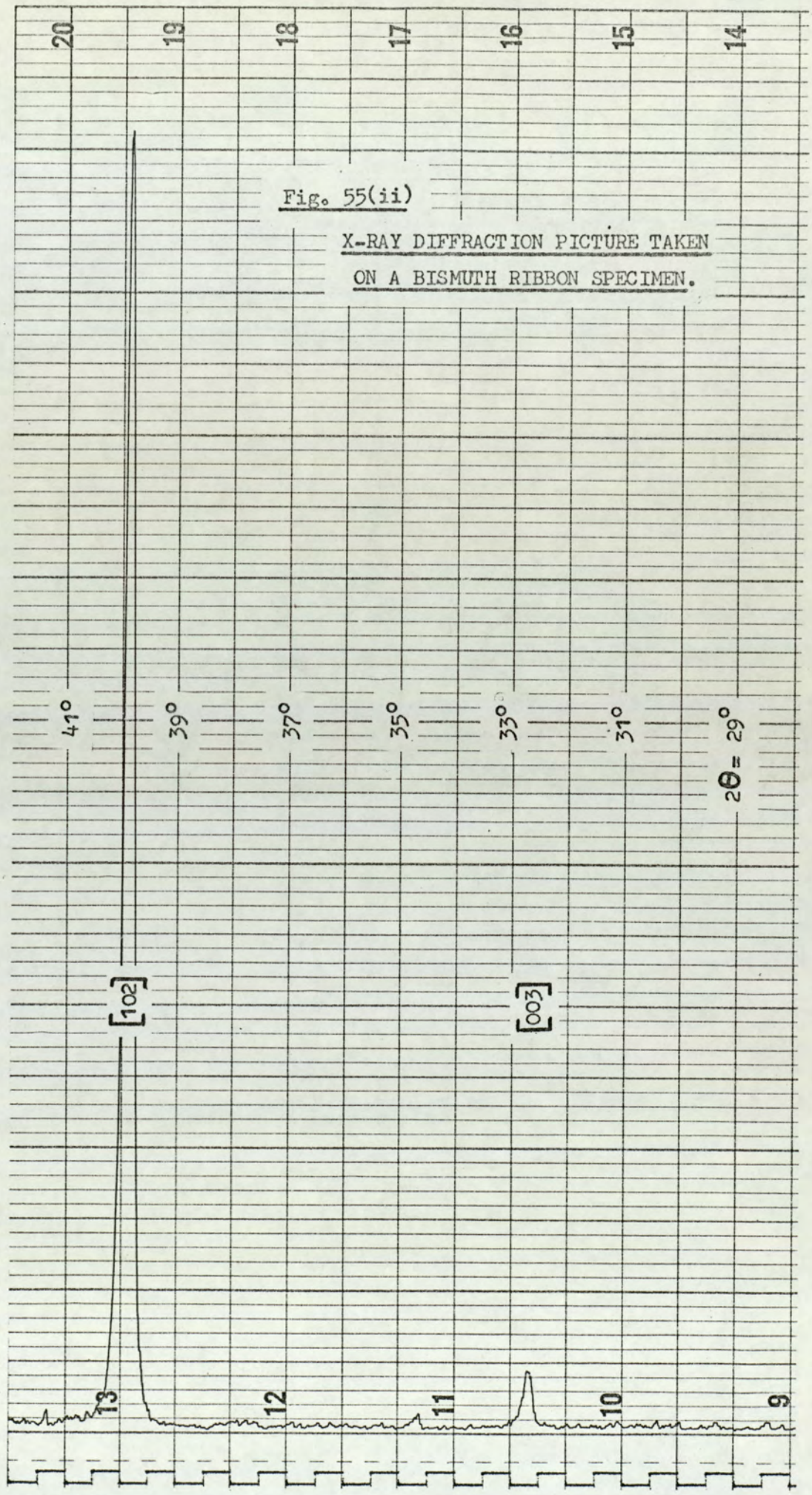

Fig. 55(ii)

X-RAY DIFFRACTION PICTURE TAKEN ON A BISMUTH RIBBON SPECIMEN.

insight into either the small angular spread of trigonal axes about the normal to the film, or a possible orientation of the isotropic axes of the crystallites within the film. An instrument capable of achieving this was the Siemens diffractometer having a rotatable goniometer head as shown in Fig. 54 . The experimental films were not of sufficient size to be used directly and a series of samples were prepared having a diameter of 1 cm. A Bragg Diffractometer check verified the expected orientation.

The essential feature of the Siemens instrument was the presence of a great circle toothed wheel meshing with an epicyclic gear. The smaller gear carried a specimen table. A motor driven assembly enabled the table to be rotated through the vertical to the inverted position such that it remained on a chordal path. A simultaneous reciprocating motion served to given an overall picture. Provision was also available for rotating the table at a fixed angle, about its normal. A collimator slit directed a fan of X-rays towards the great circle.

With the table in the 90° position the diffractomter reverted to the simple instrument and the θ and 2θ angles were set for the [003] planes. A small adjustment to obtain a maximum reading took care of mal-alignments of the goniometer head. Keeping θ° and $2\theta^{\circ}$ fixed in this way only the [003] planes were detected but their radial distribution about a vertical normal could be determined. A set of readings were taken around the great circle and the graphical plot obtained was entitled a North-South (arbitrarily defined) radial scan. Fig. 56(i) shows that within the accuracy of the experiment all the trigonal axes were aligned perpendicular to the substrate surface. An East-West radial scan gave a similar picture.

To produce a pole figure for the [102] planes it was

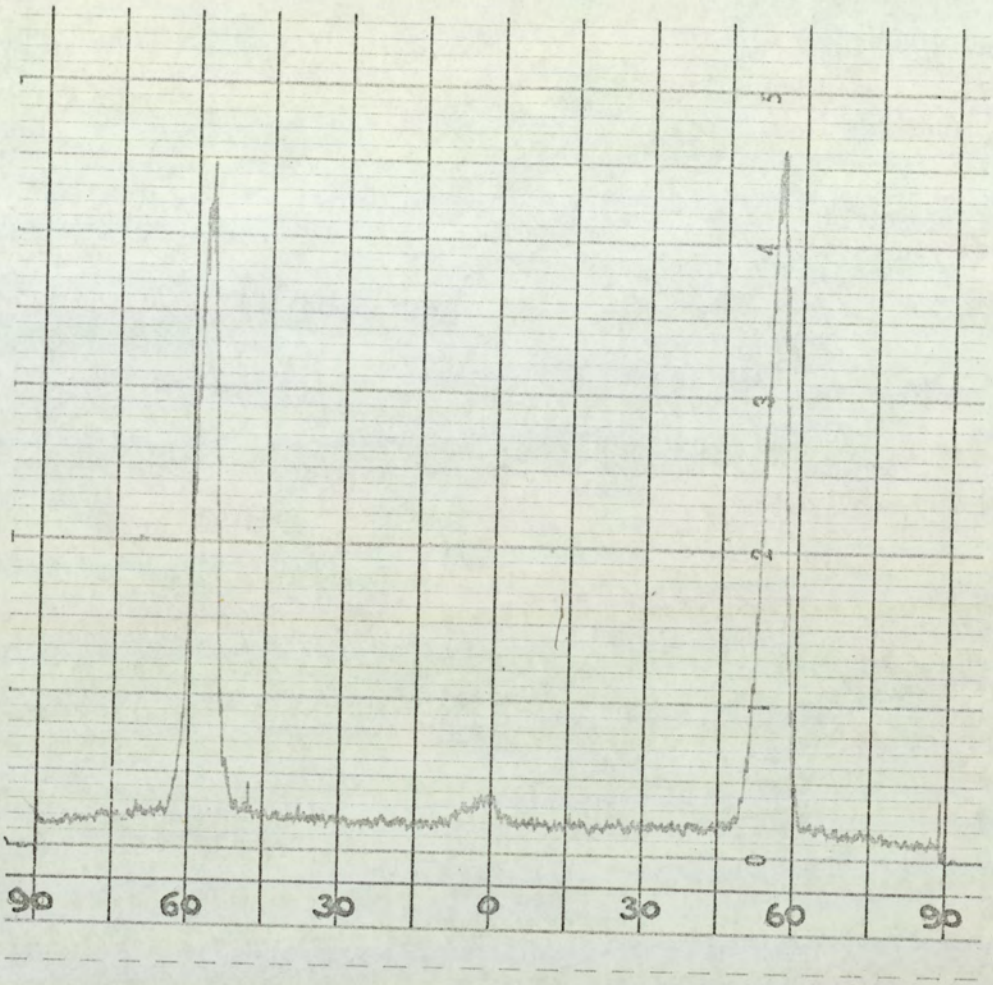

Fig. 56(i) North-south radial scan.

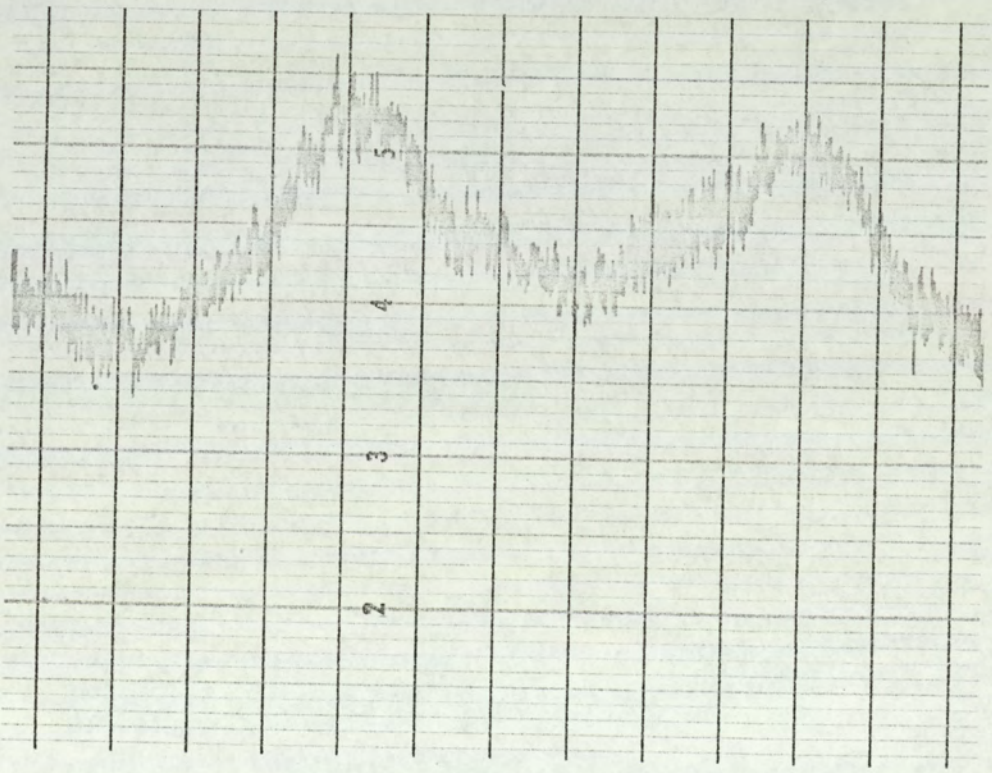

Fig. 56(ii) Circular scan.

necessary to evaluate the angle between the [003] and [102] planes and to reset the beam angle to suit.

$$\theta = \tan^{-1} \tfrac{1}{2} = 26^\circ 34'$$

$$\therefore 2\theta = 53^\circ 8' .$$

In practice an indicated setting of 57° gave a maximum reading. A north-south radial scan of the [102] planes is given in Fig.56(i). The final step was to read from the figure the exact angle of the planes with respect to any goniometer error and fix the specimen at that inclination on the great circle. A rotation about its own axis gave a circular scan indicating the distribution of crystalites in the plane of the film. The indicated preferred orientation (Fig.56(ii)) of 15 - 20% was of little significance when related to the sharpness of the radial scan peak and amounted to only about $\pm 2^\circ$ from the maximum position. The accuracy of the mechanical alignment was not guranteed to exceed this figure and a three dimensional figure produced by bracketing the setting by $\pm 1^\circ$ verified that mal-alignment was in fact the cause of an apparent orientation.

In summary therefore it can be said that the bismuth films had a near perfect orientation of the trigonal axes normal to the film surface, whilst the orientation of the crystallites in the plane of the film was random.

4.3.2. Investigations into grain size and topography of bismuth films.

The work of Newman [48] showed that for polycrystalline bismuth films with the trigonal axis aligned perpendicular to the surface normal, there existed a thickness related grain size. The mode of the crystallite diameter hystrogram was some 30% in excess of the thickness of the film. No figure was given for the varience

of the distribution, a knowledge of which would have been useful in discussing the amplitude of the quantum oscillations predicted in chapter 2. In the absence of this however an attempt was made to reproduce Newman's graph with a view to obtaining such information but met with difficulties. The sample films deposited at 1×10^{-6} torr could not generally be removed from the substrate without possible structural damage to such a mechanically weak material, even using the technique of floating into dilute nitric acid [52]. Carbon shadowing of cellulose replicas produced specimens which were far from satisfactory considering the small order of magnitude of the grain size to be studied. A sample polaroid photograph is shown in Fig. 57 taken on a film of 2000 Å. The clusters of small grains in certain areas of the picture are of the approximate size required to be in agreement with Newman but the large areas without specific detail prevented the extraction of quantitative data. Further attempts to investigate the grain size were made using a scanning electron microscope (S.E.M.)

A series of five films were examined at four magnifications up to the maximum of 155,000 times. At these magnifications the extreme flatness of the surface rendered focussing so difficult that atmospheric dust had to be admitted to the specimen surface to give depth of focus. Fig.58(i) illustrates a typical set of photographs at four magnifications taken on a film of nominally 1000 Å. A notable feature of the photographs was the absence both of intrinsic dust from the vacuum chamber (differentiated from admitted particles by shadowing) and of any trace of pinholing.

The S.E.M. technique of monitoring the intensity of a beam of electrons reflected from the conducting specimen to produce a three dimensional effect approached its maximum resolution for the anticipated grain size and an exact interpreation of the

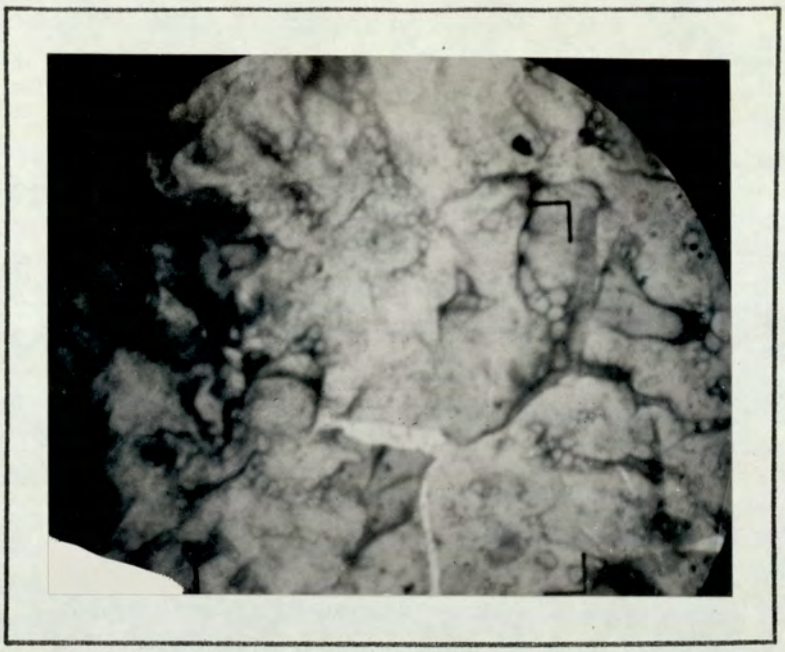

Fig. 57. Polaroid photograph of a bismuth film of 2000 Å. Approx X 4000, taken by means of a carbon replica in an electron microscope.

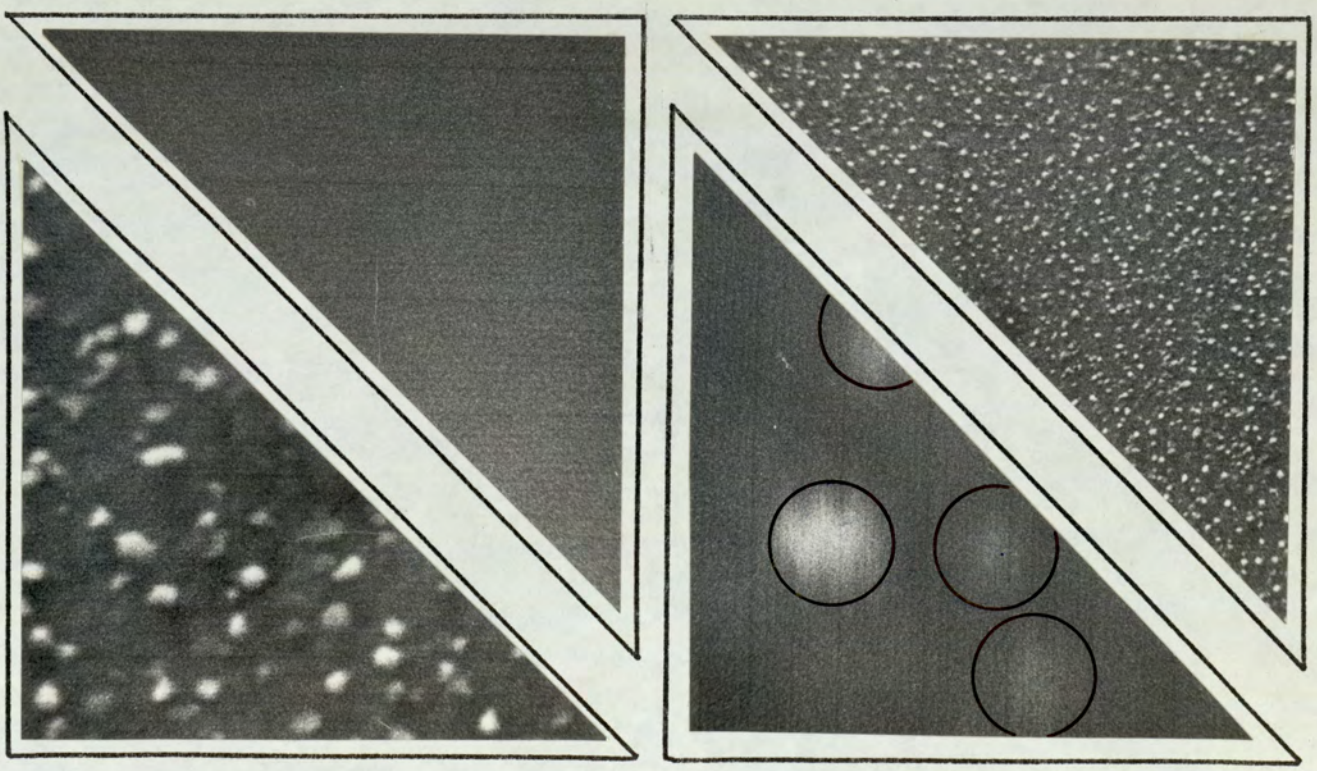

Fig. 58(i). S.E.M. photographs of a bismuth film of 998 Å at magnifications of X155, X7.5K, X30K, X150K. Overdrawn circles represent a grain diameter of 1434 Å.

photographs became more difficult. One saw as white only those parts of the surface that were inclined such that electrons were received specularily at the detector. Assuming that a single columnar growth as reported by Kooy (75) was applicable to bismuth two idealised interpretations of the S.E.M. photographs became possible:-

(i) that the density of white regions directly indicated the size of the grains on the basis of one spot per grain. A topography was envisaged similar in appearance to a bubble-raft in which there would be a contribution to the photograph from each grain by virtue of the dome-type of termination.

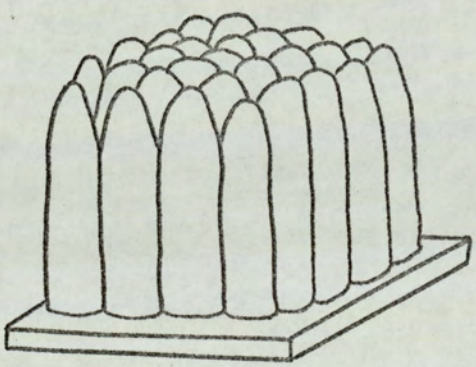

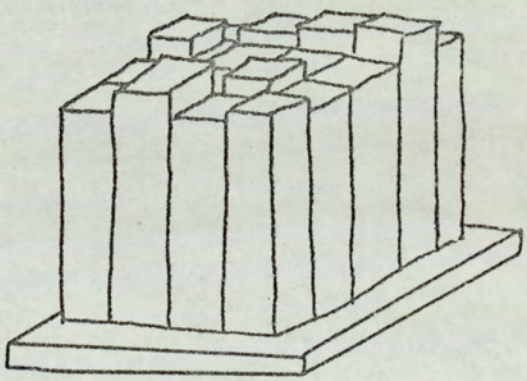

(ii) that a white region represented the upper surface of a grain, but only those grains suitably inclined towards the detector would appear on the photograph. Preferential growth of a few grains could produce such areas whereas the general background of diffuse scattering may represent many grains. The spot size itself would be indicative of grain size. The mechanism is readily feasible when reference is made

to films evaporated under conditions of oblique incidence of the vapour stream [101]. Such films exhibit a low reflectivity due to the preferential growth towards the source of surface asperities.

It is difficult to say which of these two possibities existed. A combined picture would suggest that the white region represented an upstanding grain, but that the actual grain size was somewhat larger than the area of the spot due to low intensity in the reflected beam receiving from the edges of the grain. A closer look at Fig.58 showed that the photographs consisted of a dark background having distinct white areas together with a haze of paler white regions. The paler regions can be observed on the two higher magnification photographs enabling measurements to be made. The remainder of Fig. 58 represents the range of photographs taken on the other four films examined. There is a general densening and enlarging of the white spots as the thickness increases inferring a possible increase in surface rougness with growth of grain. There is however little difference between the photographs taken at nominally 2000 Å and 4000 Å suggesting that the condensation of grains had terminated and that bulk growth was taking place. The circles drawn on the 155,000 times magnification photographs were considered to reasonably represent the area of a grain. A graph, Fig. 59 was plotted of grain diameter against film thickness indicating a 1: 1 linear relationship, displaced by some 400 Å along the grain size axis.

In conclusion a comparison of the present analysis with that of Newman and Ko certainly indicated a common trend in which the grain size was related to the film thickness. The difficulty and uncertainty in attempting to provide a more quantitative picture

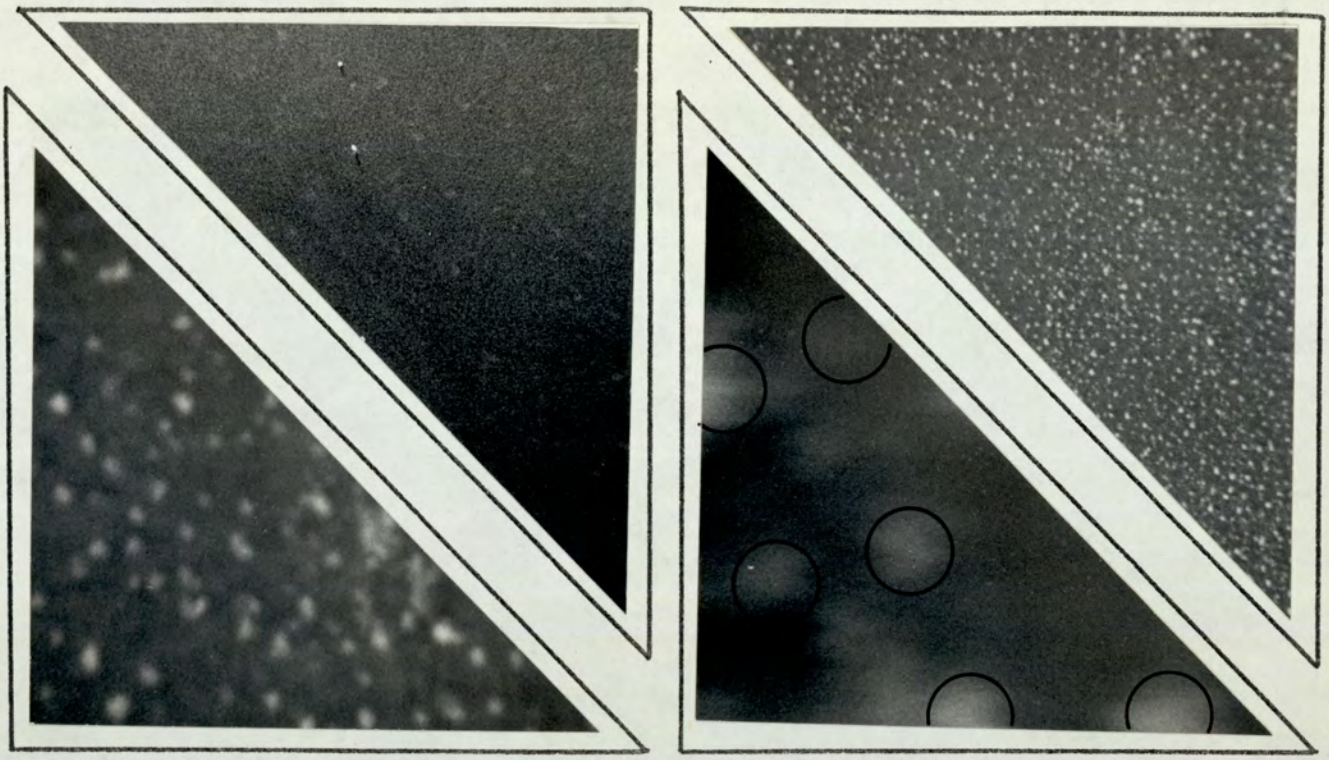

Fig. 58(ii). S.E.M. photographs of a bismuth film of 500 Å at magnifications of X155, X8K, X31K, X155K. Overdrawn circles represent a grain diameter of 956 Å.

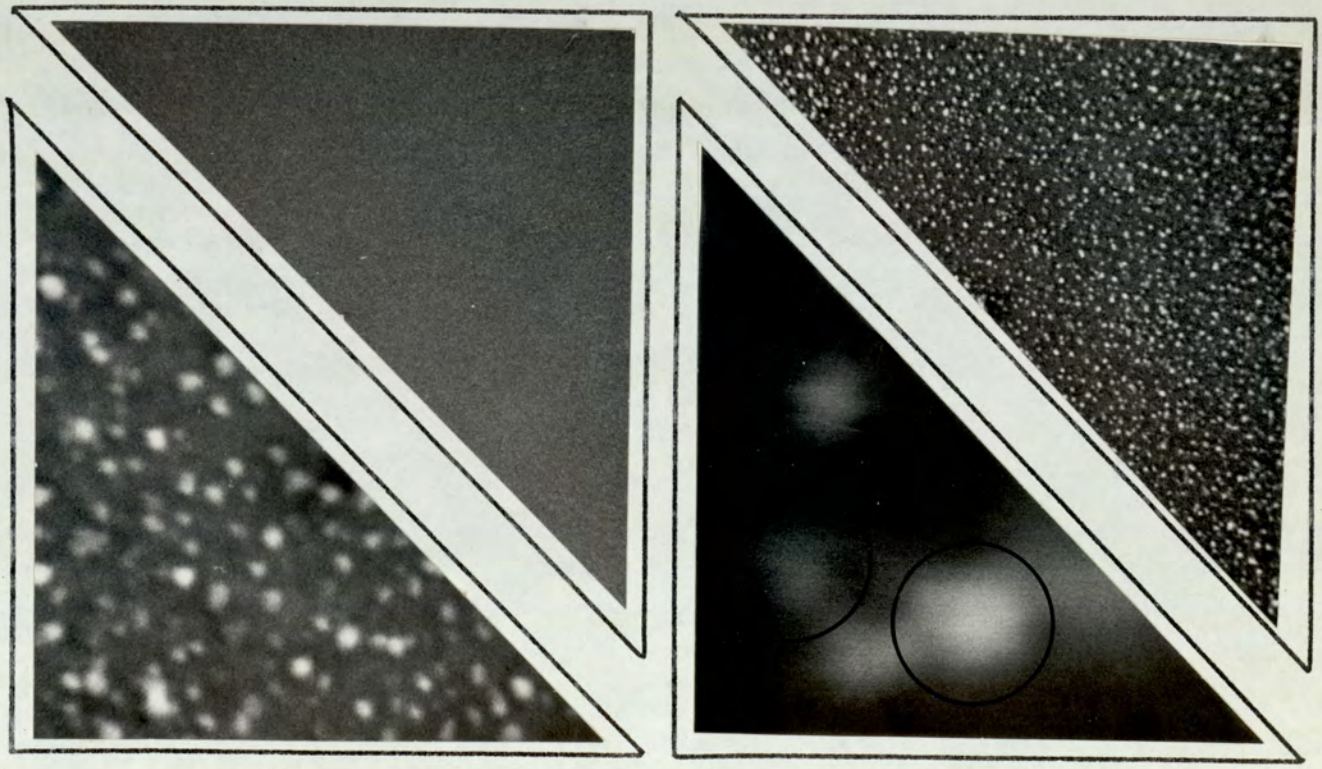

Fig. 58(iii). S.E.M. photographs of a bismuth film of 1457 Å at magnifications of X155, X8K, X31K, X155K. Overdrawn circles represent a grain diameter of 1844 Å.

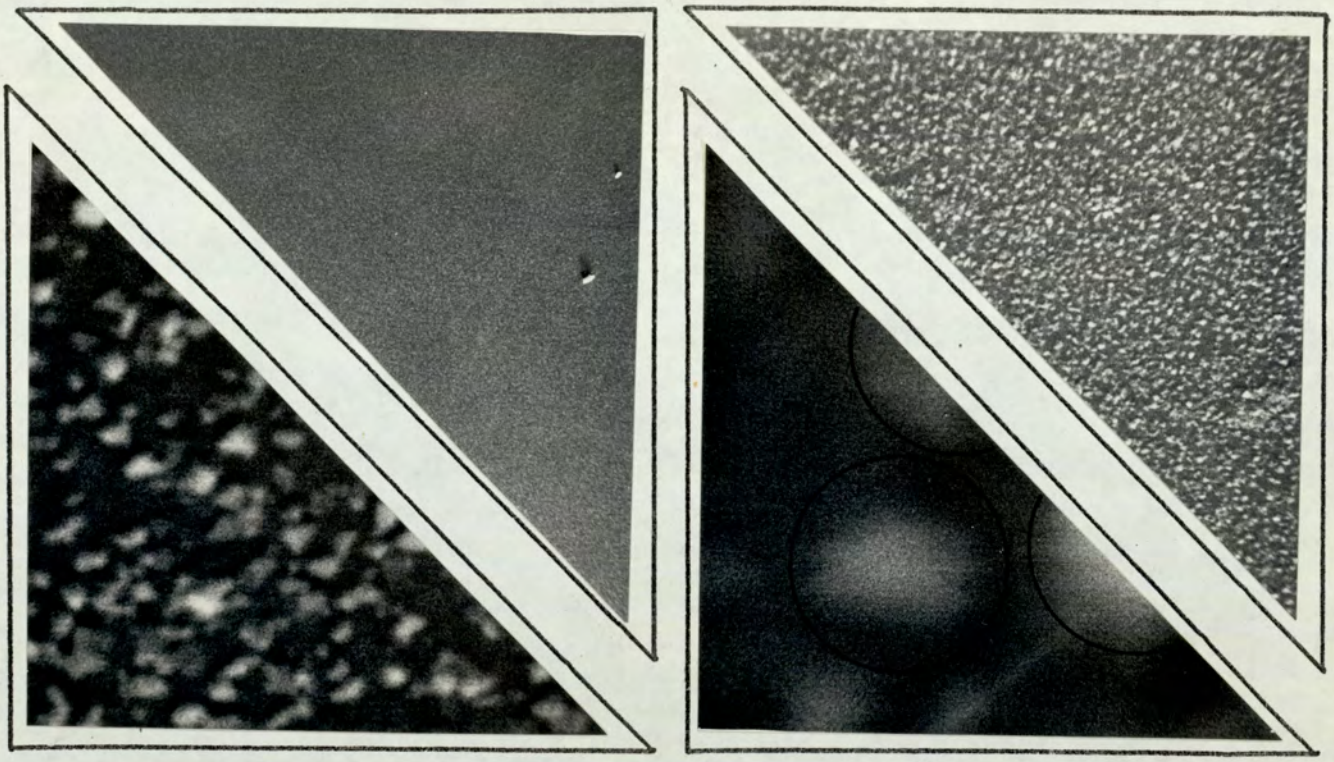

Fig. 58(iv). S.E.M. photographs of a bismuth film of 1905 Å at magnifications of X155, X7.5K, X31K, X155K. Overdrawn circles represent a grain diameter of 2458 Å.

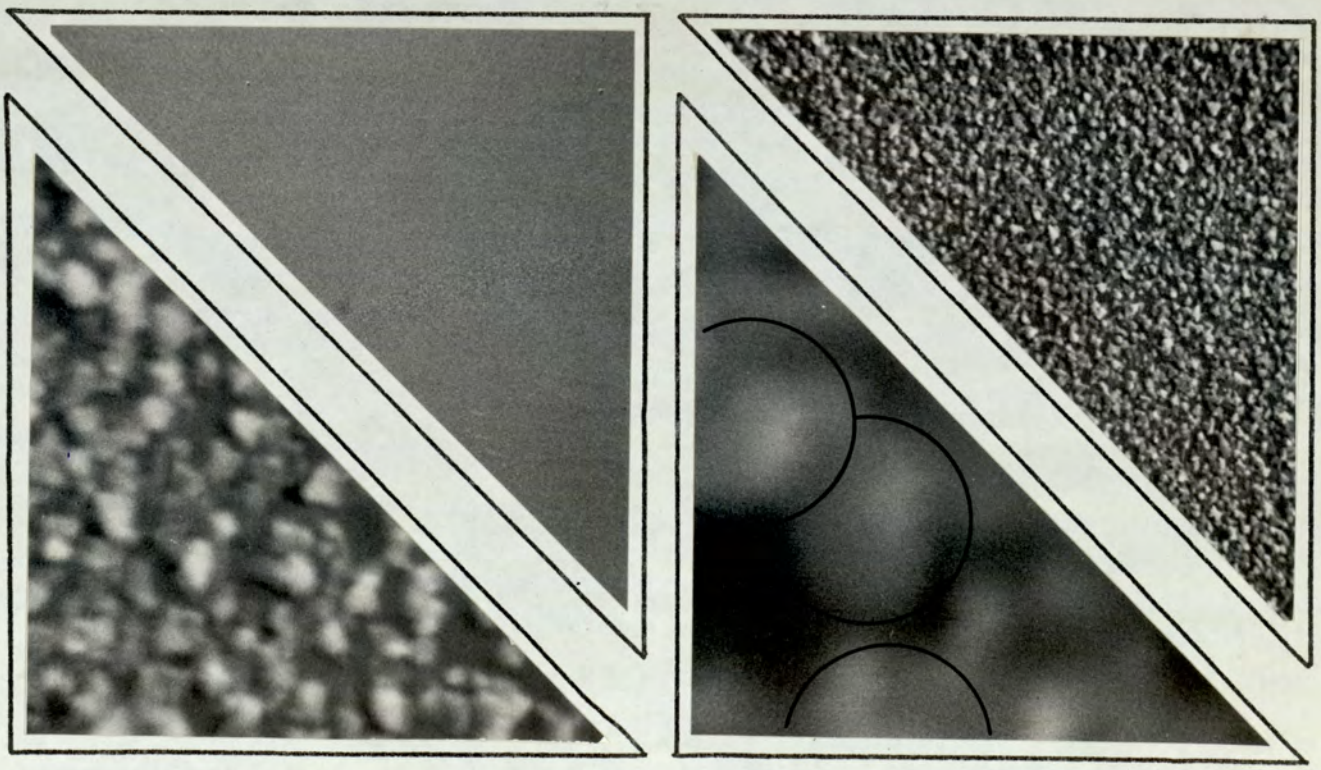

Fig. 58(v). S.E.M. photopraghs of a bismuth film of 3820 Å at magnifications of X155, X8K, X31K, X155K. Overdrawn circles represent a grain diameter of 2403 Å.

was however a limiting factor. The following chapters will be analysed in the light of a possible contribution from this source to the electrical properties of bismuth films.

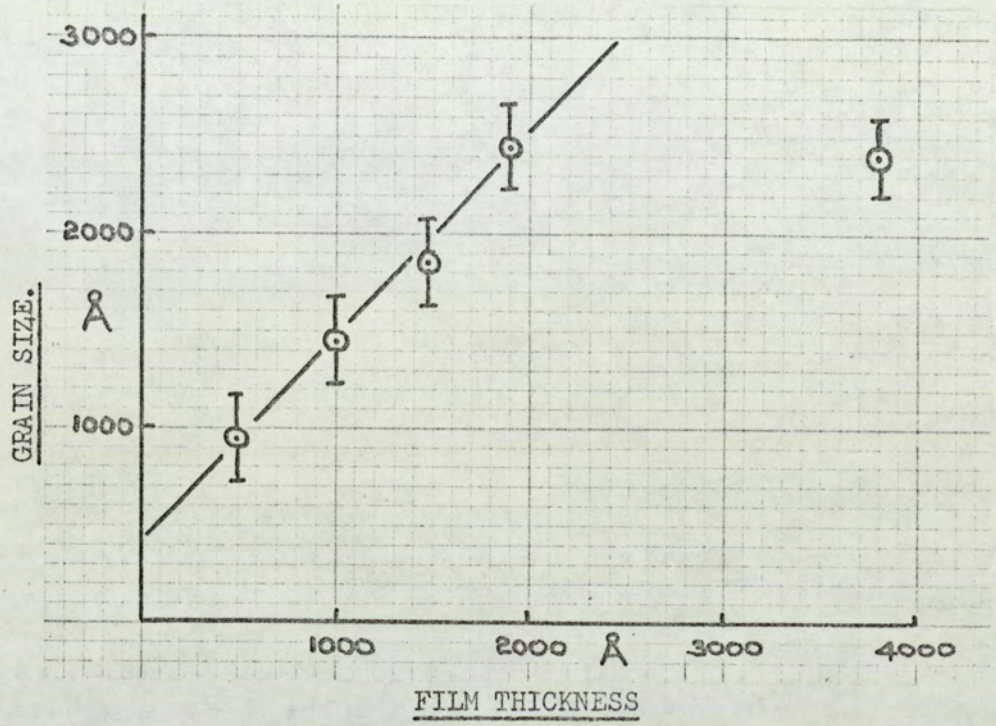

Fig. 59. Relationship between film thickness and grain size.

4.4. Evacuated rig for holding specimens

An assembly was required in which to hold a thin film perpendicular to the applied magnetic field, and at the same time enable the film temperature to be maintained within the range 77 - 300°K. Condensation considerations required the system to be evacuated, and a rig of slim proportions was desirable in order to achieve the highest possible magnetic fields. Provision was required to carry electrical leads from the film to the external measuring equipment.

An assembly meeting those requirements is shown in Fig. 60. The outer case had an upper manifold with provisions via two hand valves for evacuating the rig and for the admission of dry helium gas from a reservoir. A 2" hand screwed fitting at the upper end carried a series of transistor headers giving a total of fifteen possible leadthroughs each of 500 mA rating. The thin walled stainless steel tube terminated in an hemispherical cap from which

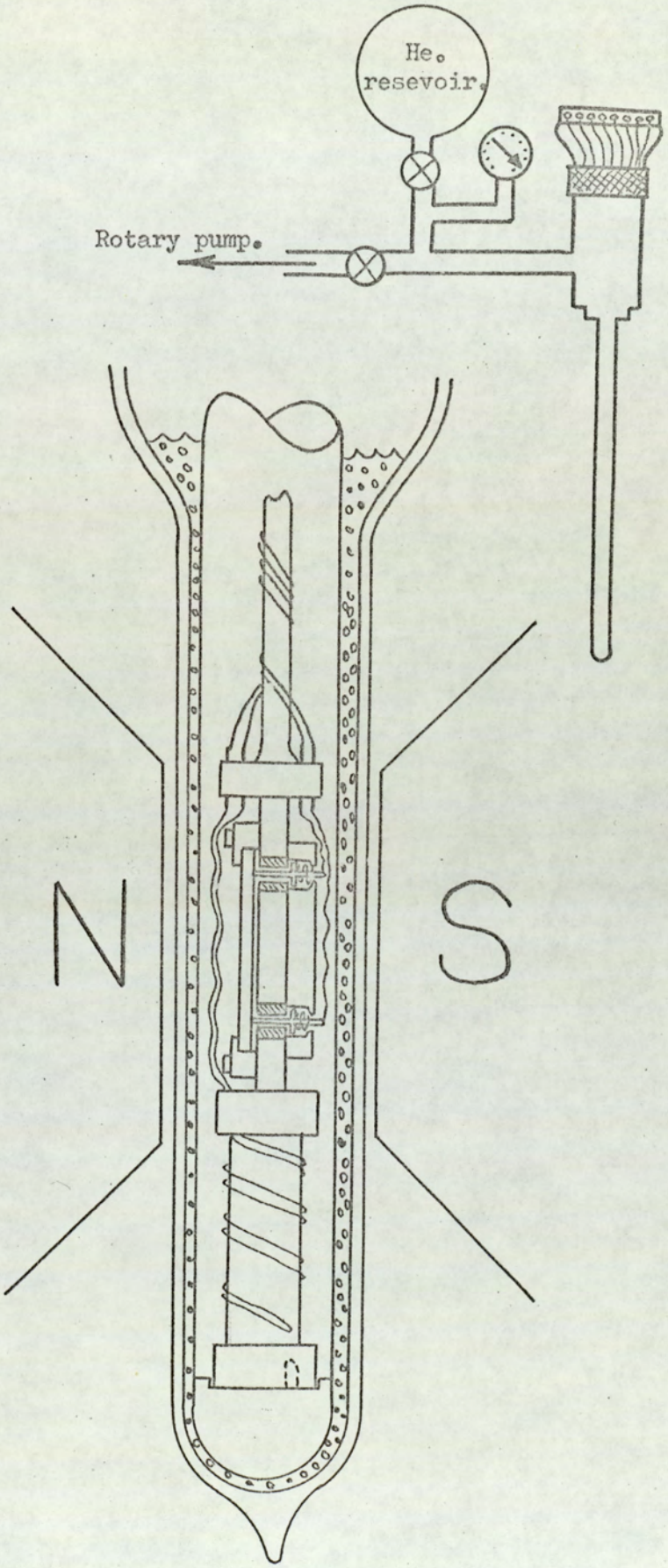

Fig. 60. Electromagnet rig showing the pressure contact assembly with two of the spring-loaded contacts.

extended a locating spiggot. The whole assembly was contained within a narrow-tailed dewar of liquid nitrogen.

The removable interior had at its lower end a brass spool carrying the substrate backing plate and perspex electrode holder. A coil of 38 s.w.g. Eureka wire was wound non-inductively around the spool giving a total resistance of 300 Ω. The small pressure contact assembly described in section 3.3. was mounted on the backing plate so that its pins extended to meet the surface of the inverted film. An applied coil voltage caused a thermal gradient to be set up within the spool enabling the temperature of the backing plate to be varied. A current of 300 mA was found to raise the temperature to 300^{o}K. The approximately 10^{o}K increment caused by a 15 mA change in heater current required 8 - 10 minutes to re-establish equilibrium, the film itself forming a sensitive resistance thermometer.

The temperature coefficient of resistivity of bismuth films in the 1000 $\overset{o}{A}$ region was determined to be approximately -2.5 mV $^{o}K^{-1}$. The photocell galvanometer amplified used had a sensitivity such that a change of 0.1 mV was readily detectable (typically $\pm$ 1 on the fourth significant figure of the voltage drop along the film). A change in film temperature of $\pm$ 0.04 ^{o}K could be observed. Following the establishment of equilibrium a variation greater than $\pm$ 0.04 ^{o}K was not observed over an extended period.

4.5. Magnetic Field Supply

A proprietory Newport Instruments Ltd. electromagnet was used as a source of magnetic field. It consisted of a 7" diameter conical pole water cooled electromagnet built on a "window frame" yoke and mounted on a rotatable base. The power supply was derived from a d.c. generator capable of developing 6.25 KW. The output of the generator was fed to a control unit which stabilised the supply to better than $\pm$ 1 part in 10^{5}. A helical potentiometer enabled the

current to the magnet to be varied up to the maximum continuous rating of 22 amperes, an external diagonal scale ammeter being used to monitor the currents. A block diagram is shown in Fig. 61.

Facilities were not available on the supply for reversing the magnetic field and hence a simple load switching network was constructed. The magnetic field was reduced to below three amps at which a chang-over switch introduced a dummy load of 11 Ω. The magnet supply leads were reversed with a second change-over switch and the dummy load removed. Failure to introduce a resistive load resulted in an automatic sweep to maximum output voltage.

Repeatable settings of the current were possible to 0.1% by means of the vernier ammeter.

Throughout the investigation only one pole gap setting of 4.0 cm. was required. A Newport Instruments type H magnetometer using a Hall effect indium arsenide sensor was used to measure the magnetic field over the whole range of magnet currents. A manufacturers calibration of true versus indicated field was employed at higher fields and the resultant graph of magnet current versus true field strength is shown in Fig. 62 . The maximum continuously available field was 1.25 Kilogauss and the quoted accuracy of the field reading was better than $\pm$ 2% over the range used.

4.6. External electrical monitoring equipment

An external electrical network was required in order to measure the longitudinal resistance and magneto resistance voltages, the transverse Hall voltages and the current through the film.

The current supply was obtained from a 0 - 30 volts d.c. power supply stabilised to better than 1 part in 10^4. The output could be varied in 0.1 volt steps and was fed to the film via a reversing switch. A 10 Ω $\pm$ 0.02% oil-filled standard resistance was placed in the line, the voltage across which was measured

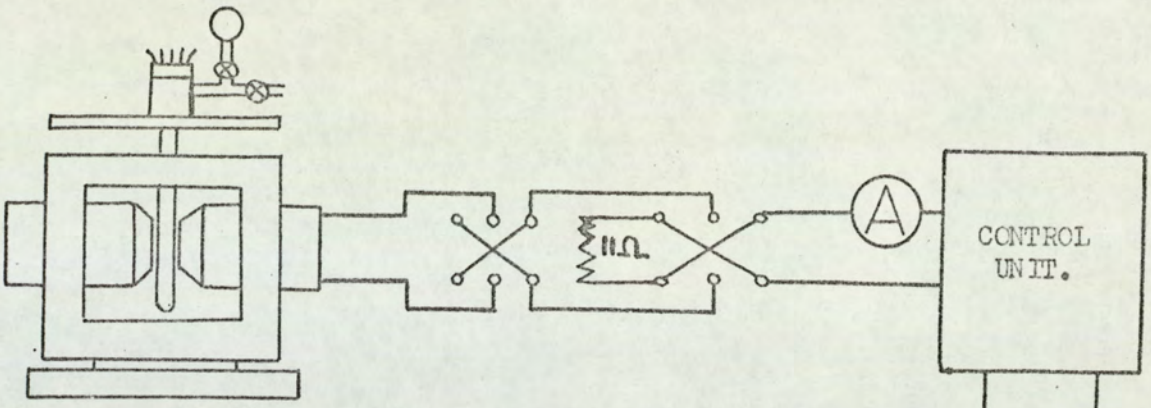

Fig.61(i). Electromagnet block diagram.

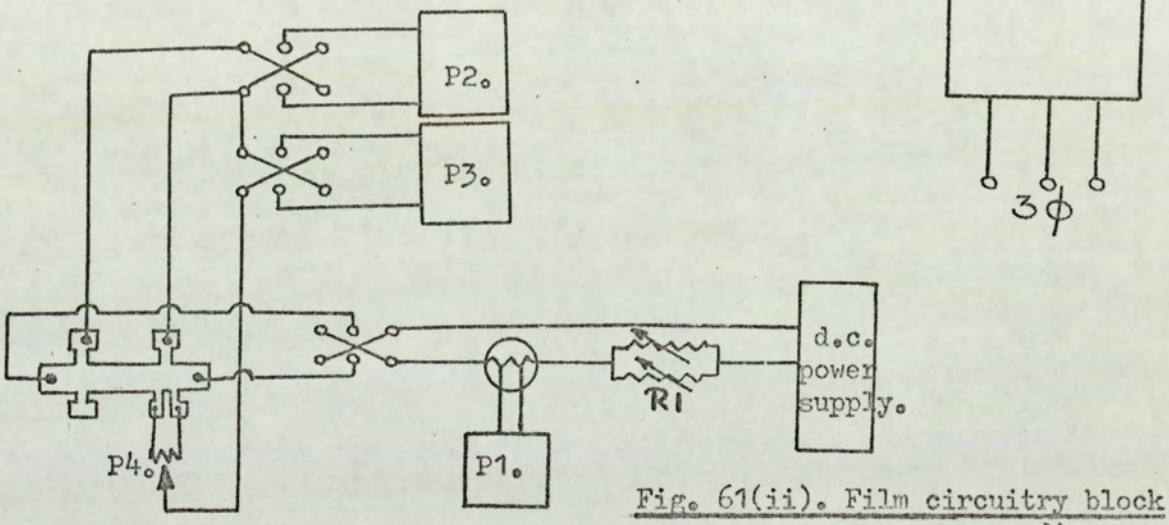

Fig. 61(ii). Film circuitry block diagram

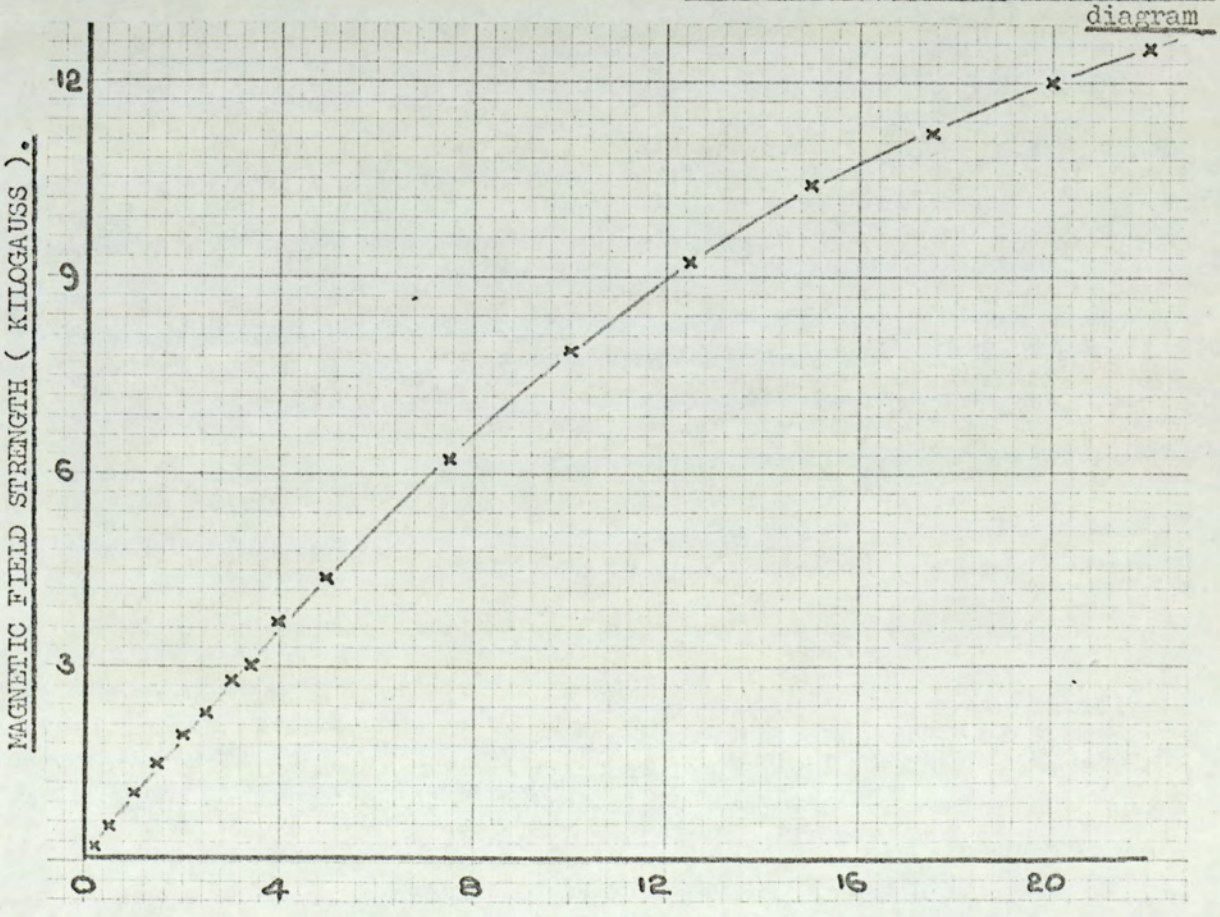

Fig. 62. Calibration curve for electromagnet.

potentiometrically on P1. (Fig. 61(ii)). At a pre-determined current a zero galvanometer deflection was maintained by adjusting the decade resistance box R1. It was found necessary to place a further box of higher resistance in parallel with the first in order to give a finer degree of control.

A centre zero reversing switch and similar potentiometer P2 reading four consecutive digets down to 1μV enabled the voltage drop along the film to be measured.

The two side arms of the film were joined by a variable potentiometer P4 of about 50Ω, whose wiper acted as a variable probe to minimise the standing voltage. A potentiometer reading five consecutive digets down to 10^{-1} μV was used.

Whilst potentiometers 1 and 2 made use of conventional "Scalamp" moving spot galvanometers, the Hall potentiometer P3 operated a photocell galvanometer amplifier. The out of balance voltage activated a spot of light directed between two photocells. The heavily damped deflection of the spot caused a differential between the outputs of the two photocells, resulting in a deflection of a second galvanometer. A gain control was available to alter the deflection sensitivity which at its maximum setting corresponded to a full scale deflection of 10^{-7} volt. Environmental conditions did not allow this maximum sensitivity to be employed and a practical compromise was a full scale deflection of about 1μV.

The reversing switches and terminals were mounted in a cabinet (observable on the general view photographs) in such a way that when the current switch dolly was in a position defined as positive, a similar position on the other two switches corresponded respectively to a positive voltage drop along the film and a positive Hall voltage. Using this simple convention a sign could be readily allocated to a given observation.

4.7. Systematic Separation of the required voltages

The required voltages V_R, the voltage drop along the film, V_M, the increment in V_R due to the application of a magnetic field, and V_H, the transverse Hall voltage cannot be read directly. They have superimposed upon them a combination of standing voltages V_S and thermal voltages V_T which need to be eliminated from the calculations. For a positive magnetic field perpendicular to the films and a positive film current direction defined consistantly with the Lorentz force on moving carriers to give a negative Hall field, Table 8 indicates the presence of the various combinations of voltages, assumed constant during a set of readings.

	Positive Magnetic Field		Zero Magnetic Field	Negative Magnetic Field	
Film current	transverse voltage	longitudinal voltage	longitudinal voltage	longitudinal voltage	transverse voltage
+	V_1 $(V_H+V_S+V_T')$	V_2 $(V_R+V_M+V_T)$	V_3 (V_R+V_T)	V_4 $(V_R+V_M+V_T)$	V_5 $(-V_H+V_S+V_T')$
-	V_6 $(-V_H-V_S+V_T')$	V_7 $(-V_R-V_M+V_T)$	V_8 $(-V_R+V_T)$	V_9 $(-V_R-V_M+V_T)$	V_{10} $(V_H-V_S+V_T')$

Table 8. Component voltages arising in thin film measurements.

The Table was drawn up on the following basis, (i) that the absolute Hall voltage changed sign when either the film current or magnetic field were reversed, (ii) the standing voltage, V_S, arising from the mal-alignment of probes inverted on changing the film current direction and (iii) the thermal voltages, V_T and V_T'

arose when the contact-film junction was at a different temperature to the adjacent film-contact junction, and was directionally invarient.

In addition to the ten voltage readings mentioned, readings were taken of the film temperature and the corresponding film current. Since the film current was maintained at a fixed value throughout, only its sign was noted.

The following shows the procedure for obtaining the individual voltages,

$$V_R = \tfrac{1}{2}(V_3 - V_8)$$

$$V_M = \tfrac{1}{4}\left\{(V_2-V_3) + (V_4-V_3) - (V_7-V_8) - (V_9-V_8)\right\}$$

$$V_H = \tfrac{1}{4}(V_1 + V_{10} - V_5 - V_6)$$

The magnetoresistance was obtained by taking the dimensionless ratio V_M/V_R, and the coefficient from further division by the squared magnetic field strength.

The resistivity was expressed as:-

$$\rho = Z_1 \times V_R \qquad \Omega\text{-M}$$

where $Z_1 = \dfrac{w \times t}{i \times L}$

w = width of film in metres

t = thickness of film in metres

i = film current in amperes

L = probe spacing in metres

The Hall coefficient was expressed as:

$$R_H = Z_2 \times V_H \qquad M^3/\text{coulomb}$$

$$\text{where } Z_2 = \frac{t}{-i \times H}$$

H = applied magnetic field strength in webers/metre^2

The computation of results was undertaken using an ICL 1905, 32K - core digital computer. The Algol programme to evaluate the galvanomagnetic and resistivity coefficients directly from Table 8 without intermediate reference to the individual component voltages is shown in Appendix 11 and entitled "primary computation". Full results are reproduced for a typical film.

Twelve observations were required to obtain a value of resistivity, magnetoresistance and Hall coefficient on one film, at one temperature and at one applied field. On each film an observation was performed at 20 fixed temperatures between 77^{o}K and 300^{o}K at each of two magnetic fields, supplemented at five fixed temperatures by observations at ten magnetic fields. For the thirty films successfully examined the total of over 32,000 observations provided no small problem in the complete representation of data, as every reading contributed equally to the ultimate quantum oscillation graphs. It is for this reason that all results will be given in the "Experimental Results" chapter at a stage immediately following the primary computation.

Whilst S.I. units form the basis of the reported work, two exceptions exist in the presentation of data. Traditionally film and optical distances have been reported in Angstrom units instead of the more correct dimension, the nanometer (1nM = 10 $\overset{o}{A}$). In addition the copious supply of measuring instruments and literature

produced by electromagnet manufacturers led to the retaining of the Kilogauss as a unit of applied magnetic field strength (1 $W/M^2 = 10^4$ gauss). The anomaly existed only until the primary computation where the conversion factors were built-in to the multiplying constants.

CHAPTER 5

EXPERIMENTAL RESULTS

5.1. Introduction

The experimental results obtained from the measurements of resistivity, magnetoresistance and Hall coefficient of thin bismuth films are presented. The purpose of this work was to investigate comprehensively the properties of films in the condition 'as evaporated' and observed after exposure to an atmospheric environment. It is appreciated that greater stability is introduced to a film by thermal or strain annealing, and the topic will be included as a suggestion for further work. However, the effect of such processing in bismuth may lead to a masking of a process of fundamental importance to the solid state "purist". No more than a preliminary introduction of the results is presented in this chapter, each section being discussed in chapter 6.

The range of observations can be represented as a three-dimensional array of points whose axes are as follows:-

(i) thickness. Films of preferred orientation were examined over a thickness range from 200 to 2000 $\mathring{A}$ in 50 $\mathring{A}$ increments, together with additional results on a film of 4500 $\mathring{A}$, a ribbon specimen 150μthick, and a randomly orientated bulk specimen.

(ii) temperature. Readings were taken at temperature intervals between 77^{o}K and 300^{o}K. Approximately 10 - 15^{o}K increments were used on runs entitled "temperature variation run", whilst a 50^{o}K increment resulting in five fixed temperatures was

used on a "field variation run".

(iii) magnetic field. Transverse magnetic fields between 0.22 Kilogauss and 12.5 Kilogauss were applied to the films. Two "temperature variation runs" were performed at fixed magnetic field strengths. The "field variation run" was then undertaken at each of the five fixed temperatures at ten magnetic field strengths.

Results will be presented of preliminary experiments designed to test the accuracy and limitations of the readings. Films as evaporated are known to undergo structural changes for several hours due to self annealing processes, followed by the formation of an equilibrium layer of oxide which may modify the conduction processes at grain boundaries. As a result it was necessary to confirm that Ohm's law held for such films. An estimate was made of the thickness of oxide formed on films during the first few days of film life.

The precise alignment of a small film within the interior of an evacuated container perpendicular to an applied magnetic field required careful adjustment. A polar diagram for Hall coefficient and magnetoresistance was plotted. Results will then be presented of resistivity, magnetoresistance and Hall effect with the magnetic field normal to the film surface.

A summary of the dimensions and current densities of the examined films is presented in Table 9 , each film being identified by its quoted thickness value. The current density range employed lay between 2 and 15 x 10^6 A/M^2.

5.2. Preliminary Investigations

5.2.1. Electrical measurements on freshly evaporated films

An analysis was performed on a film of nominally 1000 Å to observe the variation of the resistivity from the time of deposition.

Table 9 . Summary of bismuth films examined

Film thickness (Å)	Current Density $A/M^2 \times 10^{-6}$
Bulk (3.8 x 5.5 mm)	0.025
Ribbon (150 μ)	0.60
4500	12.86
2045	12.73
1697	4.09
1587	4.38
1501	4.62
1409	4.93
1287	5.40
1270	5.47
1220	3.79
1201	3.85
1100	4.21
1067	4.34
1025	4.70
927	4.99
862	9.67
801	5.78
744	5.60
735	6.30
650	2.14
609	6.08
552	2.52
504	6.89
451	3.08
401	8.13
357	3.89
309	8.24
258	5.38
211	6.57

A series of 40 s.w.g. enamelled copper wires were soft-soldered to a substrate having evaporated copper borders. The evaporator was evacuated to 1×10^{-6} torr. The use of the maximum output from the d.c. power supply together with a suitably high series "buffer" resistor predetermined the film current. A film of 1000 Å was evaporated at 10.6 Å/second and the termination of evaporation defined the time T = 0. Readings were taken over several hours until no further change in resistance was observed. The film was then exposed to the atmosphere and readings taken over several days. Fig. 62 illustrates the observations taken on a 1000 Å film.

The film resistivity was observed to decrease with time over the initial period when the effect of substrate cooling alone following deposition would cause the resistivity to increase. Bismuth films of this thickness are shown to have a negative temperature coefficient of resistivity. The magnitude of the decrease was some 3% and was considered to be due to the self-annealing of the film. 100 minutes after deposition a minimum was observed in the resistivity, followed by a region of linear increase due to the final return of the chamber interior to laboratory temperature. No further change was observed after 180 minutes. Extrapolating the linear portion of the curve to the ordinate led to the conclusion that the substrate (as opposed to the film surface) suffered a temperature change of 1° K during evaporation. The copper heat sink and re-entrant cold finger contributed to the thermal inertia of the substrate.

The system was returned to atmospheric pressure with an air supply dried by passage through liquid nitrogen. An immediate increase in resistivity occurred within the first 15 seconds of admission of the gas, but readings showed a maximum to occur after a total of 30 seconds had elapsed, followed by a minimum after 60 seconds. A logarithmically linear increase in resistivity was

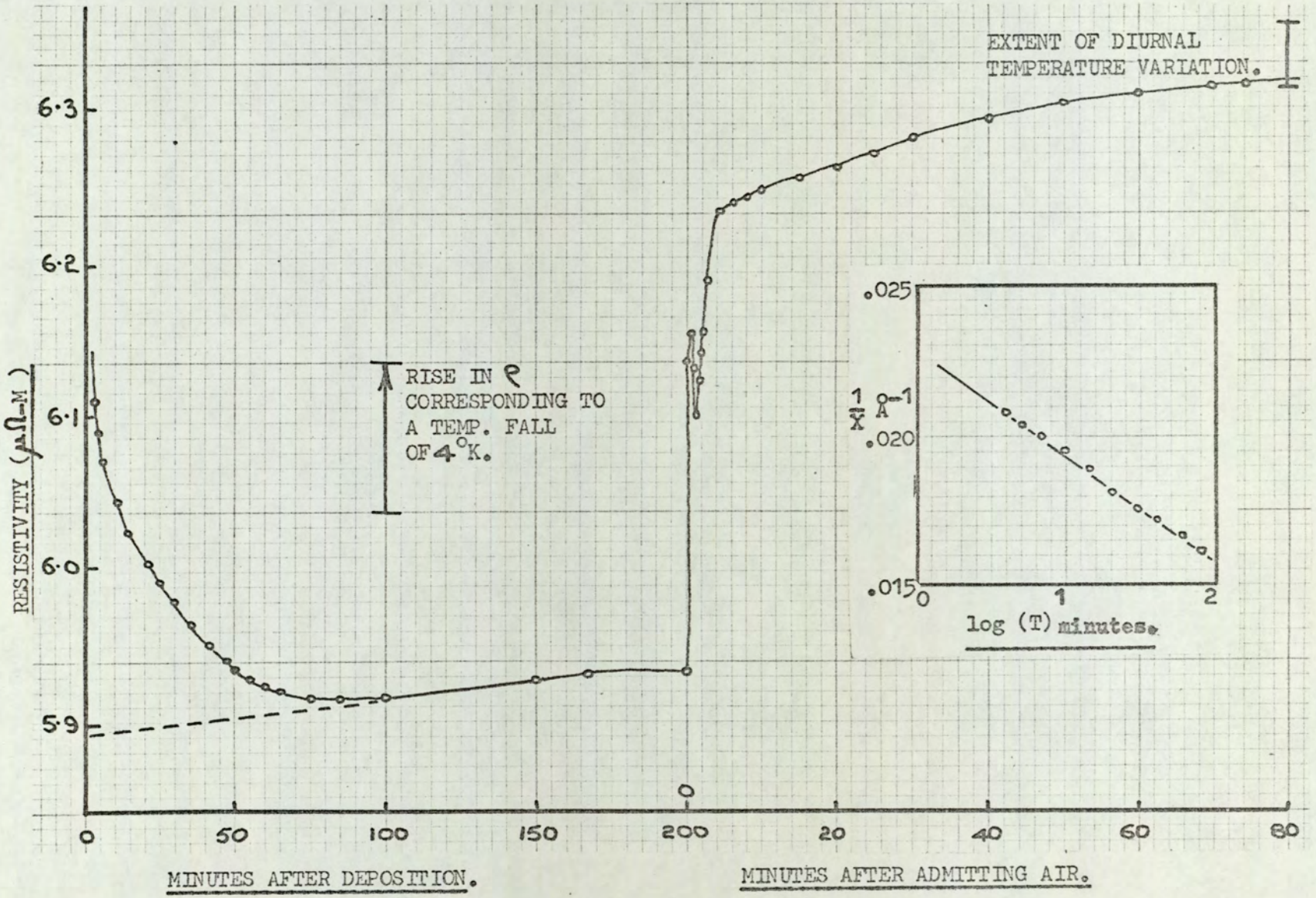

Fig. 62. The oxidation and self-annealing of bismuth films.

then observed for 30 minutes as the equilibrium layer of oxide grew. An hour later, further changes were masked by the diurnal variation in laboratory temperature which could be easily monitored. The initial peak superimposed on the oxidisation curve was equivalent to a $2^{o}K$ fall in film temperature and could have arisen due to the chilling effect of the refrigerated admitted air.

5.2.2. Ohms Law

At a film-age of three days a range of electric fields was applied to verify that Ohms law held for the polycrystalline thinly oxidised films (Fig.63.). For fields in the interval $1 - 20 \times 10^{6}$ A/M^{2} the mean deviation from a constant resistivity value of $6.325 \mu\Omega$-M was less than 0.3%.

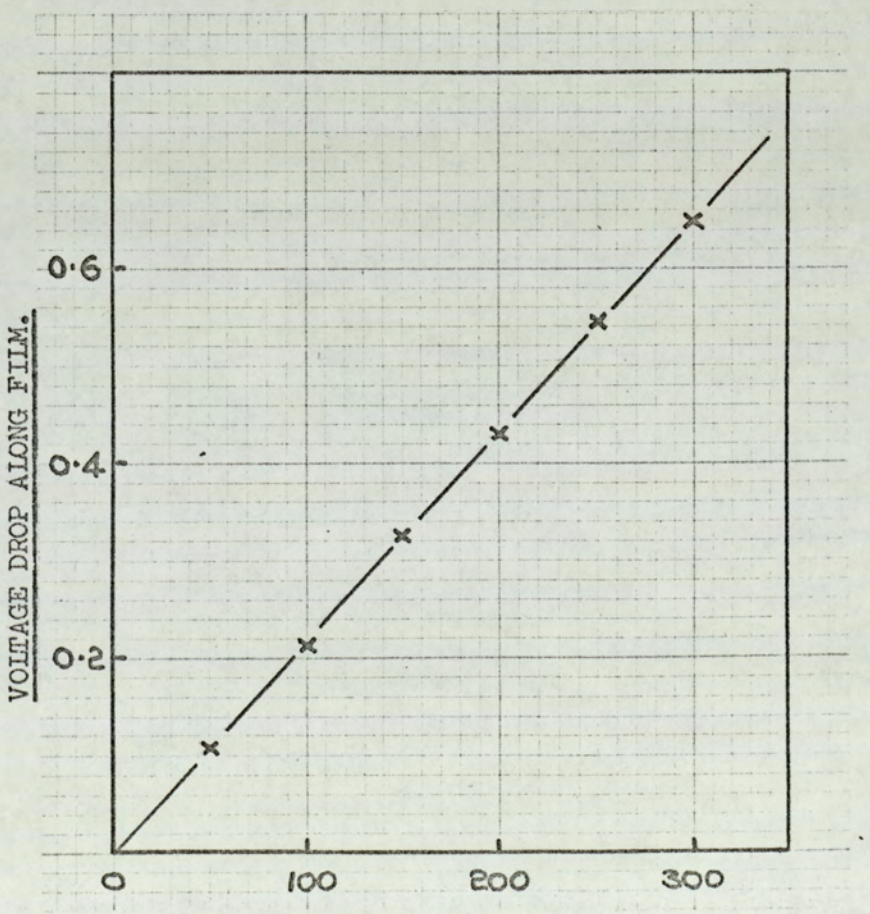

Fig. 63. The validity of Ohm's Law for bismuth films.

5.2.3. Hall coefficient and magnetoresistance pole figures

A simple protractor device was attached to the electromagnet film carrying jig to enable the film to be rotated through 360°. Measurements were taken of Hall and magnetoresistive voltages for the 552 Å film at 5° intervals. A polar diagram (Fig. 64) shows the magnitude of the two coefficients with respect to the fixed film. An arbitary scale has been used.

The Hall coefficient was a maximum with the magnetic field perpendicular to the film, and zero in the orthogonal position. As the magnetic field moved from the normal position the Hall field, which was mutually perpendicular to the magnetic field and current, had a reduced component at the fixed Hall probes, resulting in a reduction in R_H. The slight depression of the Hall coefficient in the normal position was however not explained.

As discussed in chapter 2 a magnetoresistance results from the decreased mean free path due to the Lorentz Force. This is somewhat offset by the Hall effect which constrains the carriers of an optimum velocity to a straight path. Film boundaries however restrict the magnetoresistance further for carrier directions not orthogonally related to the magnetic field. Rotating the film introduced a large dimension perpendicular to the Hall field thus removing the boundary contribution. The pole figure is seen to have a minimum with the magnetic field normal to the film. A close look will reveal small deviations from an otherwise smooth curve which reflect the presence of crystal planes of symmetry (102). This is additional evidence of the precise orientation of the crystallites in the film.

Utilising the unexplained depression in the otherwise maximum value of the Hall coefficient it was possible to ensure

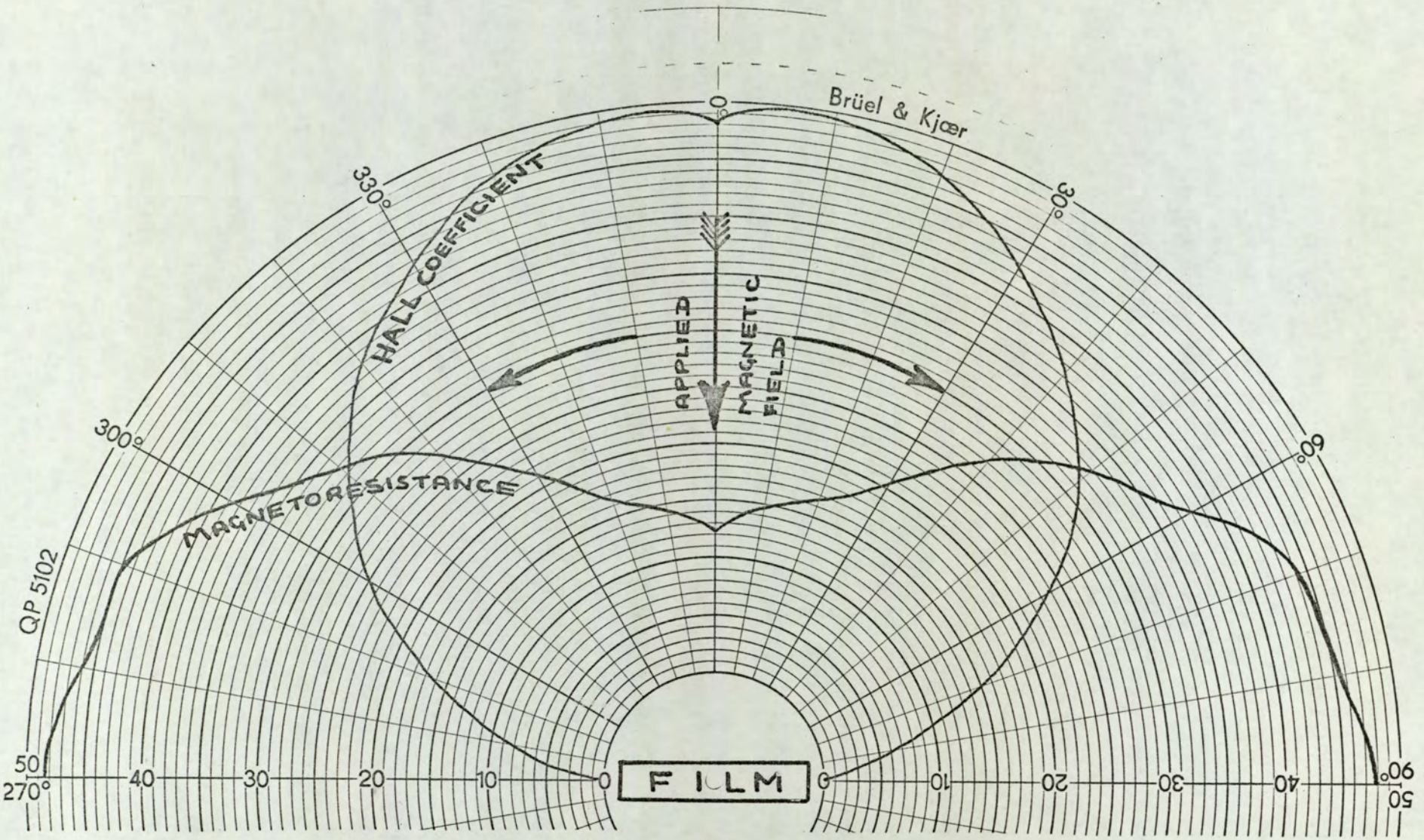

Fig. 64 . Polar Diagram for Hall effect and magnetoresistance

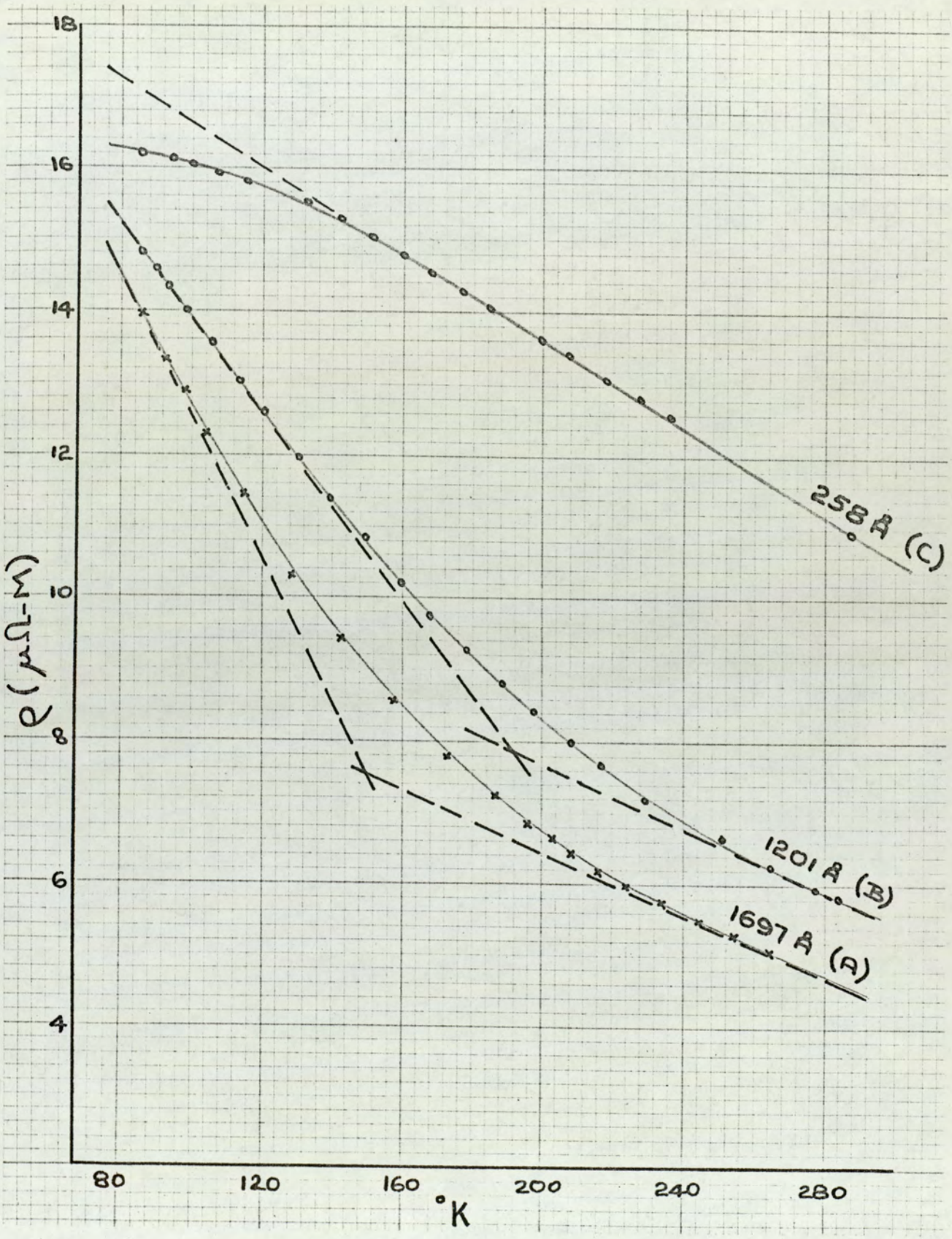

Fig. 65. Resistivity vs. temperature for three typical films

was not precisely defined. The exponential variation of bulk mean free path with temperature for bismuth was such that the temperature change associated with an order of magnitude change in film thickness was too small to be observed quantitatively from the resistivity results. The uncertainty of producing the asymptotes further precluded the analysis.

The relative displacement of the curves signified the differential contribution to the total resistivity of intersticial atoms, vacancies and dislocations. After the initial self-annealing process at room temperature these were observed to be invarient on repeated thermal cycling over the experimental range.

Graph C was typical of the measurements taken on the three thinnest films. The asymptotic regions cannot be distinguished due to the small gradient, but a low temperature saturation of the resistivity was observed. Similarities existed between curve C and the graph of Aubrey et. al. and of Friedman and Koenig (Fig. 6) on bulk bismuth at 4.2 ^{o}K. The results reported here are the first observation of this phenomena reported at 77^{o}K.

Figs. 66 to 79 represent the resistivity results taken on thirty films. The outlined features were observed to hold for the entire range of films examined and in particular the boundary scattering temperature coefficient was observed to depend in an oscillatory manner on the thickness of the film. The high temperature asymptotes were seen to be parallel within the limits of experimental error.

Fig. 80 represents the observations on a proprietory rolled ribbon of 150μ thick and of a randomly orientated vacuum cast polycrystalline bulk specimen. Both were observed to display a positive temperature coefficient of resistivity and are compared with the bulk single crystal resistivity values presented by

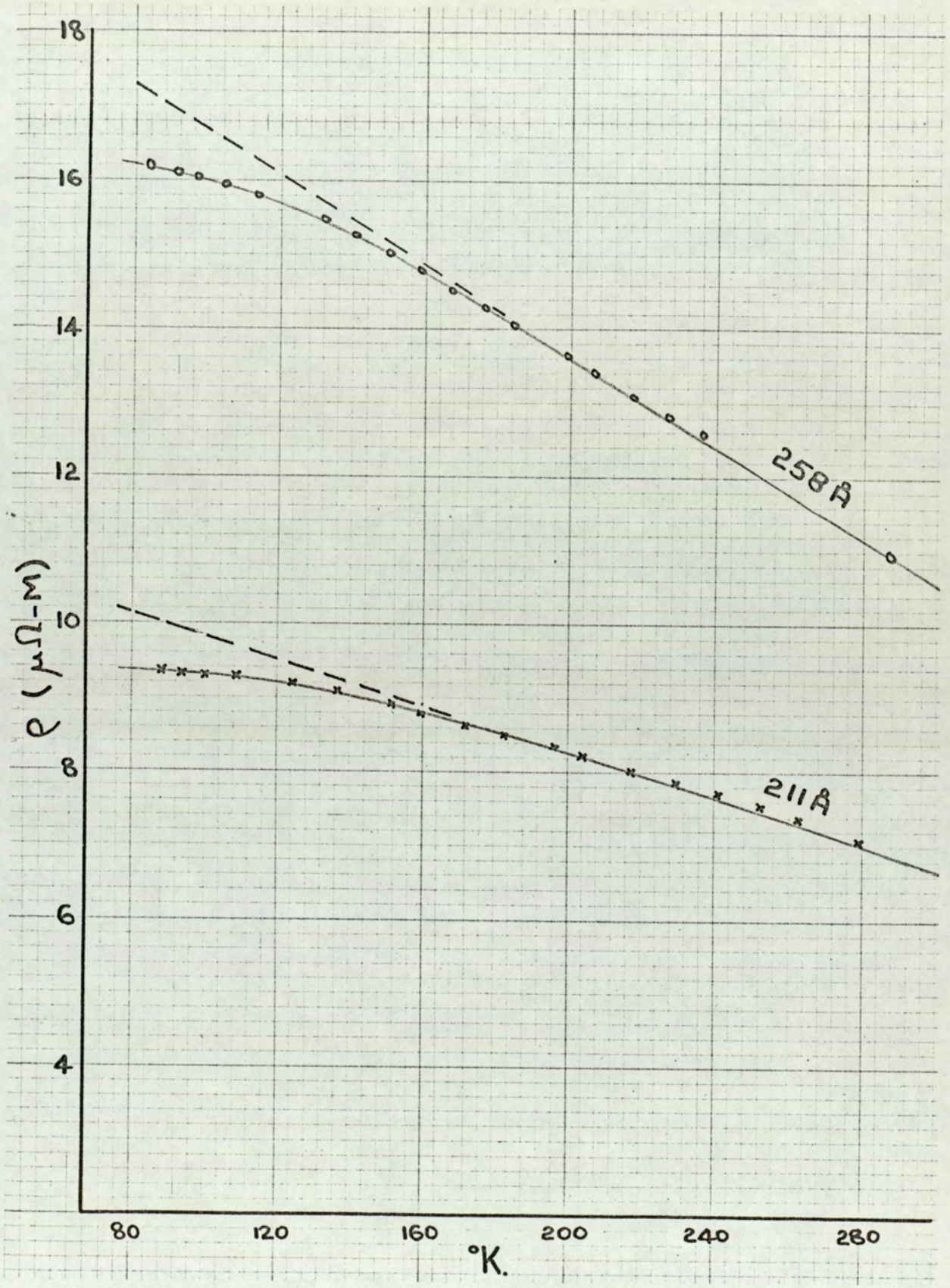

Fig. 66. Resistivity vs. temperature for bismuth films.

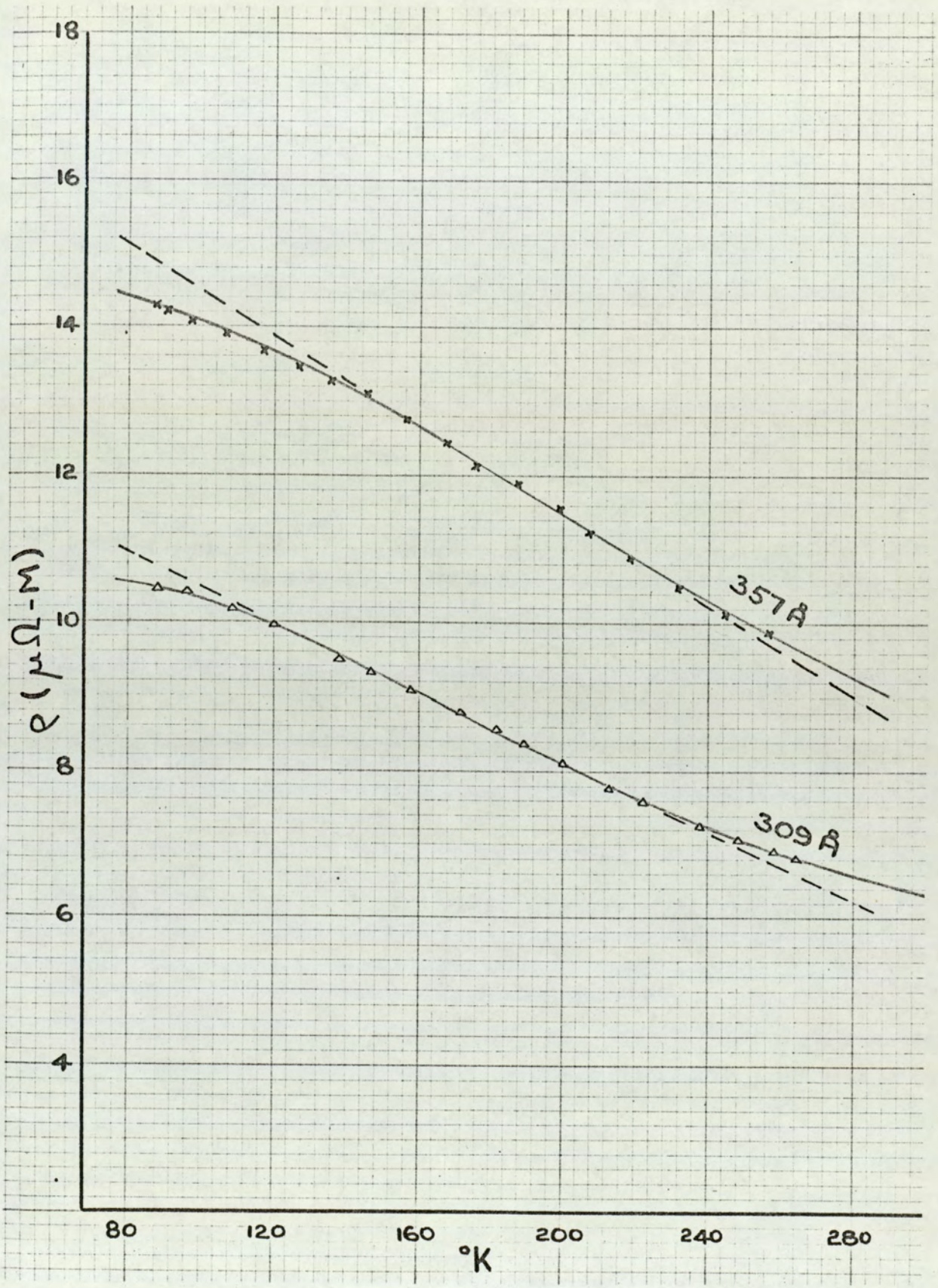

Fig. 67. Resistivity vs. temperature for bismuth films.

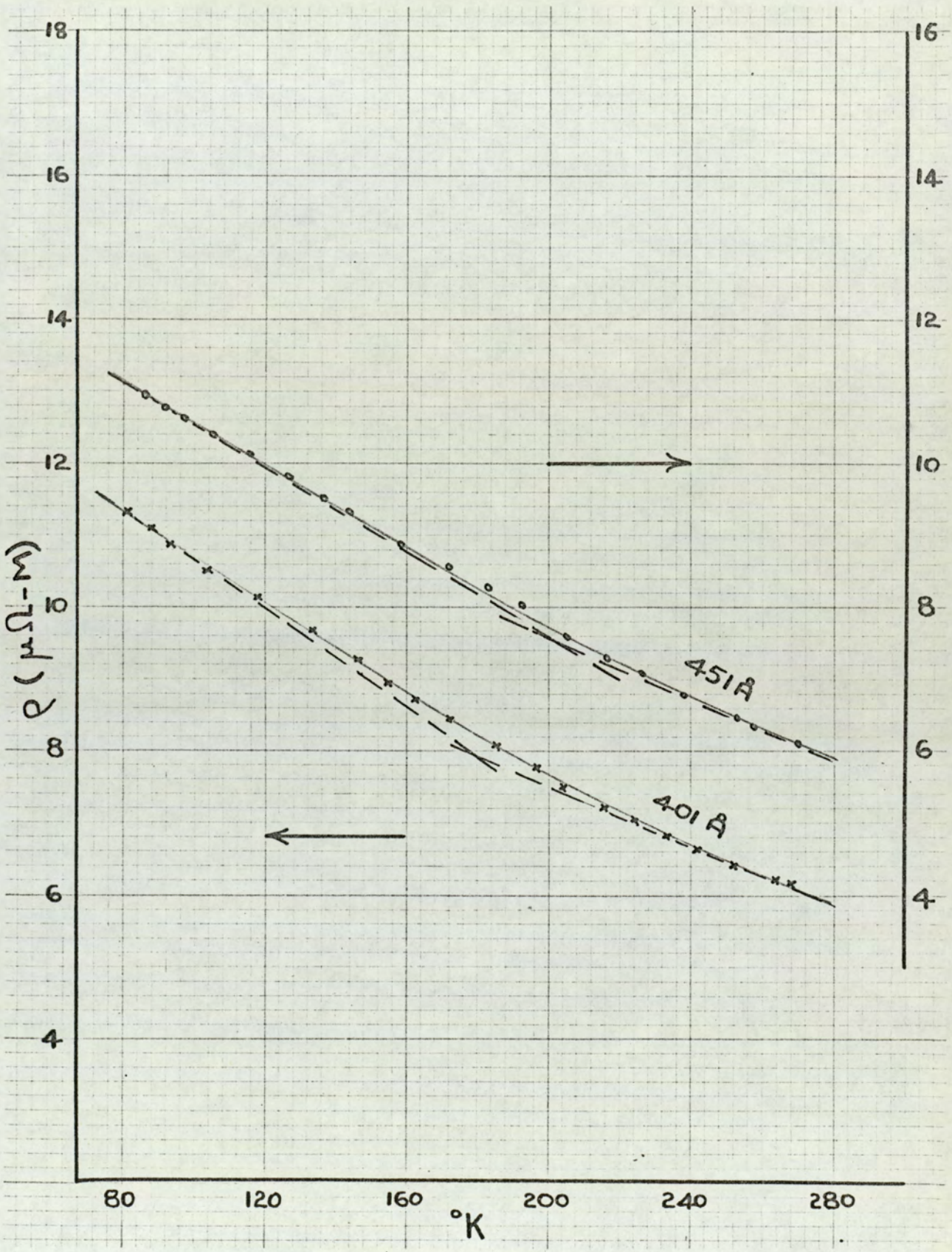

Fig. 68. Resistivity vs. temperature for bismuth films.

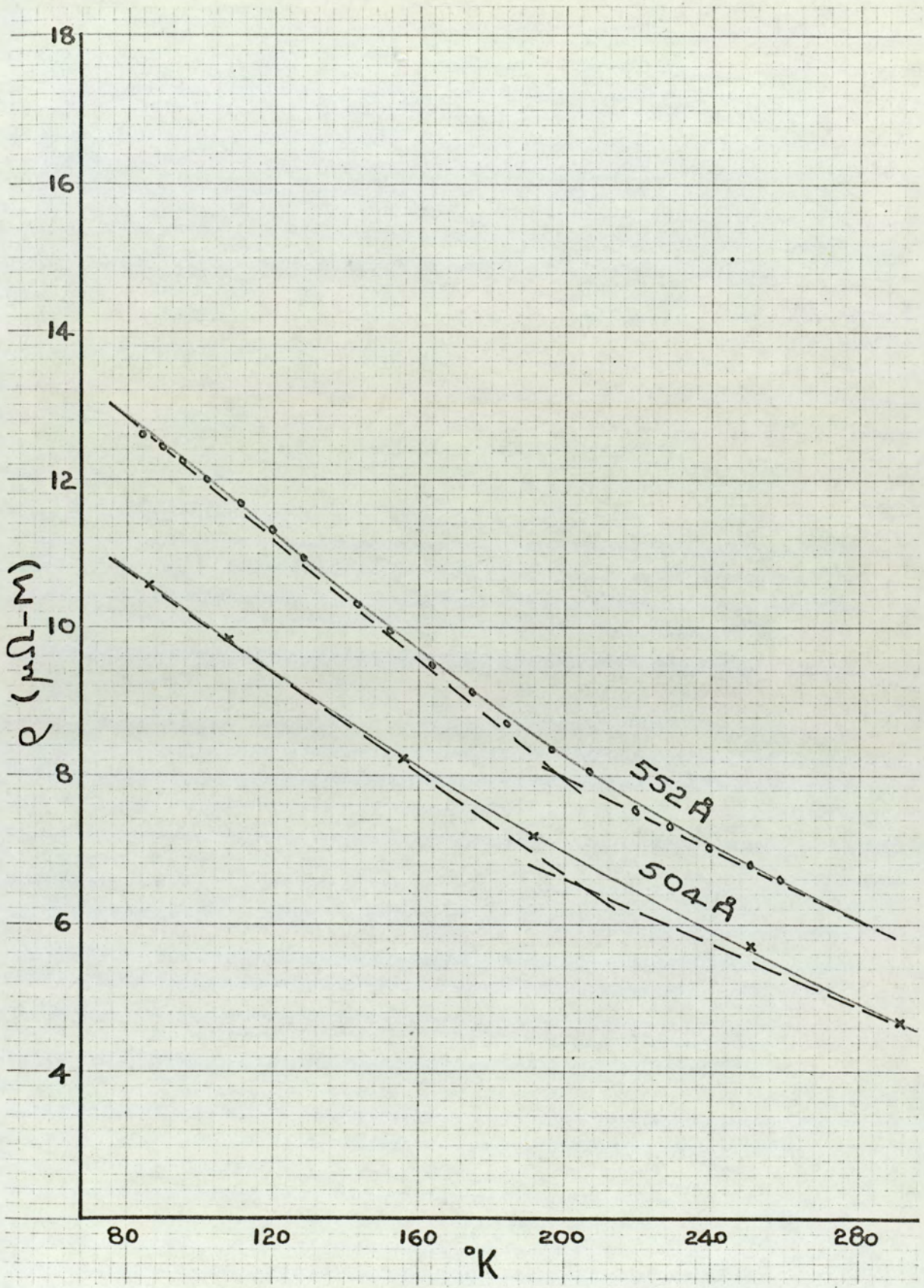

Fig. 69. Resistivity vs. temperature for bismuth films.

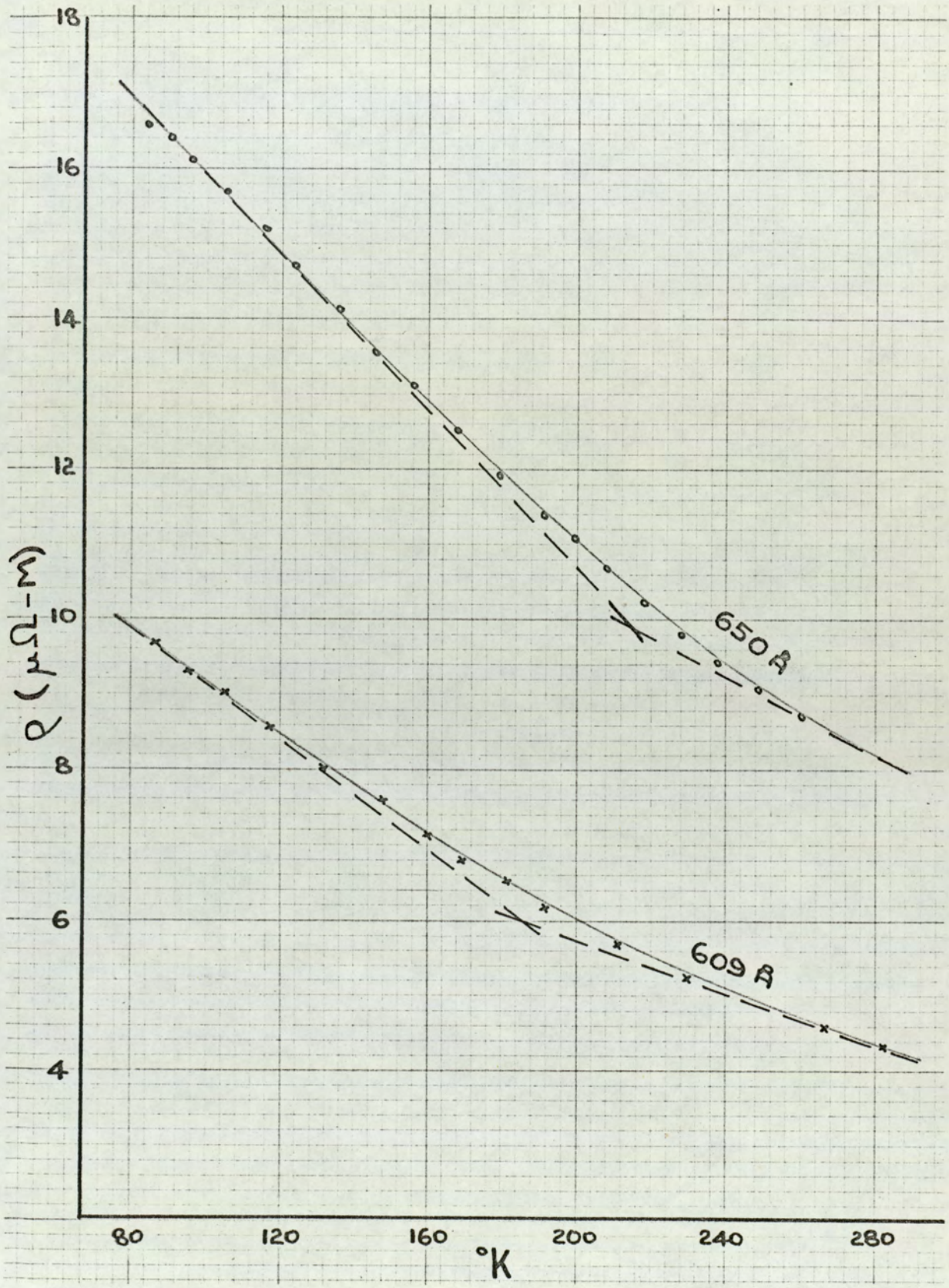

Fig. 70. Resistivity vs.temperature for bismuth films.

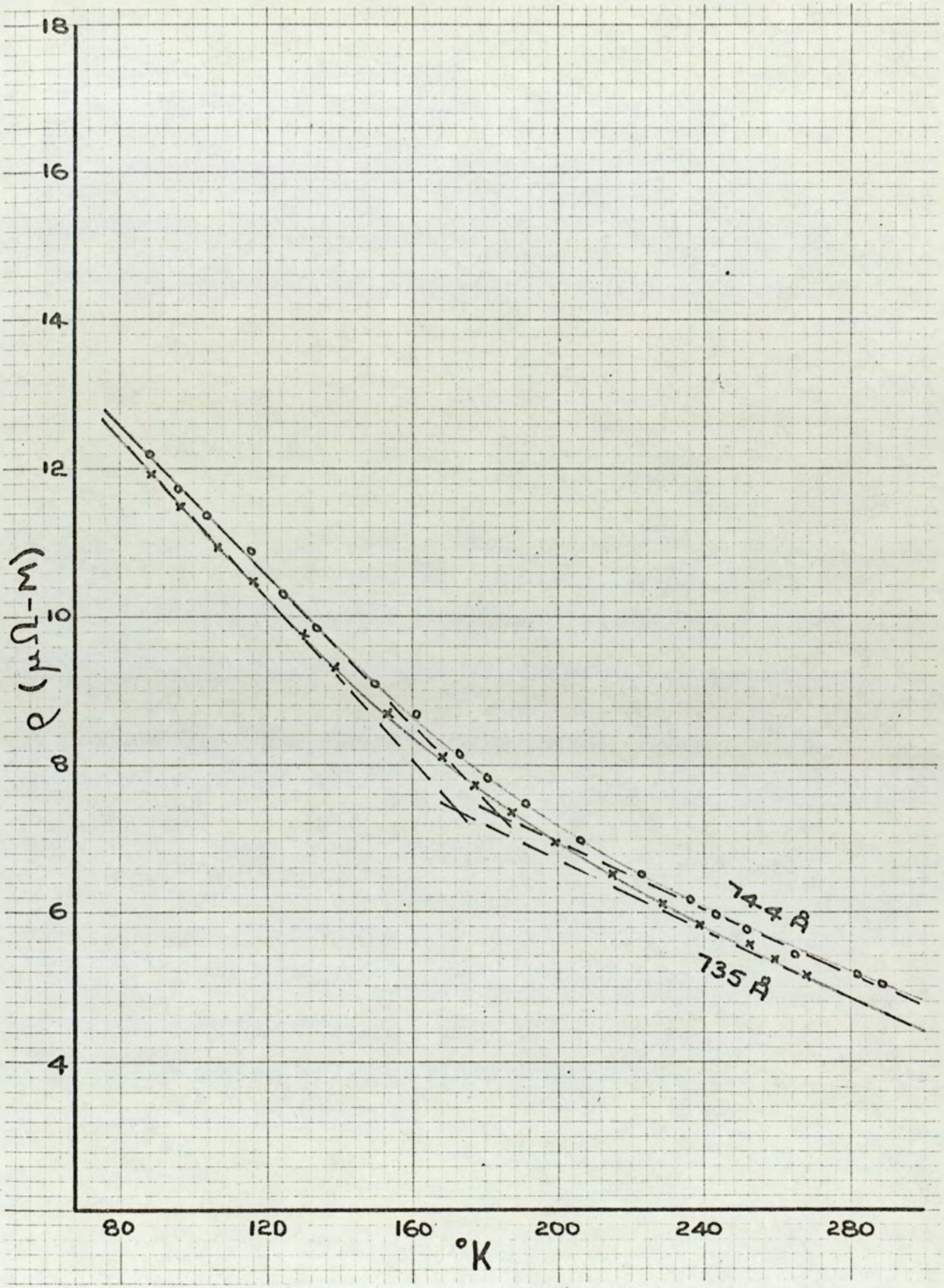

Fig. 71. Resistivity vs. temperature for bismuth films.

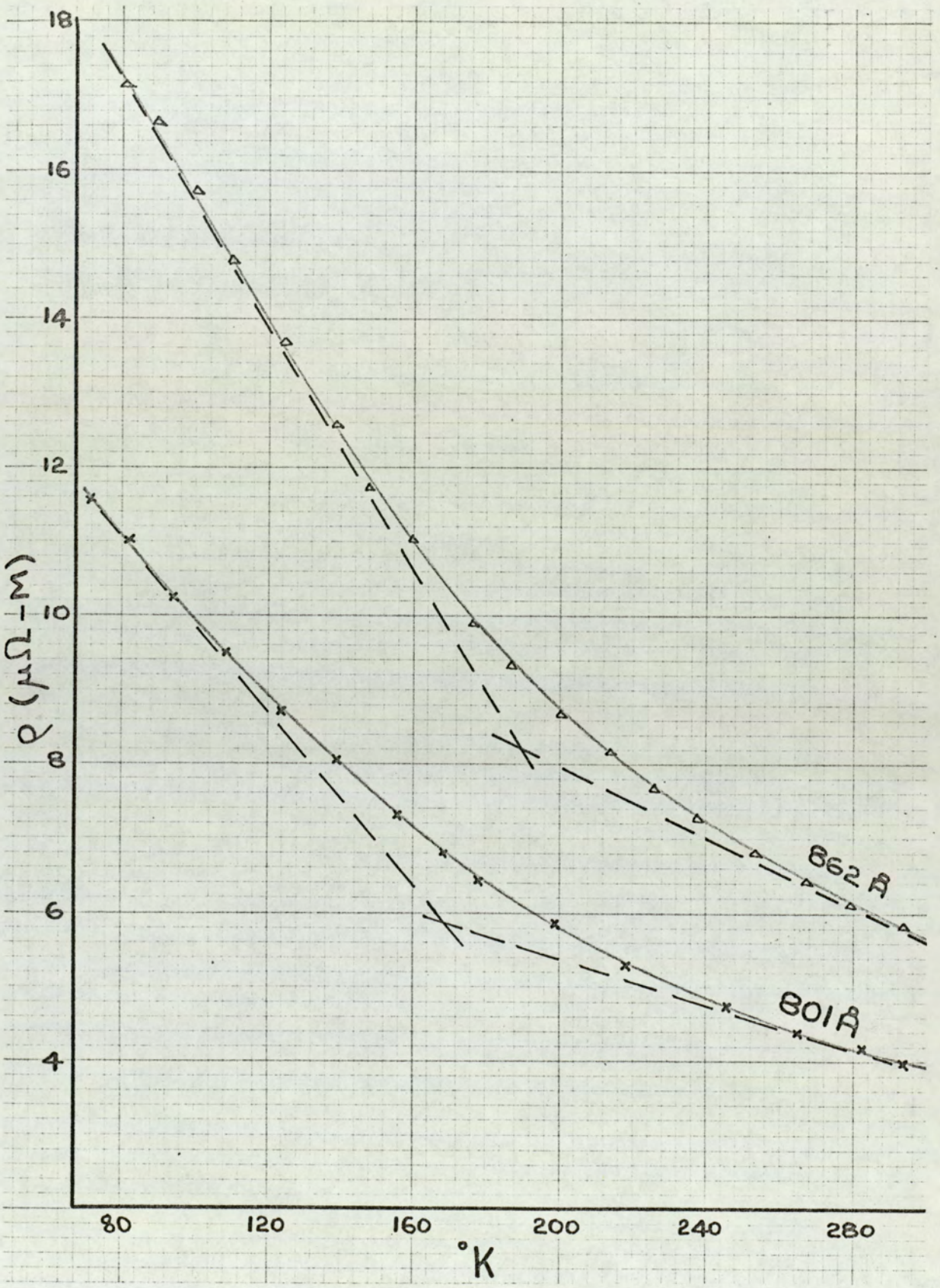

Fig. 72. Resistivity vs. temperature for bismuth films.

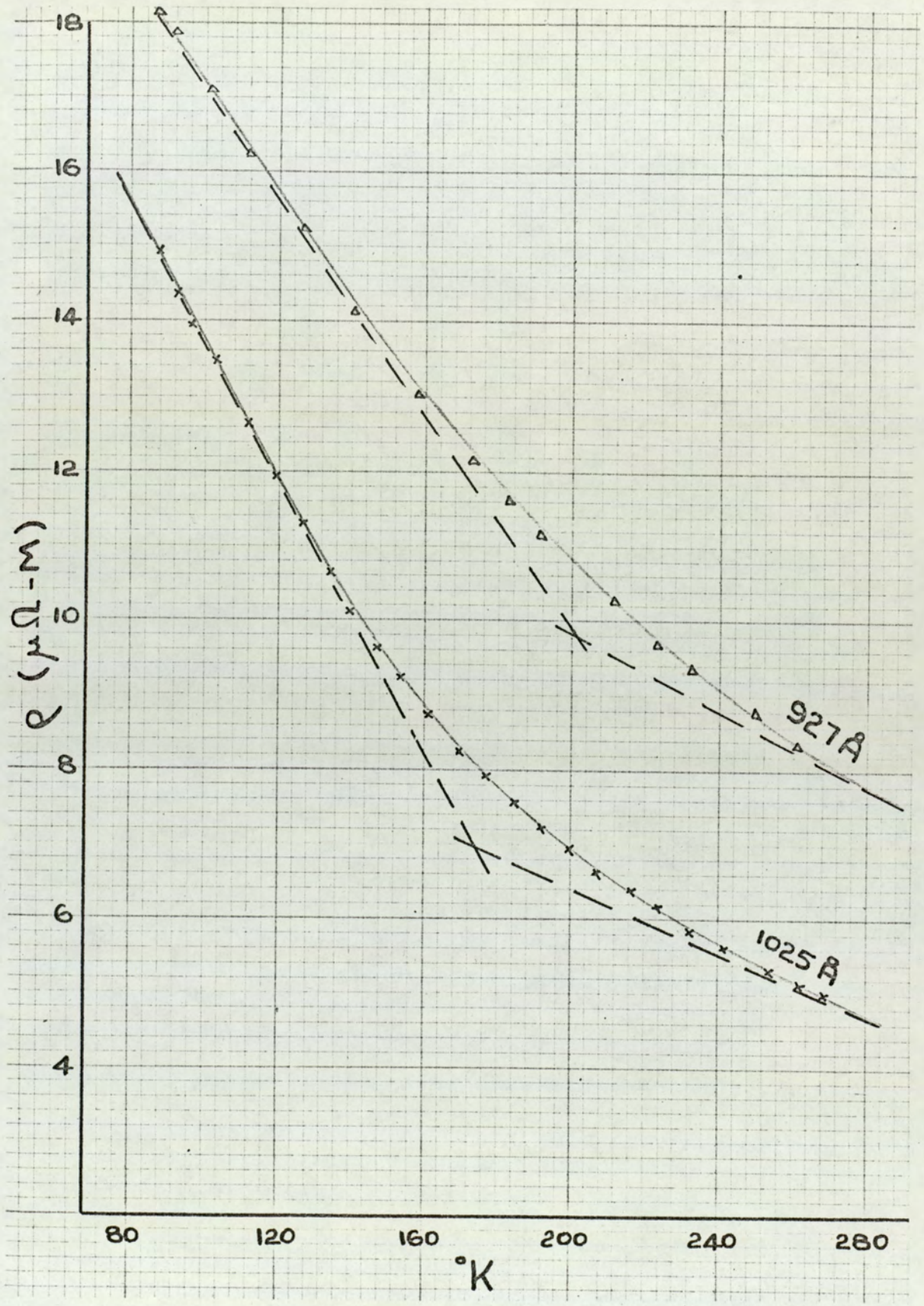

Fig. 73. Resistivity vs. temperature for bismuth films.

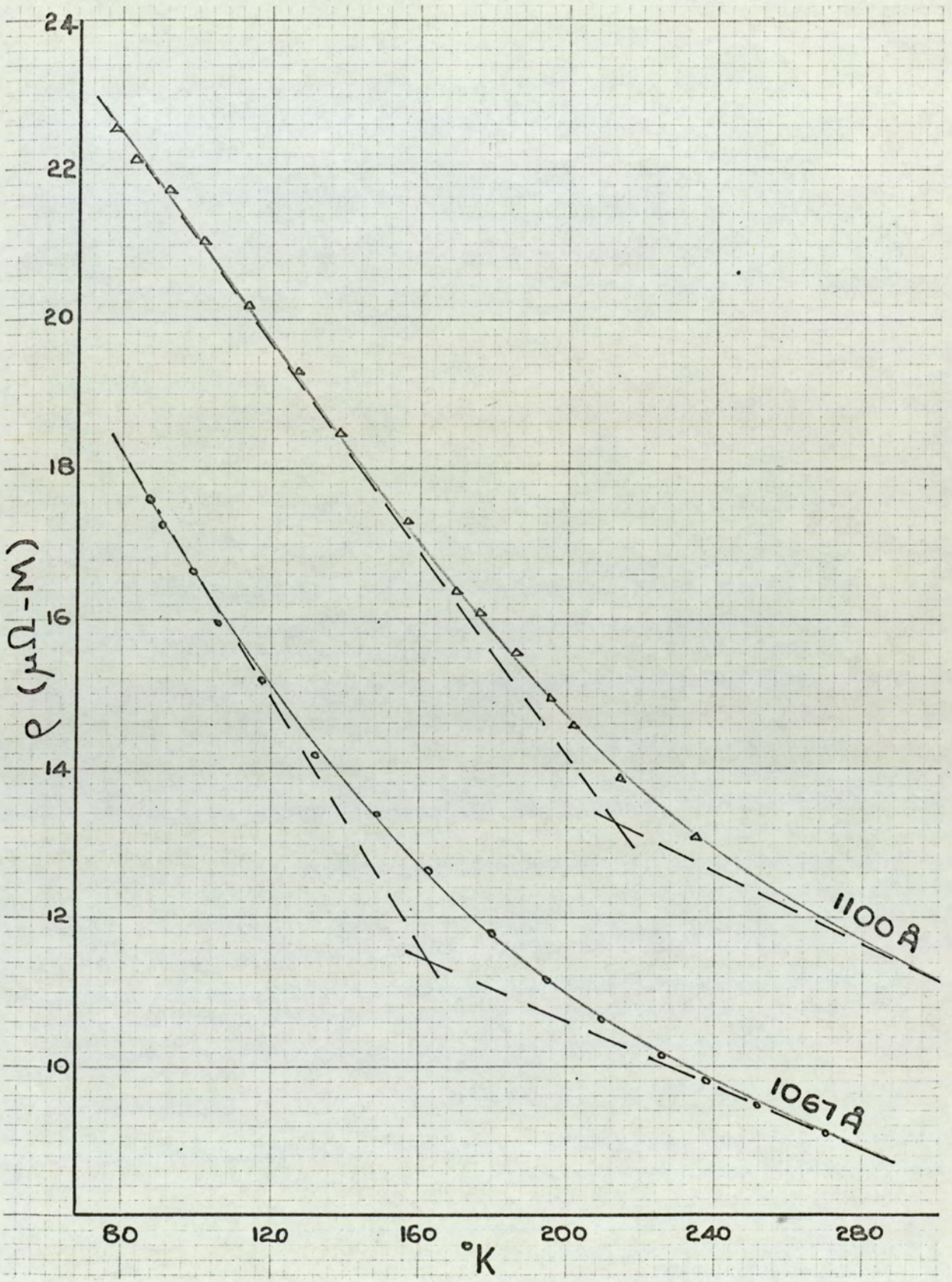

Fig. 74. Resistivity vs. temperature for bismuth films.

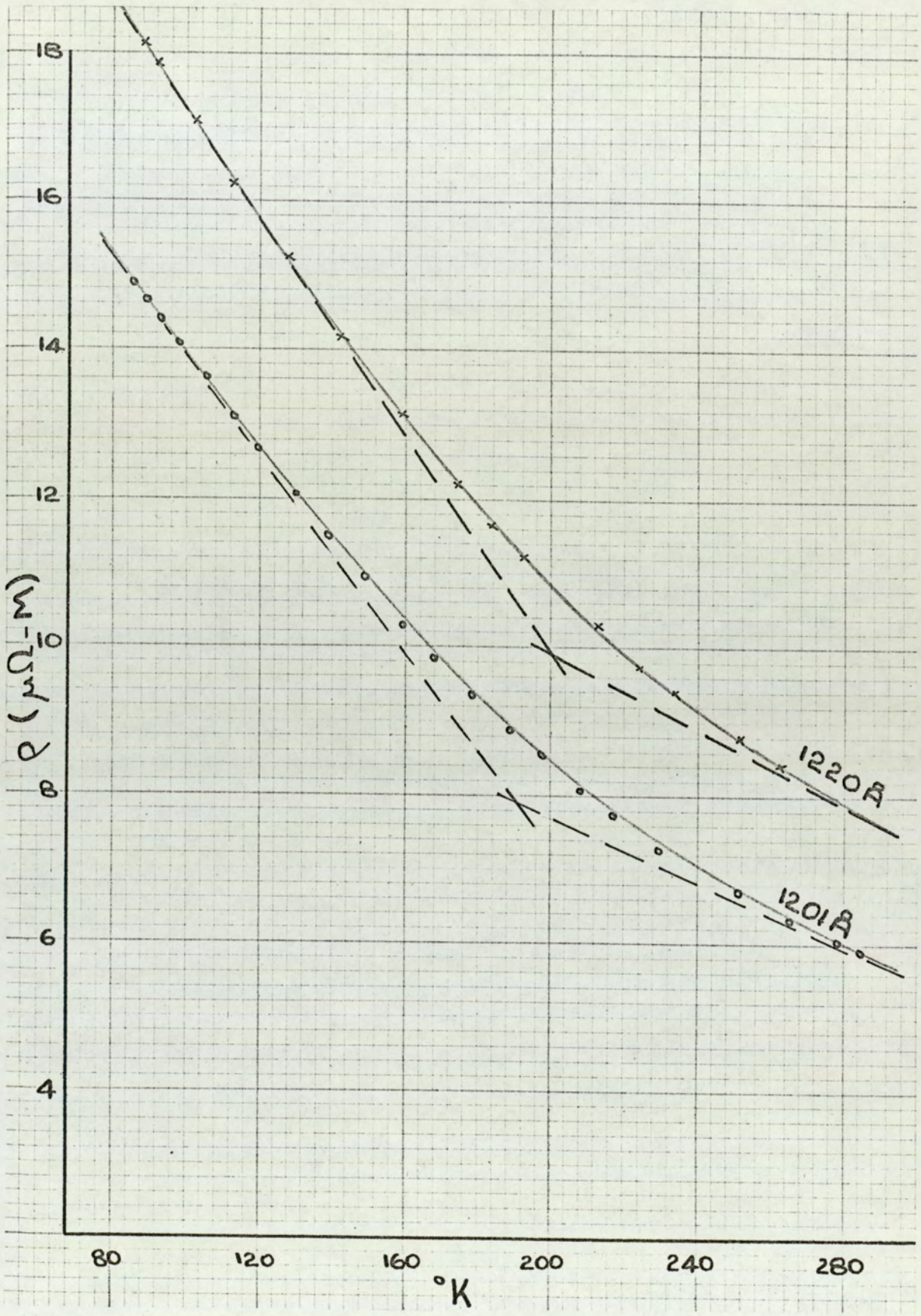

Fig. 75. Resistivity vs. temperature for bismuth films.

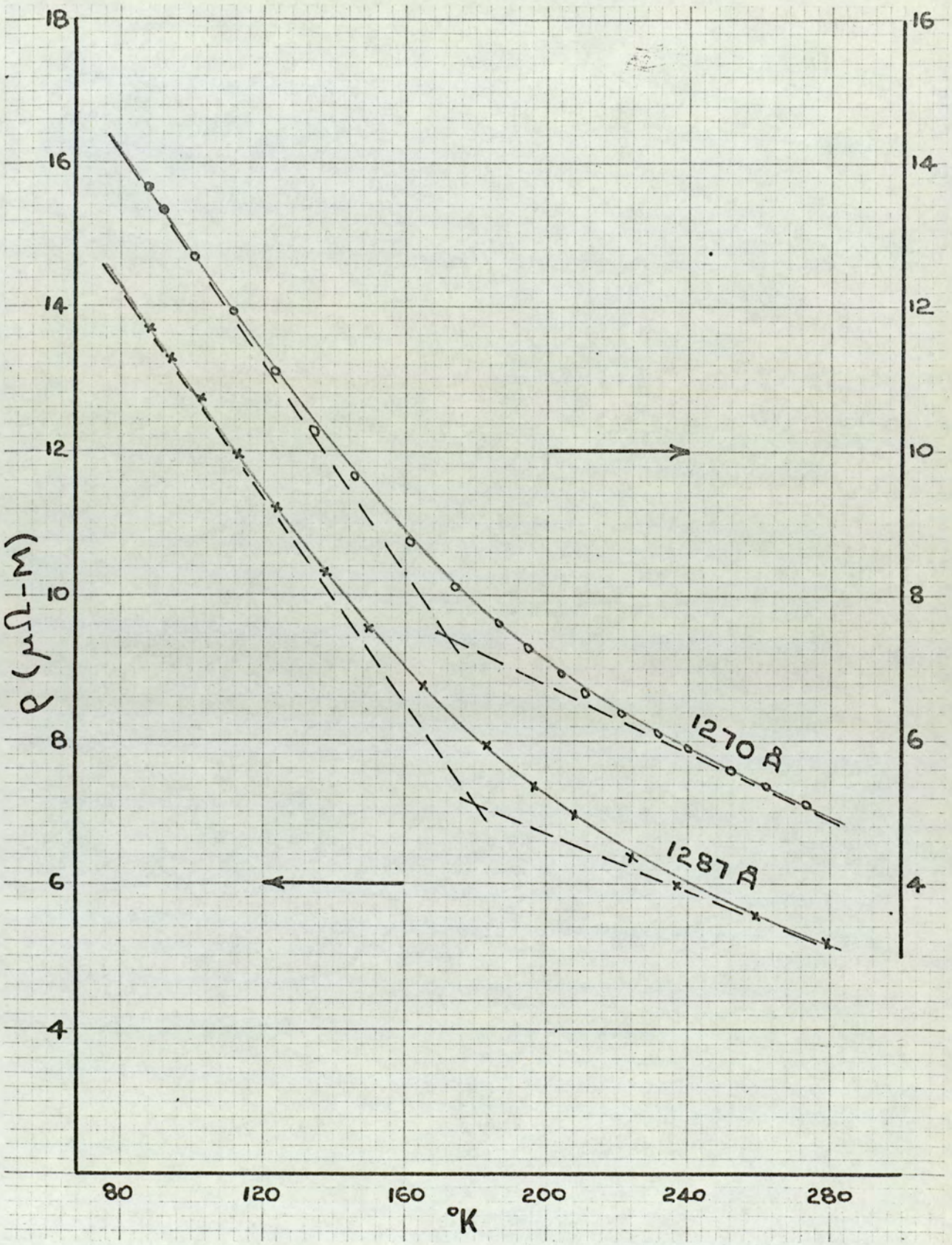

Fig. 76. Resistivity vs. temperature for bismuth films.

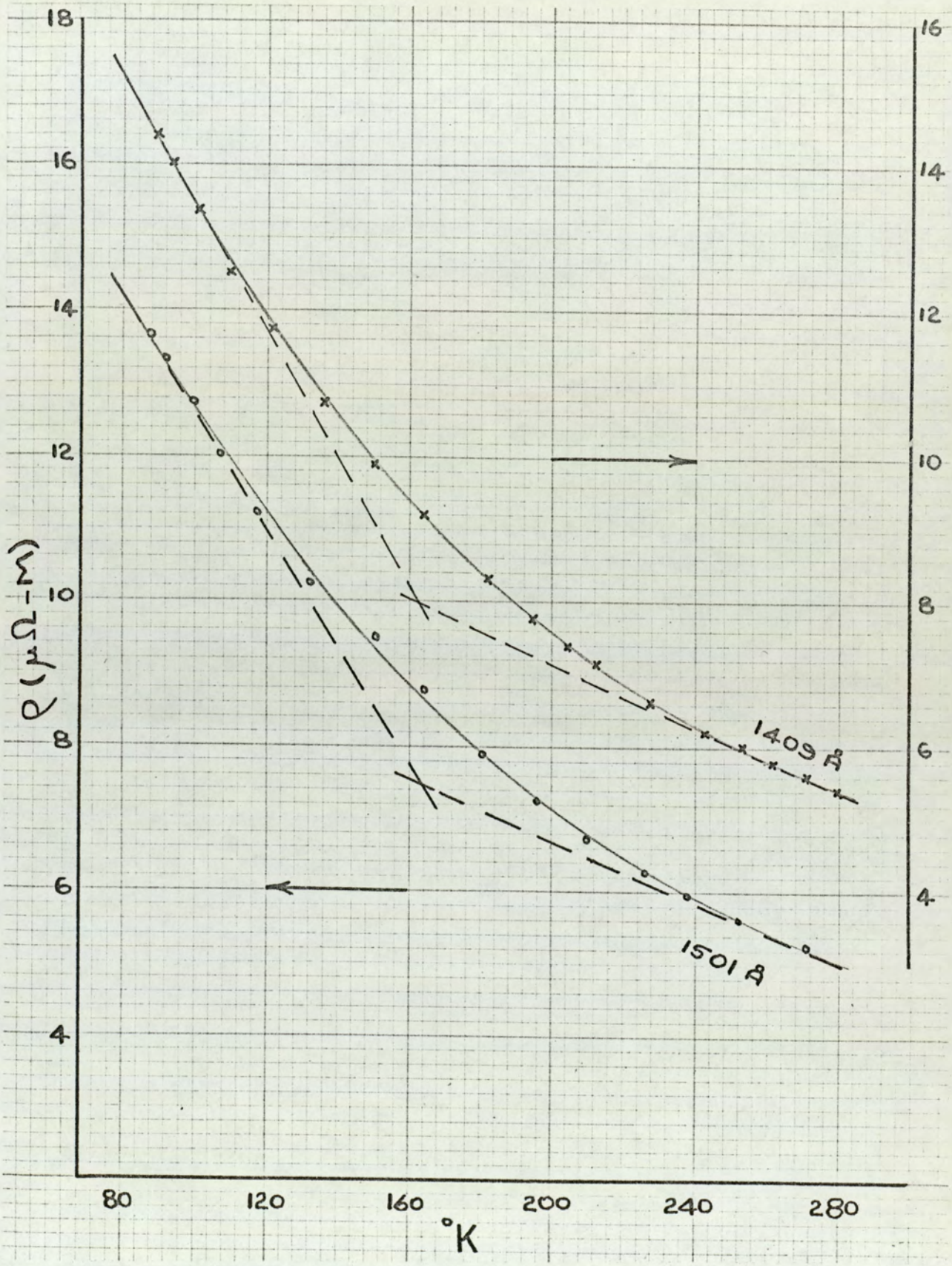

Fig. 77. Resistivity vs. temperature for bismuth films.

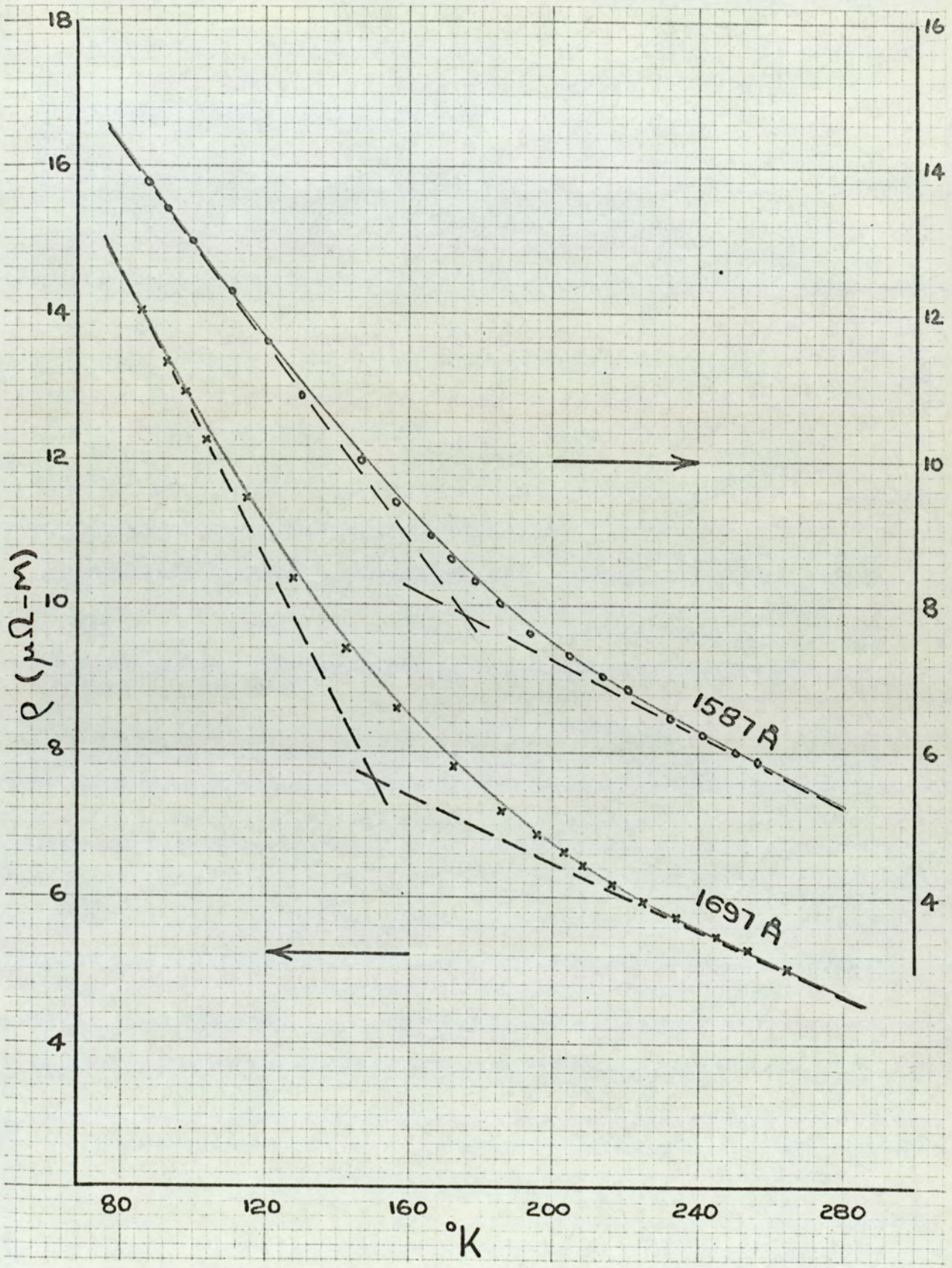

Fig. 78. Resistivity vs. temperature for bismuth films.

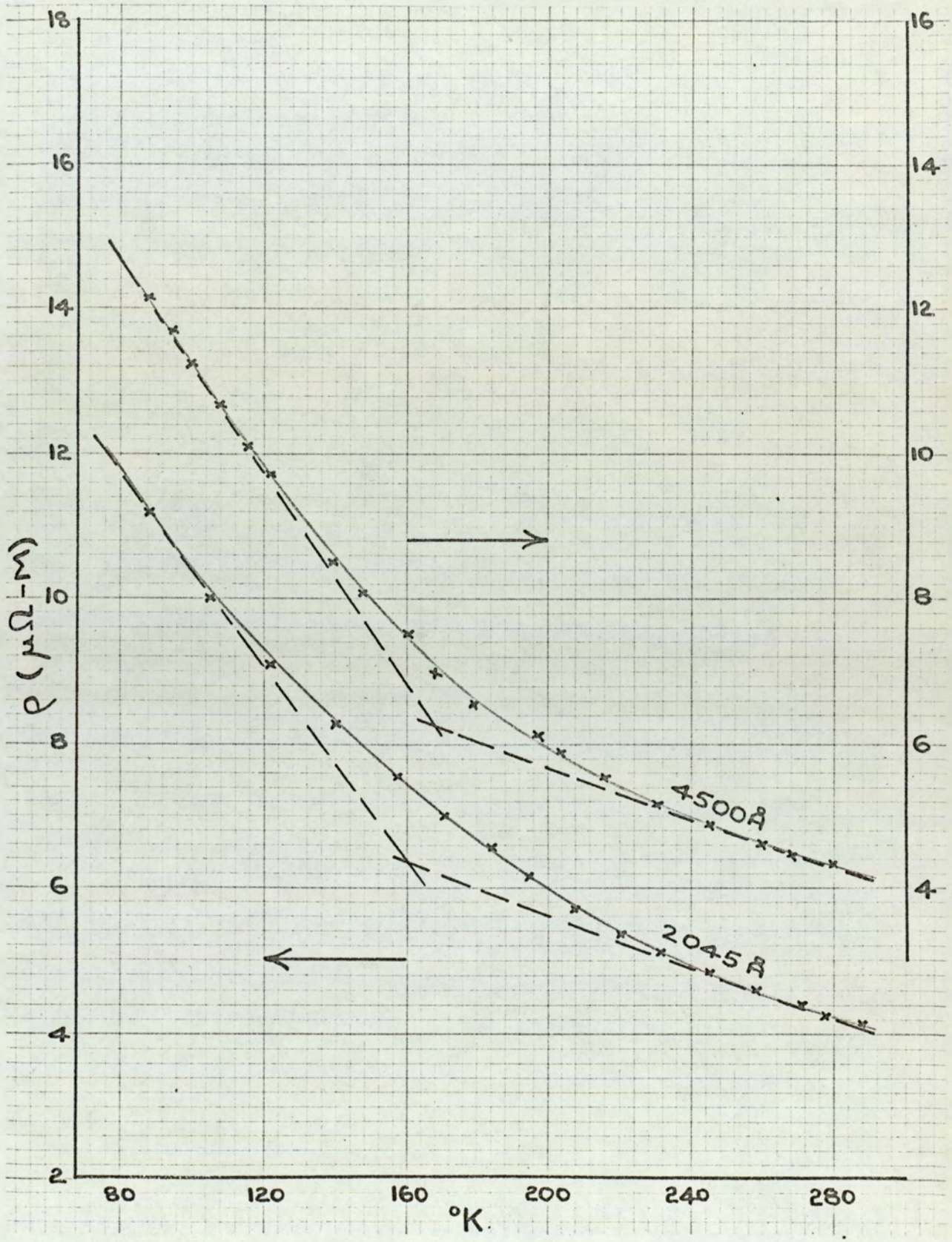

Fig. 79. Resistivity vs. temperature for bismuth films.

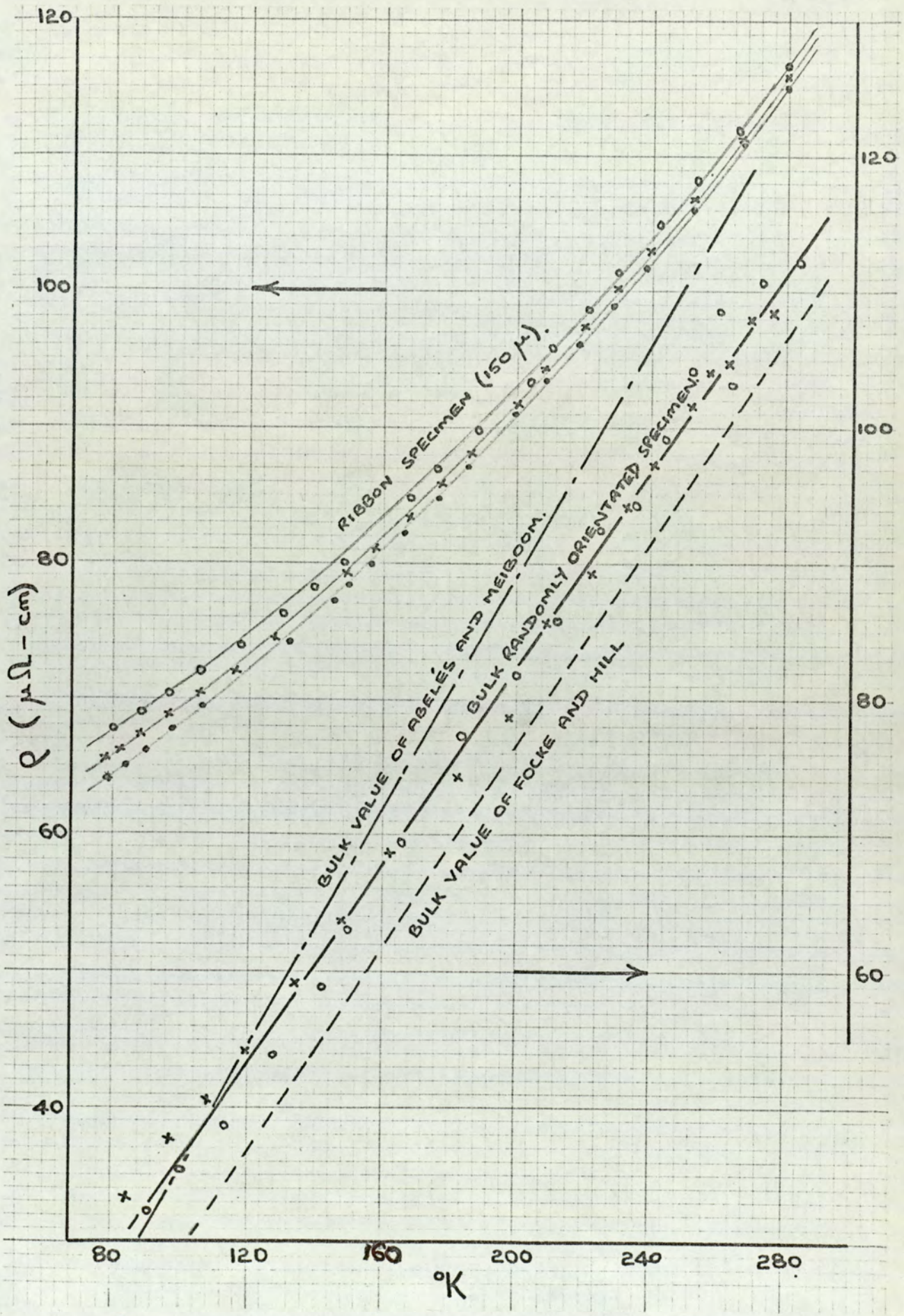

Fig. 80. Comparison between the resistivity of randomly orientated bulk and ribbon specimens and published single crystal values.

Abeles and Meiboom [28] and Focke and Hill [27].

The room temperature resistivity values of the films extended from a factor of 3 to 7 times the corresponding value obtained for bulk specimens and was consistant with similar observations on 'as evaporated' films.

5.4. Magnetoresistance

The analysis of Borovik indicated that the resistivity of bismuth specimens should increase without limit in an increasing magnetic field, and has been observed in pulsed magnetic fields at 4.2°K to reach 10^6 times the value in zero field. As demonstrated in the pole figure of section 5.2.3. however, despite the intrinsic greatness of the magnetoresistance phenomena the effect of additional boundary scattering was likely to have a marked effect. The increased mean free path with decreasing temperature resulted in an unlimited growth of the magnetoresistance in bulk material. In thin films the number of carriers having velocity components out of the plane of the film decreased in the thin limit and thus a decrease in magnetoresistance at low temperatures might be expected. This will be discussed in chapter 6.

The appearance of certain features in the curves of the magnetoresistive coefficient against temperature resulted in the need to present a selection of the data both in the form of the direct magnetoresistance ratio, $\Delta\rho/\rho$, and of the coefficient, B. Figs. 81 and 82 show the magnetoresistance ratio plotted linearly against temperature for both the bulk randomly orientated specimen and for the 150 μ ribbon specimen. Both series of graphs display a similar profile in which the values of $\Delta\rho/\rho$ at reduced temperatures increased far out of proportion to the corresponding increase in mean free path.

The value of the magnetoresistance ratio reduced by

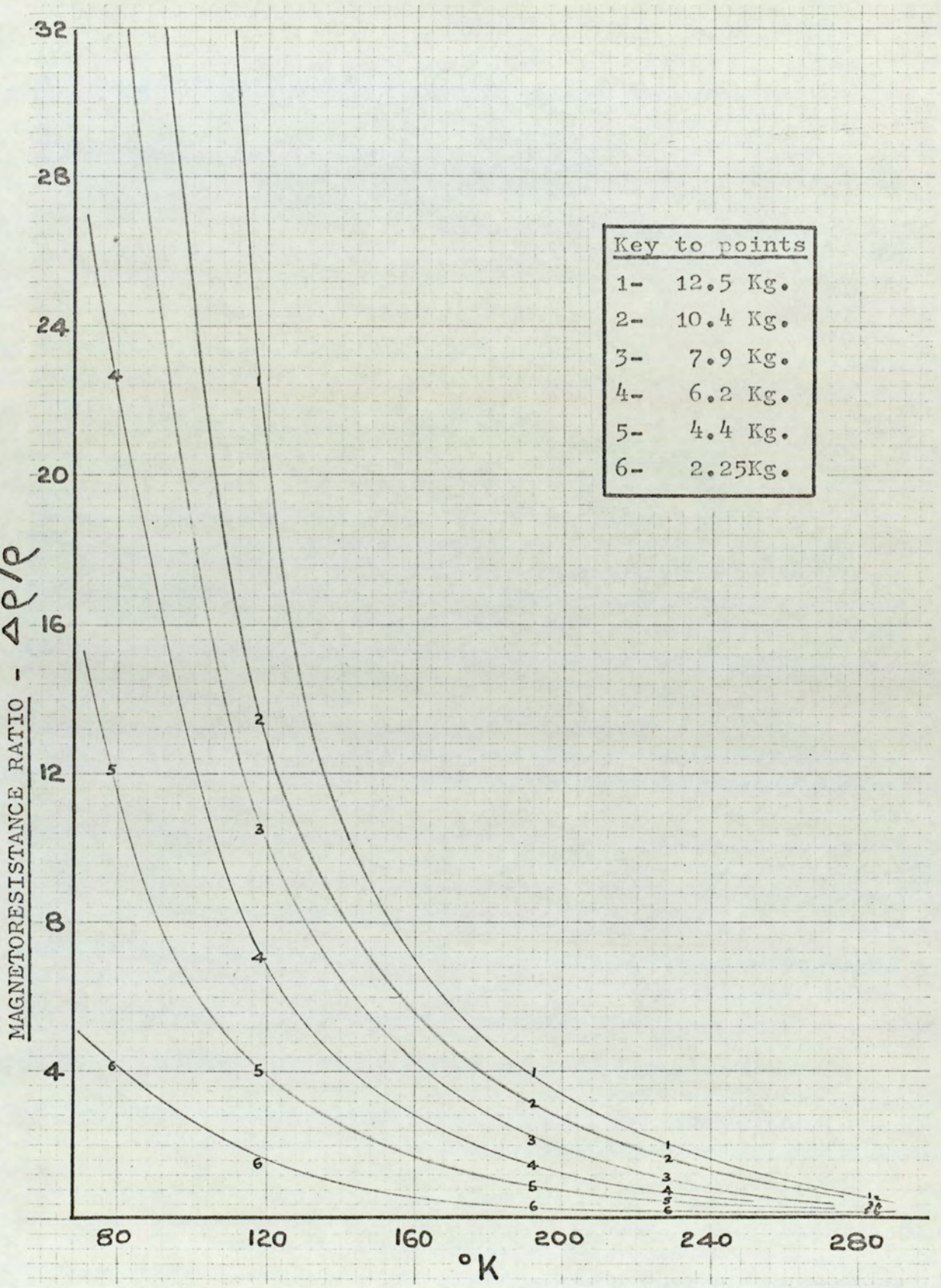

Fig. 81. Magnetoresistance ratio vs. temperature at selected magnetic fields for the randomly oriented bulk specimen.

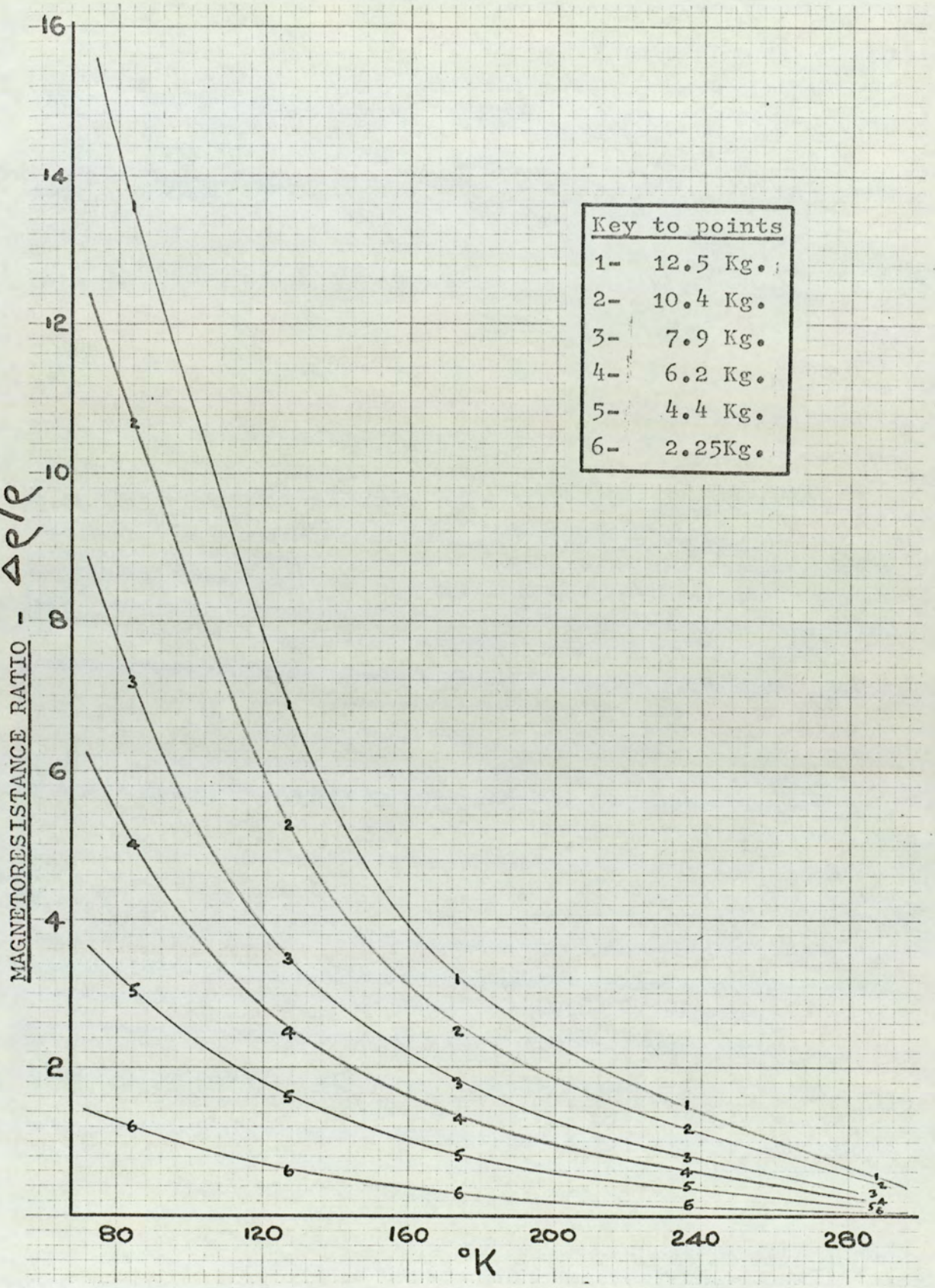

Fig. 82. Magnetoresistance ratio vs. temperature at selected magnetic fields for the ribbon specimen.

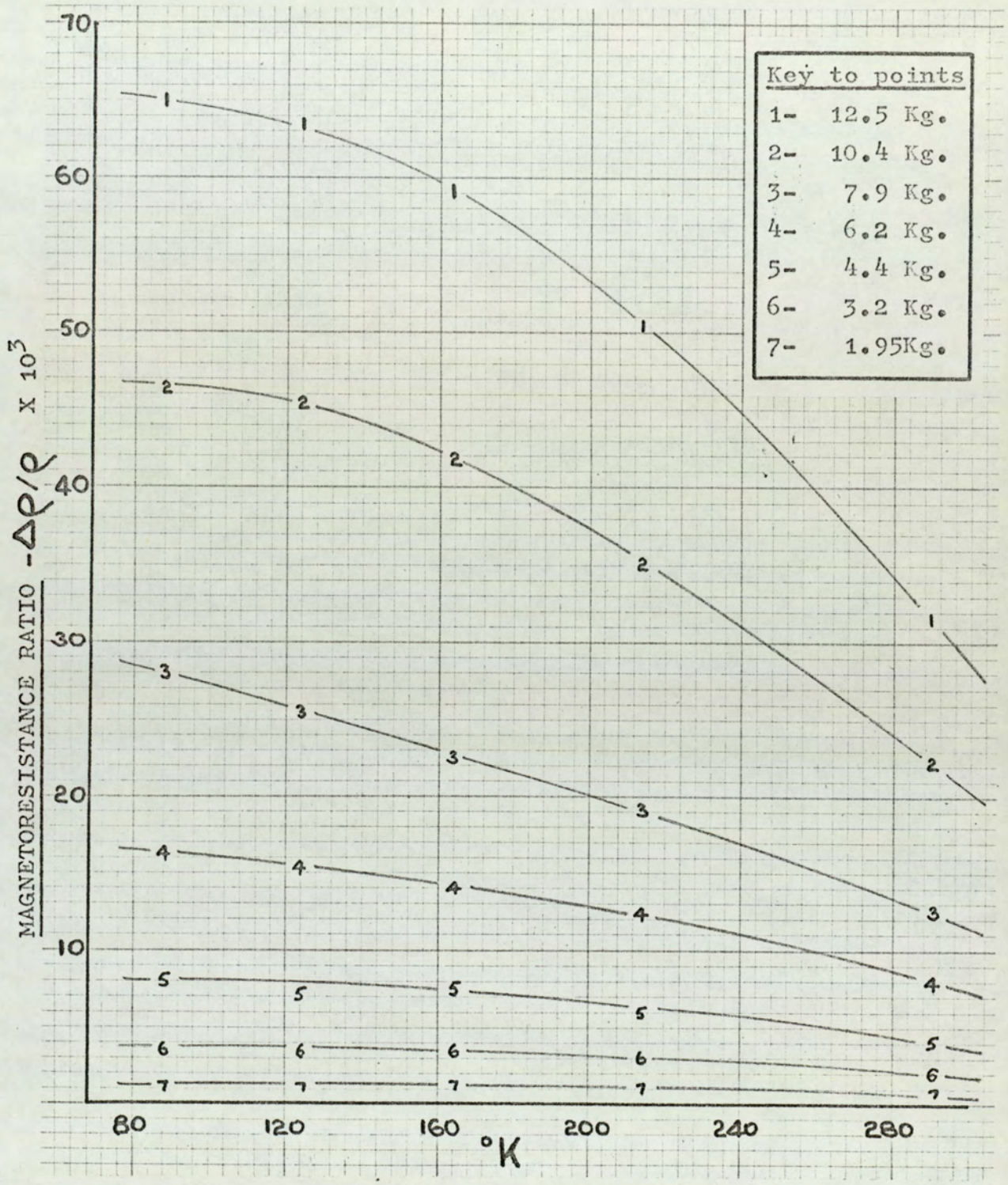

Fig. 83. Magnetoresistance ratio vs. temperature at selected magnetic fields for a film of 4500 Å.

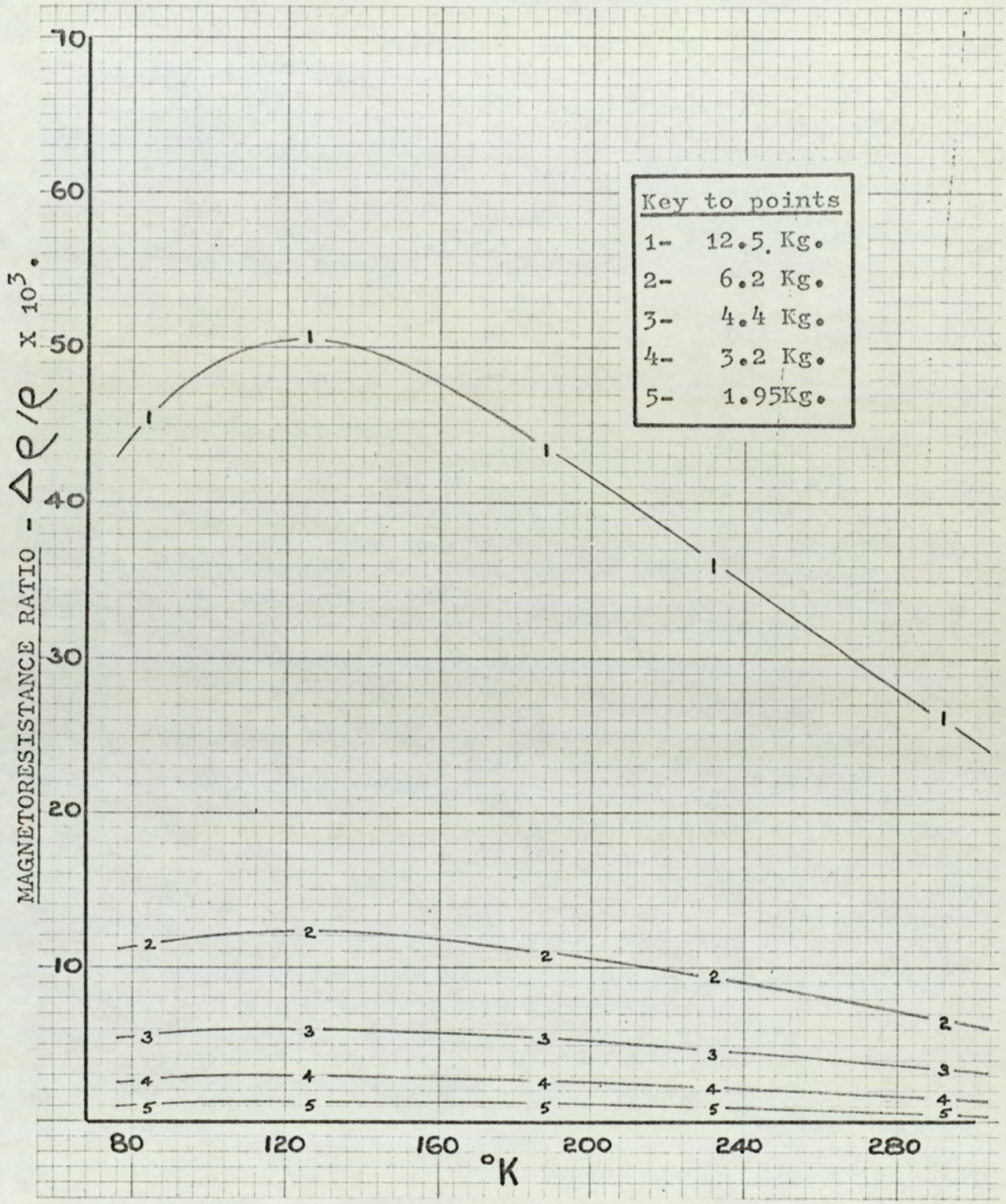

Fig. 84. Magnetoresistance ratio vs. temperature at selected magnetic fields for a film of 2045 Å.

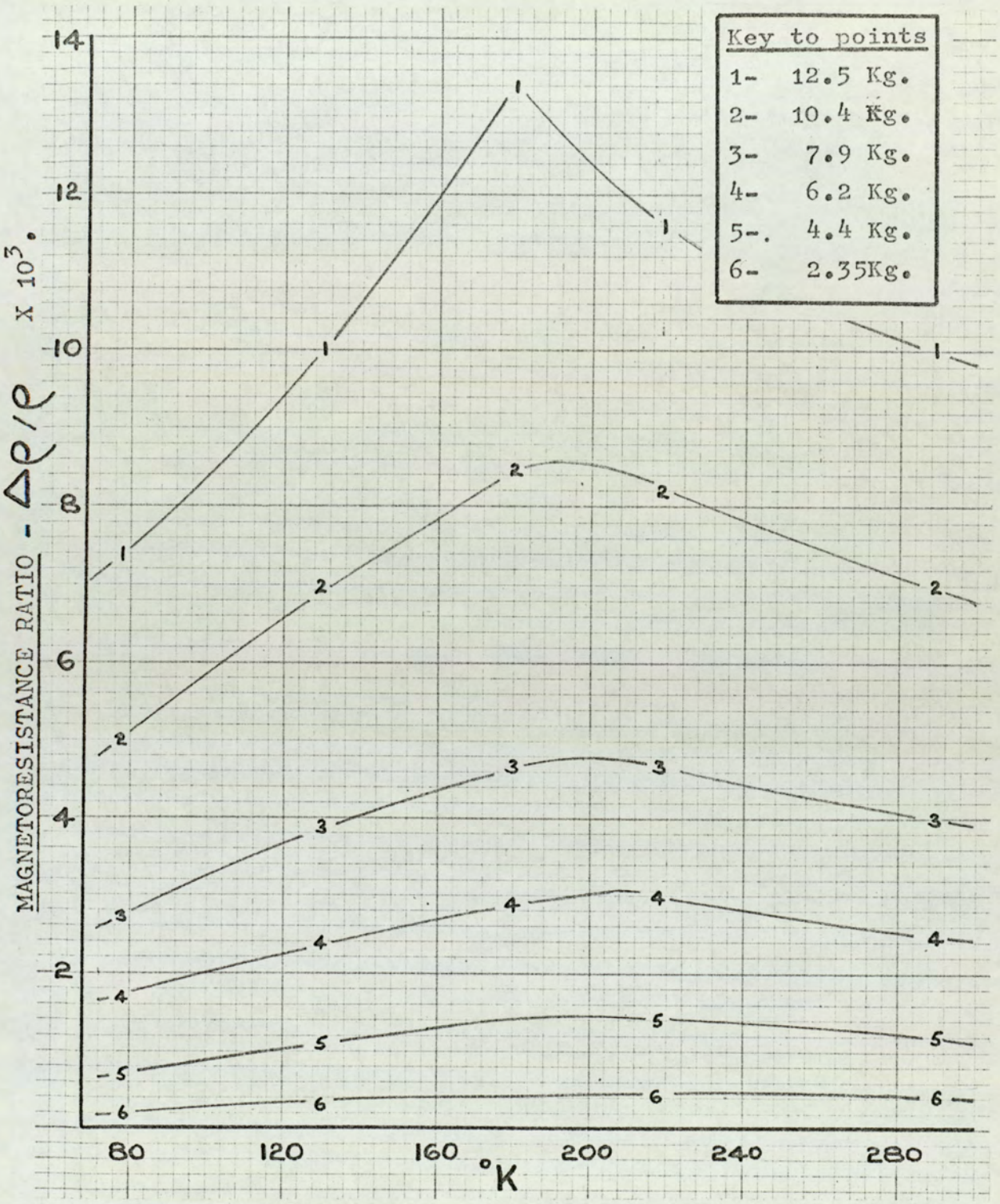

Fig. 85. Magnetoresistance ratio vs. temperature at selected magnetic fields for a film of 862 Å.

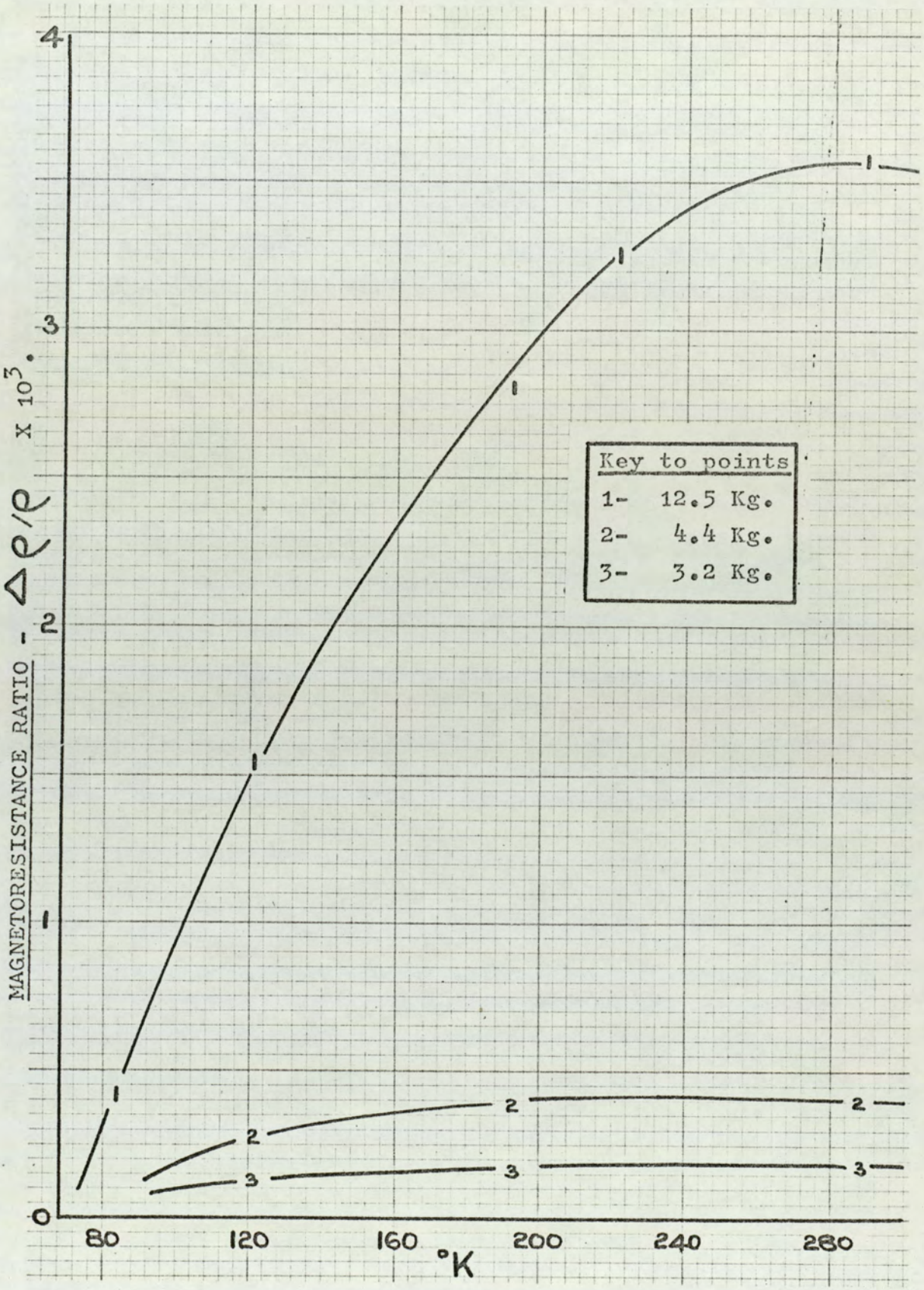

Fig. 86. Magnetoresistance ratio vs. temperature at selected magnetic fields for a film of 309 Å.

several orders of magnitude on approaching the thin film region. Fig. 83 shows the values of the ratio for a film of 4500 Å. It is seen that the exponential-type of increase in bulk material no longer occurred and that a maximum value was observed at the lowest temperatures attained. The maximum value was more noticeable in Fig. 84 taken at 2045 Å.

The trend is continued in Fig. 85 as the film boundaries further supress the increase in resistivity under the influence of the transverse magnetic field. The maxima of the curves do however show a distinct displacement towards the higher temperatures as the magnetic field is reduced. The effect of the displaced maxima would be to produce a series of magnetoresistance coefficient curves which were non-coincident.

At the thinner films examined the magnetoresistance became extremely small and at a maximum resolution of $\pm$ 1 digit on a four figure number the results decreased in accuracy. Fig. 86 taken on a film of 309 Å does however show that at these thicknesses the slope of the curve was positive at all temperatures.

All curves of resistivity shown in section 5.3. have an asymptotic origin extending over only a small range of temperatures. The effect of specimen size would appear to be far wider reaching in the magnetoresistance observations in that the maxima in the curves extend beyond the limits of temperature covered.

The curves of magnetoresistance coefficient, B , against temperature are shown for all films in Figures 87 to 110 and are drawn from the $\Delta\rho/\rho$ results assuming an inverse square law relationship:

$$B = \frac{\Delta\rho}{\rho H^2}$$

A selection of the results are presented from the "Field

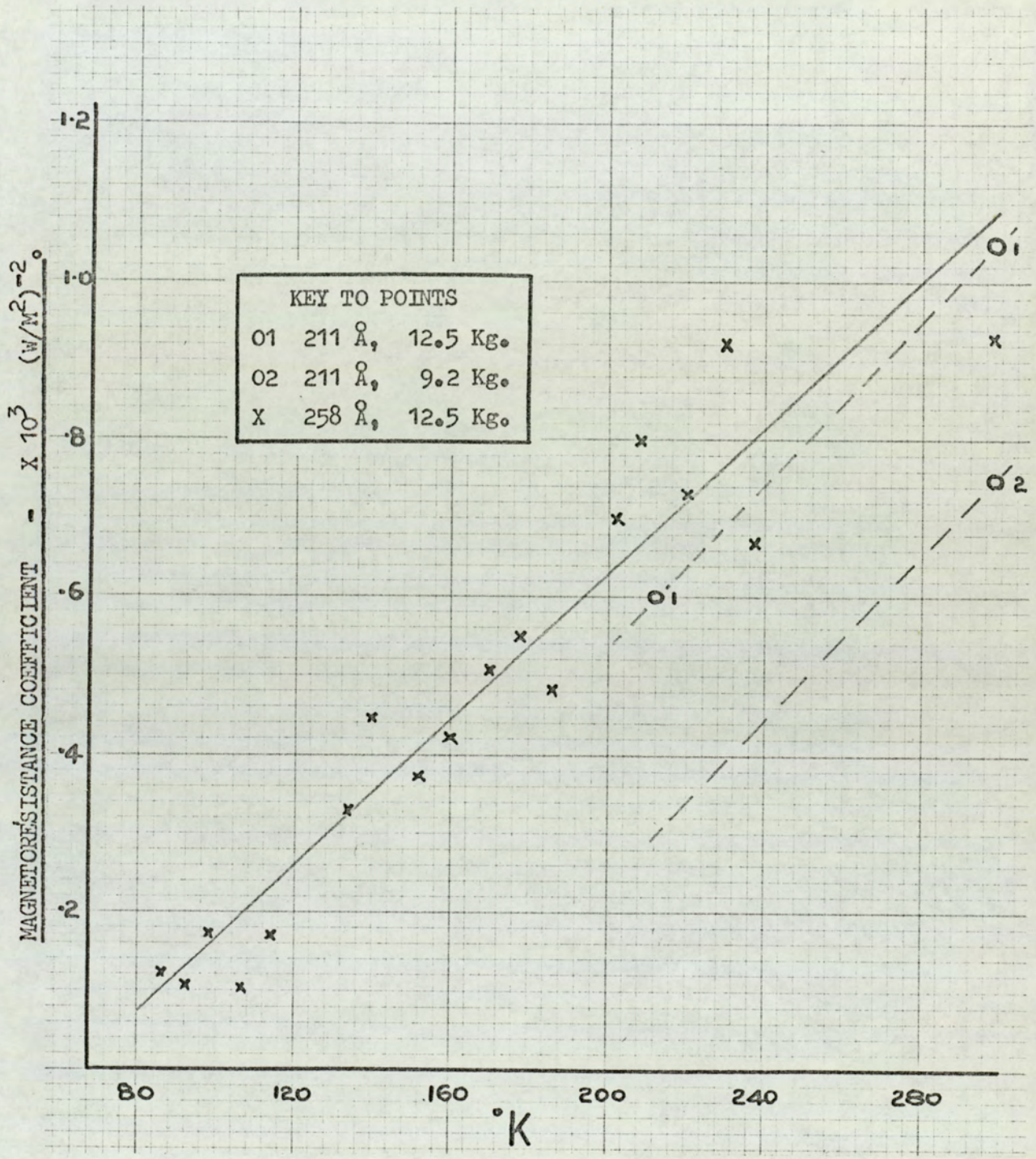

Fig. 87. Magnetoresistance coefficient vs. temperature for bismuth films of 211 Å and 258 Å.

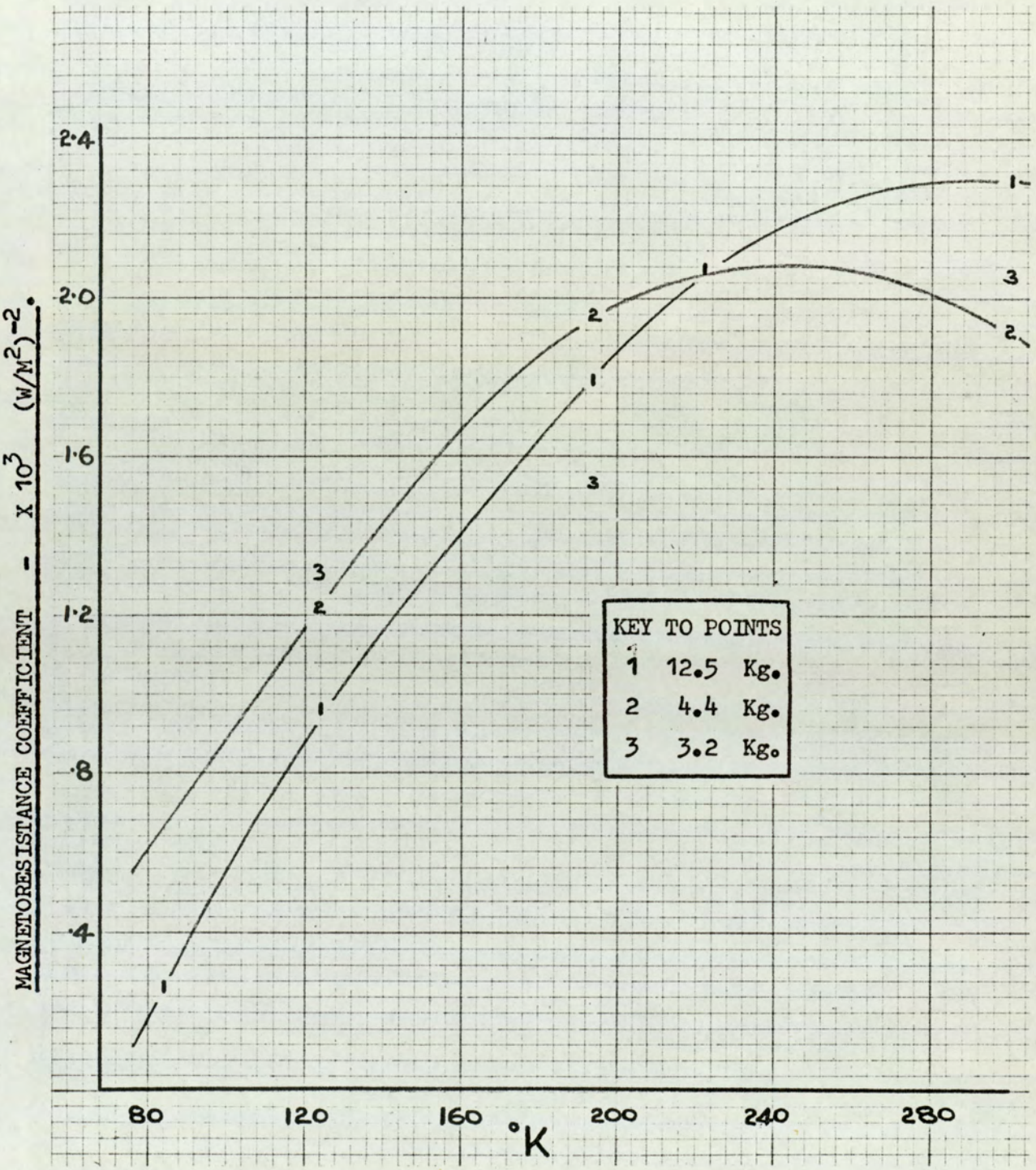

Fig. 88. Magnetoresistance coefficient vs. temperature at a selection of magnetic fields for a bismuth film of 309 Å.

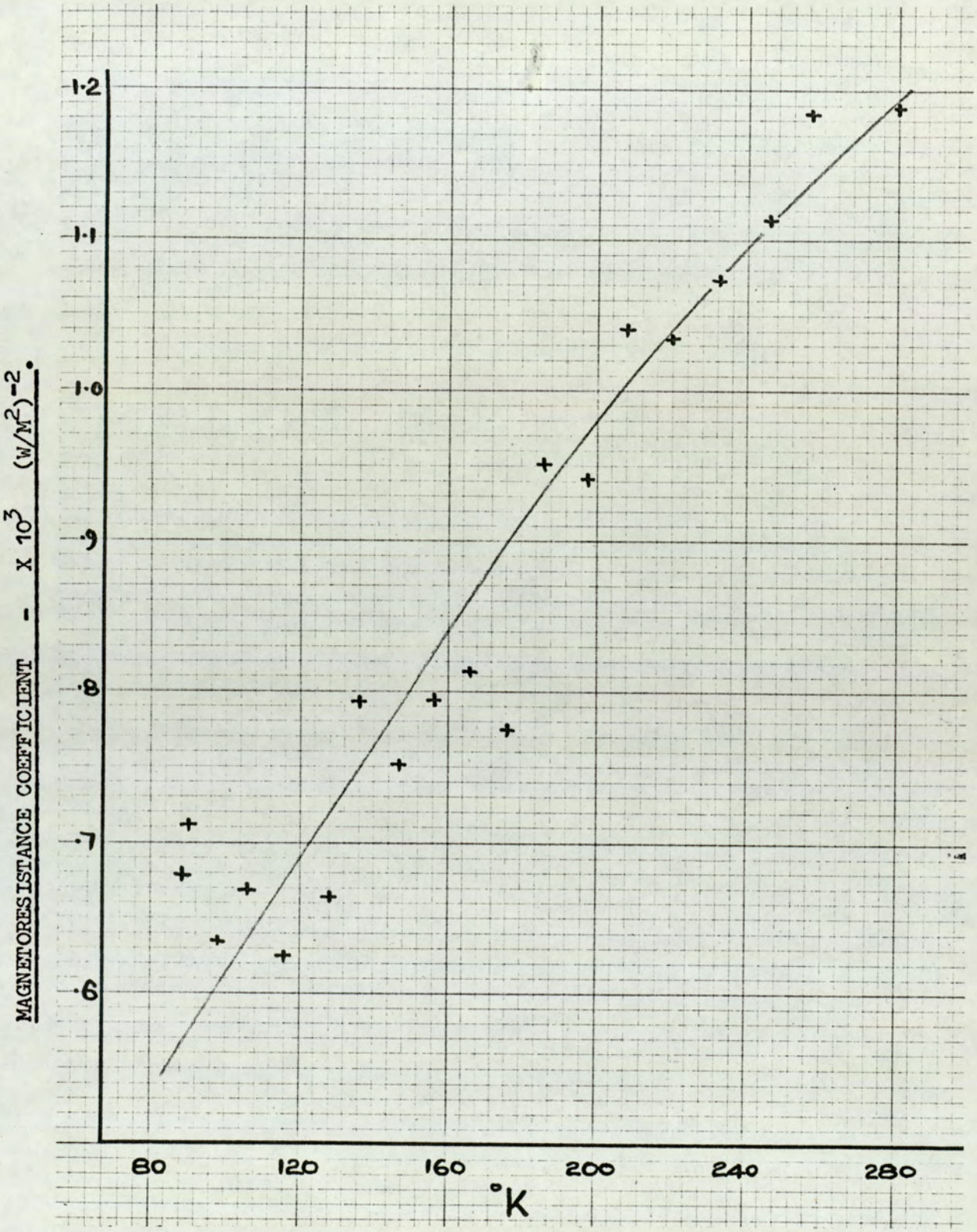

Fig. 89. Magnetoresistance coefficient vs. temperature at 12.5 Kilogauss for a bismuth film of 357 Å.

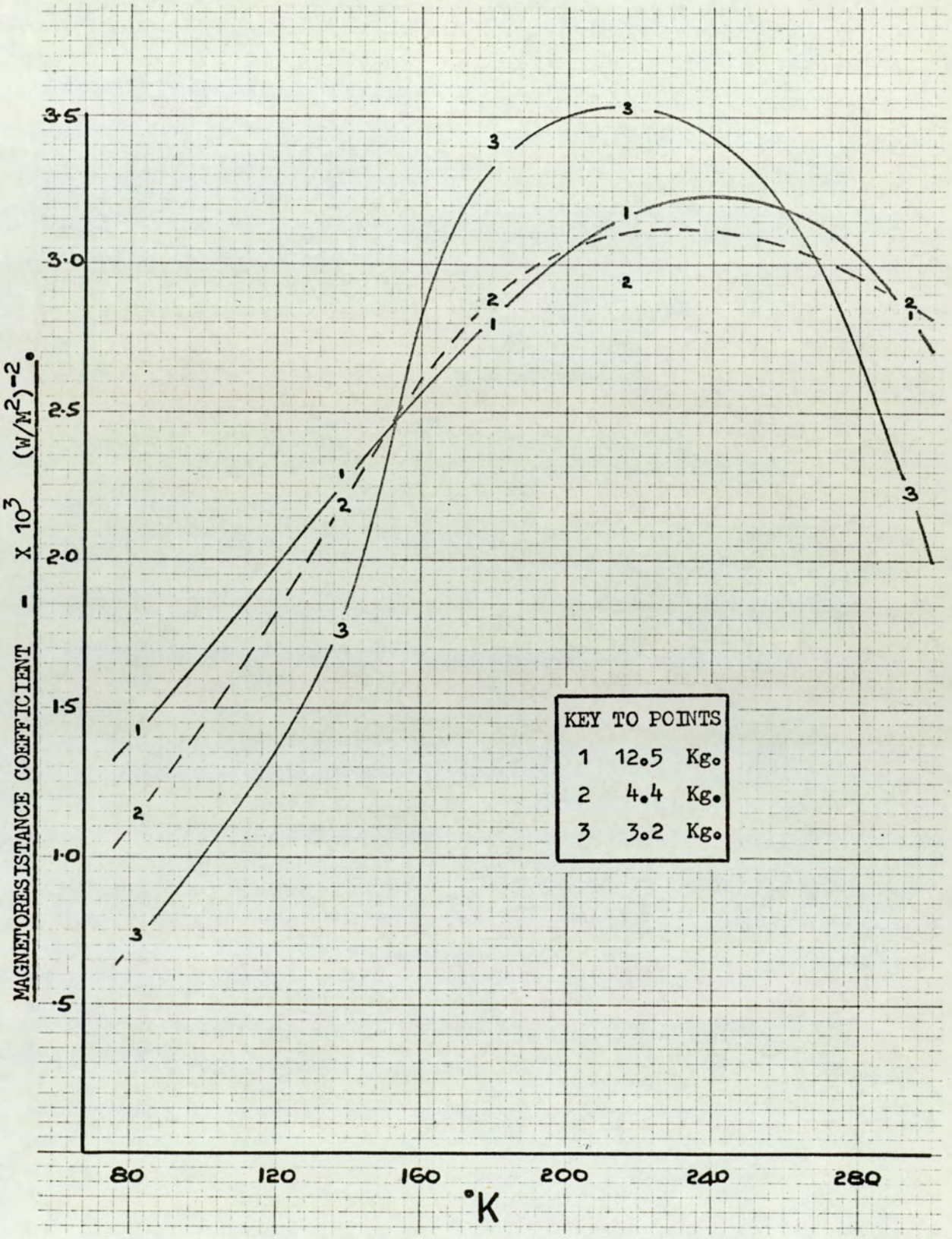

Fig. 90. Magnetoresistance coefficient vs. temperature at a selection of magnetic fields for a bismuth film of 401 Å.

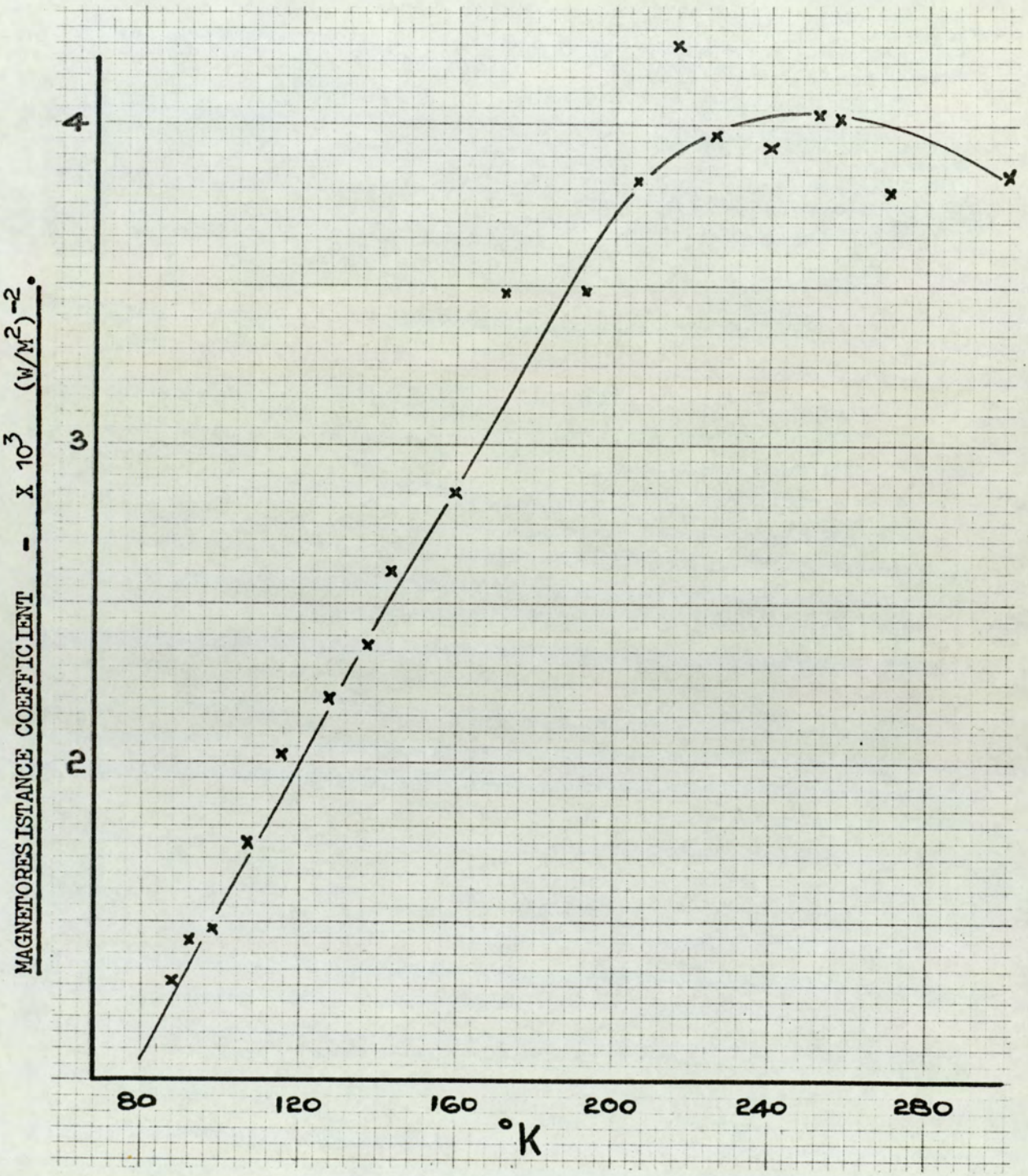

Fig. 91. Magnetoresistance coefficient vs. temperature at 12.5 Kilogauss for a bismuth film of 451 Å.

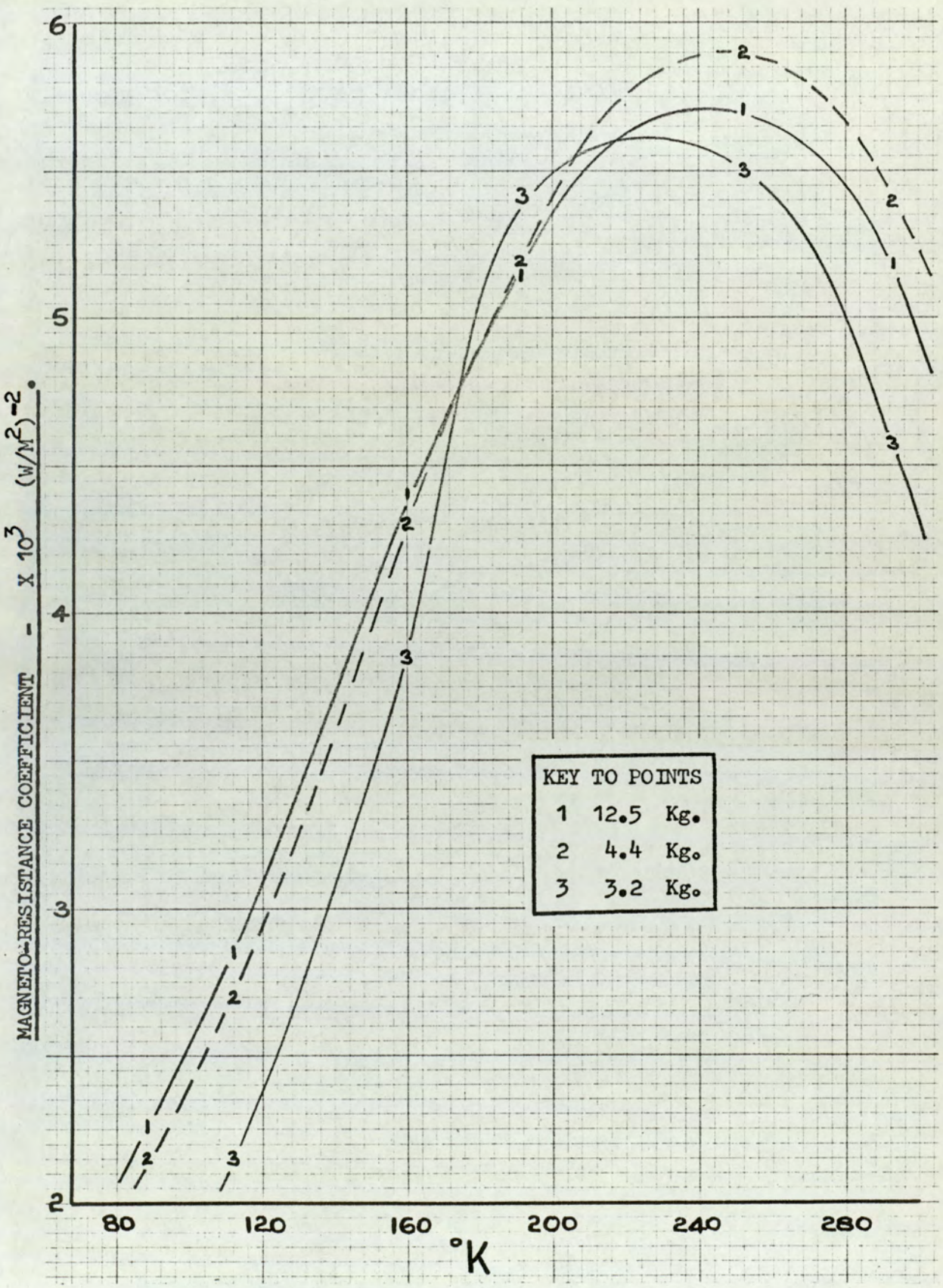

Fig. 92. Magnetoresistance coefficient vs. temperature at a selection of magnetic fields for a bismuth film of 504 Å.

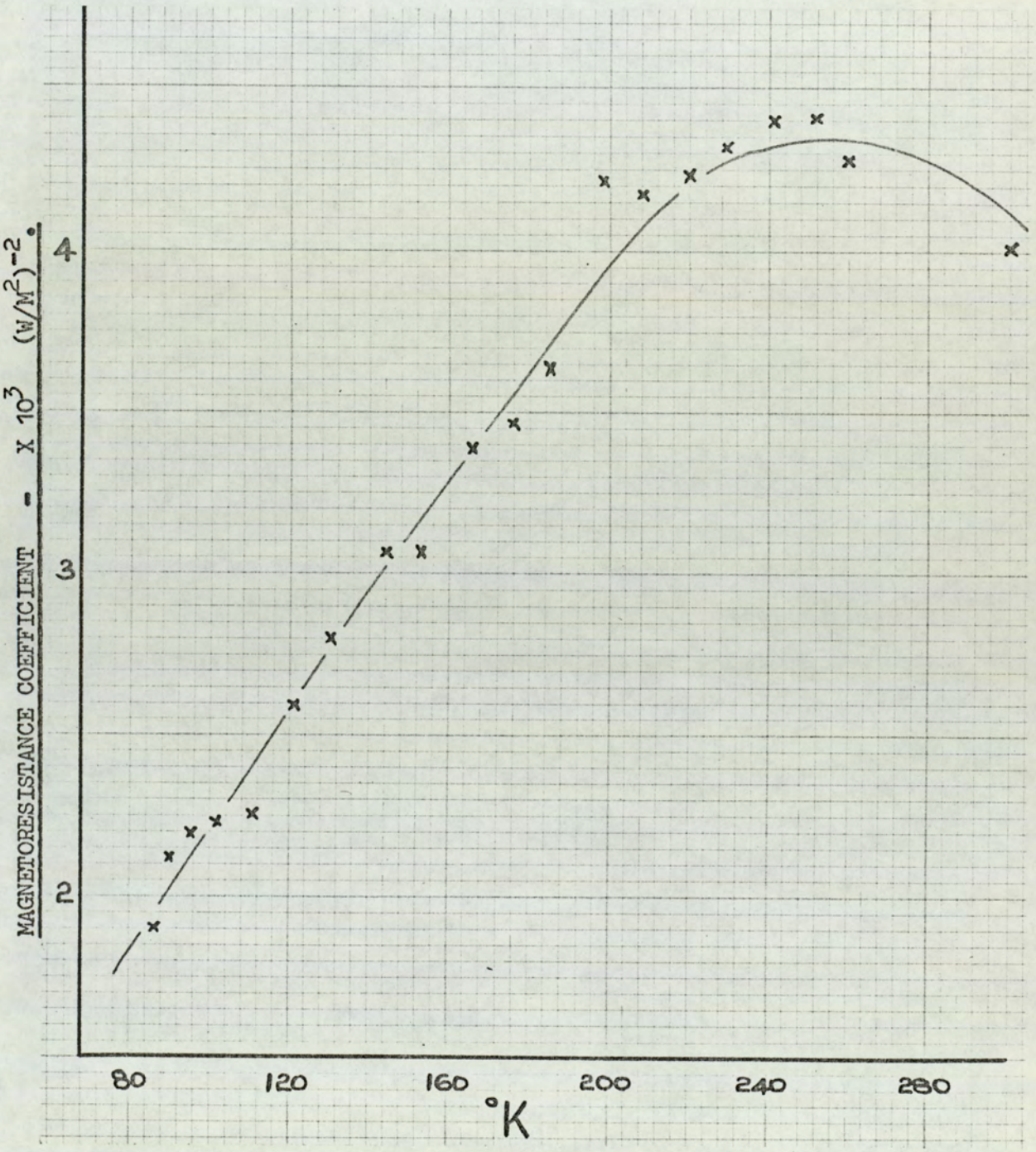

Fig. 93. Magnetoresistance coefficient vs. temperature at 12.5 Kilogauss for a bismuth film of 552 Å.

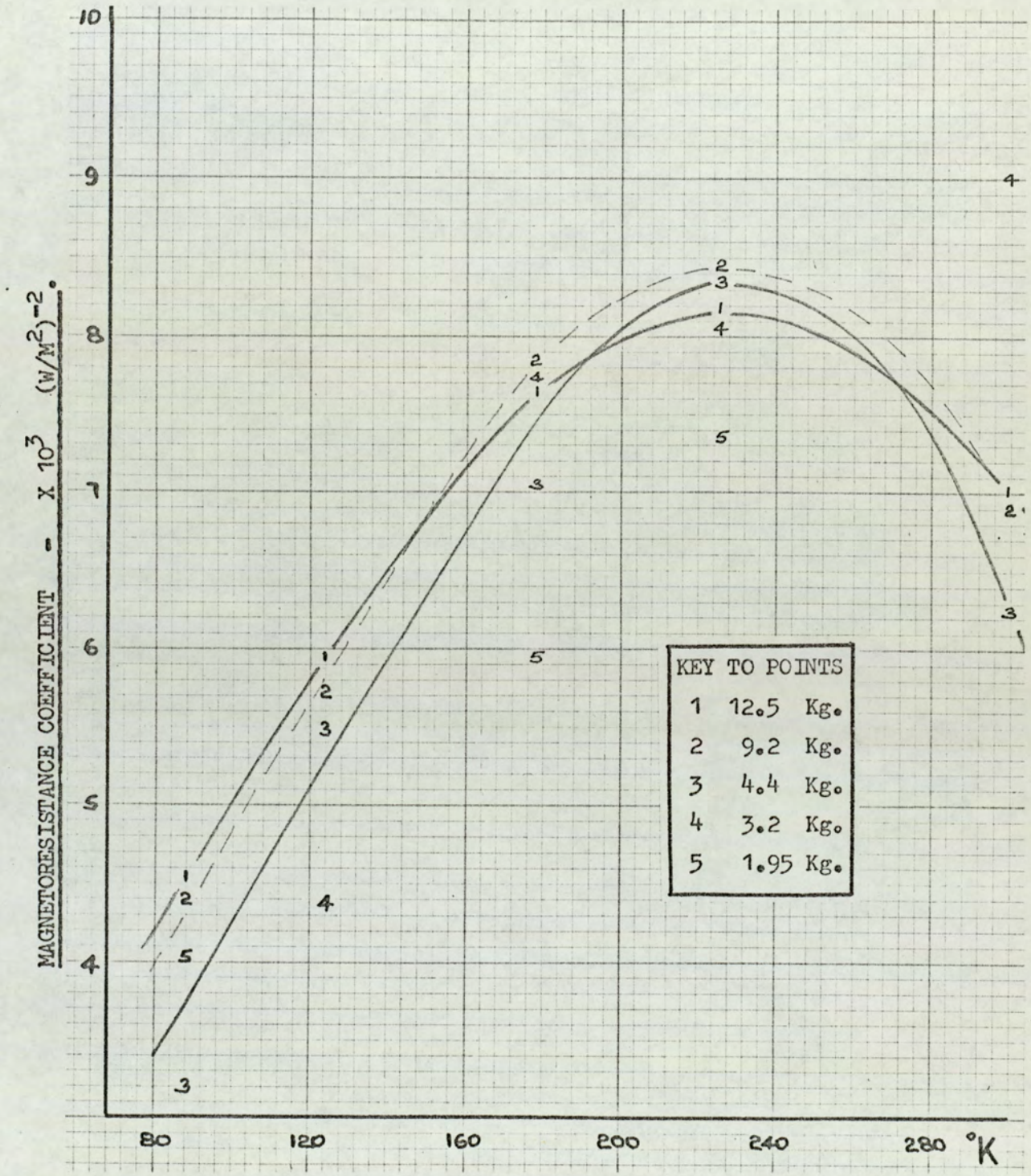

Fig. 94. Magnetoresistance coefficient vs. temperature at a selection of magnetic fields for a bismuth film of 609 Å.

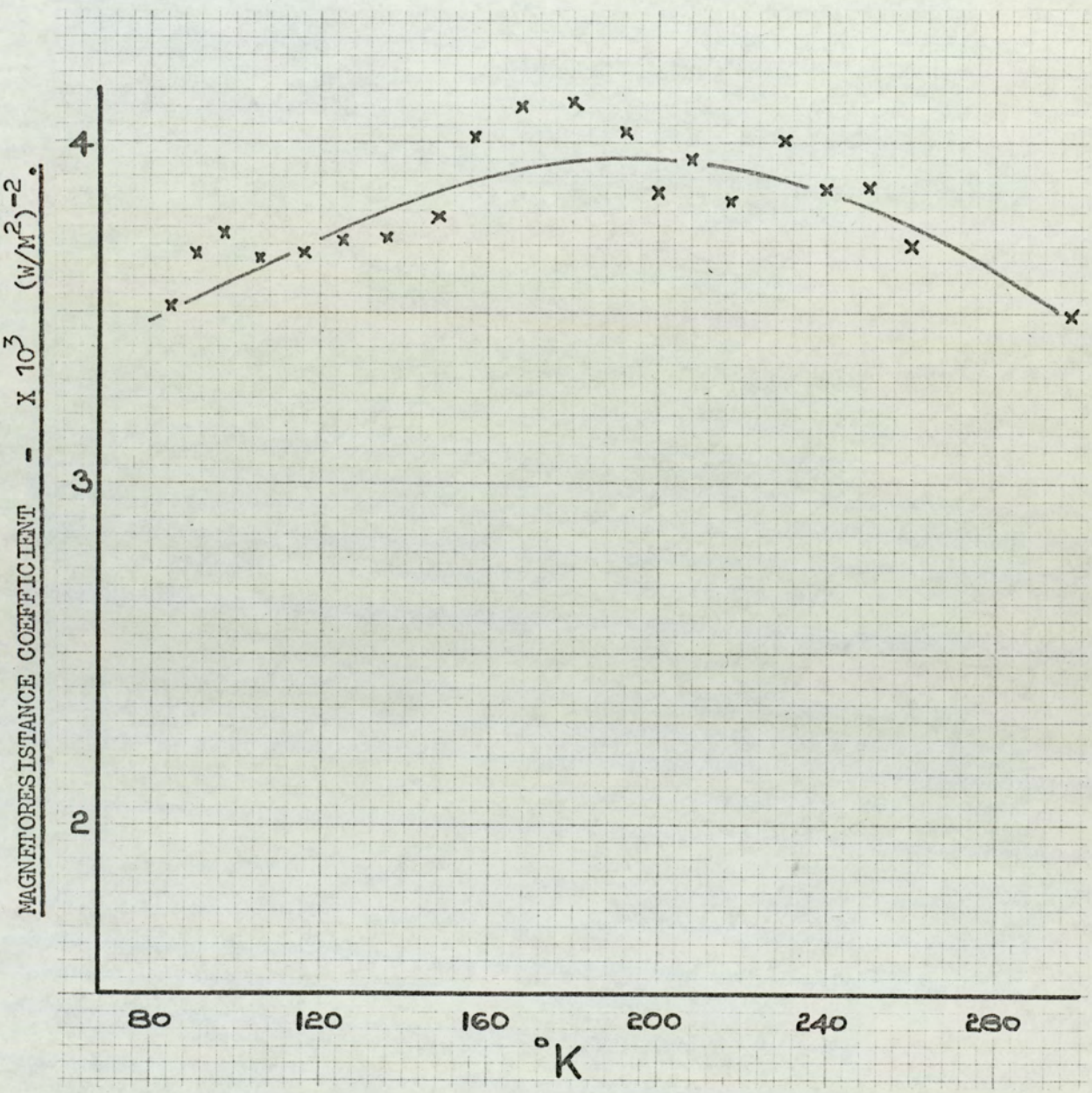

Fig. 95. Magnetoresistance coefficient vs. temperature at 12.5 Kilogauss for a bismuth film of 650 Å.

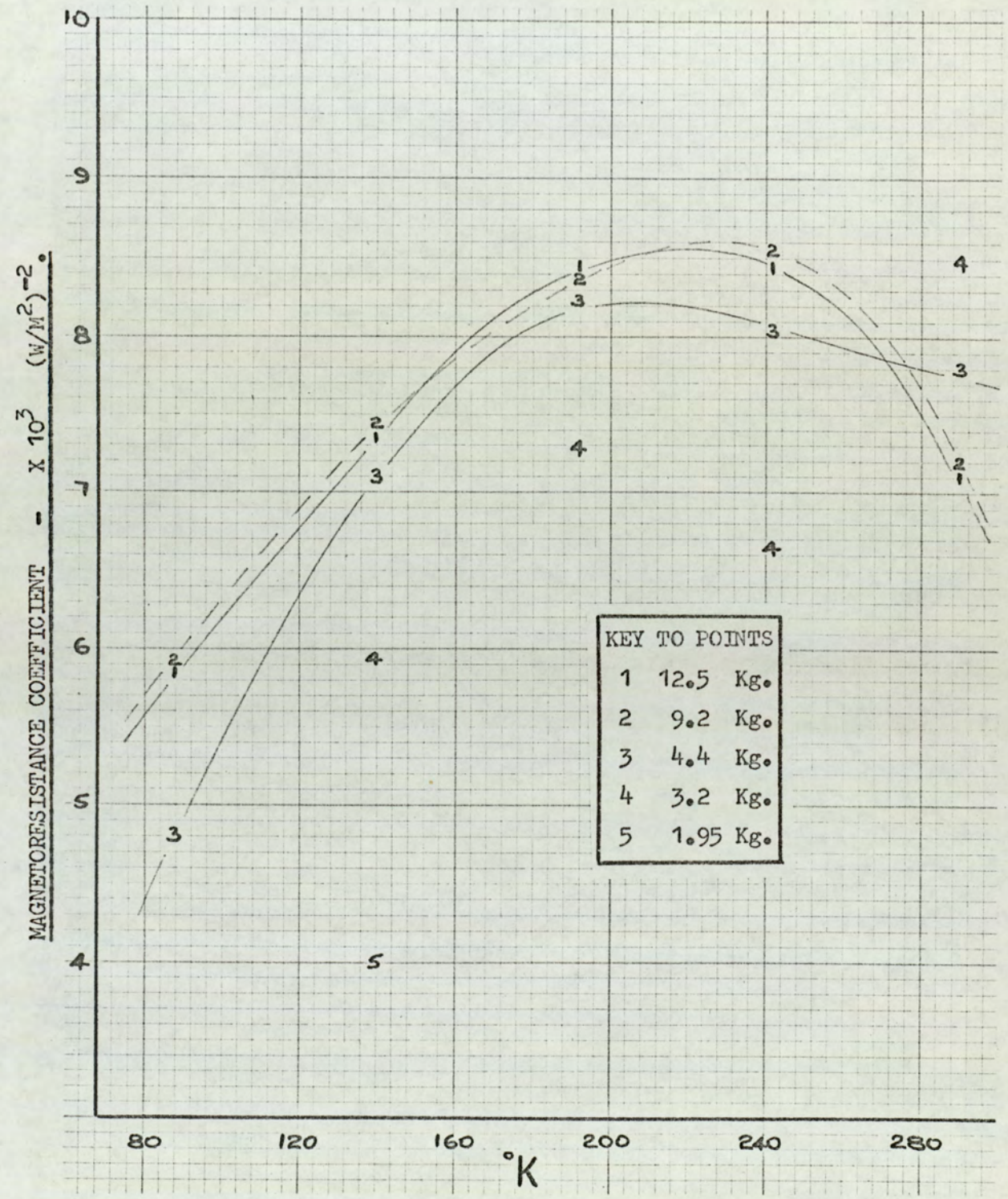

Fig. 96. Magnetoresistance coefficient vs. temperature at a selection of magnetic fields for a bismuth film of 735 Å.

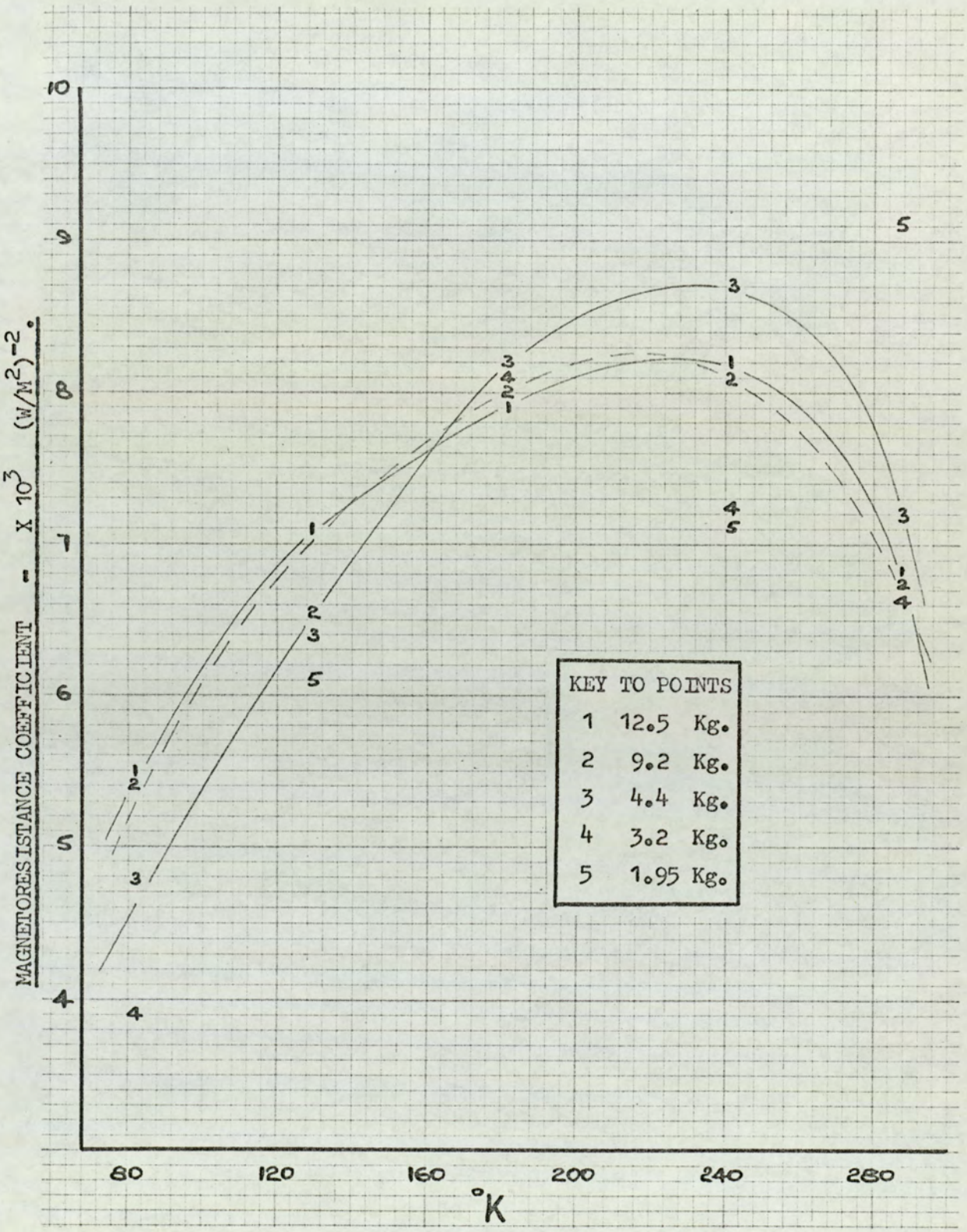

Fig. 97. Magnetoresistance coefficient vs. temperature at a selection of magnetic fields for a bismuth film of 744 Å.

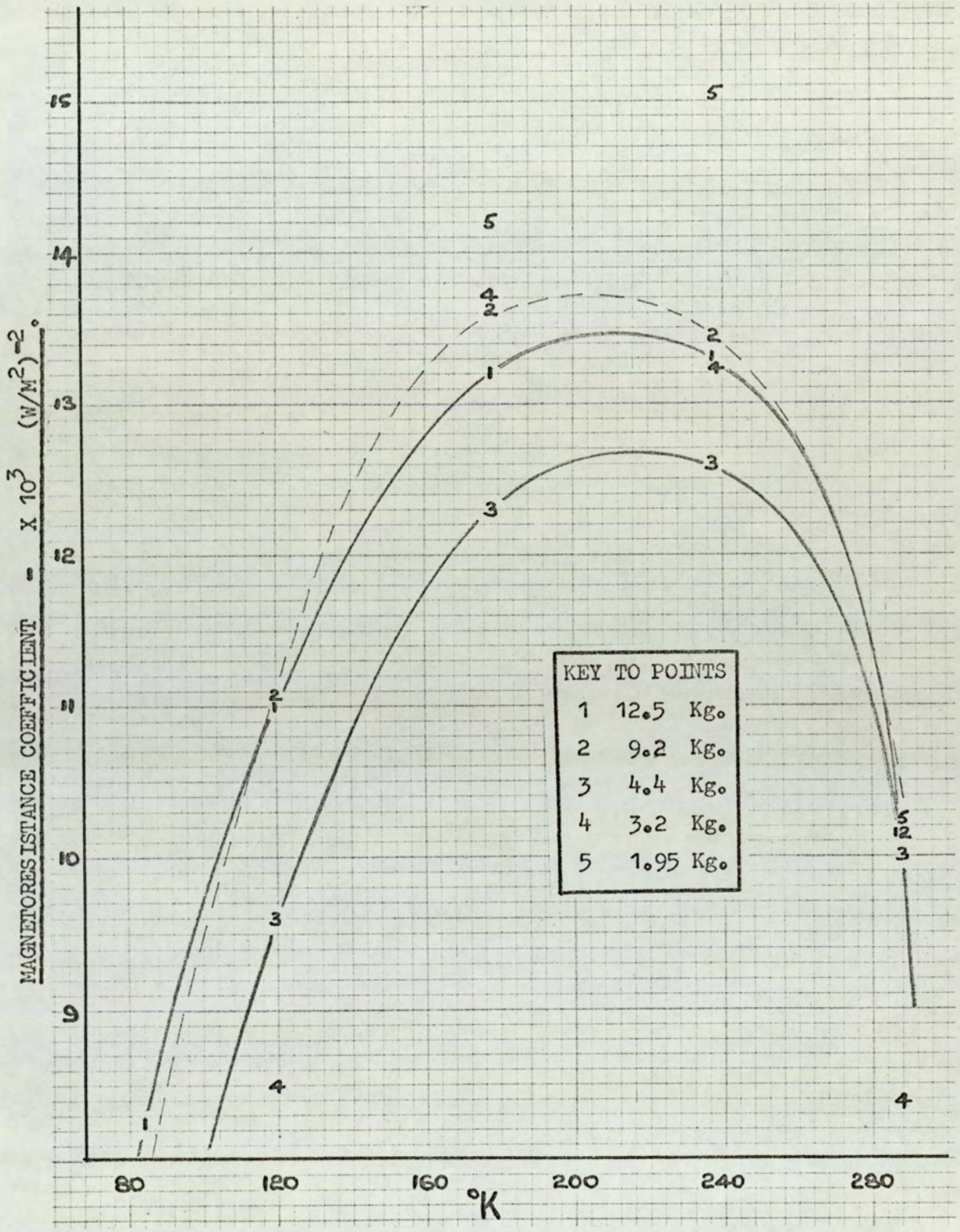

Fig. 98. Magnetoresistance coefficient vs. temperature at a selection of magnetic fields for a bismuth film of 801 Å.

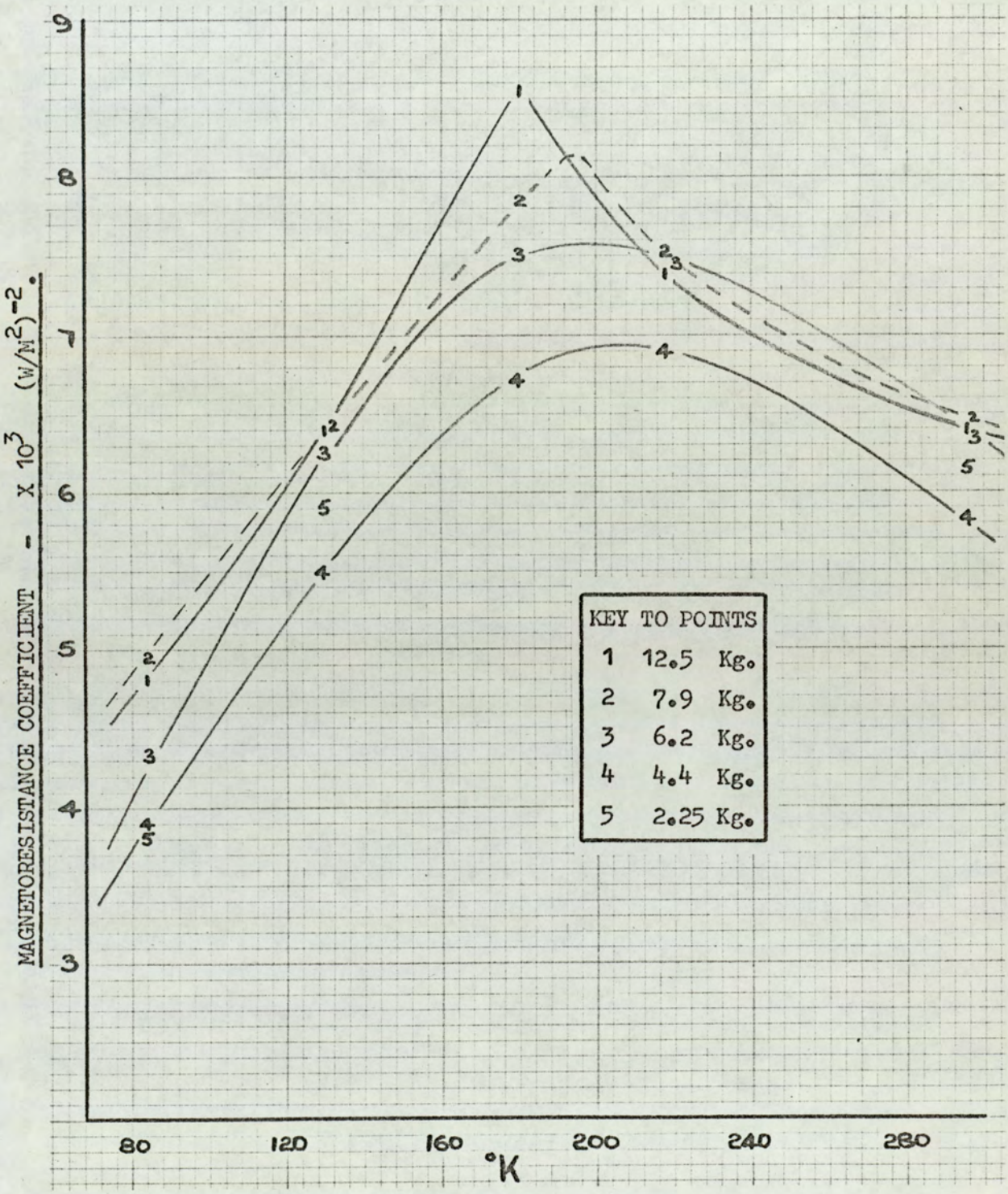

Fig. 99. Magnetoresistance coefficient vs. temperature at a selection of magnetic fields for a bismuth film of 862 Å.

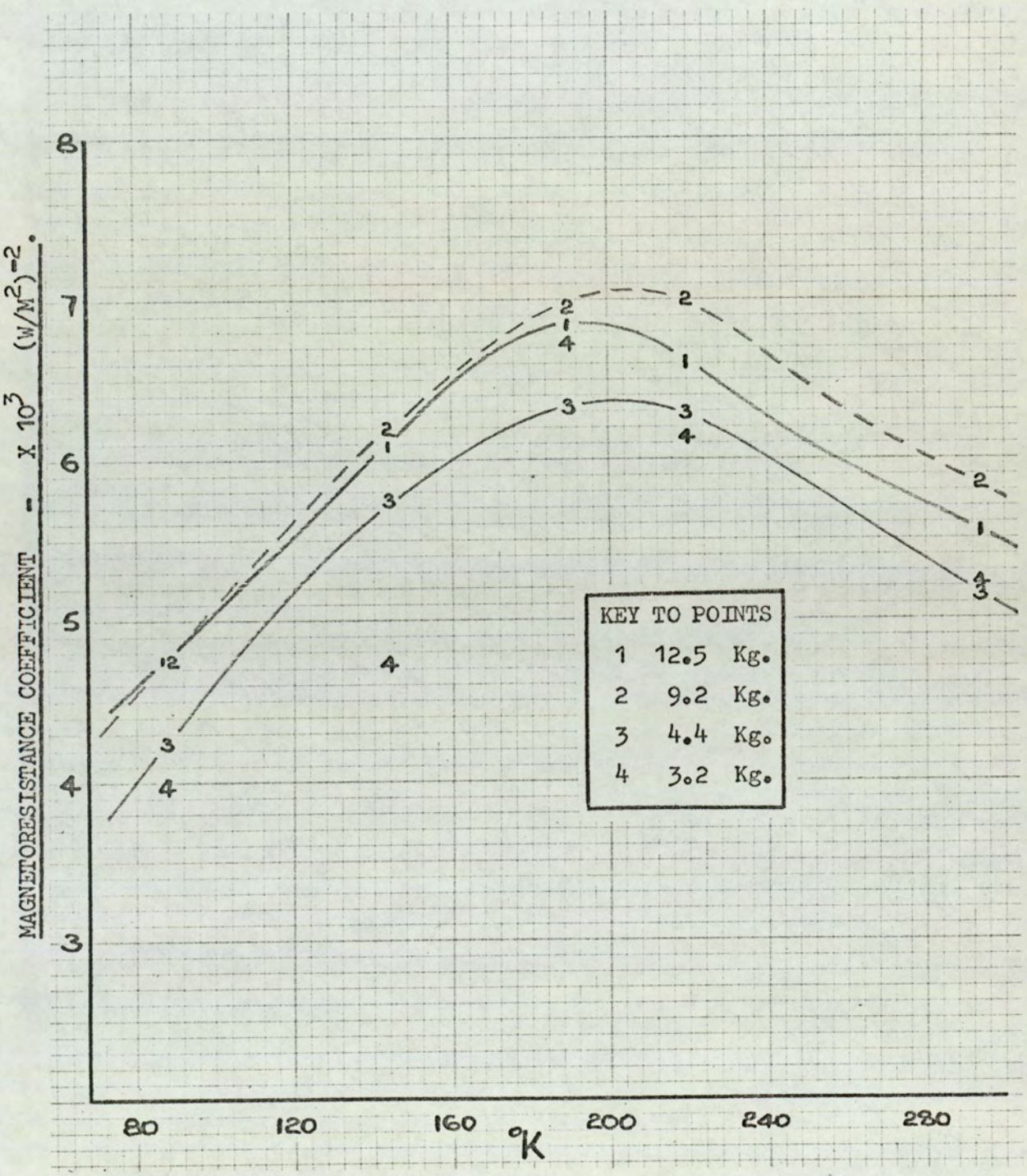

Fig. 100. Magnetoresistance coefficient vs. temperature at a selection of magnetic fields for a bismuth film of 927 Å.

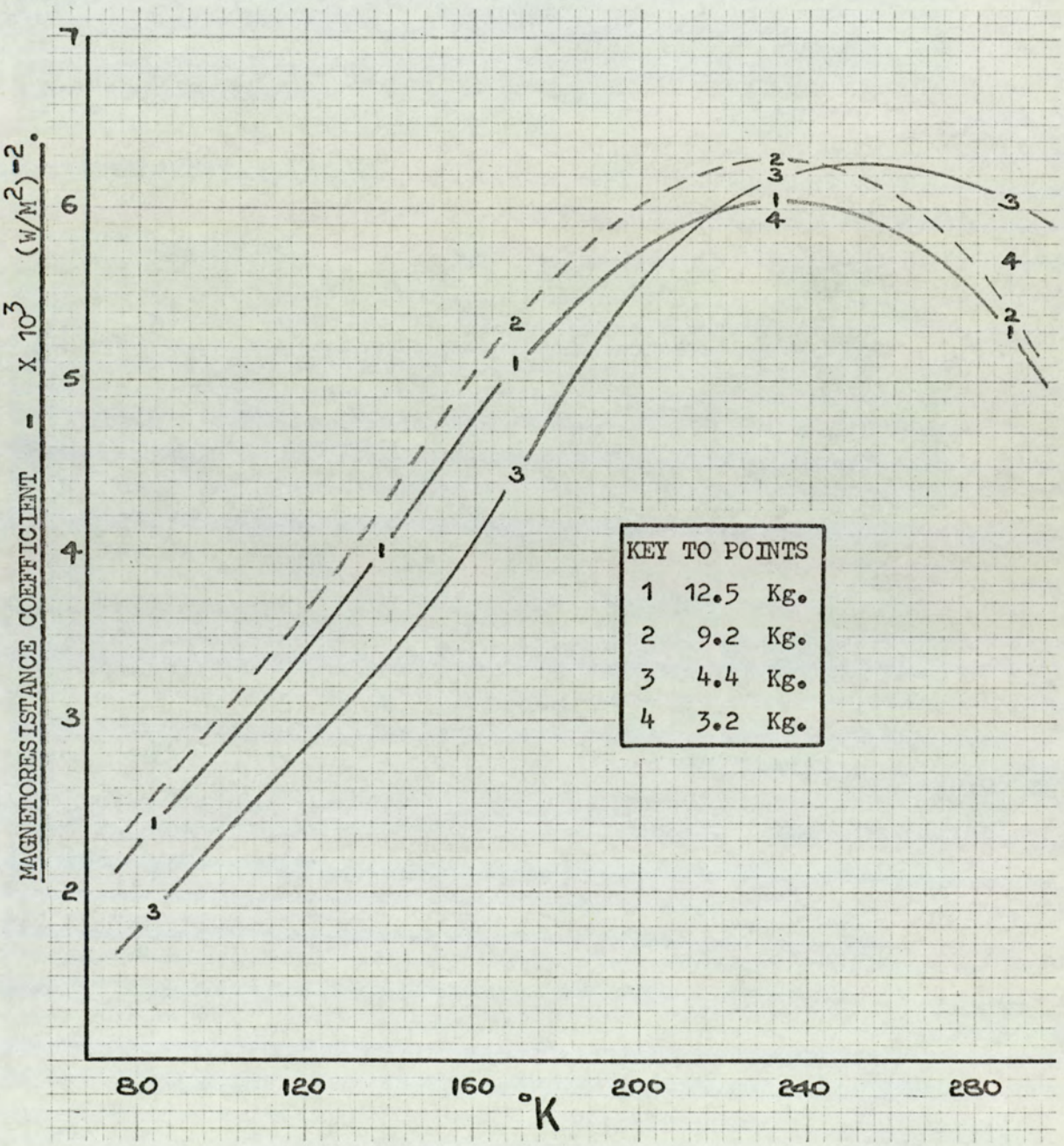

Fig. 101. Magnetoresistance coefficient vs. temperature at a selection of magnetic fields for a bismuth film of 1100 Å.

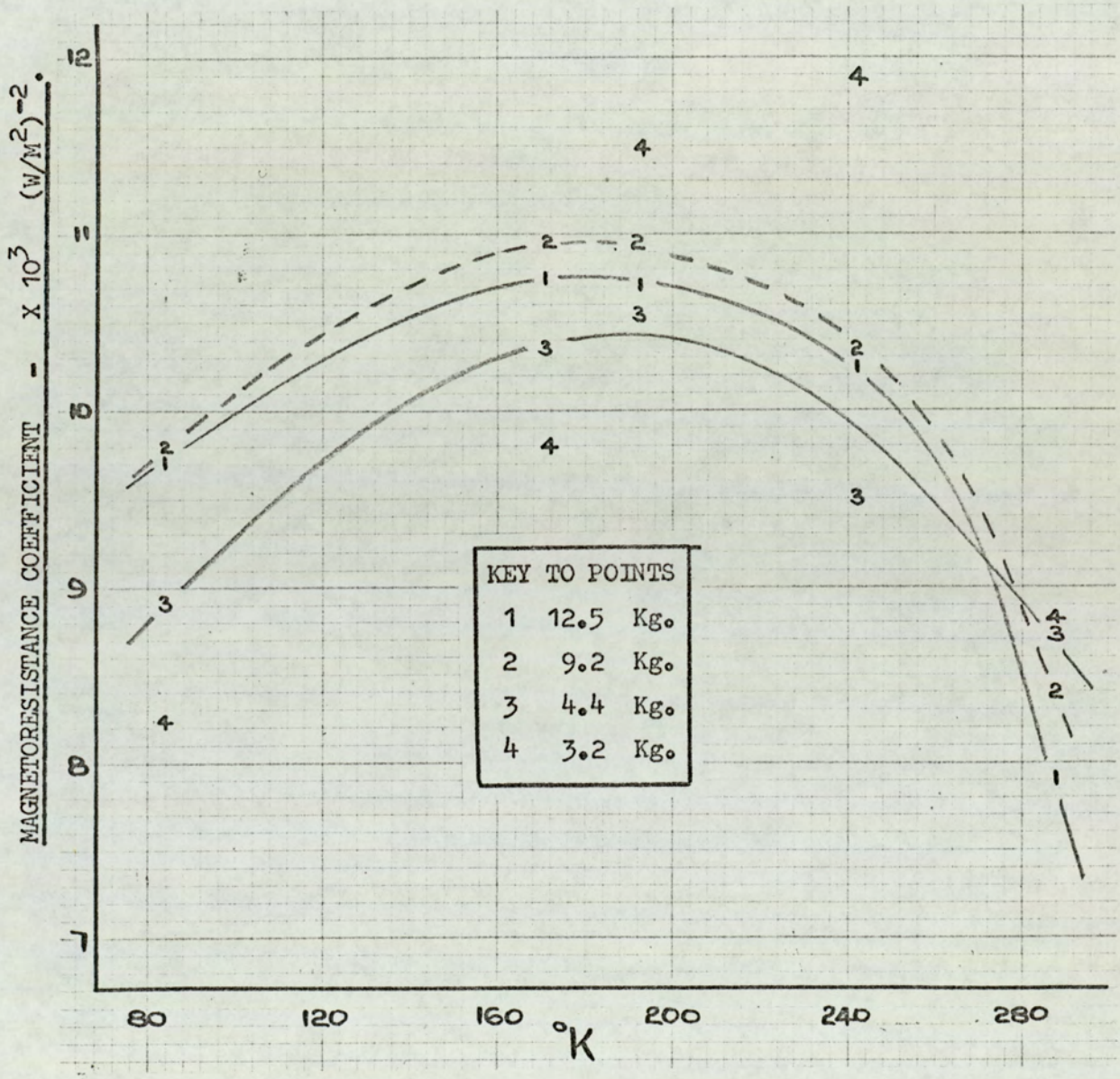

Fig. 102. Magnetoresistance coefficient vs. temperature at a selection of magnetic fields for a bismuth film of 1201 Å.

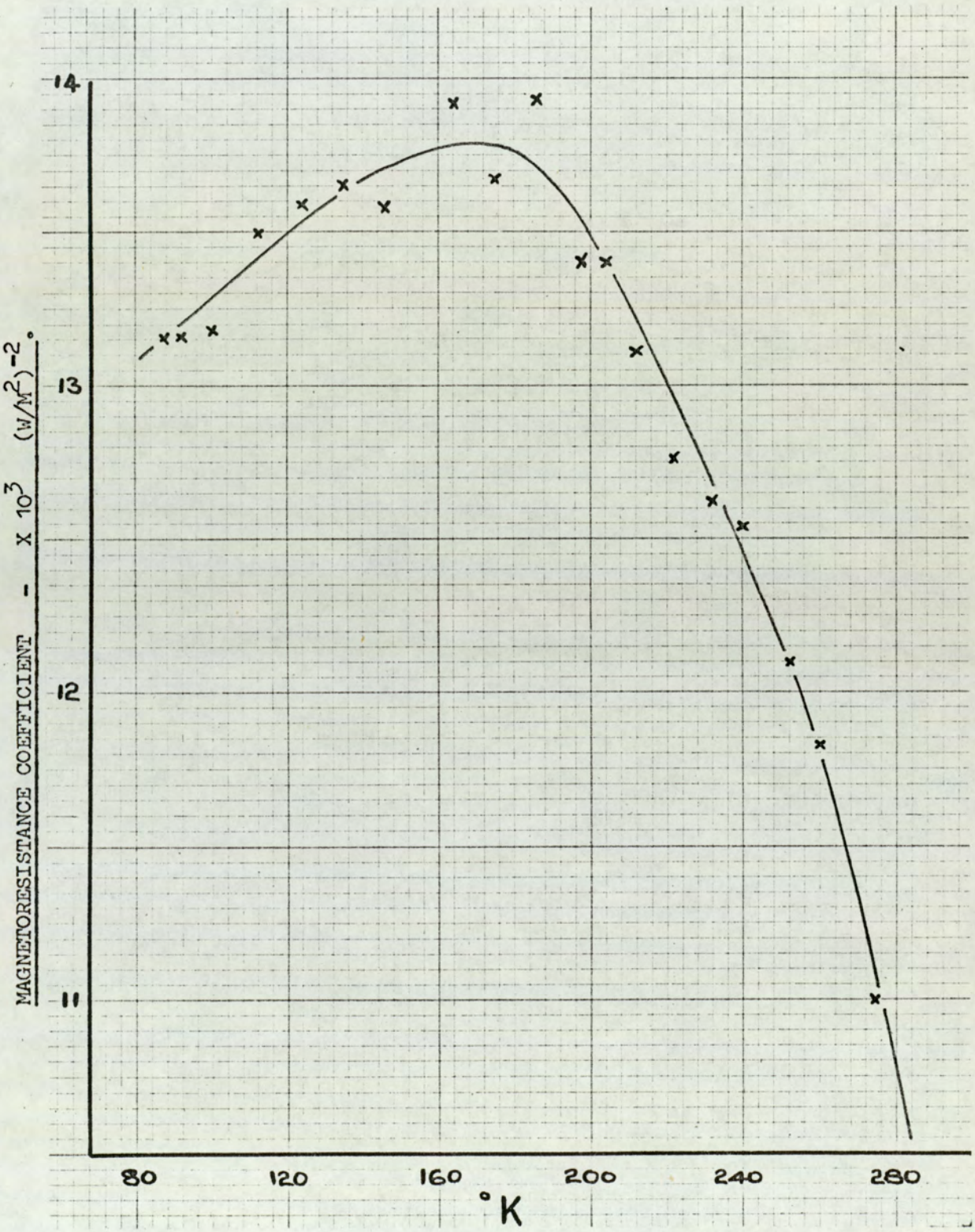

Fig. 103. Magnetoresistance coefficient vs. temperature at 12.5 Kilogauss for a bismuth film of 1270 Å.

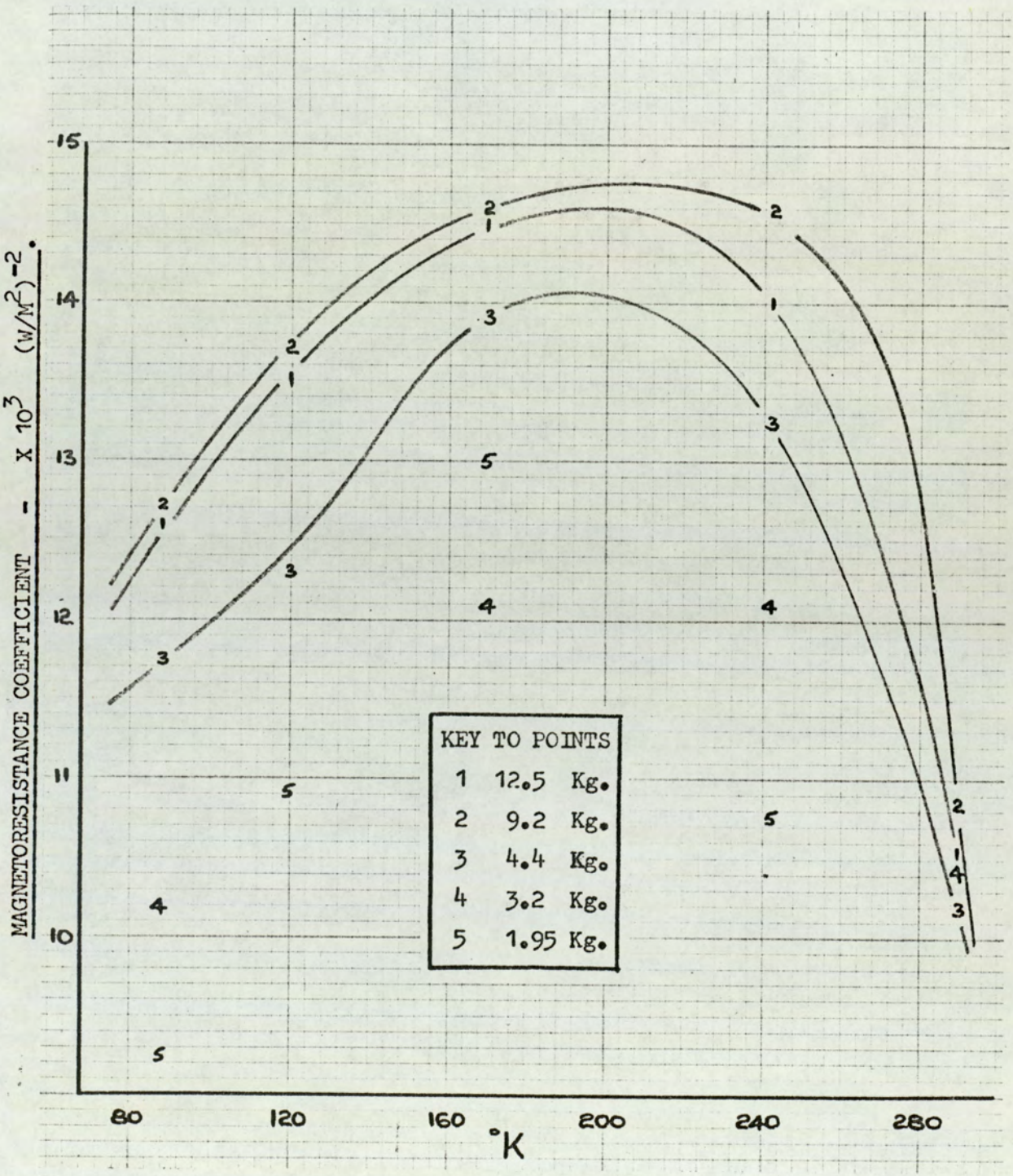

Fig. 104. Magnetoresistance coefficient vs. temperature at a selection of magnetic fields for a bismuth film of 1287 Å.

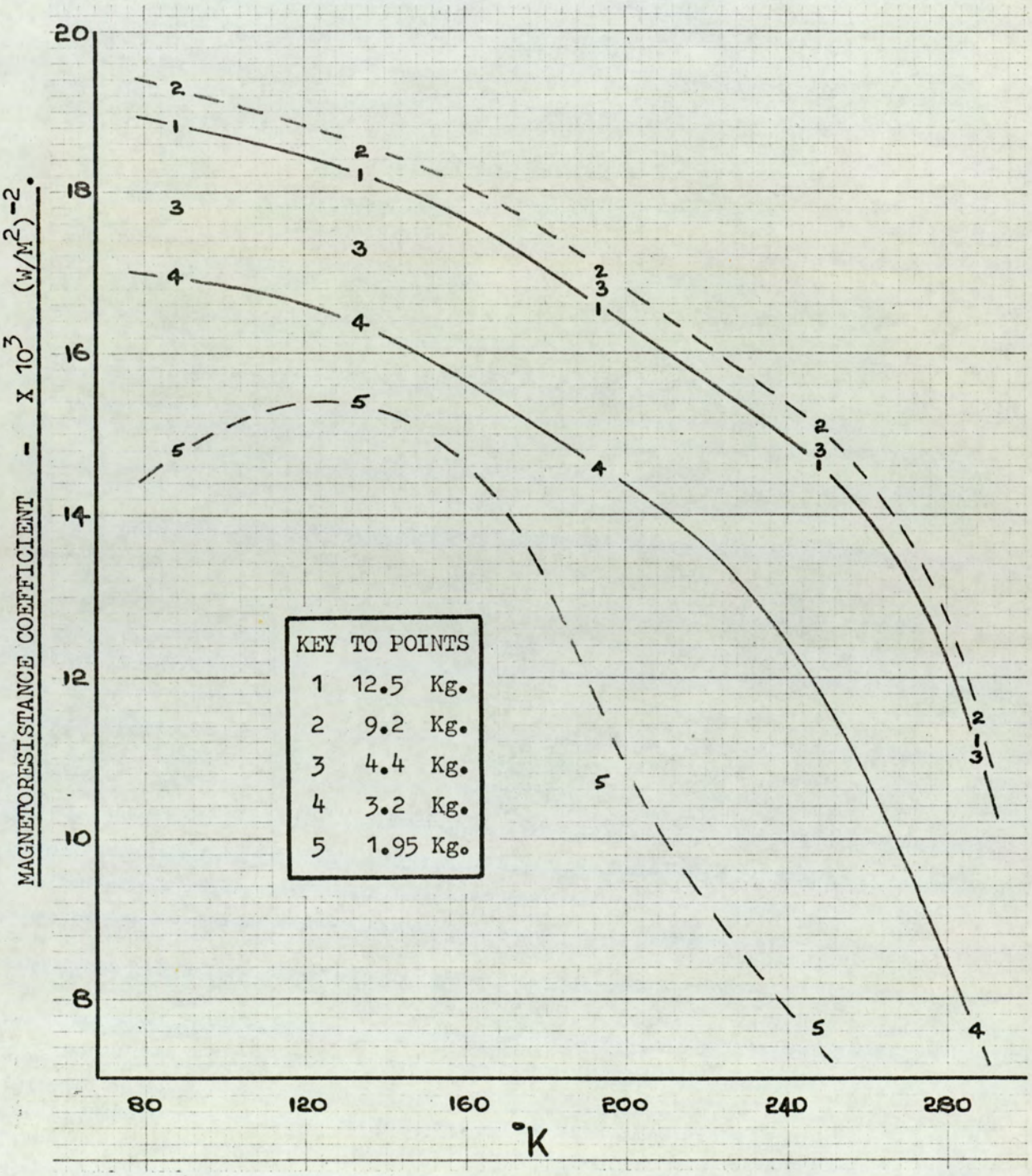

Fig. 105. Magnetoresistance coefficient vs. temperature at a selection of magnetic fields for a bismuth film of 1409 Å.

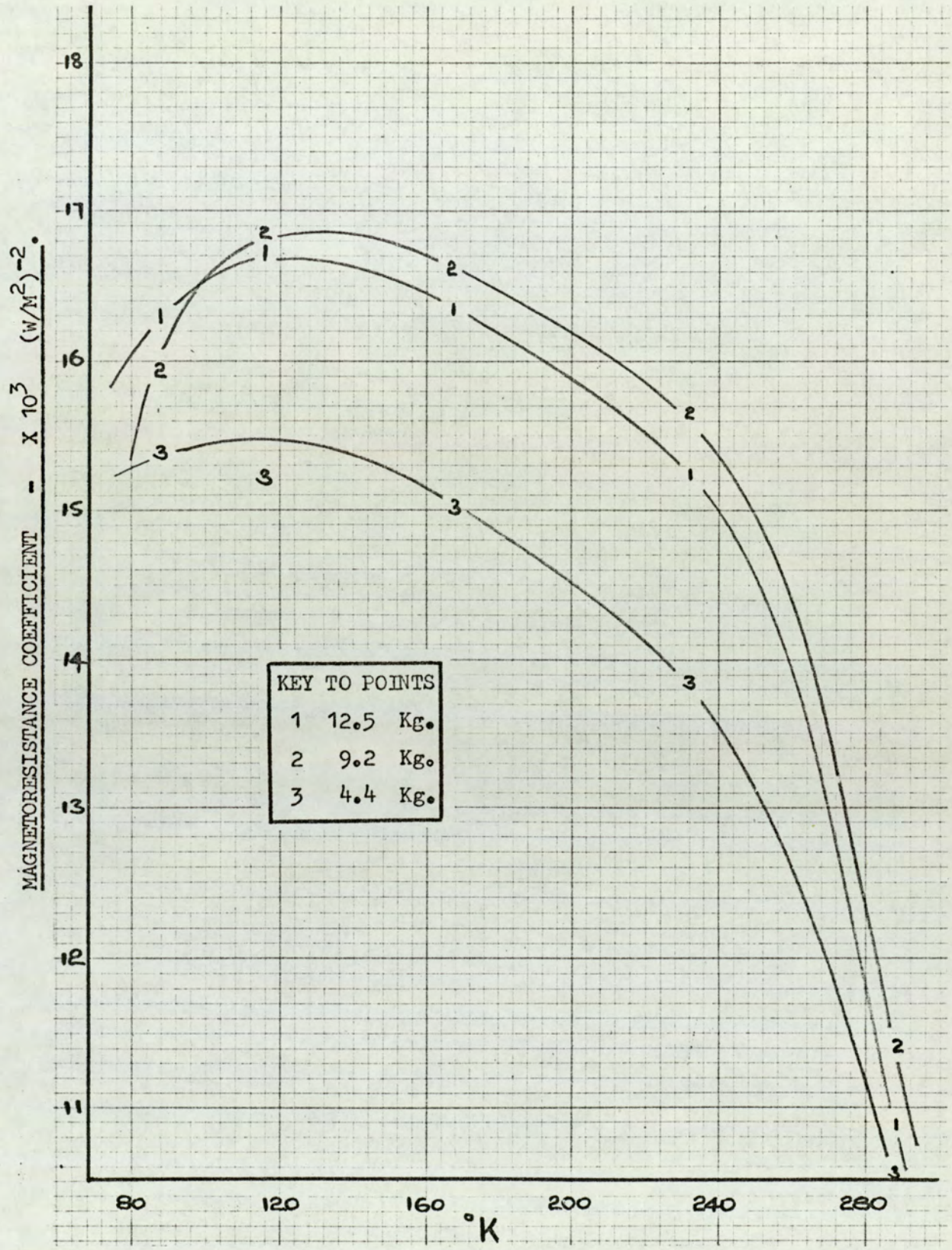

Fig. 106. Magnetoresistance coefficient vs. temperature at a selection of magnetic fields for a bismuth film of 1501 Å.

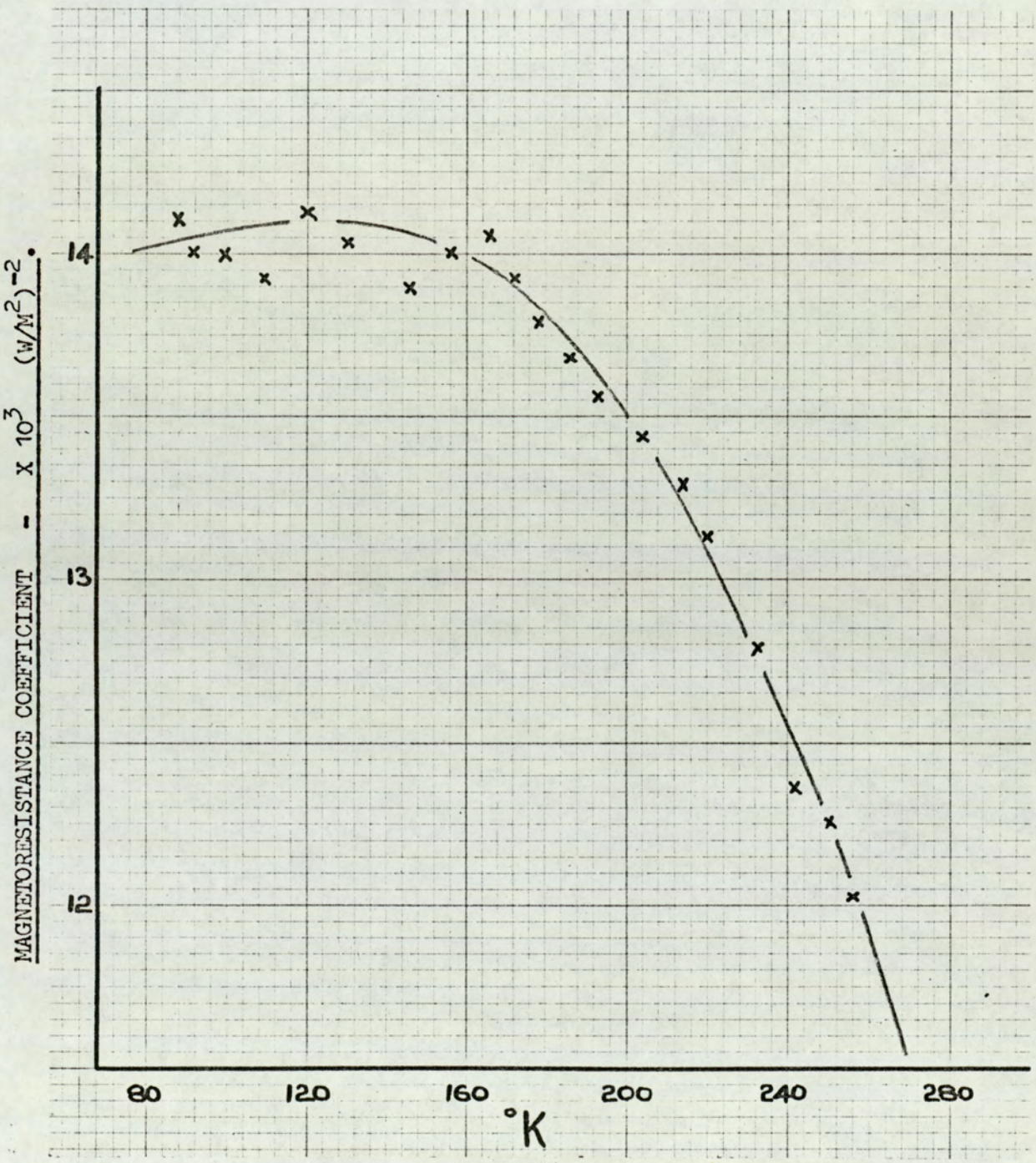

Fig. 107. Magnetoresistance coefficient vs. temperature at 12.5 Kilogauss for a bismuth film of 1587 Å.

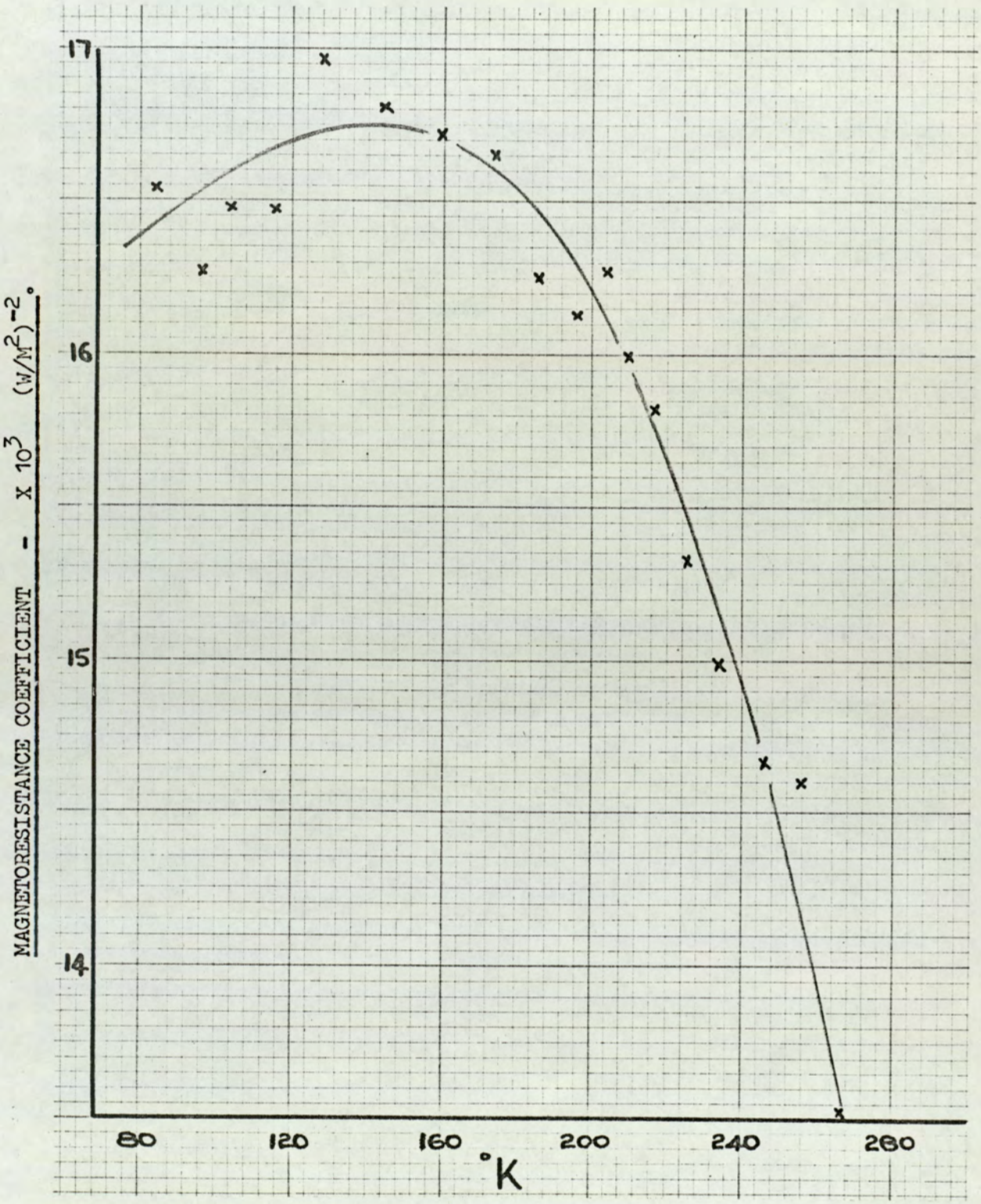

Fig. 108. Magnetoresistance coefficient vs. temperature at 12.5 Kilogauss for a bismuth film of 1697 Å.

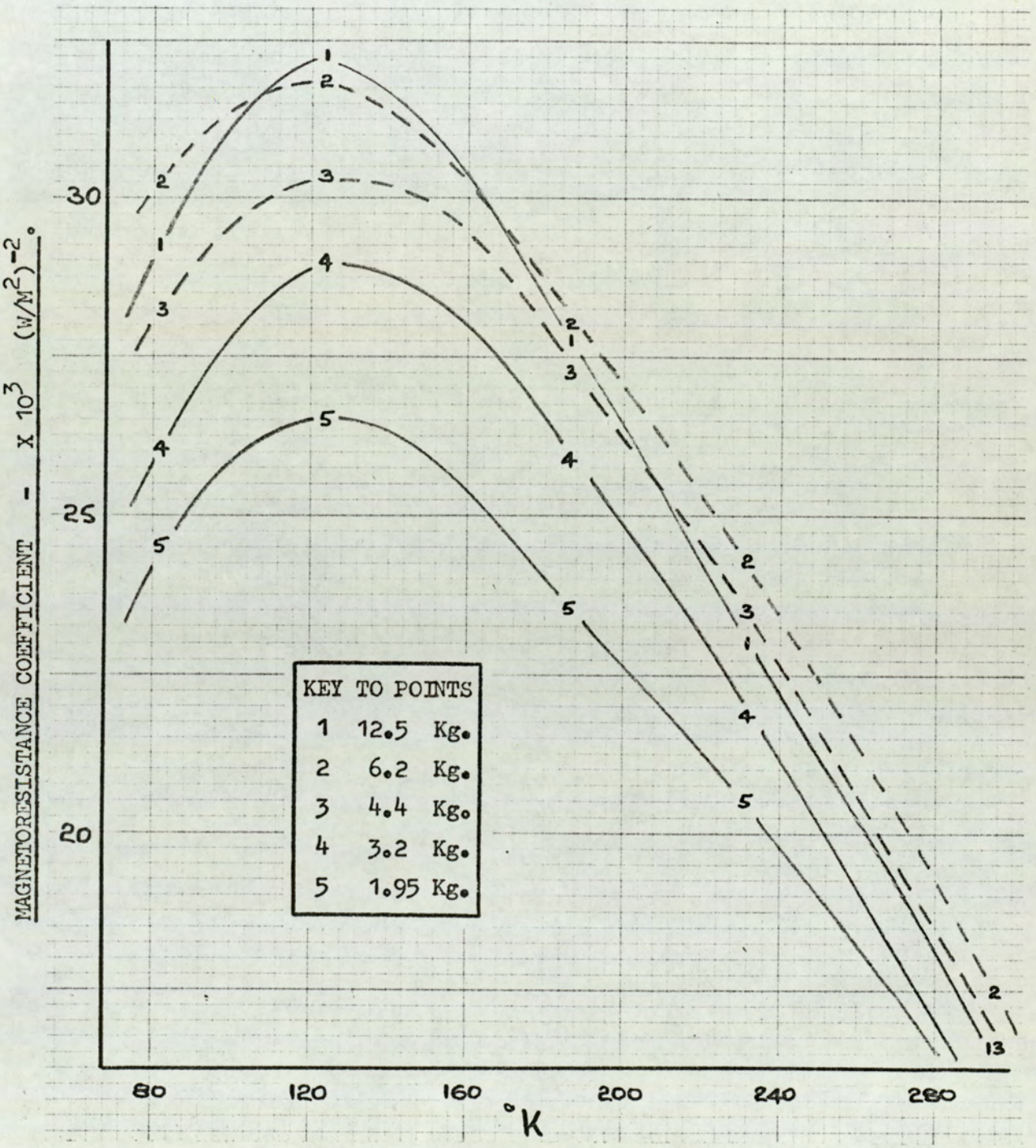

Fig. 109. Magnetoresistance coefficient vs. temperature at a selection of magnetic fields for a bismuth film of 2045 Å.

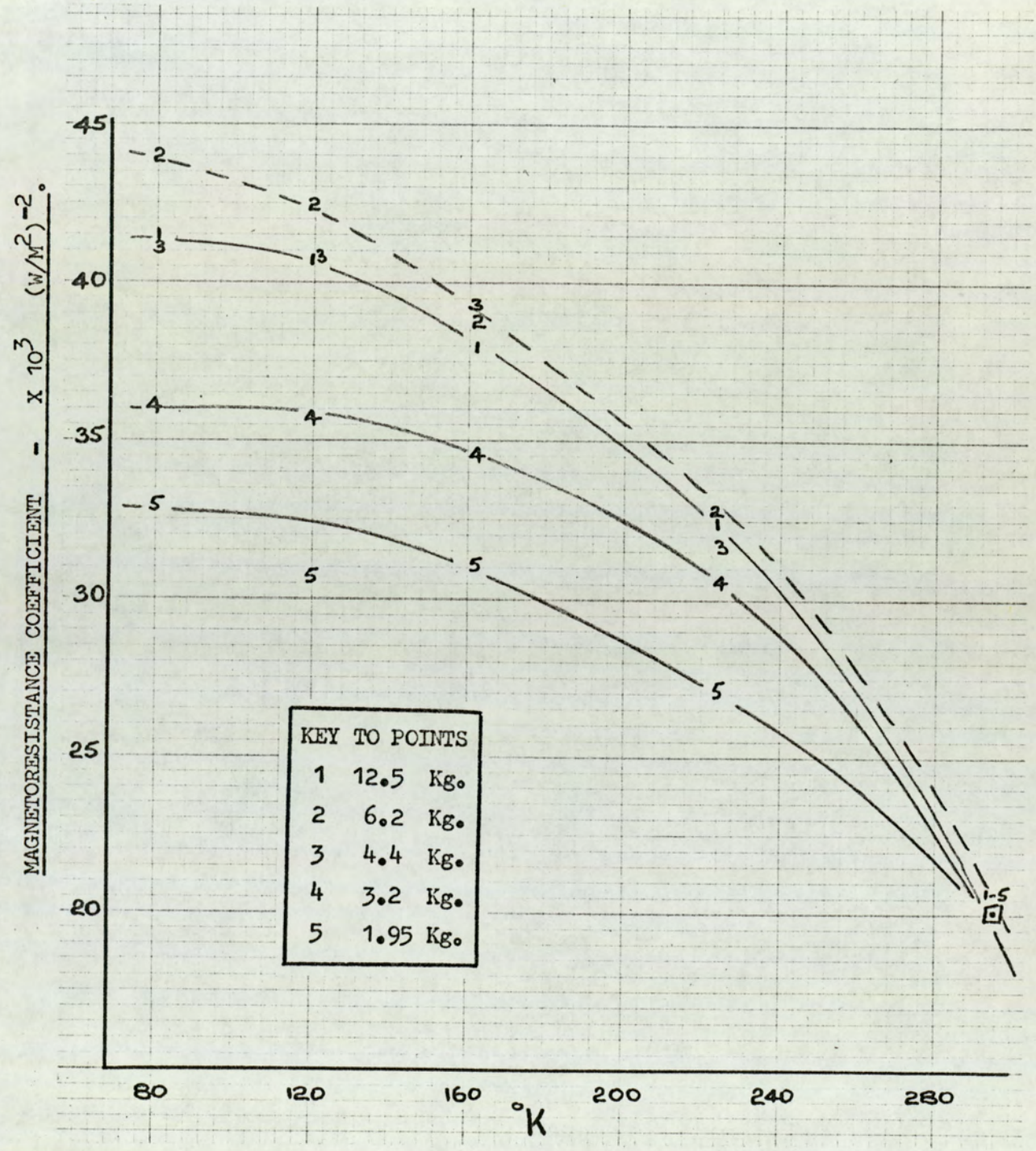

Fig. 110. Magnetoresistance coefficient vs. temperature at a selection of magnetic fields for a bismuth film of 4500 Å.

variation" runs whilst the remainder are derived from the "temperature variation" runs.

5.5. Hall coefficient

The presence of a Hall voltage is a direct manifestation of the Lorentz force on a charged carrier moving in a magnetic field. For a two carrier system in which the Hall coefficient expression is the difference of two terms, the sign of the Hall voltage is directly related to that of the majority carrier. The quantitative problem is however more complex in that the variation of the number of carriers in bismuth under the influence of a magnetic field reported in the literature [10] affects the magnitude of the Hall coefficient.

The simple two carrier Hall expression for bismuth

would suggest that at a fixed temperature the Hall coefficient depends only on N, the number of carriers. Landau splitting of energy levels in a quantising magnetic field is however known to exist in bismuth, but it may be possible to reduce the perturbation to an effective change in the number of carriers at constant mobility.

Fig. 121 shows the results obtained on a film of 735 Å at a selection of magnetic fields, and whose features generalise those of the series. Observations were taken over the temperature range 77 - 300°K. The prabolic nature of the curve is seen in which conduction by electrons predominated at the lower temperatures. The Hall coefficient decreased with increase in temperature until a zero value was obtained in the region of 180°K, resulting from the equality of the electron and hole mobilities. At higher temperatures holes

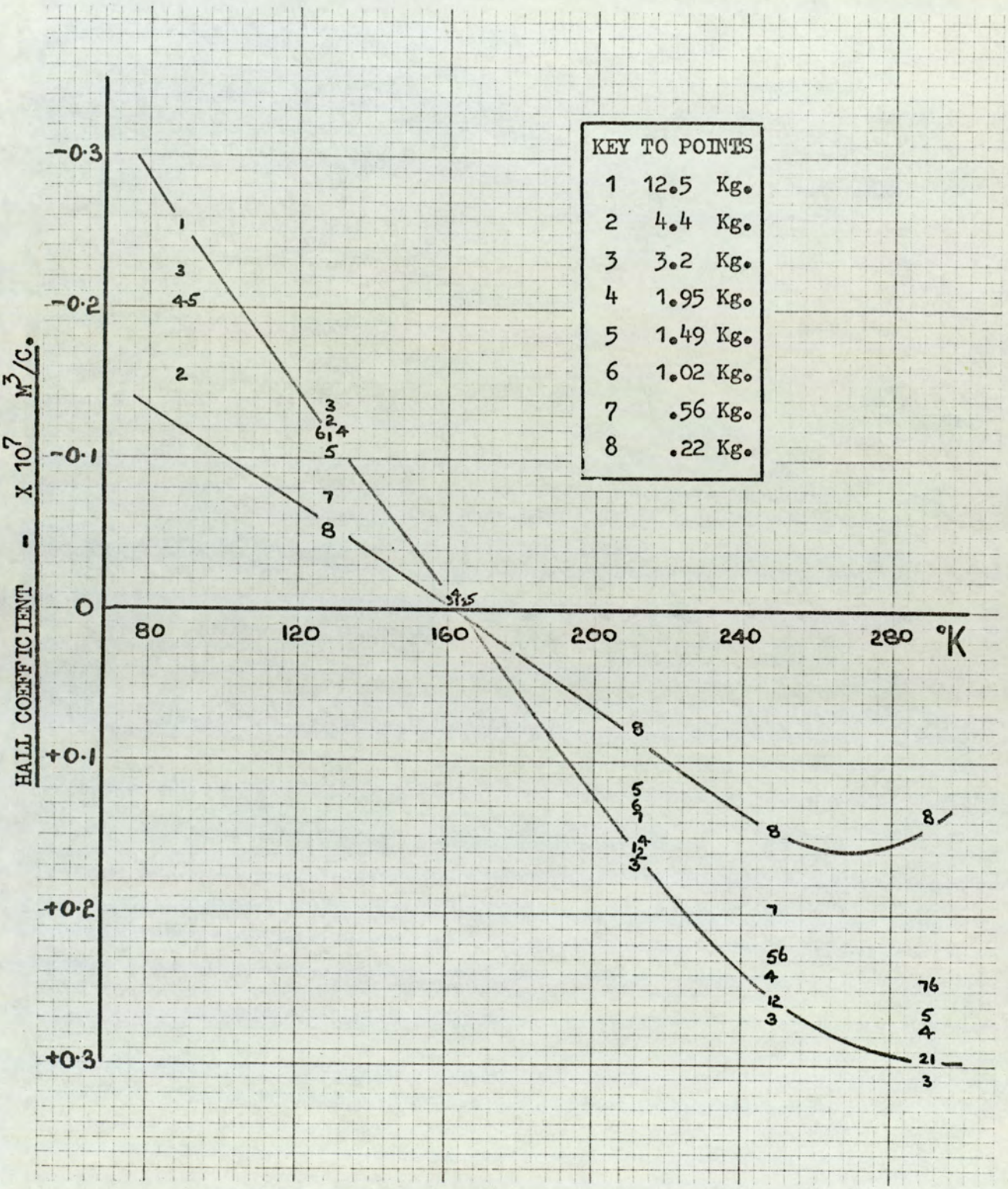

Fig. 111. Hall coefficient vs. temperature at a selection of magnetic fields for a bismuth film of 211 Å.

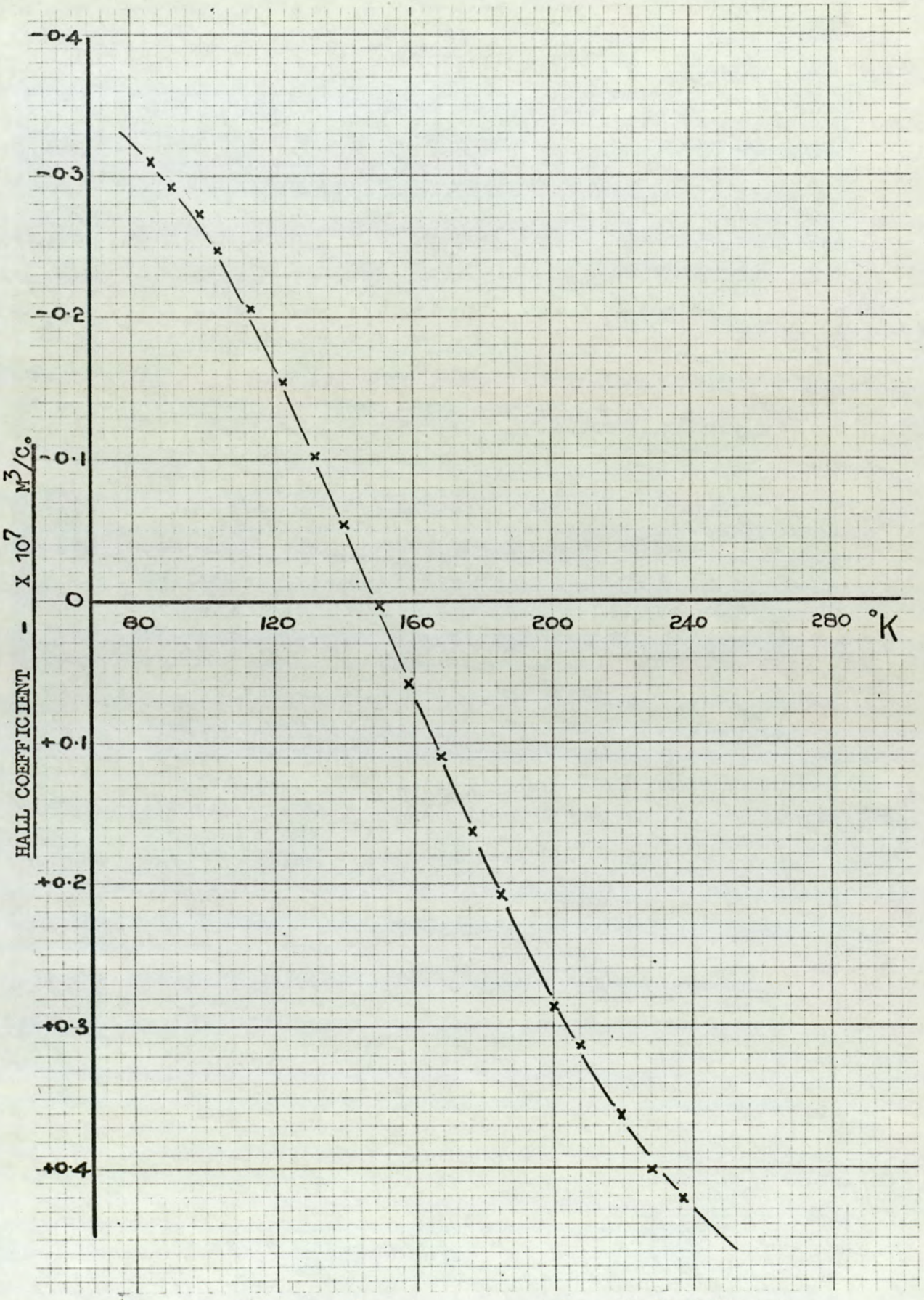

Fig. 112. Hall coefficient vs. temperature at 12.5 Kilogauss for a bismuth film of 258 Å.

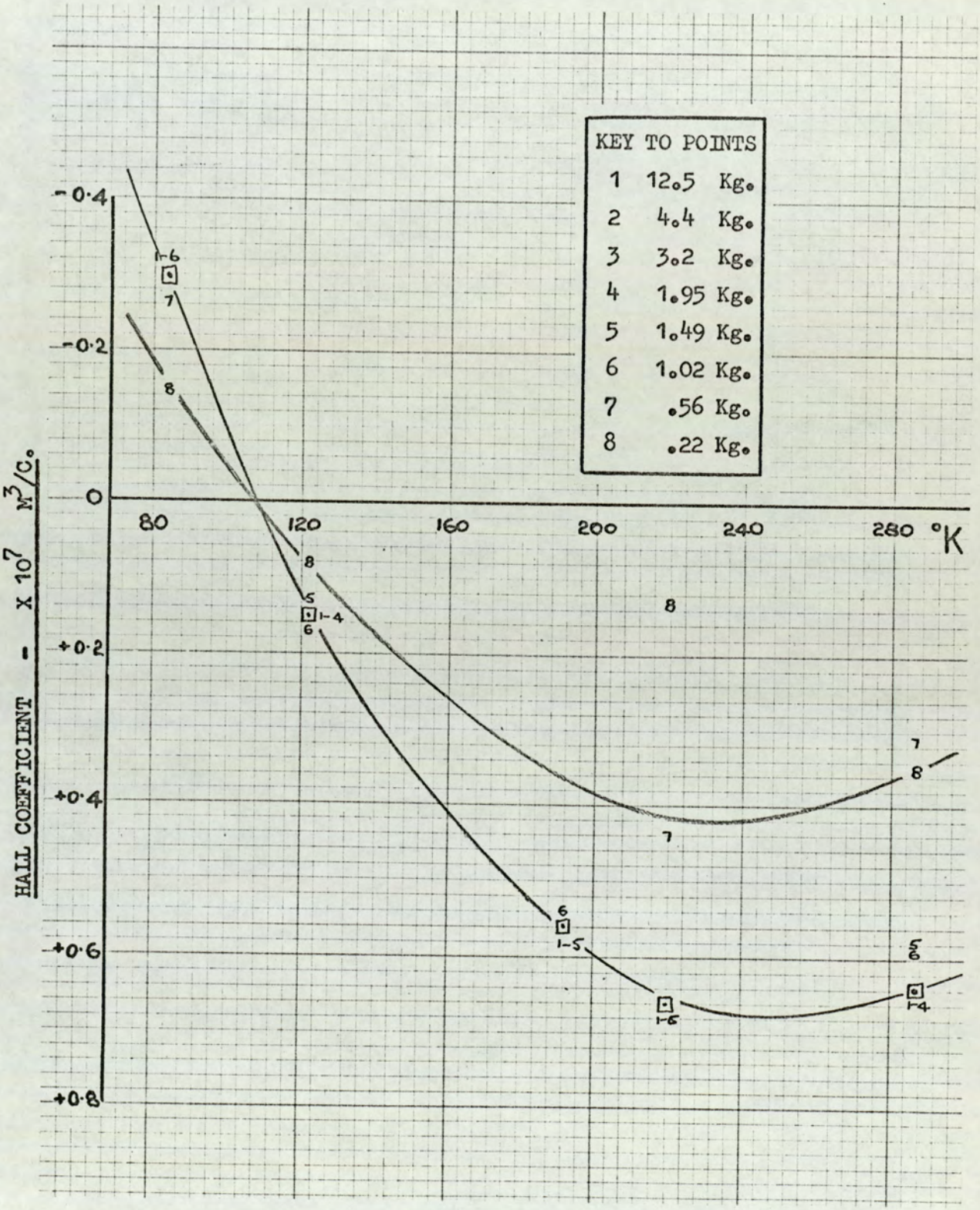

Fig. 113. Hall coefficient vs. temperature at a selection of magnetic fields for a bismuth film of 309 Å.

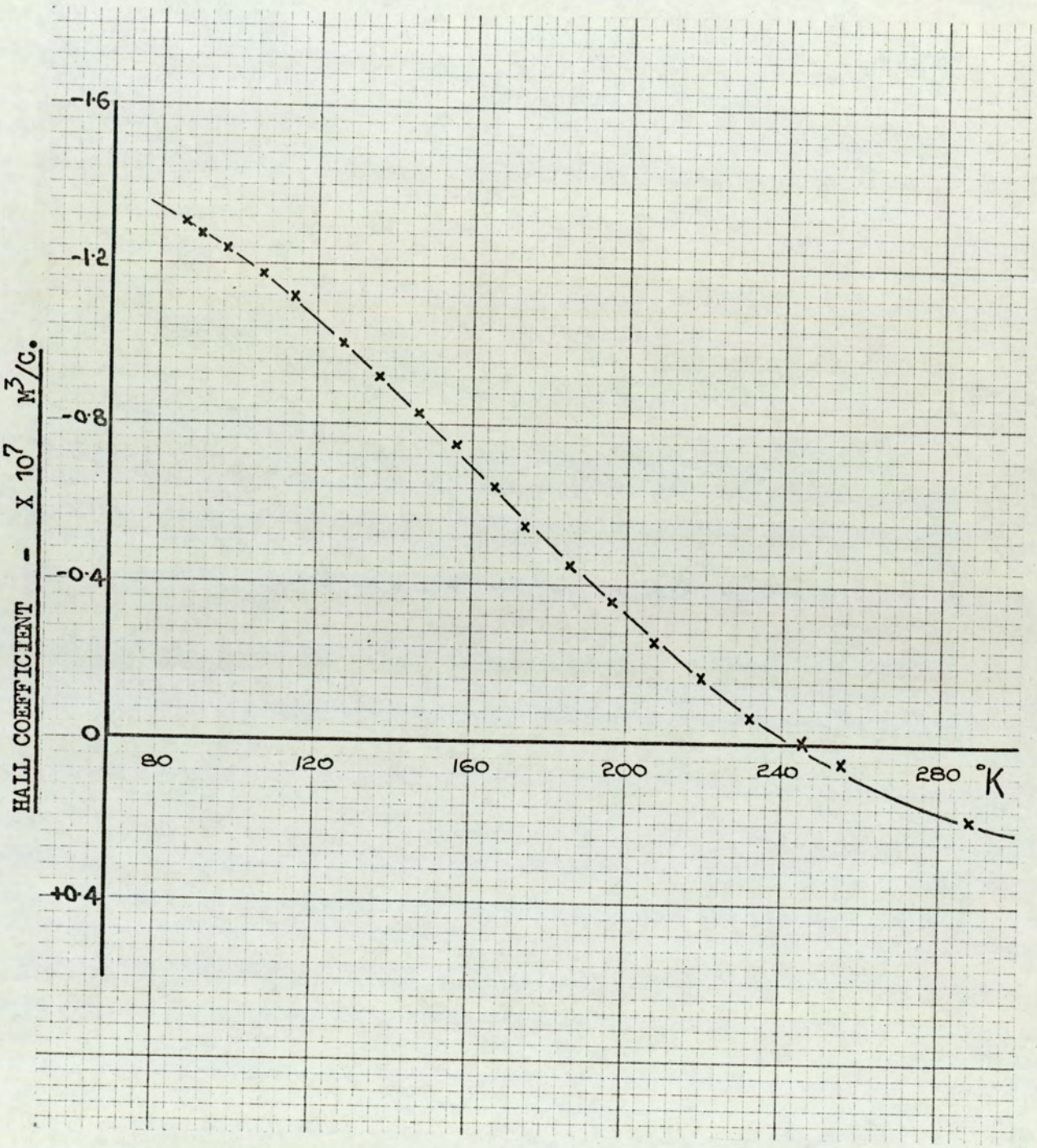

Fig. 114. Hall coefficient vs. temperature at 12.5 Kilogauss for a bismuth film of 357 Å.

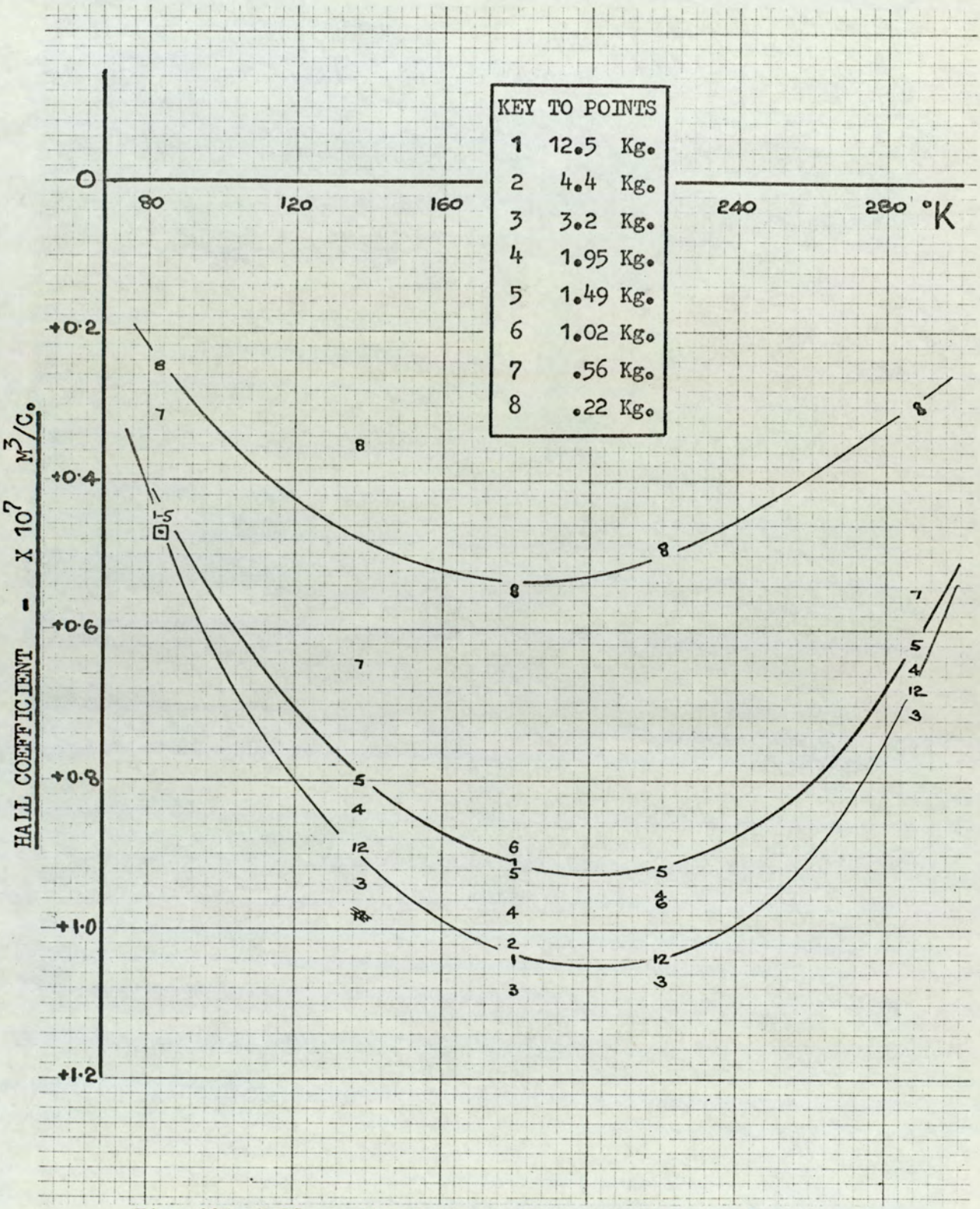

Fig. 115. Hall coefficient vs. temperature at a selection of magnetic fields for a bismuth film of 401 Å.

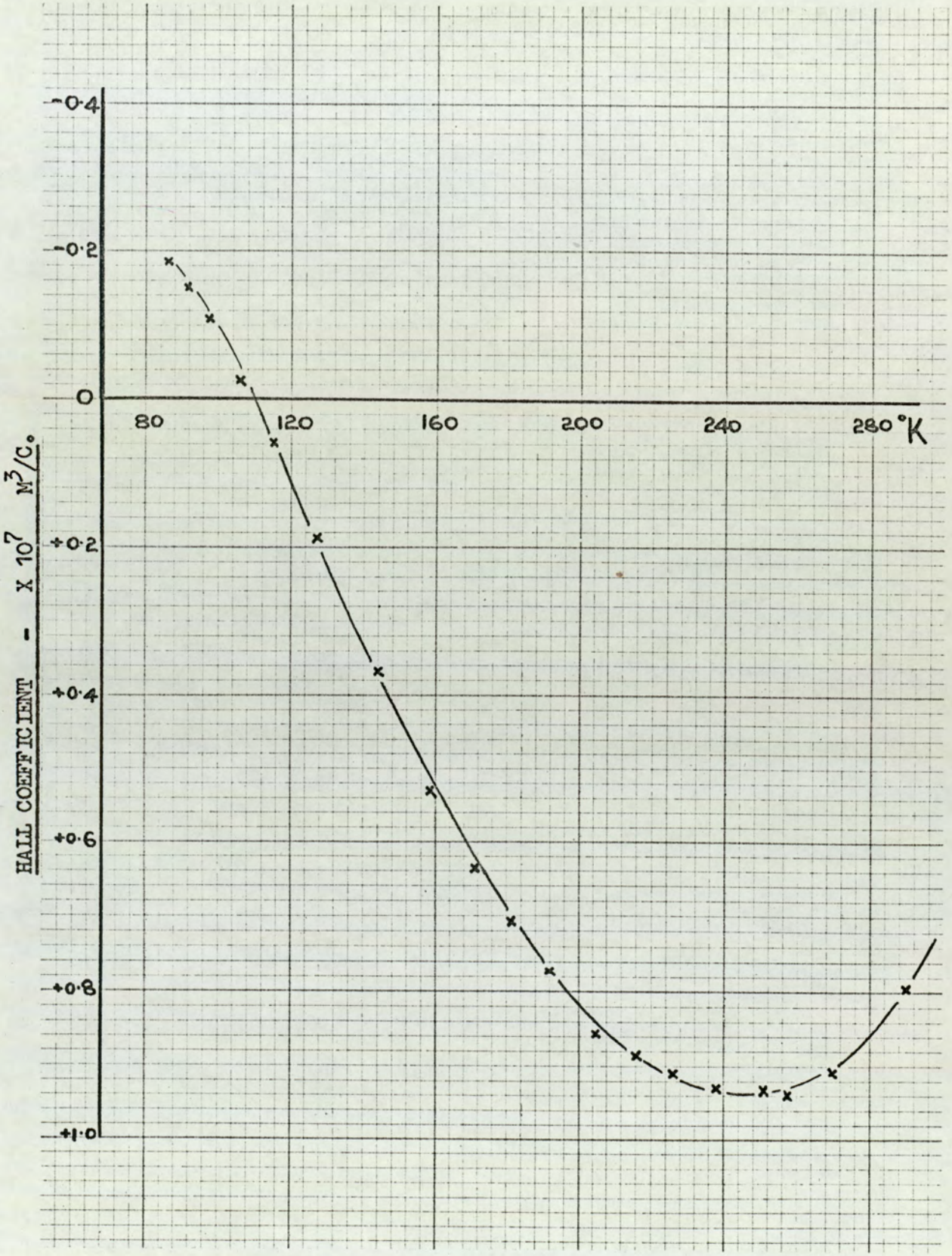

Fig. 116. Hall coefficient vs. temperature at 12.5 Kilogauss for a bismuth film of 451 Å.

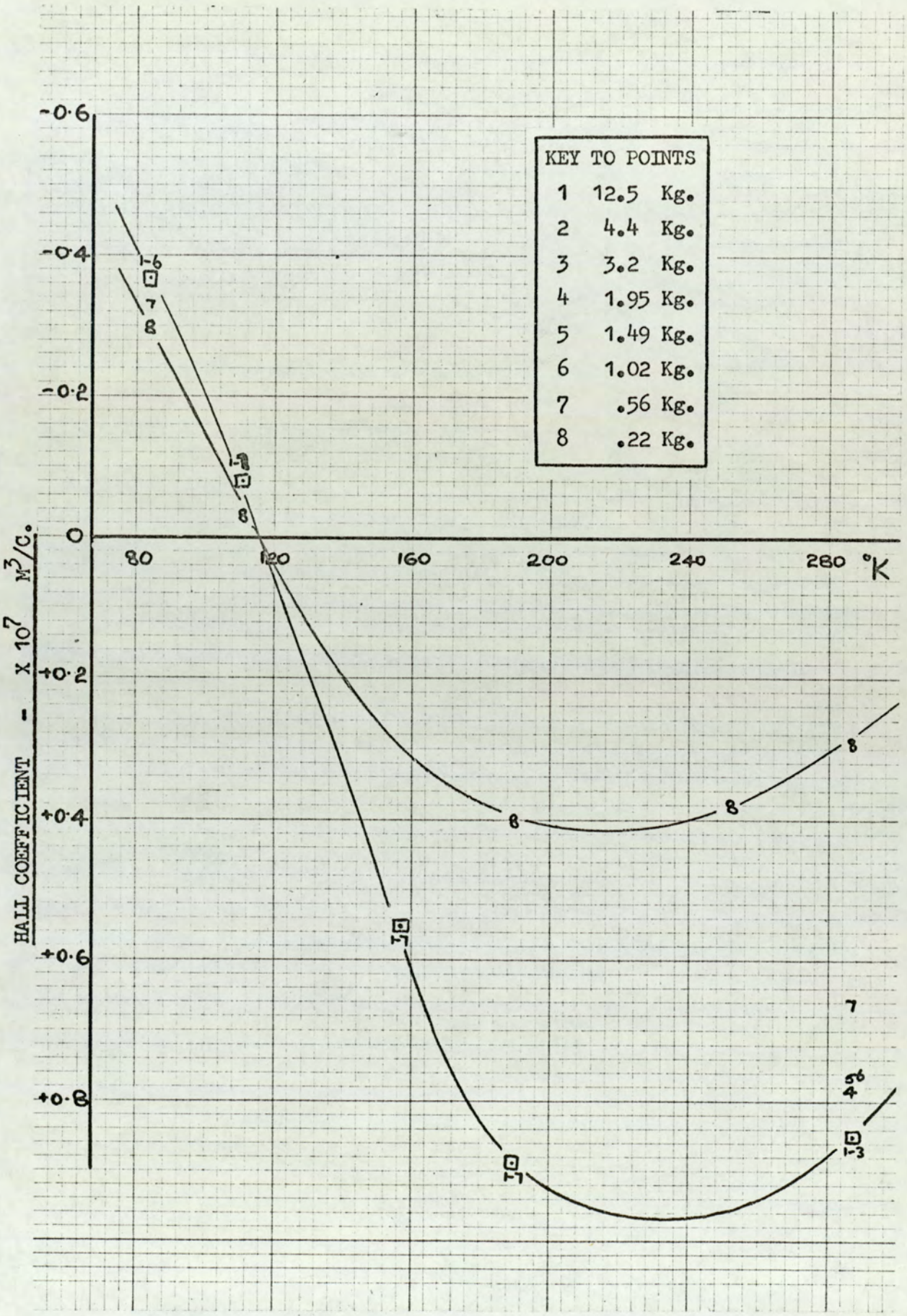

Fig. 117. Hall coefficient vs. temperature at a selection of magnetic fields for a bismuth film of 504 Å.

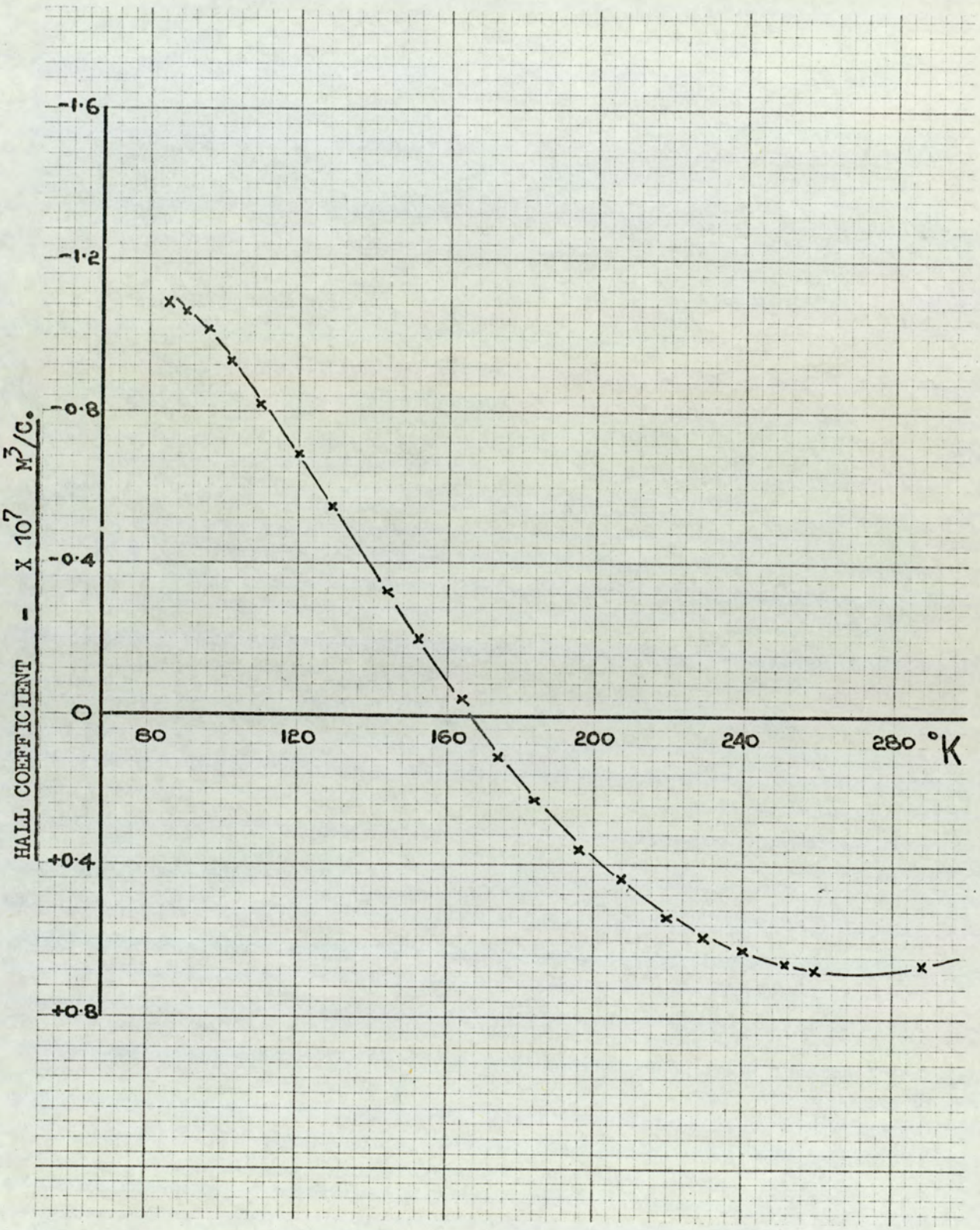

Fig. 118. Hall coefficient vs. temperature at 12.5 Kilogauss for a bismuth film of 552 Å.

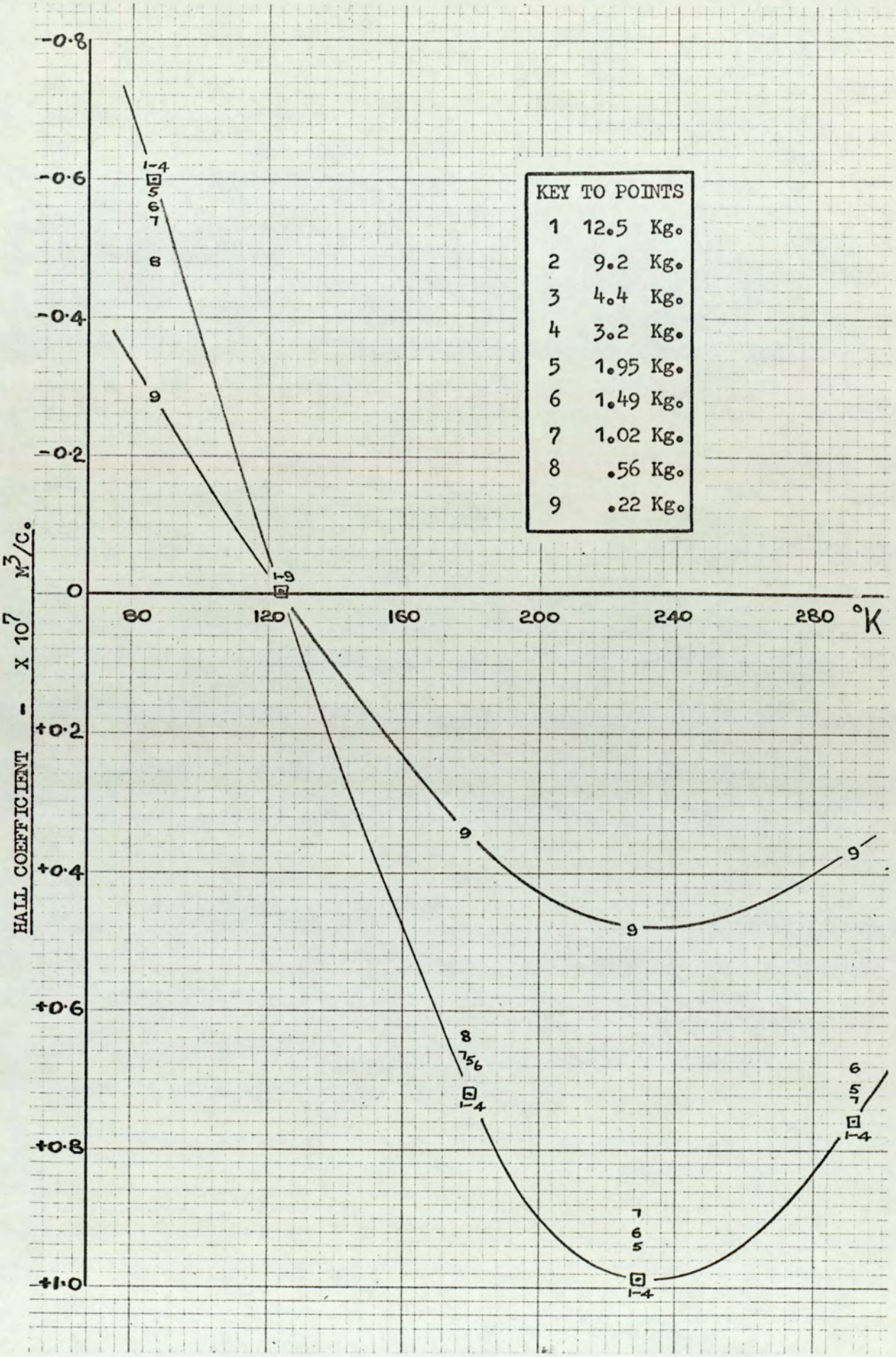

Fig. 119. Hall coefficient vs. temperature at a selection of magnetic fieldssfor a bismuth film of 609 Å.

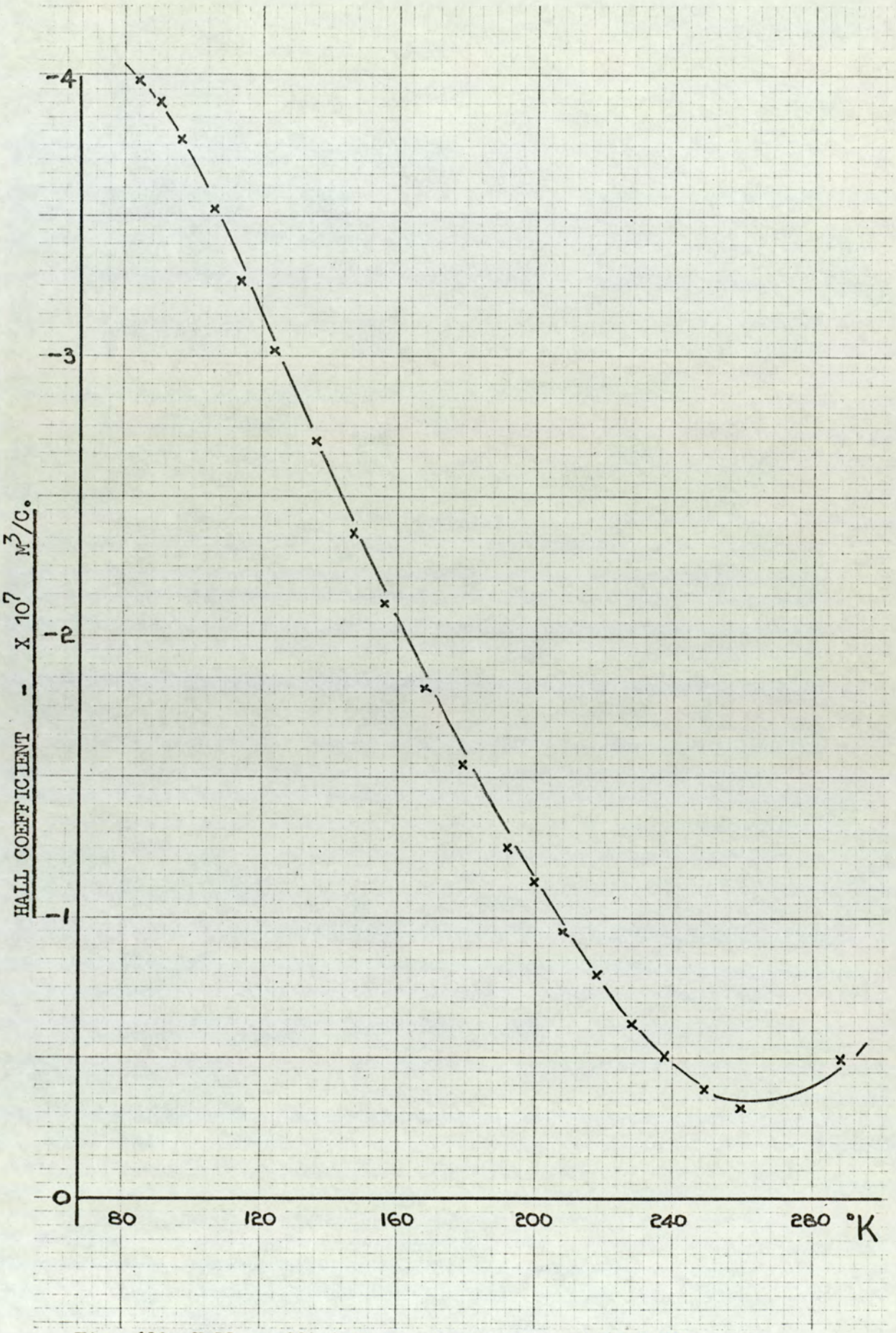

Fig. 120. Hall coefficient vs. temperature at 12.5 Kilogauss for a bismuth film of 650 Å.

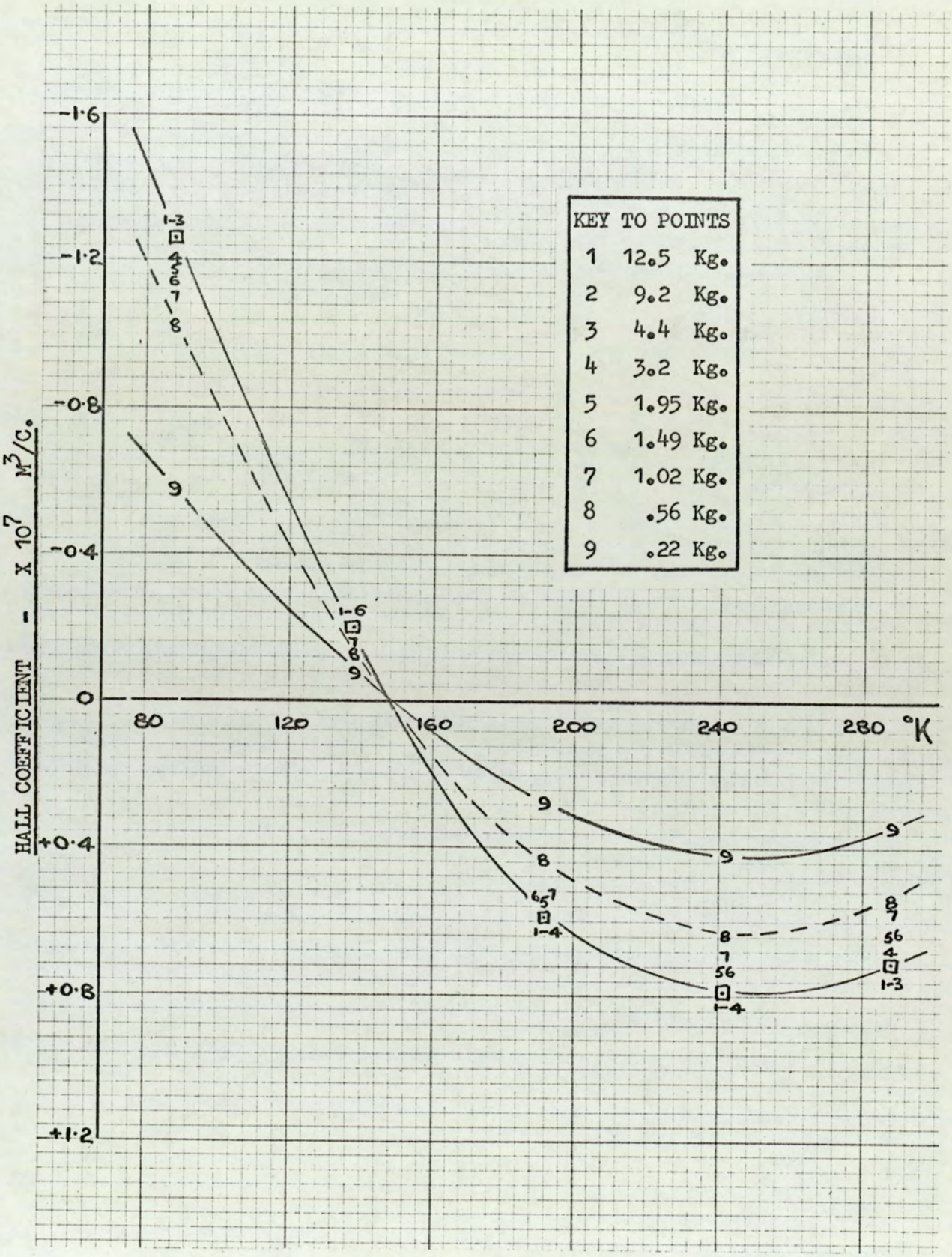

Fig. 121. Hall coefficient vs. temperature at a selection of magnetic fields for a bismuth film of 735 Å.

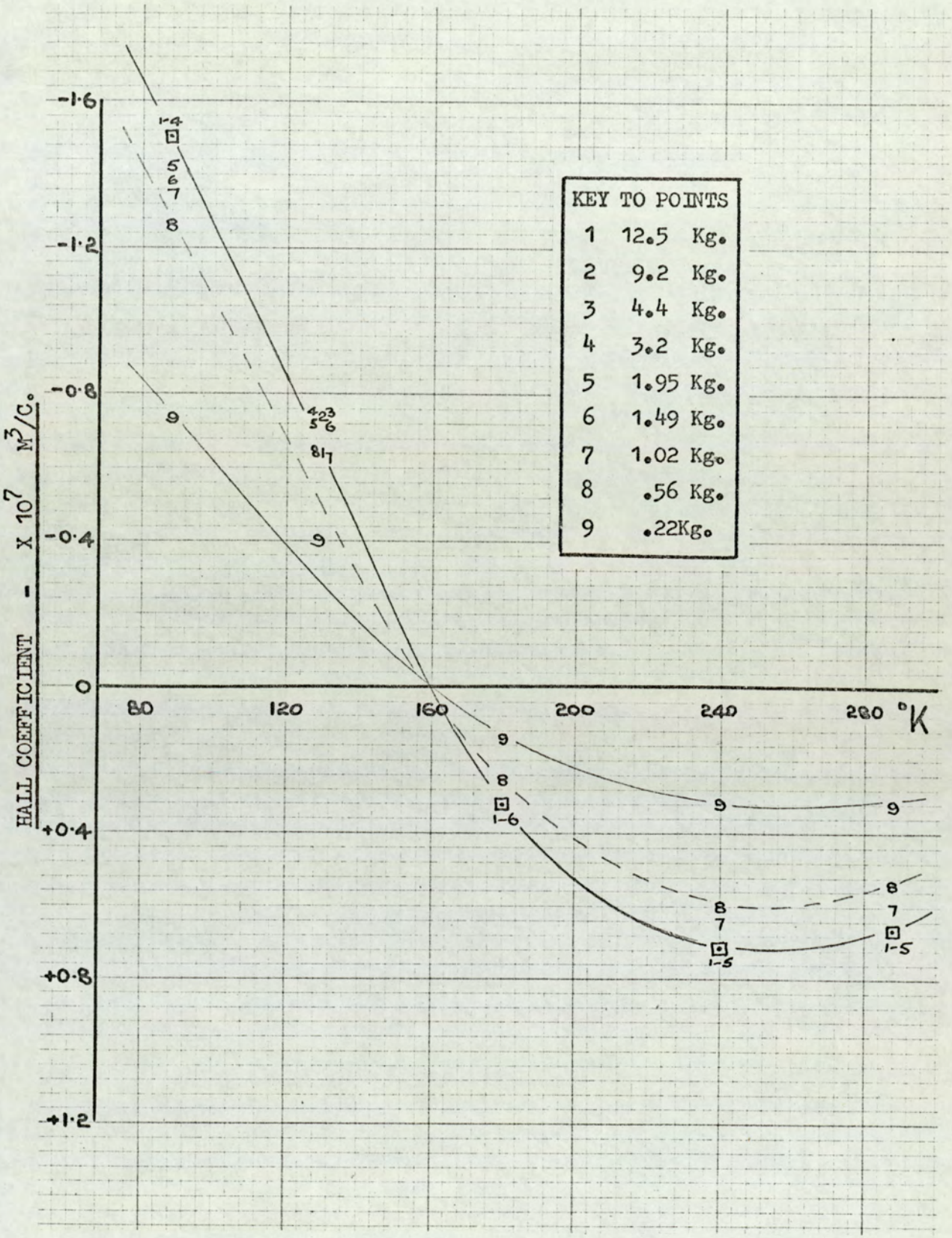

Fig. 122. Hall coefficient vs. temperature at a selection of magnetic fields for a bismuth film of 744 Å.

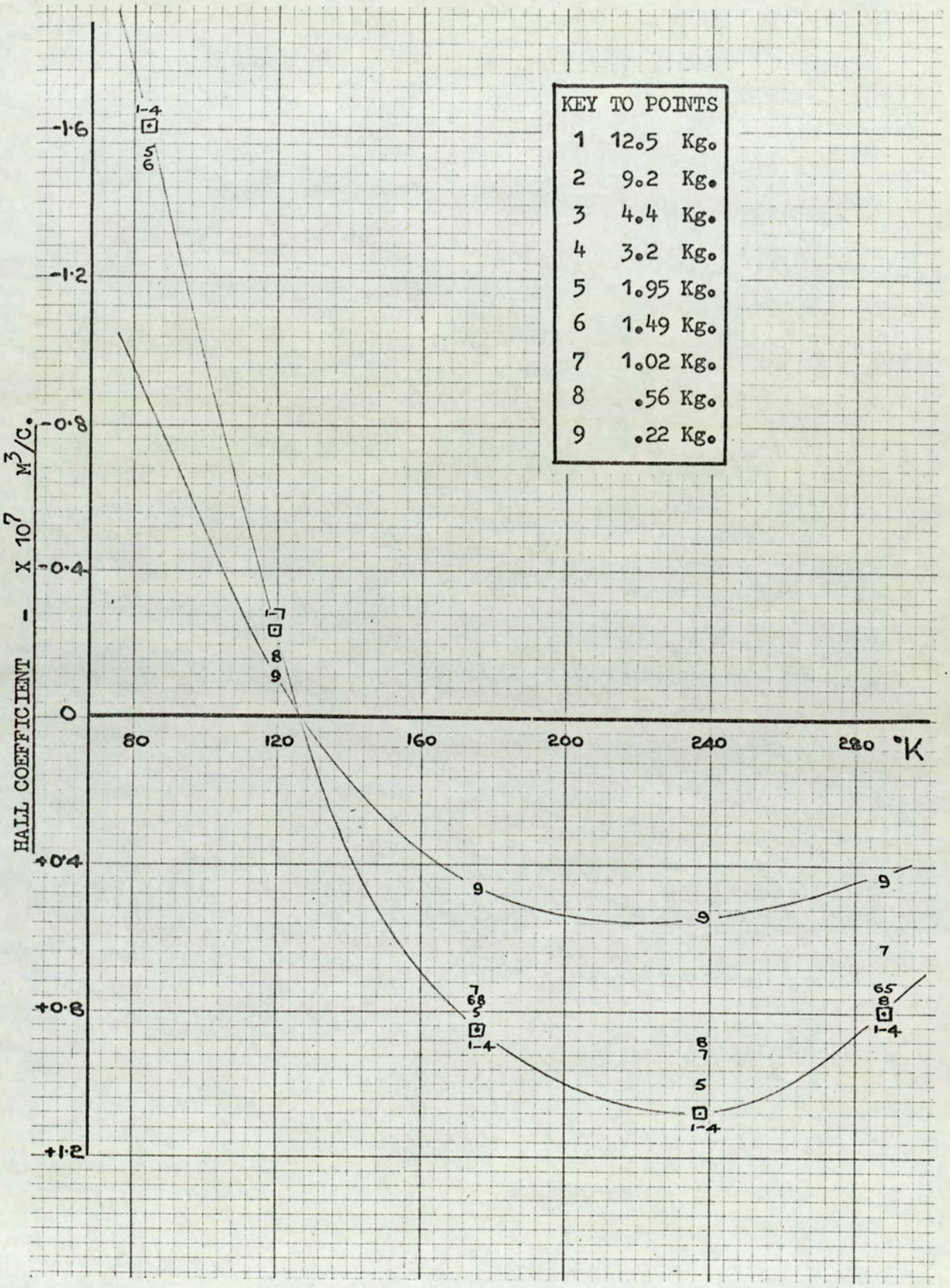

Fig. 123. Hall coefficient vs. temperature at a selection of magnetic fields for a bismuth film of 801 Å.

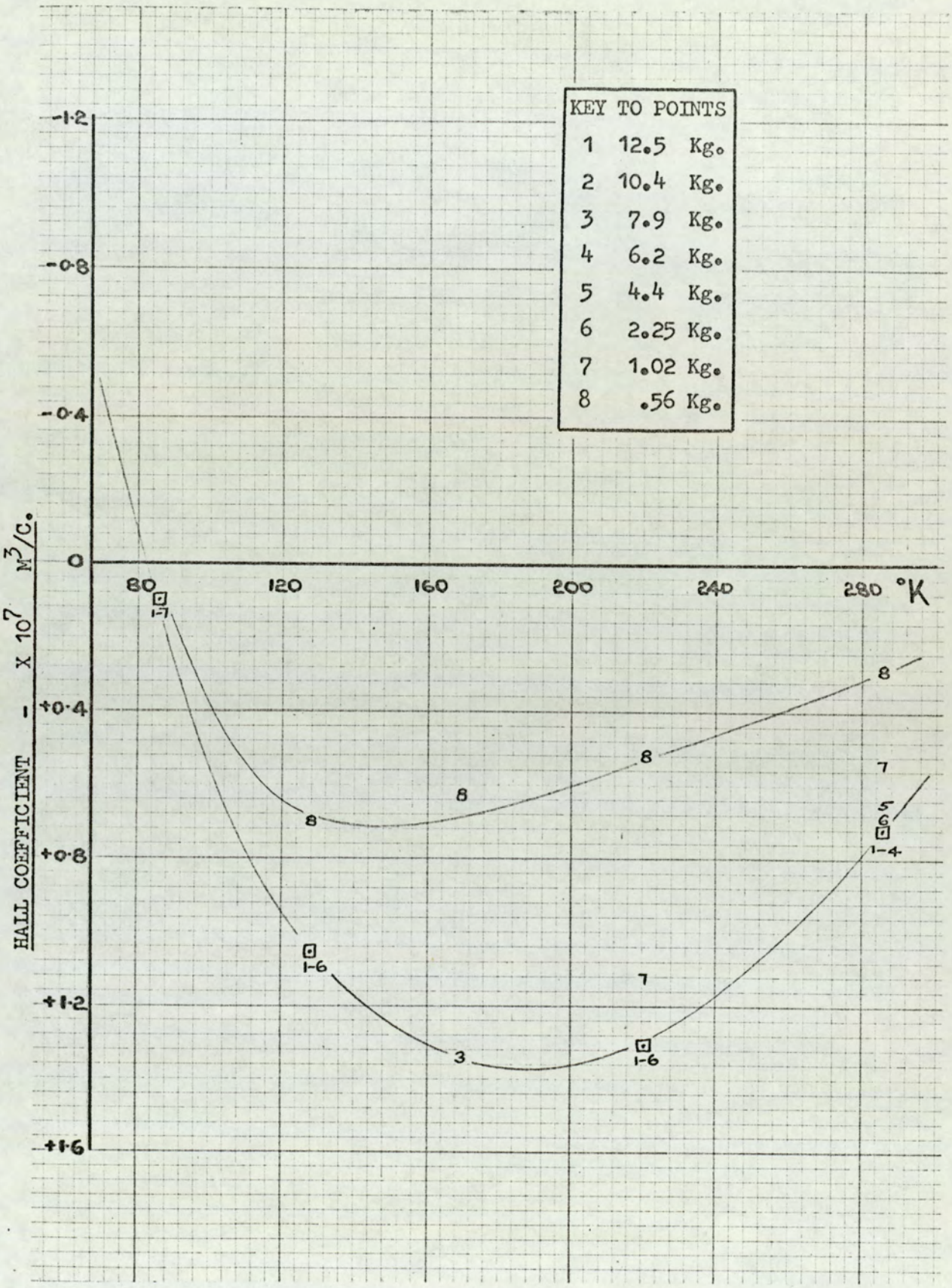

Fig. 124. Hall coefficient vs. temperature at a selection of magnetic fields for a bismuth film of 862 Å.

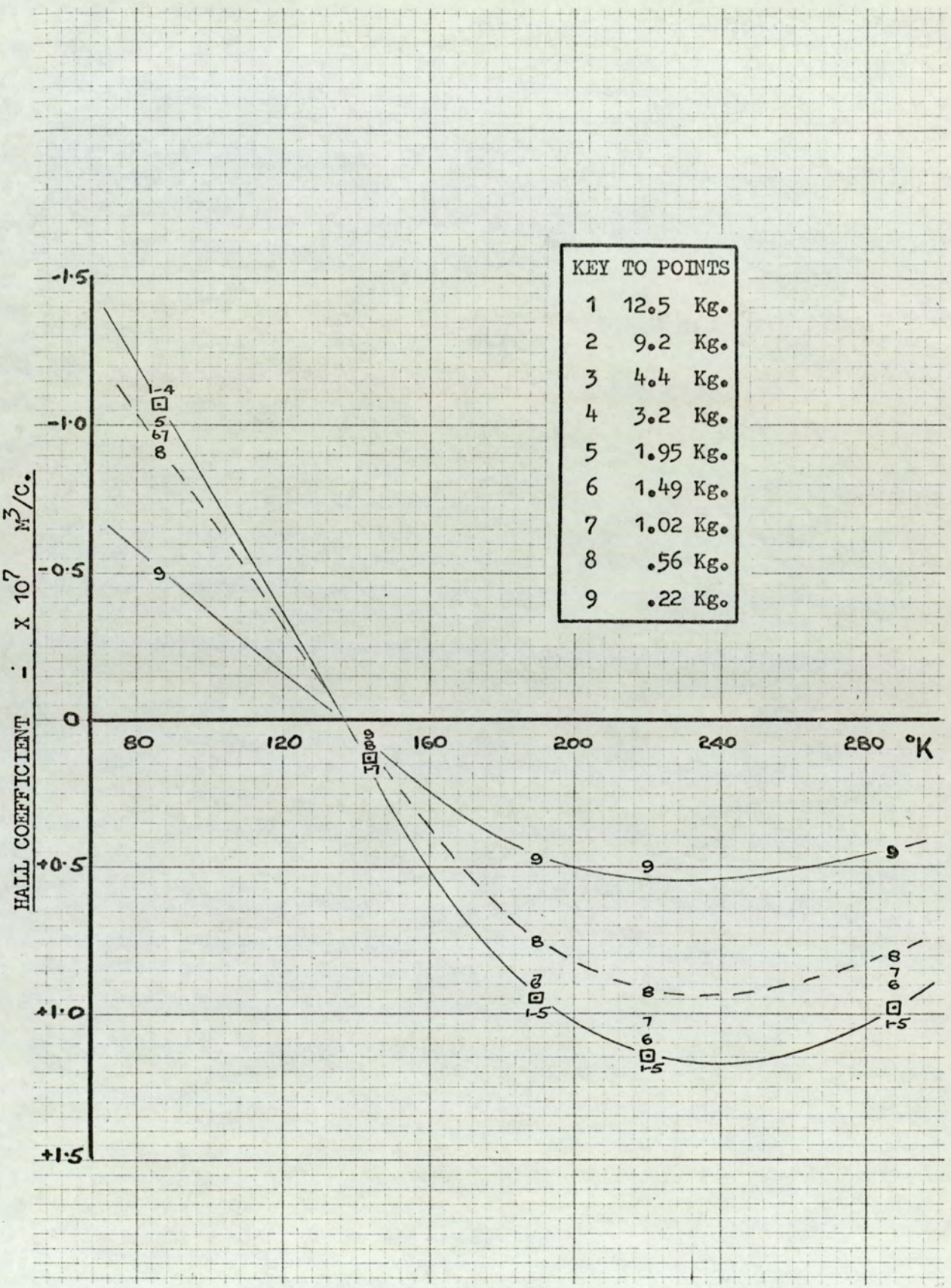

Fig. 125. Hall coefficient vs. temperature at a selection of magnetic fields for a bismuth film of 927 Å.

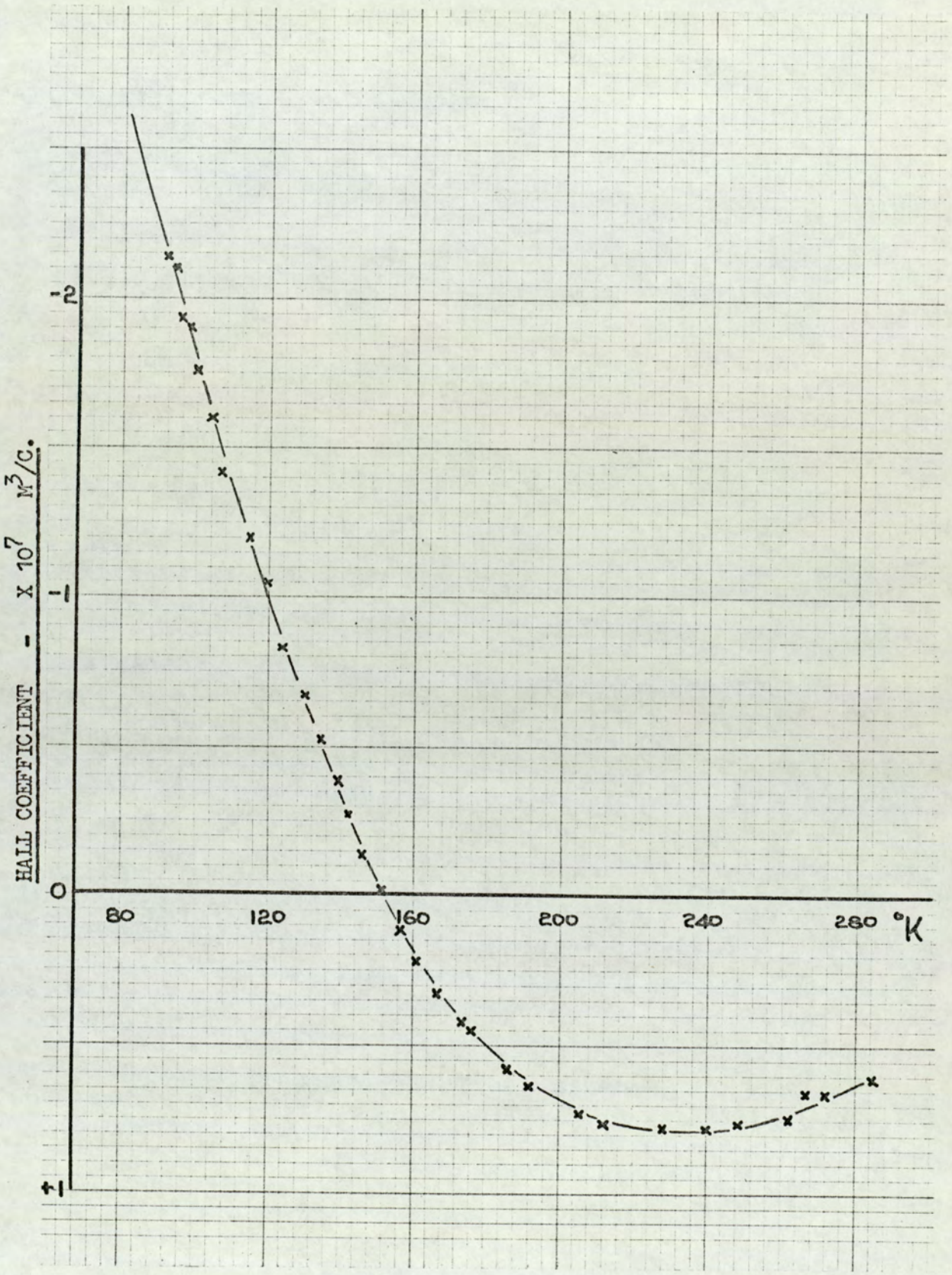

Fig. 126. Hall coefficient vs. temperature at 12.5 Kilogauss for a bismuth film of 1025 Å.

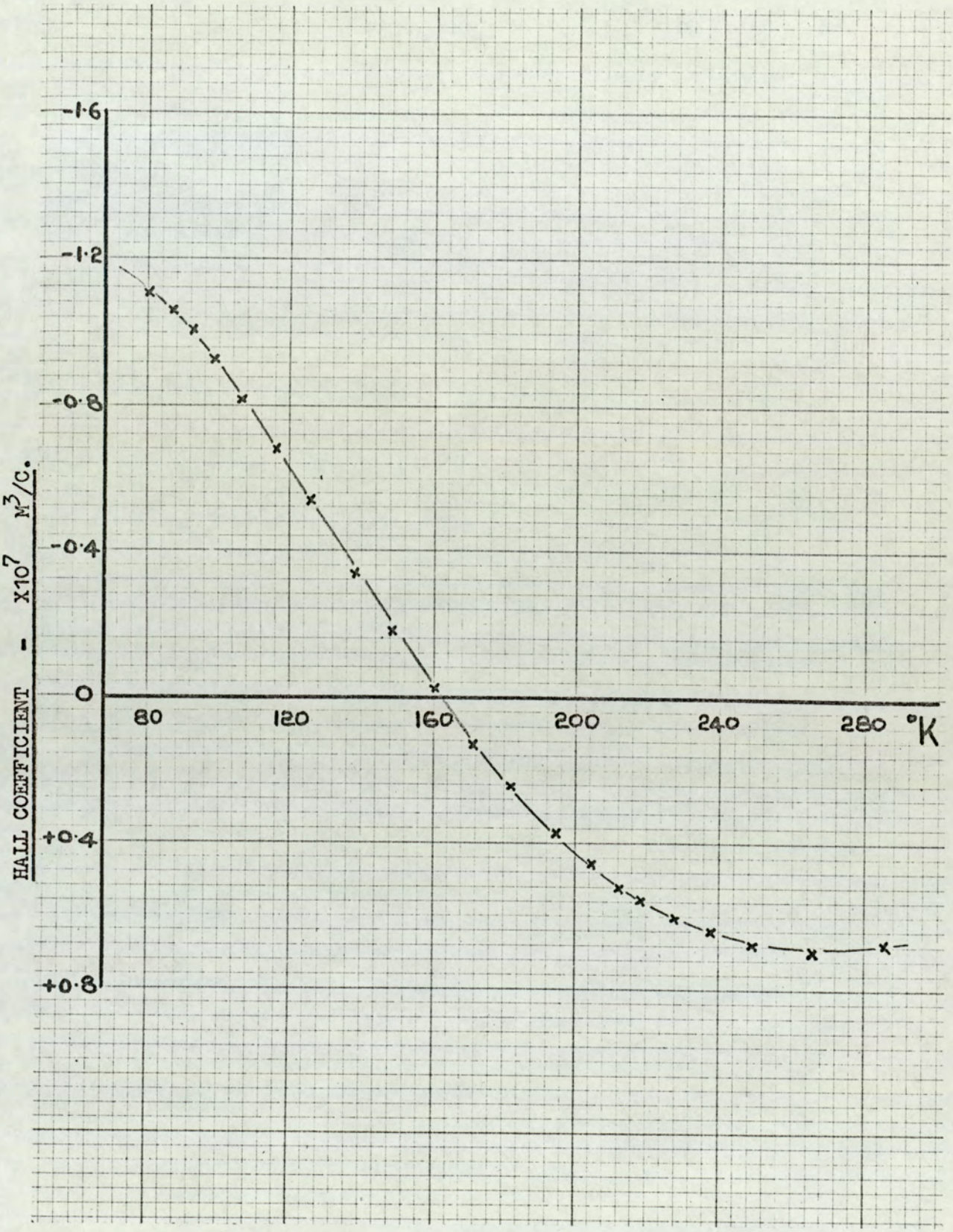

Fig. 127. Hall coefficient vs. temperature at 12.5 Kilogauss for a bismuth film of 1067 Å.

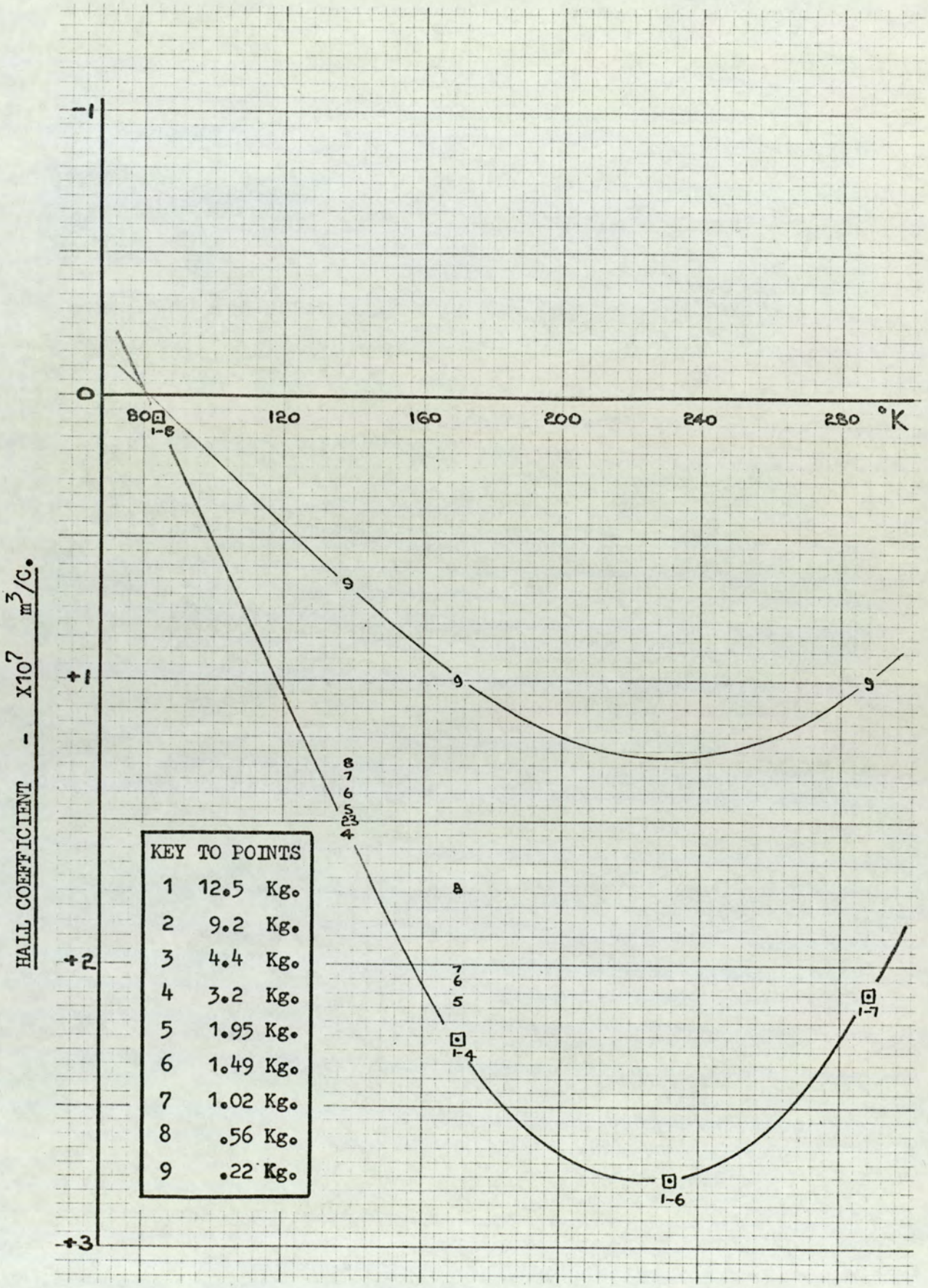

Fig. 128. Hall coefficient vs. temperature at a selection of magnetic fields for a bismuth film of 1100 Å.

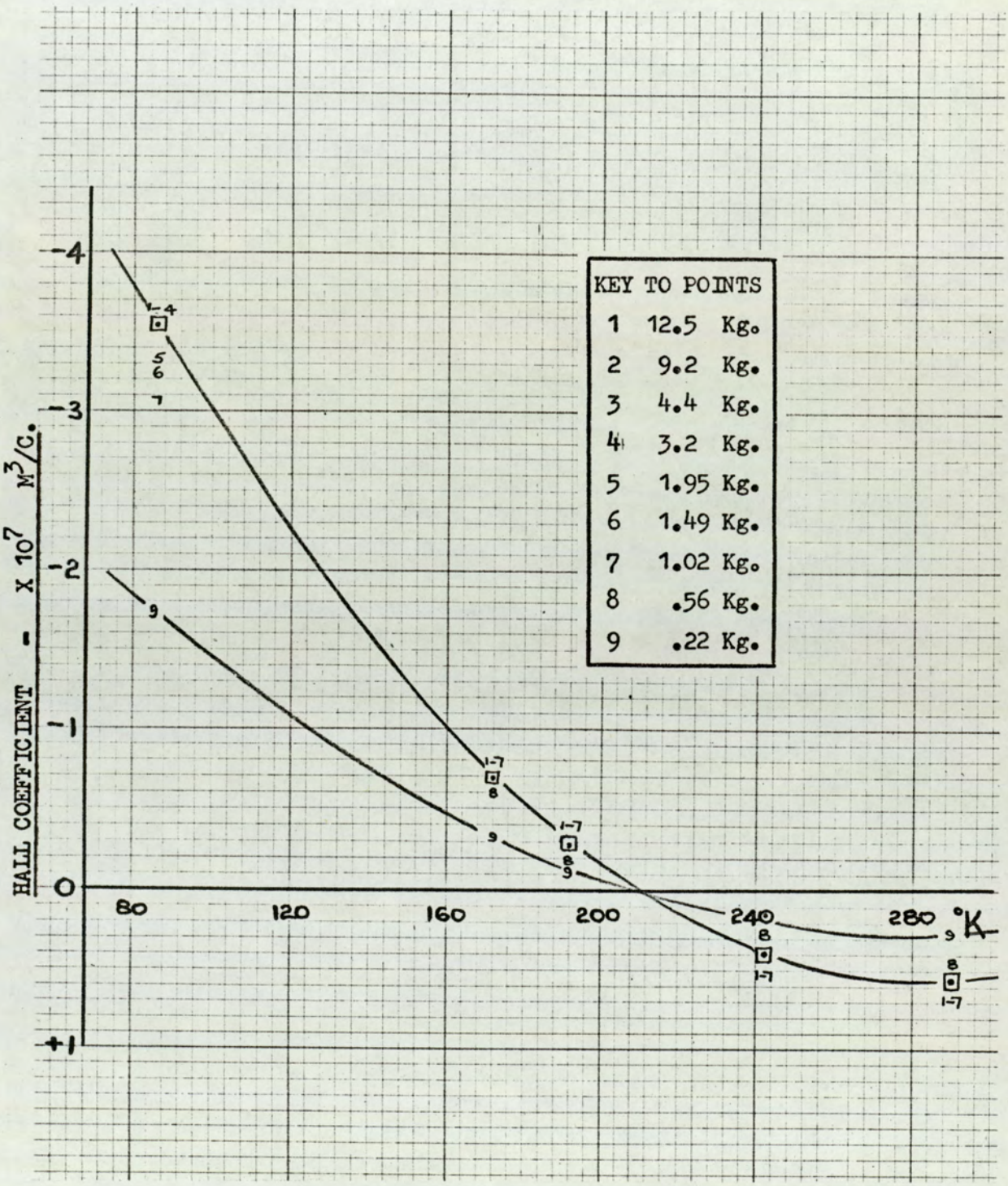

Fig. 129. Hall coefficient vs. temperature at a selection of magnetic fields for a bismuth film of 1201 Å.

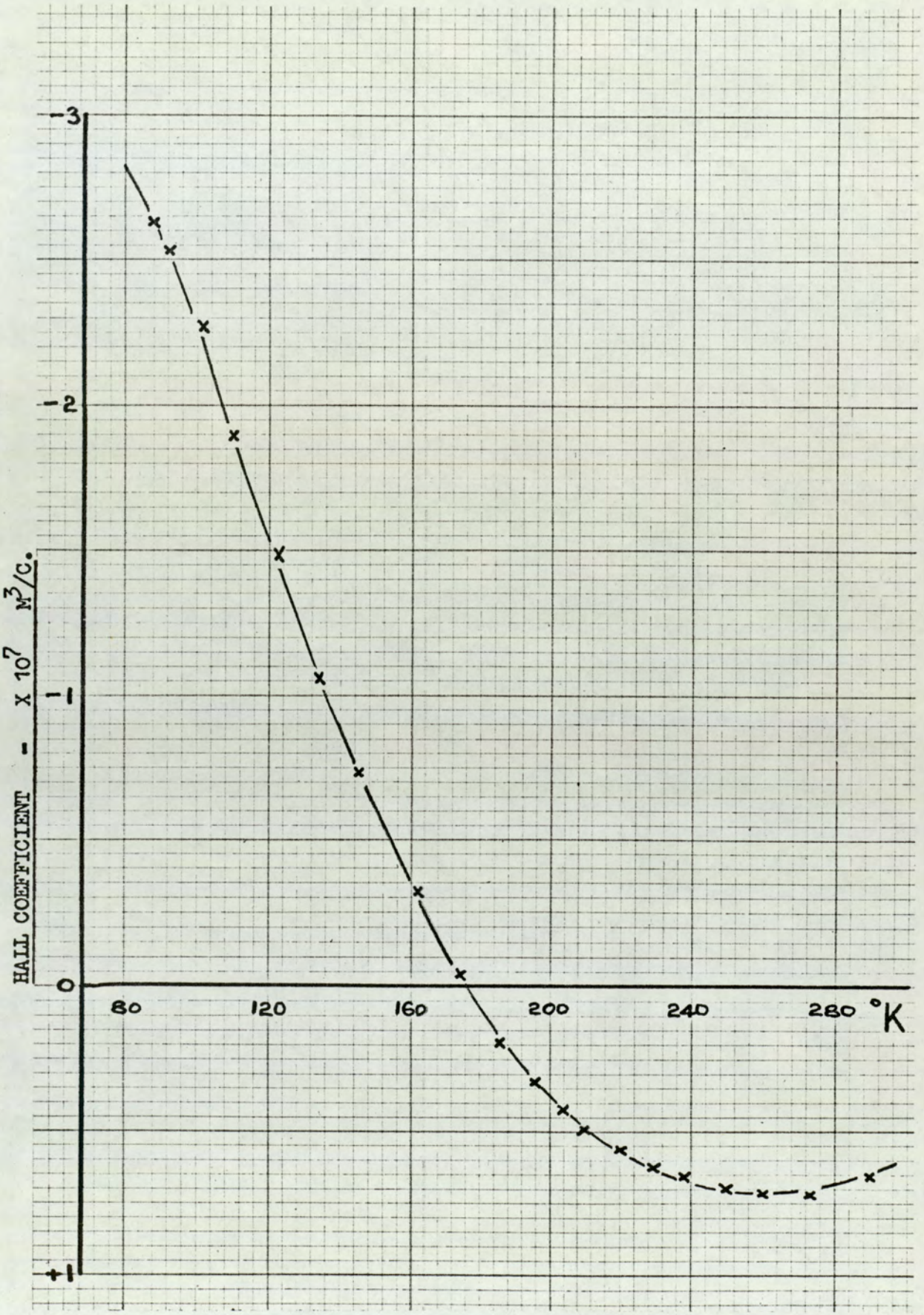

Fig. 130. Hall coefficient vs. temperature at a selection of magnetic fields for a bismuth film of 1270 Å.

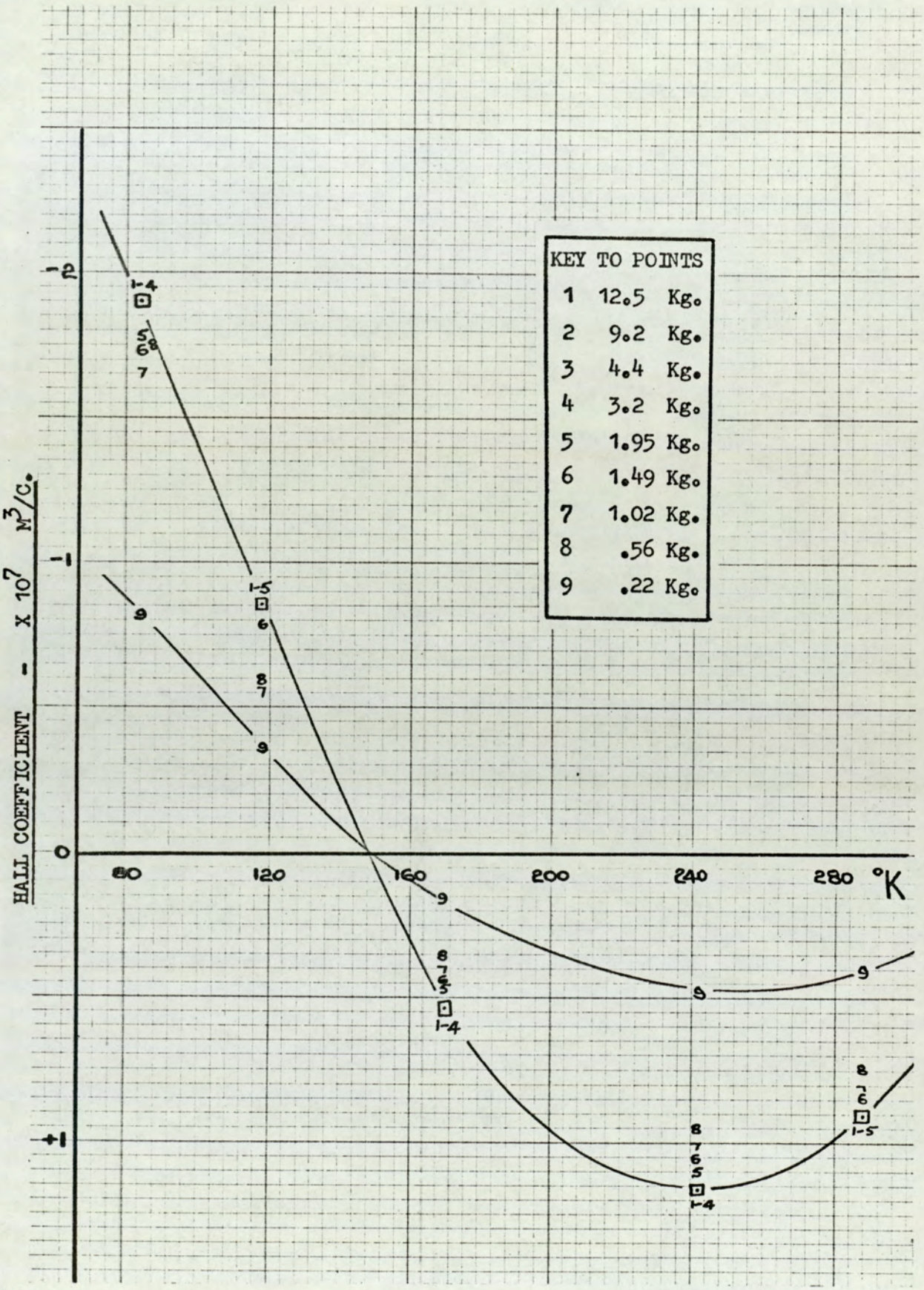

Fig. 131. Hall coefficient vs. temperature at a selection of magnetic fields for a bismuth film of 1287 Å.

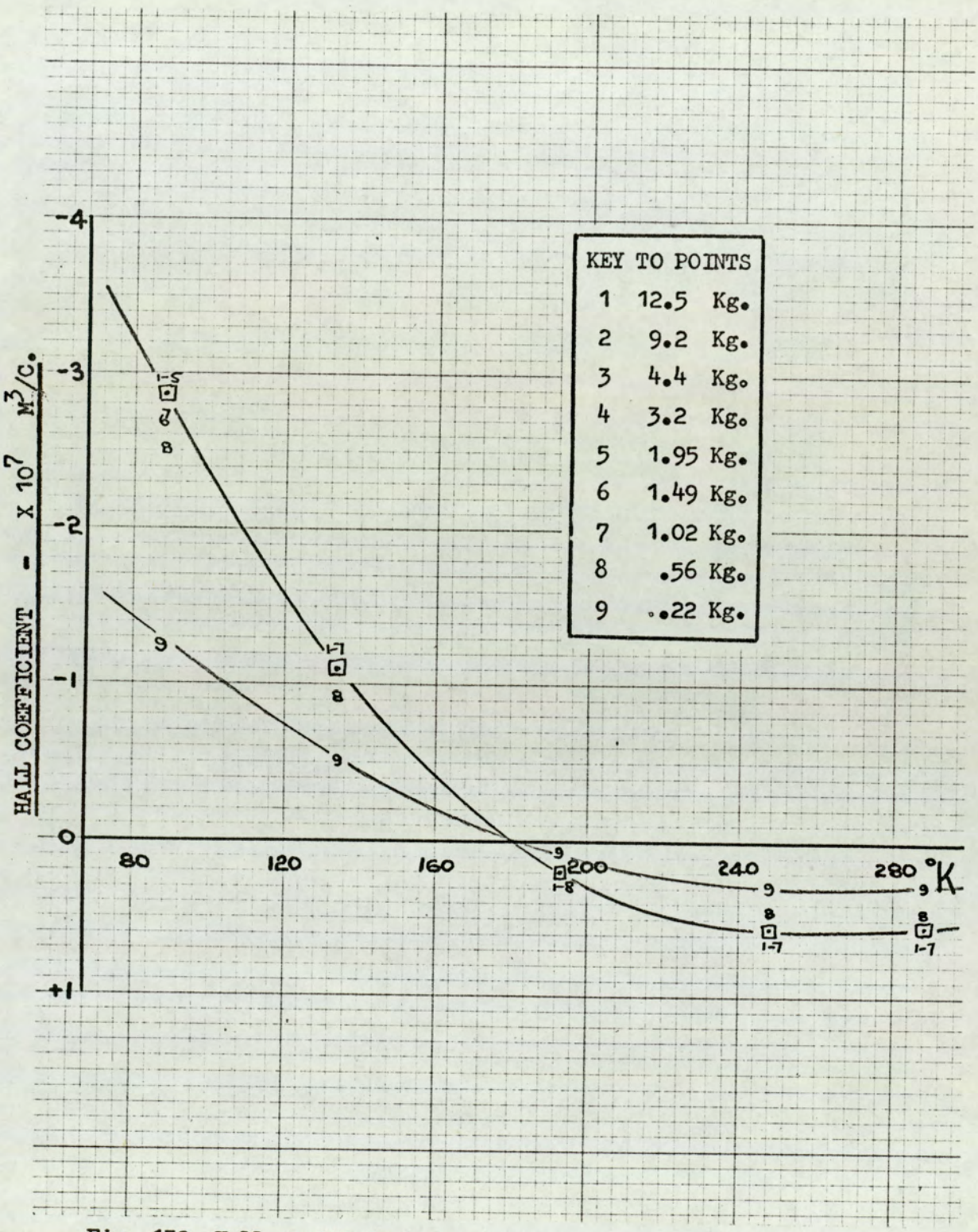

Fig. 132. Hall coefficient vs. temperature at a selection of magnetic fields for a bismuth film of 1409 Å.

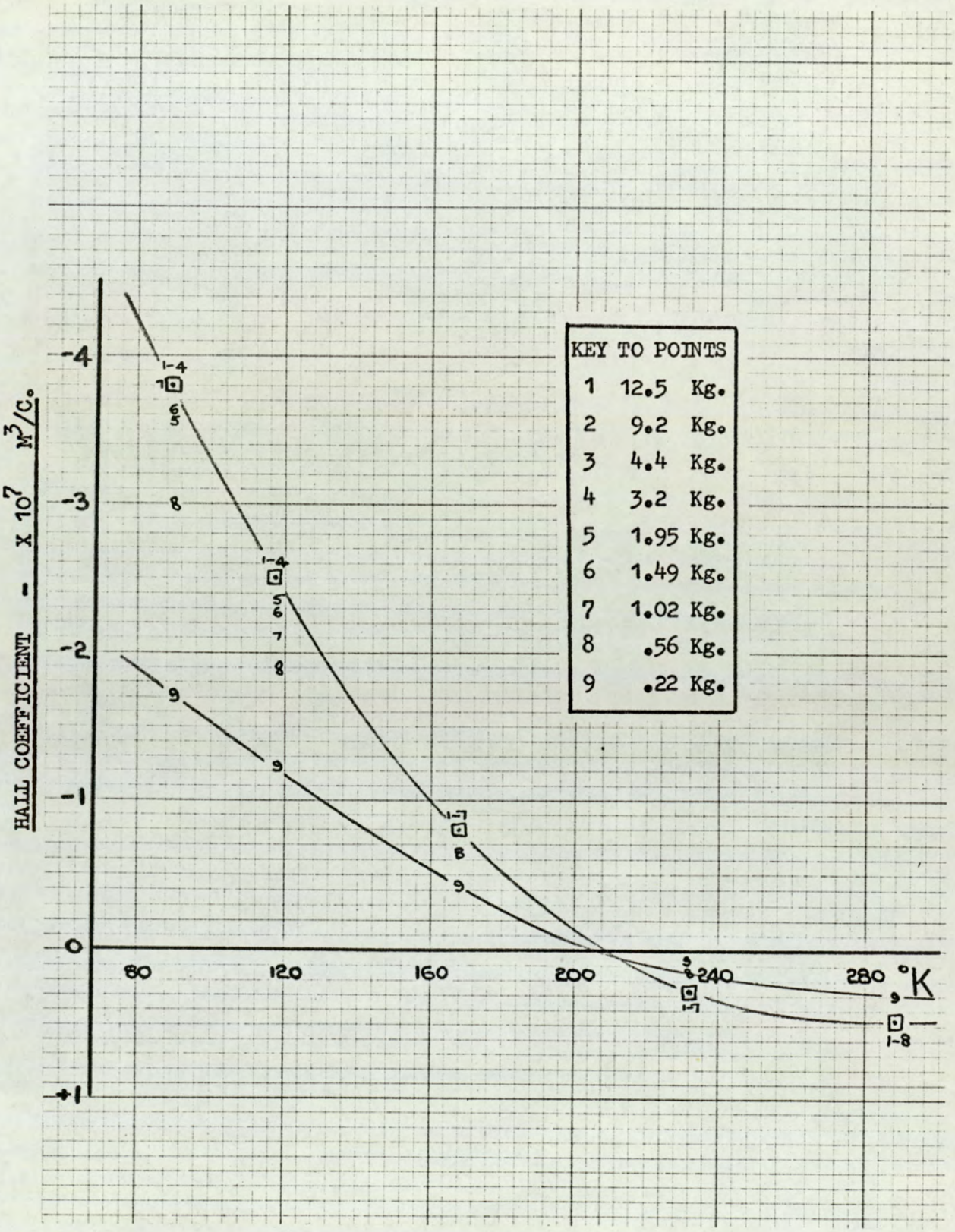

Fig. 133. Hall coefficient vs. temperature at a selection of magnetic fields for a bismuth film of 1501 Å.

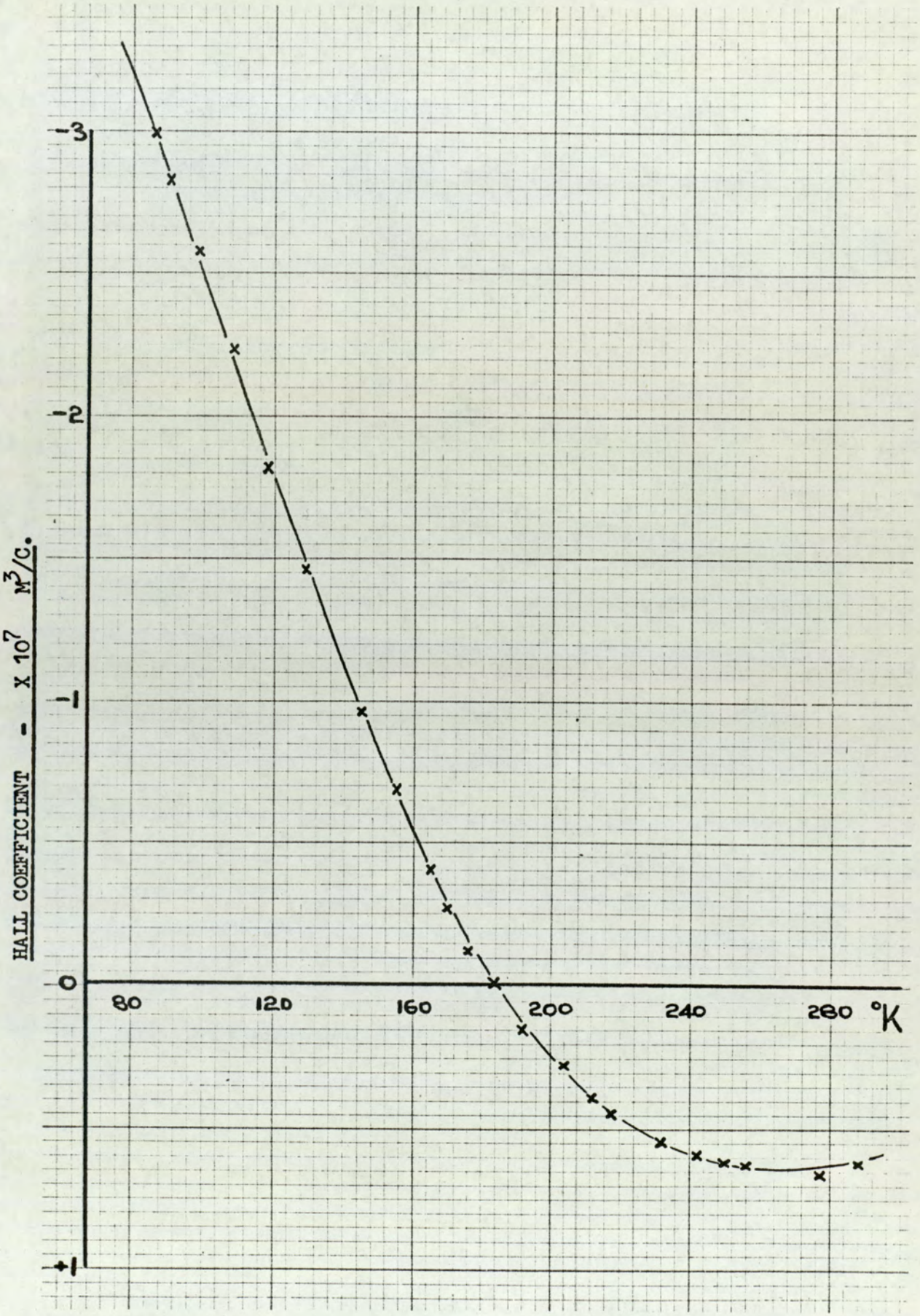

Fig. 134. Hall coefficient vs. temperature at 12.5 Kilogauss for a bismuth film of 1587 Å.

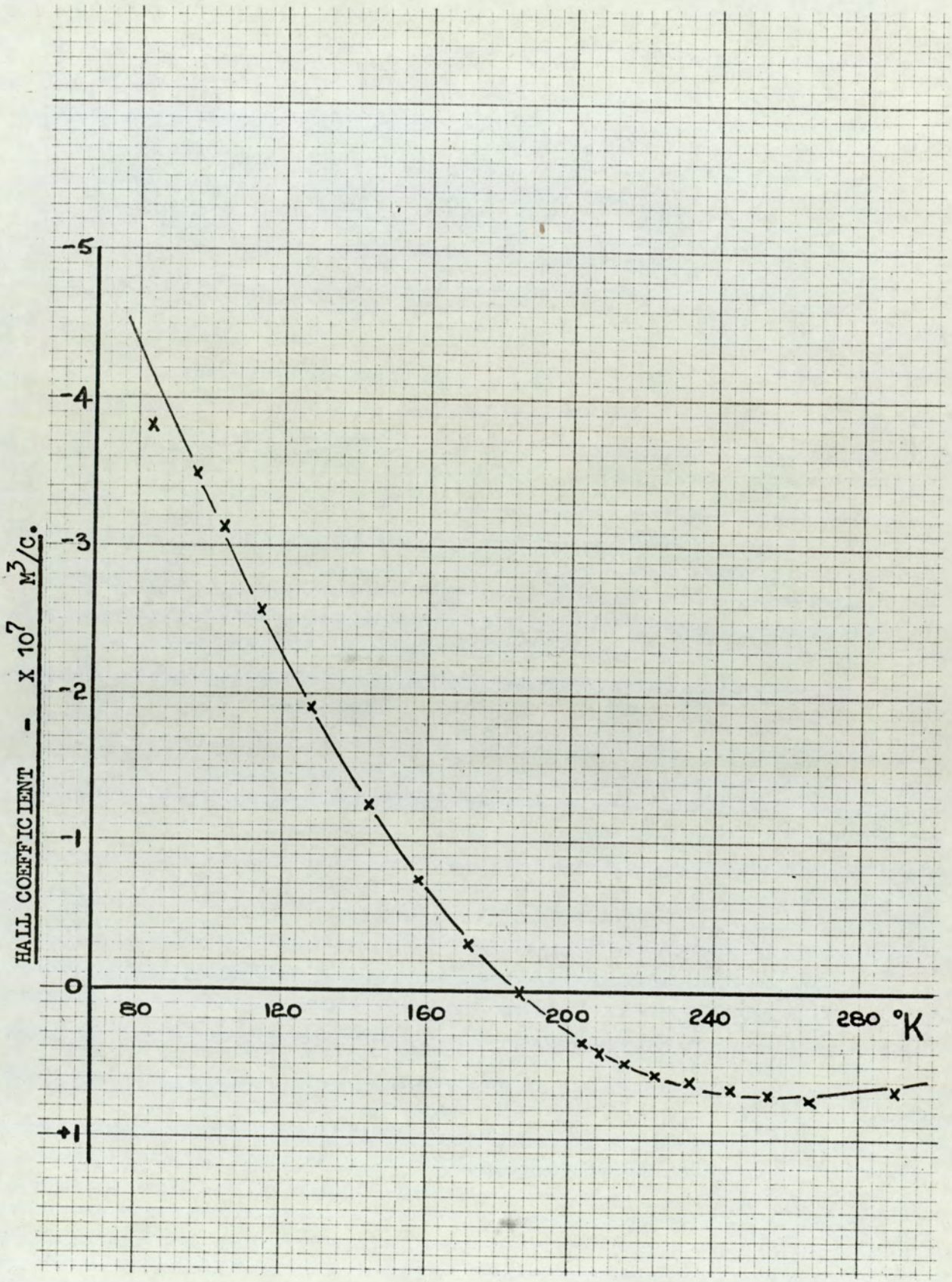

Fig. 135. Hall coefficient vs. temperature at 12.5 Kilogauss for a bismuth film of 1697 Å.

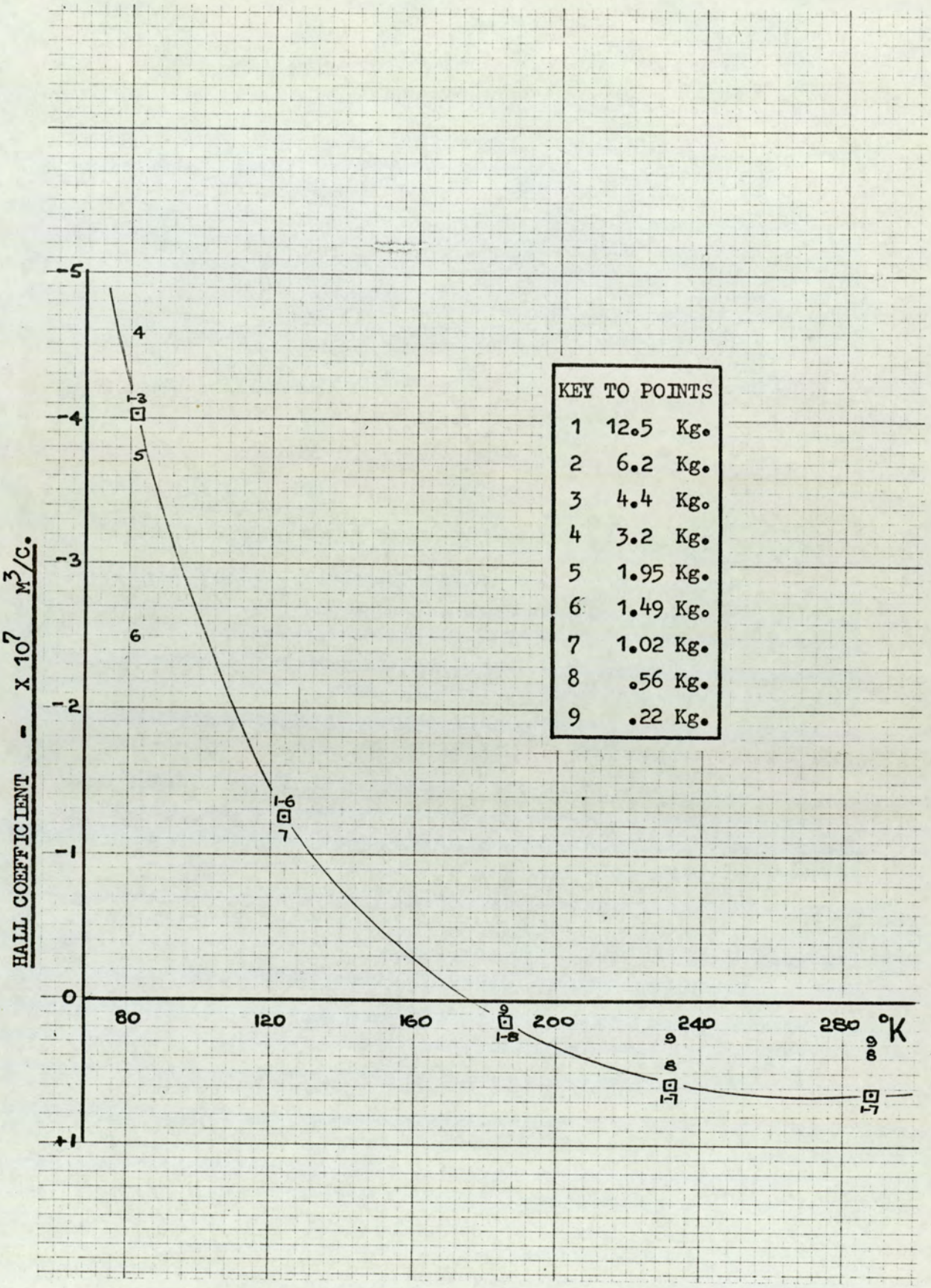

Fig. 136. Hall coefficient vs. temperature at a selection of magnetic fields for a bismuth film of 2045 Å.

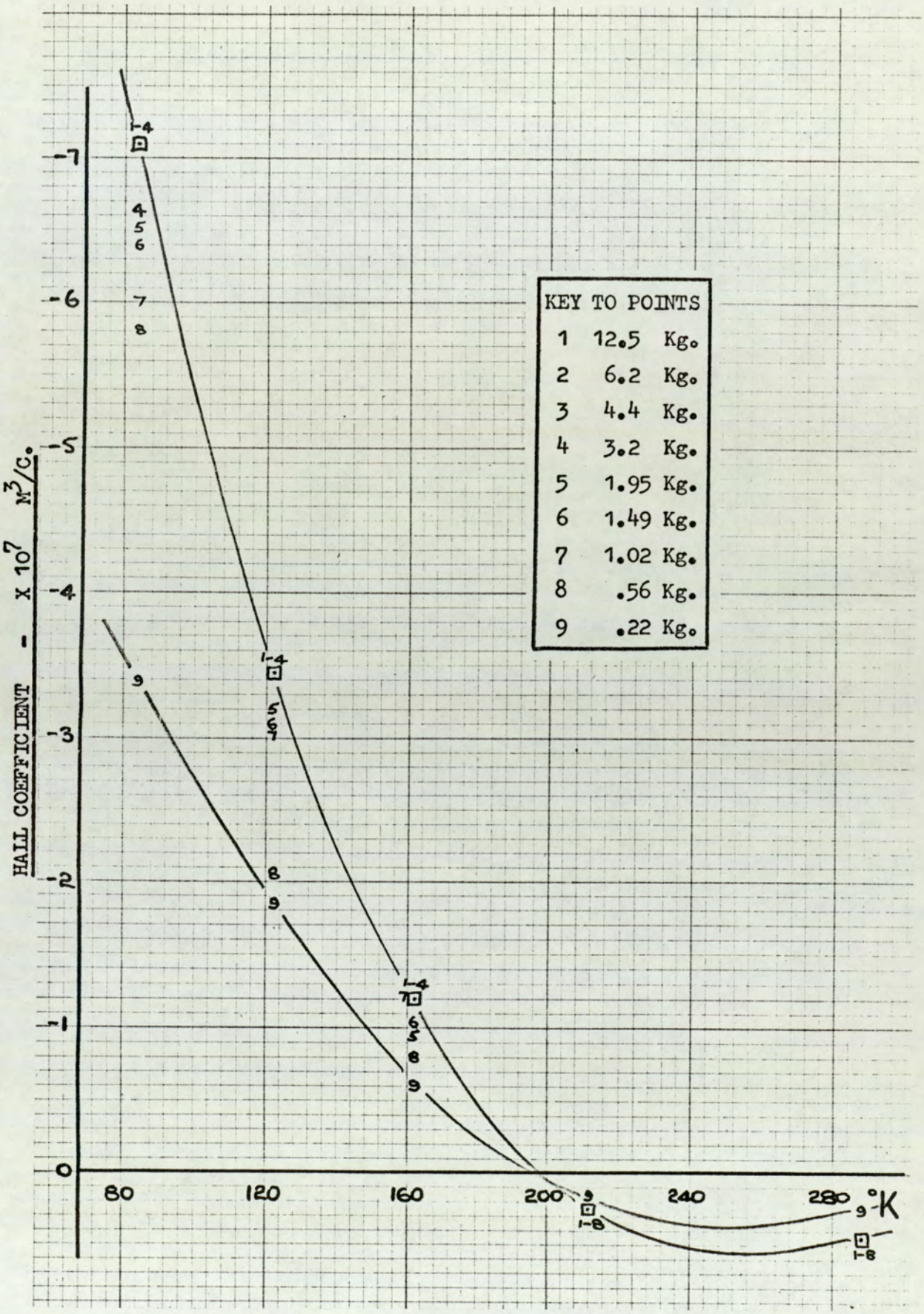

Fig. 137. Hall coefficient vs. temperature at a selection of magnetic fields for a bismuth film of 4500 Å.

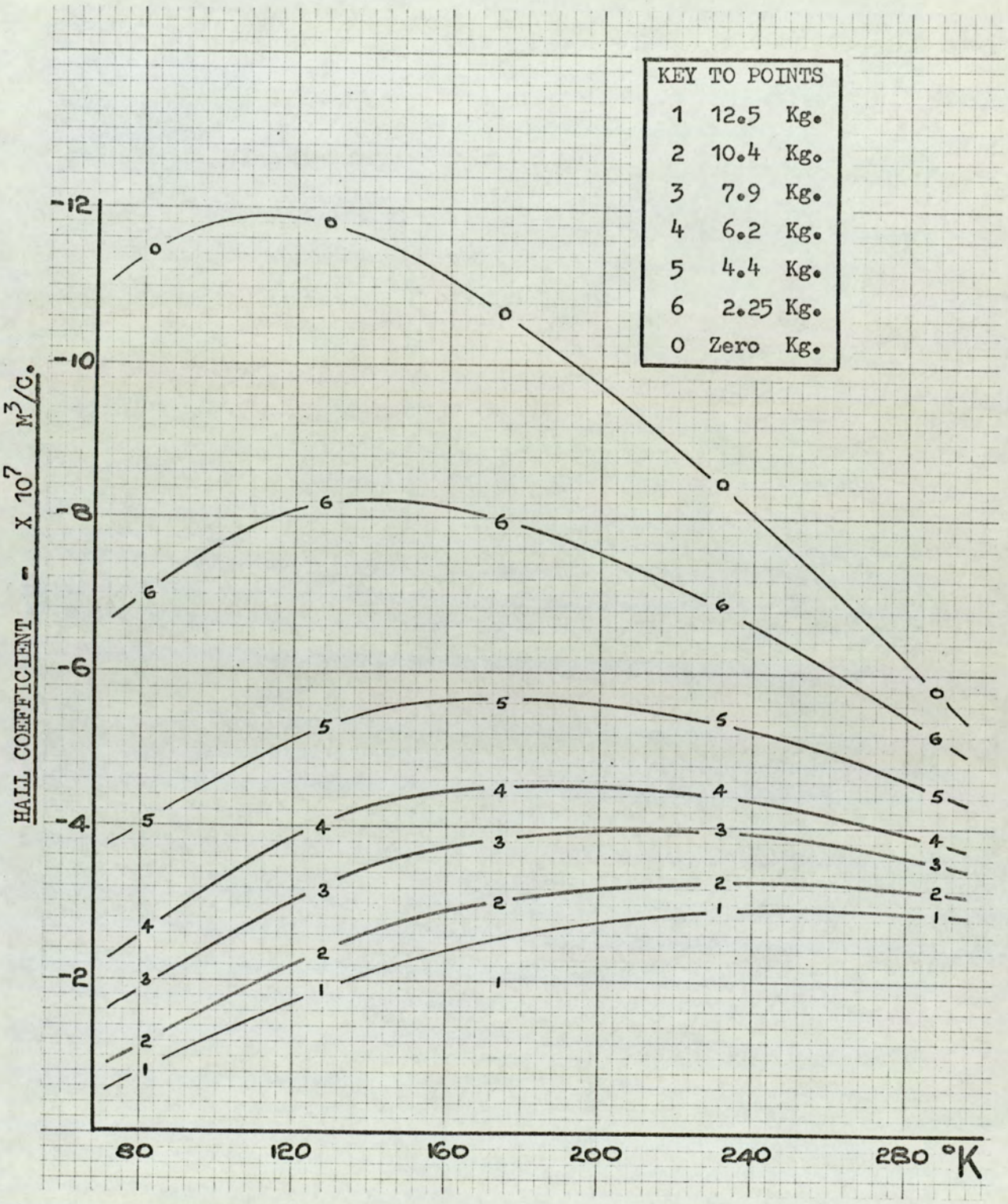

Fig. 138. Hall coefficient vs. temperature at a selection of magnetic fields for a ribbon specimen.

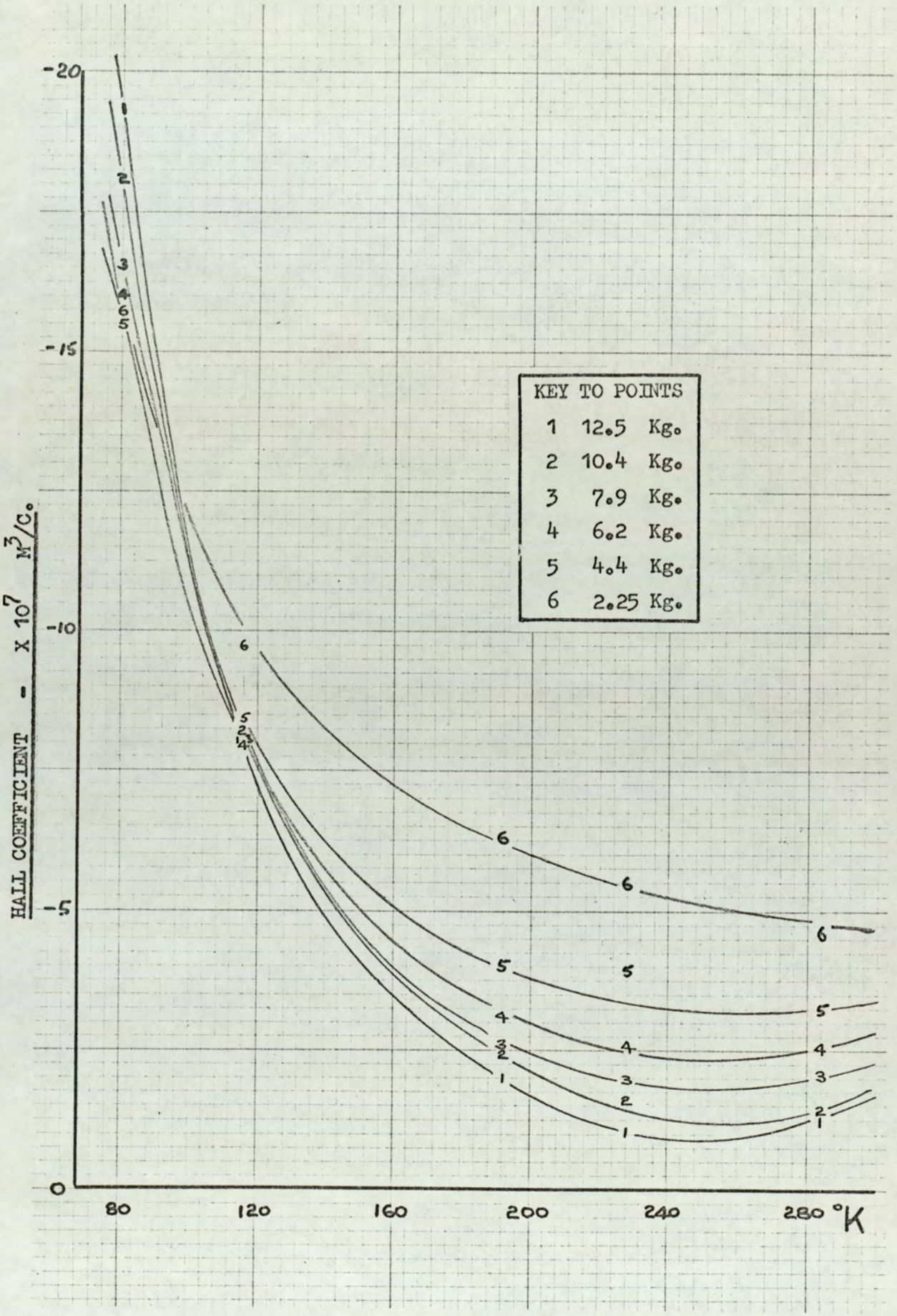

Fig. 139. Hall coefficient vs. temperature at a selection of magnetic fields for a bulk bismuth specimen.

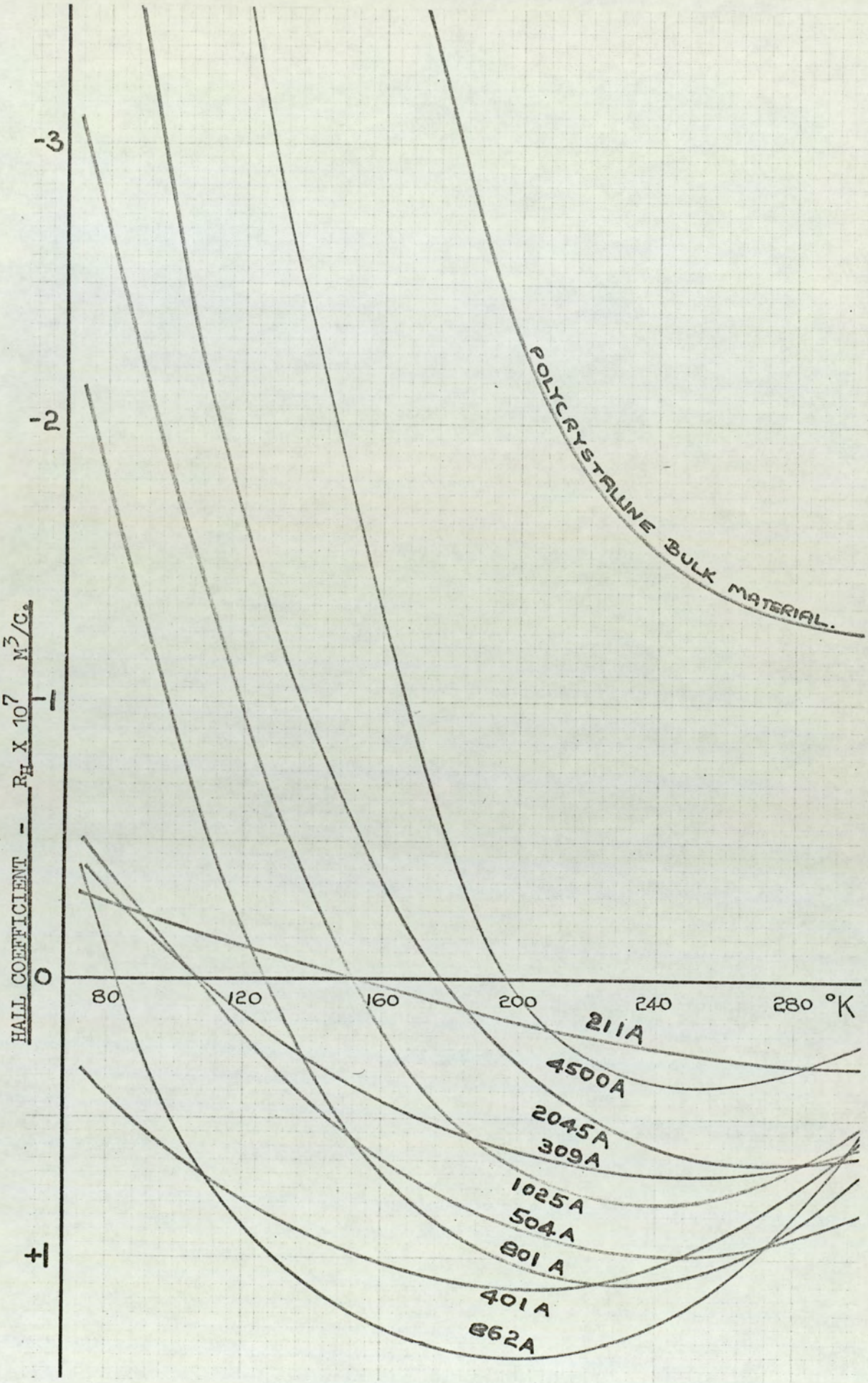

Fig. 140. Saturation Hall coefficient vs. temperature for a selection of bismuth films.

became the majority carrier, the curve experiencing a minimum just below room temperature. In bulk material electron conduction predominated at all temperatures.

The effect of a different magnetic field strength was to produce a curve of similar features differing only in the modulus of R_H. The curves were observed to reduce in separation at higher fields until a saturation curve was obtained. A notable feature was the coincidence of all the zero Hall coefficient values.

Figures 111 to 139 show the results obtained at a number of applied magnetic fields for the range of films and bulk specimens investigated. Whilst the results of all the films had exactly the same profile, attention is drawn to the different scale between the various graphs. Fig.140 has been included in which the saturation Hall coefficients of a selection of films has been represented against temperature on the same scale. The inclusion of all curves in Fig. 140 would lead to confusion, so only nine lines have been selected at this stage in the interests of clarity.

Commencing from the bulk material a lowering of the Hall coefficient occurred with decrease in thickness. At 4500 Å the curve had a point of equal mobility of carriers resulting in hole conduction at room temperature. Further reduction in thickness produced additional displacement until at 800 Å the curve was almost completely represented by hole conduction. Below this thickness however, the curves were observed to displace back towards the abscissa but at the same time having a more flat appearance. Along any chosen isothermal the value of R_H may be observed to behave in an oscillatory manner when related to the thickness of the film.

5.6. Summary

The results following the primary computation have been presented. The accuracy of the measured voltages was better than

0.1 % due to the galvanometer techniques involved. The quoted accuracy of the magnetic field strength measurements was 2%, but once calibrated, settings were repeatable using the vernier ammeter to better than 0.1%. Despite the many auxiliary experiments performed to assess the validity of the assumptions made to separate V_H, V_S and V_T an intrinsic error lay in the interpretation of the observations made. The differential nature and wide range of values of the measured quantities made an assessment of the overall error a complex task. As an alternative approach it may be assumed that if the variability of the quoted coefficients arose from the internal configuration within the specimens, then mutural consistancy should arise in the solution of the equations yielding the transport parameters. The accuracy of the points would thus be confirmed.

Whilst all resistivity measurements have been presented graphically in this section, only a selection of values at typical magnetic field strengths have been presented for the Hall and magnetoresistance coefficients. The remaining curves will however be included in the discussion of results in which the effect of magnetic field as the sole variable will be analysed. A set of mutually consistant curves will be derived whose only variable was the film thickness. It is only in this way that the detection of quantum effects will have their true significance.

CHAPTER 6

DISCUSSION OF RESULTS

6.1. Introduction

A problem exists in discussing concisely the wide range of results presented in this investigation. On the one hand there is opportunity for discussion of the individual properties of resistivity, magnetoresistance and Hall coefficient, and their dependence on temperature, and on applied magnetic fields. Each section has however a common thread in that the classical size effects, recurring in all sets of data are dependent on the thinness of the specimens and the size of the grains. The variation of the parameters with thickness is not monotonic due to quantum size effects, which are best discussed as a separate section. The difficulties associated with relating the practical to theoretical results in bismuth films are numerous. The complex Fermi-surface, the uncertainty of the mode of carrier scattering and highly anisotropic properties are just a few of the problems which are encountered in an analysis. In many cases an exact explanation of the properties observed in thin bismuth films is not possible but comparison will be made where appropriate with corresponding results taken on bulk specimens both in the present work and in the literature.

6.2. Resistivity of freshly evaporated films

Experimental circumstances resulted in the need to remove the prepared bismuth films from the vacuum environment prior to taking experimental observations. Such a technique had to be approached with some caution considering the chemical and physical nature

of the material. Piezoresistivity measurements on bismuth by Bate [103] have shown that stresses caused by change in pressure can have a marked effect on its properties. Furthermore the rapid oxidisation which takes place in bismuth exposed to atmospheric oxygen has a two-fold effect. A reduction in thickness of the metallic film occurs resulting in a modified resistance and current density. An overall change in the electrical properties is also likely to occur by the uptake of oxygen at the grain boundaries of the film.

A short programme of work was undertaken with a view to observing the change in properties arising from these sources over the working life of a bismuth film. A film of nominally 1000 Å was evaporated at 10.6 Å/S in a vacuum of 1×10^{-6} torr. Using the maximum output from the d.c. power supply, together with a suitably high series 'buffer' resistor readings were taken of the film resistivity from the time of termination of the evaporation. Over a period of 100 minutes the resistivity was observed to fall quite smoothly as in Figure 62 . As the temperature coefficient of resistivity in bismuth films will be shown to be negative, the possible cooling of the film following evaporation would give rise to an increase in resistivity. The fall must therefore have its origin in the relief of internal stresses by a process of self-annealing. The motivation for the annealing can arise in part from the stresses introduced in the solidification of the bismuth vapour onto the substrate which amounts to about 3.5% by volume. Uozumi [104] evaporated bismuth films onto cantilevered copper shims and electrically observed the deflection caused by the differential stress. Having corrected the results for radiation effects of the filament he observed the relief of stress by the gradual return of the shim to the equilibrium position. Though only very thin films were used by Uozumi the time scale for the process was quite short, and even for thicker films

would remain below 60 seconds. The origin of the total fall of 3% in resistivity in the present investigation cannot be attributed solely to this source. A possible explanation would be charge-induced coalescence of grains as described by Chopra (62).

As the rate of self-annealing diminished a linear increase in resistivity was observed and was attributed to the final return of the substrate to laboratory temperature following the deposition. Extrapolating the time to the ordinate would suggest that the substrate, as opposed to the film surface, suffered a temperature change of only $1^{o}K$ during the evaporation. The re-entrant cold finger and copper heat sink favourably contributed to the thermal inertia of the substrate.

Under conditions of thermal equilibrium, atmospheric air, dried by passage through liquid nitrogen, was admitted to the chamber. A rapid increase in film resistivity was observed. Within minutes the resistivity showed signs of saturation until after about 1 hour further change was masked by the diurnal variation in laboratory temperature. An initial maximum occuring after the first 15 seconds was attributable to the film surface chilling by the refrigerated atmosphere and amounted to a $2^{o}K$ fall in temperature.

The resistance of the film was an inverse measure of the amount of material remaining behind after oxidisation. Assuming negligable oxide was present at the onset of admission of dry air then from the change in resistance the remaining thickness of bismuth could be readily calculated,

$$t' = \frac{\rho_o}{\rho} \times 1000 \text{ Å}$$

To a first approximation the thickness of oxide may be taken to equal the thickness of bismuth removed. This is unlikely

to be very accurate, but as we are more interested in the remaining bismuth, the analysis will be acceptable. The process of oxidisation in metals for which the uptake of oxygen in excess of a few monolayers occurs at ordinary temperatures is given by Mott [105]. The theory is based on the assumption that oxygen atoms are adsorbed onto the surface of the oxide. A strong field is set up in the oxide due to the contact potential difference between the metal and adsorbed oxygen, and enables the metal ion to migrate through. Mott dismissed the possibility of the diffusion of oxygen through the oxide. A logarithmic law, as given by Cabrera [106], can be applied to materials which form an equilibrium oxide layer:

$$\frac{1}{X} = A - B \ln T \quad \ldots\ldots\ldots\ldots (6.1)$$

where X = oxide thickness

T = time

A,B = constants.

A deduction of the thickness of oxide in the present analysis using the approach given above resulted in a linear plot of equation 6.1 as in the inset of Figure 62 . The 60 Å of oxide formed over 2 hours was likely to be in excess of that formed under experimental conditions in which the film was subjected to a nitrogen environment until mounted in a residual atmosphere of dry helium. A total lapse of less than 10 minutes could result in the oxidisation of approximately 30 - 50 Å of bismuth.

6.3. Resistivity

The resistivity results taken on thirty bismuth films are presented in Figures 66 to 79 . The results are plotted at temperatures between 77°K and 300°K, and it will be recalled (chapter 4) that the films have been shown to consist of small

single crystals whose diameter was of the same order as the film thickness, and whose orientations were such that the trigonal axes lay along the normal to the film.

For the whole range of films examined a negative temperature coefficient of resistivity (T.C.R.) was observed, a feature which was not the case either in the bulk polycrystalline specimens presented here or in the values for bismuth single crystals quoted for example by Abeles and Meiboom [28]. The origin and significance of the negative T.C.R. will be discussed presently. Dismissing for a moment the results obtained on films below 400 Å in thickness, the curves for all films were observed to display a change in gradient within the temperature range 150 - 210°K. On either side of this range there was a tendency towards an asymptotic value. The change in gradient was a manifestation of the classical size effect, and arose from the contribution to the conductivity of carriers scattered from the surfaces of the film, and from the grain boundaries.

The temperature dependence of Mattheisons rule, chapter 2, is given by:

$$\frac{\partial \rho}{\partial T} = \frac{\partial \rho_L}{\partial T} + \frac{\partial \rho_S}{\partial T} \quad \ldots\ldots \quad (6.2)$$

At high temperatures where the mean free path of carriers is only of the order of a hundred atomic distances the contribution due to surface scattering is insignificant. The variation of the measured resistivity with temperature is thus that which would arise solely due to the vibrations of the lattice. The effect of reducing the thickness of bismuth films below those of bulk values will be discussed in relation to quantum size effects, but essentially there is an effective decrease in the overlap energy between the valency and conduction bands. As a result of the reduced band gap the carrier concentration is more sensitive to temperature, and causes

increased elevation of electrons to the conduction band at higher temperatures. The resulting negative T.C.R in thin bismuth films thus arises, but observations of the gradual change from a positive to negative coefficient are more difficult due to the several orders of magnitude difference between the thickest films and thinnest foils.

The quoted thickness below which films attain a negative coefficient varies widely in the literature. The extensive work of Kioke (33) placed the value at 5000 Å, the value of the coefficient levelling out below 2000 Å to a constant value of between -2 and -3 x 10^{-3} $\mu\Omega$-M/°K (Figure 7 VI). The coefficient observed by Duggal (32) however changed sign at 1000 Å and decreased rapidly as the thickness was reduced (Figure 7 IV). Both authors evaluated the T.C.R. from measurements at room temperature, where the contribution to the resistivity arose solely from the vibrations of the lattice. Figure 141 illustrates the asymptotic slope of the curves at 280°K against film thickness for the present work. From 400 - 1700 Å a constant value of -2.25 x 10^{-2} $\mu\Omega$-M/ °K $\pm$ 15% was obtained, falling slightly to - 1.7 x 10^{-2} for films of 4500 Å in complete agreement with the results of Kioke.

The relative displacement of the curves at 280°K signified the contribution to the conductivity due to interstitial atoms, vacancies and dislocations ever present in evaporated thin films. Following the initial self-annealing and surface oxidisation discussed in section 6.2 there were no changes in resistivity as a result of thermal cycling over the range 77 - 300 °K. Consequently the temperature dependence of the appropriate term, ρ_I , in the Matthieson equation may be equated to zero. In all cases the resistivity values at 280°K in the present work were in excess of the corresponding bulk values of 1.10 $\mu\Omega$-M. Assuming that the origin of the negative T.C.R. in bismuth films may be attributable to a modification of

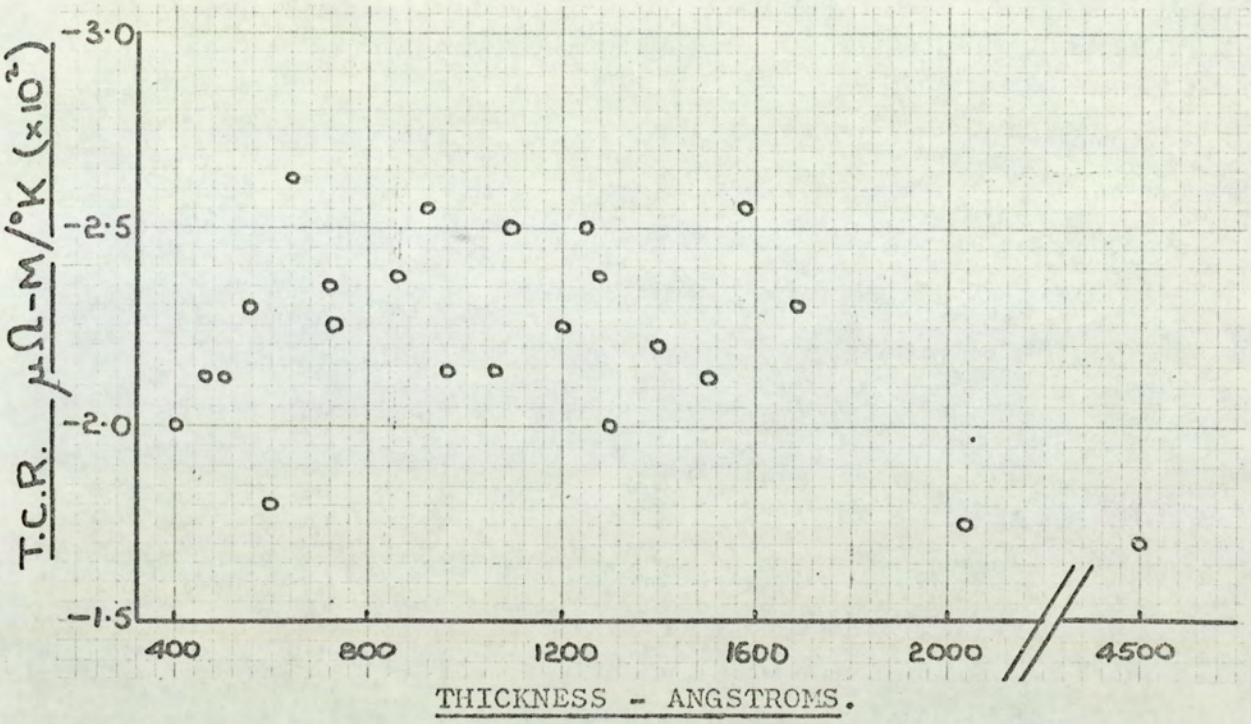

Fig. 141. Temperature coefficient of resistivity at 280°K vs. film thickness.

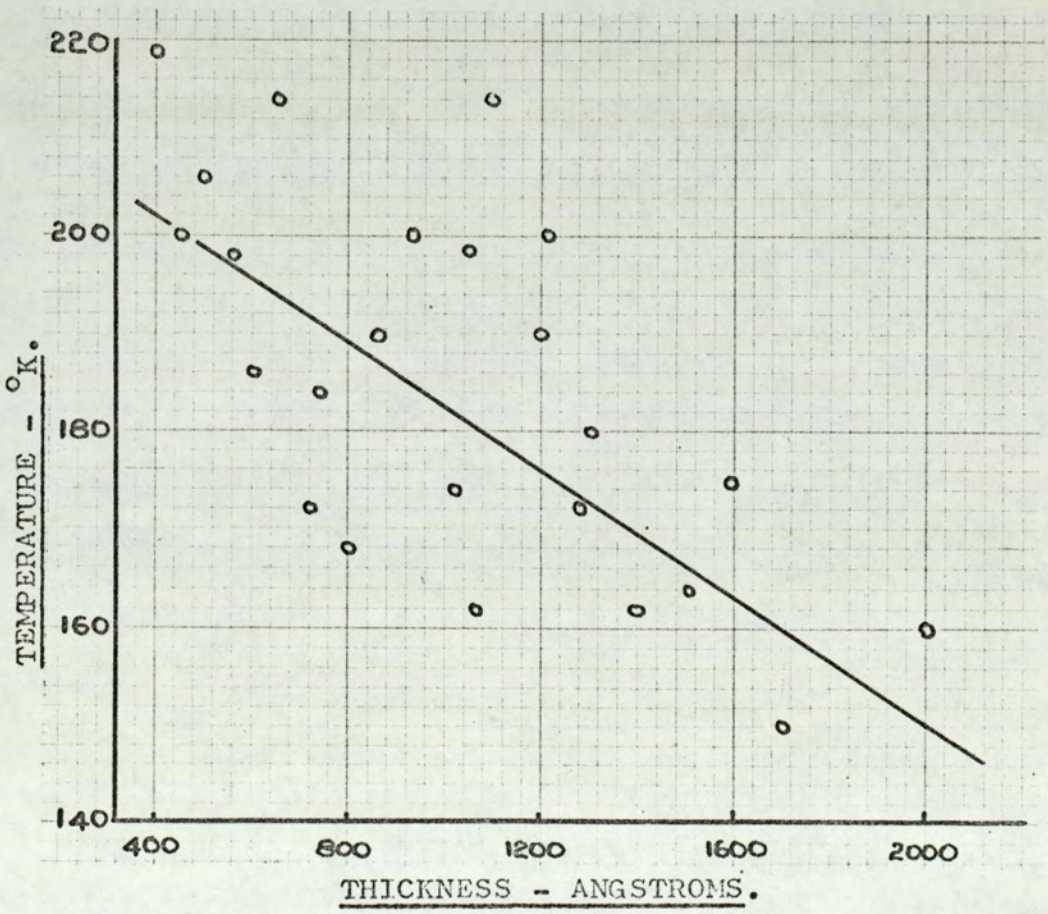

Fig. 142. Temperature corresponding to the asymptotic origin in the resistivity curves vs. film thickness.

the band structure the general increase in resistivity is in itself not unreasonable. The effect of interstitials and dislocations does however have a similar effect, and as has been demonstrated by both Duggal and Kioke the increase in absolute value of the resistivity is accompanied by a significant scatter in the experimental points. The present values of 4 - 10 $\mu\Omega$-M for films showing a thick limit value of the resistivity are in agreement with Kioke, but higher than those of Duggal. Subsequent heat treatment of the evaporated films prepared by Duggal accounts for the difference between his results and those of the present work. The larger grains known to be associated with evaporation onto 400 ^{o}K mica substrates followed by thermal annealing result in resistivity values closer to those of bulk material. The change in resistivity due to annealing at a constant film thickness does however indicate the significance of grain boundary scattering in the overall conductivity process. The hypothesis was confirmed by Clawson (Figure 18) in which the properties of thin films were observed to display a mildly positive T.C.R. and near bulk values following recrystallisation from the liquid phase.

In an attempt to establish the degree of reproducibility of the results of the present work, readings were taken on two films of nominally equal thicknesses evaporated under similar conditions. The graph of resistivity against temperature for films of 735 ^{o}A and 744 ^{o}A are presented in Figure 71 . The relative displacement between the two curves was quite small and contributed to the general conclusions that the properties of the films could be reliably reproduced.

The contribution to the resistivity due to surface scattering becomes progressively more significant as the temperature is reduced. The increase in the number of free paths prematurely terminated by the boundary due to a decrease in temperature results in

a temperature coefficient for surface scattering which must essentially be negative. The actual temperature dependence of the coefficient is not however likely to be straightforward, and depends greatly on the mechanism of scattering at the boundaries. If we consider a simple picture of the thin film scattering process in which all carrier paths commence at the boundary then the total effective mean free path is the sum of contributions of all component paths. The effective path, λ_{eff}, is the distance to the next surface intersection, λ_s, or the bulk mean free path, λ_b, whichever is the least.

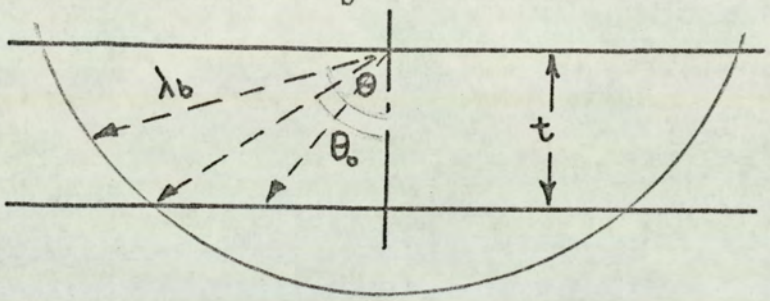

It can be readily seen that the effective path parallel to the applied field for diffuse scattering can be expressed as;

$$\lambda_{eff} = \int_0^{\theta_o} \frac{t}{\cos\theta} \cdot \sin\theta \, d\theta + \int_{\theta_o}^{\frac{\pi}{2}} \lambda_b \sin\theta \, d\theta \qquad \ldots\ldots(6.3)$$

where $\theta = \cos^{-1} \frac{t}{\lambda_b}$

On integration,

$$\lambda_{eff} = t(\log (\lambda_b/t) + 1) \qquad \ldots\ldots\ldots\ldots\ldots\ldots(6.4)$$

which for small thicknesses is the conductivity expression given in equation 2.20. An examination of the integrals however shows that the contribution to the effective path is greater at angles close to θ_o and therefore in the thin limit the significant carriers are those travelling almost parallel to the surface. In

this case $\lambda_{eff} \simeq \lambda_b$. The number of carriers executing paths corresponding to θ_o is however vastly reduced by the surfaces resulting in enhanced resistivity. Though fewer in number the contributing carriers are similar to those in bulk conductivity, and hence a similar temperature dependence is expected.

For films in excess of 400 Å the curves can be seen in the present work to approach the asymptotic axes defining the thick and thin limit contributions to the conductivity. In contrast to the almost parallel nature of the high temperature asymptote however those at the low temperature are not parallel, and indeed are a function of film thickness.

The overall temperature coefficient in bismuth films may be presented in several ways, the most frequent presentation being the ratio of the resistivities at, for example, 77°K and 300°K for a range of thicknesses [52]. Such ratios provide information used in discussions such as the quantum size effect. The wide qualitative knowledge of the contribution of boundary scattering to the shape of the resistivity temperature curve does however make the unique nature of the current presentation seem rather surprising. It can be readily seen that basic effects, quantum or otherwise, may be disadvantageously hidden in calculating the ratio $\rho_{77}/\rho_{300°K}$ because of the spread in values of ρ 300°K for thin films. The basically parallel nature of the high temperature portion of the curves led to the present approach of using the slope of the low temperature asymptote as a property best reflecting the quantum nature of the observations. In this way the effect of surface scattering may be uniquely separated from both bulk and impurity contributions.

A plot of the slope of the asymptote against film thickness is shown in Figure 143 in which the oscillatory nature of the curve can be readily seen. The significance of the periodic oscillation

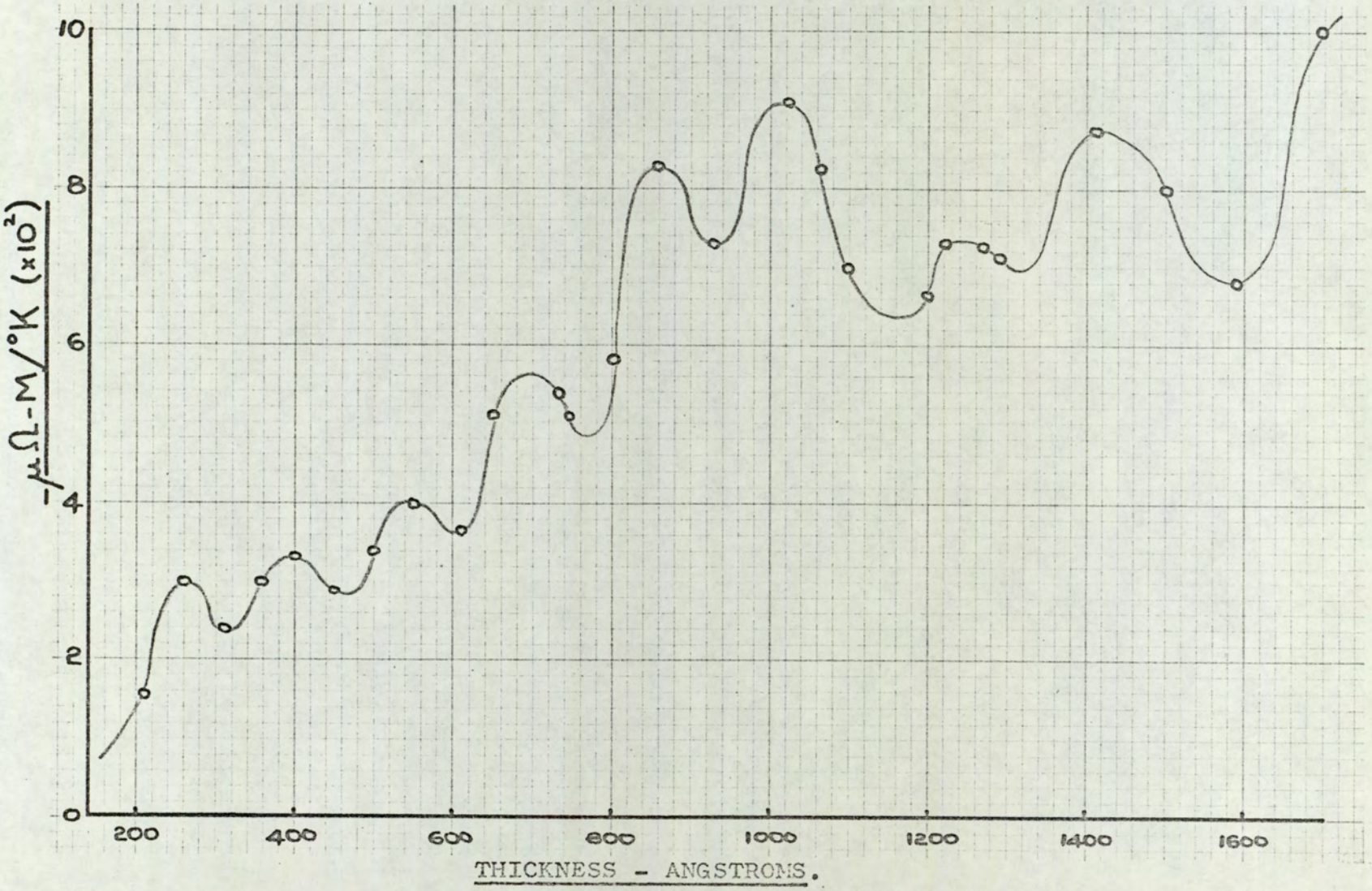

Fig. 143. Temperature coefficient of low temperature asymptote vs. film thickness.

may be described thus. If all curves were normalised so that both the high temperature asymptotes and asymptotic origins were coincident then at any temperature for which boundary scattering is important the degree to which the grain and film boundaries affect the conductivity is a function of the thickness of the film. At certain thicknesses carriers may preferentially traverse the length of the film. The observation is introduced at this stage, but will be discussed fully under the heading of quantum effects.

Under the idealised conditions of two distinct asymptotes the problem ofstudying the effect on the asymptotic origin of varying the film thickness should in principle be straight forward. As the thickness is increased, the temperature at which boundary scattering contribution equals the lattice contribution to the conductivity, should correspondingly decrease. However, the experimental change in thickness of only an order of magnitude, and an extreme uncertainty in drawing the axes would in itself render the quantitative exercise very difficult. In addition the presence of the oscillatory nature of the asymptote leads to the query as to the location of the fulcrum about which the curve pivots. On the assumption that the origin remains independent of the gradient of the low temperature asymptote, Figure 142 was drawn to illustrate the temperature at which boundary scattering becomes significant for various thicknesses of film. Despite the distribution of points a trend is observed in which the average free path, assumed to be around the film thickness at this point, increased with decrease in temperature. The curve indicated an inverse relationship between the mean free path and temperature as would be expected at temperatures above the Debye characteristic temperature.

From the uncertainties one would conclude that a quantitative correlation between the temperature variation of the resistivity of

thin bismuth films, and the effective path of the carriers is impractical by this type of analysis.

Hitherto, no mention has been made of the effect on the conductivity of specular rather than diffuse scattering of carriers at the surface of the specimen. It is known that in bismuth the long carrier wavelengths, being unable to adequately resolve surface asperities, have a coefficient of specular reflection which is very close to unity. The conventional Sondheimer treatment of the classical size effect in thin films shows that the size effect will only be observed in the case of diffuse scattering from the boundaries. The boundary in fact acts as a scattering centre, and thus free paths are terminated prematurely. In the case of specular reflection in which the electron is 'optically' reflected back into the lattice the path is not terminated and the conductivity becomes independant of sample size. An important analysis by Price (31) and by Ham and Mattis (107) has however shown that in the case of non-spherical energy surfaces there is still a size dependence for the electrical conductivity interpreted by the fact that the electron velocity vector no longer lies along the momentum vector. It was further shown, and this is a unique feature of specular reflection, that the size effect would reach a limiting value. The arguments are complex, but the saturation essentially depends on the shape of the constant energy surfaces. For the case of diffuse scattering a monotonic decrease in conductivity with increase in mean free path is observed independant of the shape of the energy surfaces. Figure 6 illustrates the observations on bulk material of Friedman and Koenig (17) and of Aubrey et al (22) in which the saturation effect is observed in a plot of conductivity against sample thickness at 4.2 ^{o}K. Goldsmit attributed the large discrepancy to the internal stresses introduced by Friedman and Koenig in removing the specimens from the

liquid helium for machining. Aubrey utilised a wedge shaped specimen. The specular coefficient was invarient to mechanical abrasion of the surface so that surfaces which were optically flat were also specular to these long wavelength carriers.

The results presented here on the four thinnest films are of particular interest in that at the lower temperatures a saturation of the resistivity is seen to occur. The saturation is interpreted as being of a similar origin to the above results on bulk specimens. On all four films the departure from the expected boundary scattering line was quite marked and this is in fact the first report specifically mentioning the occurrence of this phenomena in thin films. The effect can however be observed in the normalised results of Ogrin (46) in which a plot of $\rho_T/\rho_{4.2^\circ K}$ is presented against temperature from 4.2 - 280 $^\circ$K. In agreement with the present work only films below 400 $\mathring{A}$ show evidence of a saturation at 80°K. The 309 $\mathring{A}$ film in the present work is of particular interest in that both the classical mean free path and the specular reflection saturation size effect may be observed on one film. As would be anticipated the temperature at which the saturation occurs increased with decrease in thickness, and it is notable that the saturation may be resolved despite the general increase in resistivity which accompanied the thinnest films.

The analysis performed on the bulk and ribbon specimens was primarily intended to give insight into the difference between the polycrystalline galvomagnetic properties of films and bulk material. The resistivity results are presented in Figure 80. The resistivity of the bulk polycrystalline specimen lay between the single crystal values of Focke and Hill and of Abeles and Meiboom. A similar resistivity was obtained using the proprietory bismuth ribbon. A notable feature was that three separate runs

resulted in curves which were non-coincident and slightly non-linear. The non-linearity did not have its origin in a size effect and was qualitatively explained by the residual magnetic field retained in the pole-pieces of the electromagnet, the effect of which became more pronounced at lower temperatures.

In summary therefore it may be said that the orientated bismuth films displayed a resistivity in which the temperature coefficient of resistivity was negative. By varying the temperature over the range 77 - 300 ^{o}K the classical mean free path size effect was observed. The temperature coefficient arising from the effect of boundary scattering displayed an oscillatory dependence on film thickness, a discussion of which will be presented later. A quantitative assessment of the mean free path of carriers from the classical size effect was barely possible, but evidence exists for the presence of a size effect in the thinnest films arising from the shape of the complex energy surfaces.

6.4. Hall coefficient

The presence of a Hall voltage in a material is a direct manifestation of the action of the Lorentz force on a charged carrier moving in a magnetic field. It has long been recognised as a powerful phenomenon for studying the electronic properties of materials. In a material in which there is only one type of carrier present the Hall coefficient is determined by:

$$R_H = \frac{1}{ne}$$

and thus its measurement reveals directly the total effective number of carriers. The advantage of the method is that it is available for use at all temperatures whereas the more sophisticated methods usually require specialist techniques at low temperatures. For a two carrier system the holes and

electrons, being opposite in both charge and direction, are deflected to the same side of the specimen and thus the simple two carrier Hall expression for a compensated material was shown (equation 2.45) to be,

$$R_H = \frac{1}{Ne}\left[\frac{\mu_h - \mu_e}{\mu_h + \mu_e}\right] \quad \ldots\ldots\ldots (6.5)$$

The action of the Hall field is to oppose the Lorentz force on the moving carrier so that it is constrained to move in its original path. This theoretical ideal is, however, not met in a real solid, because of the velocity distribution of the carriers both within an individual carrier energy spectrum and between different energy bands. Even in the presence of an equilibrium Hall field the majority of carriers will be influenced in their motion by the magnetic field, and it is interesting to note the consequence of the additional field force term, $e(V \wedge B)$. The rate at which energy is supplied to a carrier is given by

$$\frac{\partial W}{\partial t} = F.v = e\left[v.v \wedge H\right] \quad \ldots\ldots (6.6)$$

The scalar triple product vanishes in the orthogonal case and thus the magnetic field does not supply energy to the system. In the case of carriers of equal mobility the Hall field becomes zero since, although the nett Hall current is zero, the partial flow of electrons and holes are in opposition. Under these conditions the nett effect is the generation of electron hole pairs at one face of the specimen and annihilation at the opposite face. The process is very energetic and the resultant ionisation energy is transferred across the specimen. The electronic flow of energy continues until it is balanced by the conduction of heat in the opposite direction. The process is known as the Ettingshausen

voltage.

The observations of the Hall effect in thin bismuth films in the present investigation were of two types. In some cases a set of observations were performed in a fixed magnetic field at about thirty temperatures between 77°K and 300 °K. On other films the magnetic field was varied over the range zero to 12.5 Kilogauss at five fixed temperatures within this range. Figure 126 taken on a film of 1025 Å was typical in profile of the range of films examined. The quadratic nature of the curve is readily seen in which conduction by electrons predominated at lower temperatures. The Hall coefficient decreased with increase in temperature until at about 150°K a zero Hall coefficient was observed. Under these conditions the mobilities of the electrons and holes were equal. Further increase in temperature resulted in holes becoming the majority carrier, the curve having a minimum value somewhat below room temperature. The graph is to be compared with a similar contribution by Fritsche et al [6] as shown in fig. 15 (i). Sparsity of points in the low temperature region led Fritsche to present a line showing a linear change in R_H followed by a saturation region in which R_H was independant of temperature. The minimum was not observed in Fritsche's graph although the present work confirms the feature to be real. Colombani and Huet [9] showed that in the temperature range 20 - 200 ° Celsius the coefficient continued to return towards the abscissa. The normalised results of Ogrin et al [3] fig. 15(ii), are in complete agreement with the present investigation showing a minima whose corresponding temperature decreased with increase in thickness. A higher degree of disorientation may have been present in the thicker films of Ogrin causing films in access of 2000 Å to show a negative Hall coefficient at 300 °K. As will be discussed later

the minima arise from a particular combination of the anisotropic Hall coefficients present in polycrystalline films.

A variation of the number of carriers with magnetic field is known to exist in bismuth, but quantitatively the problem has only been considered in bulk material. Azbel and Brandt (108) considered the relative displacement of the energy bands for carriers having a quadratic dispersion law, along similar lines to the derivation leading to the Landau sub-bands occurring in materials at low temperatures. The action of the magnetic field is to displace the energy bands relative to each other in such a way that an increase in band overlap causes an increased spillage of carriers from the valence to the conduction band. In addition to the general movement of bands, a fine structure appears on graphs of low temperature galvomagnetic properties of bismuth against magnetic field, which originate from the quantisation of the electron energy levels, and gives rise to Schubnikov-de Haas oscillations. The oscillatory properties of bismuth films as a function of magnetic field were not studied in the present investigation.

Azbel and Brandt deduced that in bulk bismuth the variation in the number of carriers with applied magnetic field was directly proportional to $H^{3/2}$. As a result of the increase in carriers the Hall coefficient becomes functionally dependent on the magnetic field and has been reported by several authors. Quantitatively the correlation between the theory and experiment for either bulk or films does not appear in the literature.

The effect of applying a different magnetic field to the film was to produce a curve of similar profile to that described above, differing only in the magnitude of the values of R_H, as for example in fig 137. The graphical points refer consequently to a decrease in magnetic field from 12.5 Kg to 220 gauss. From

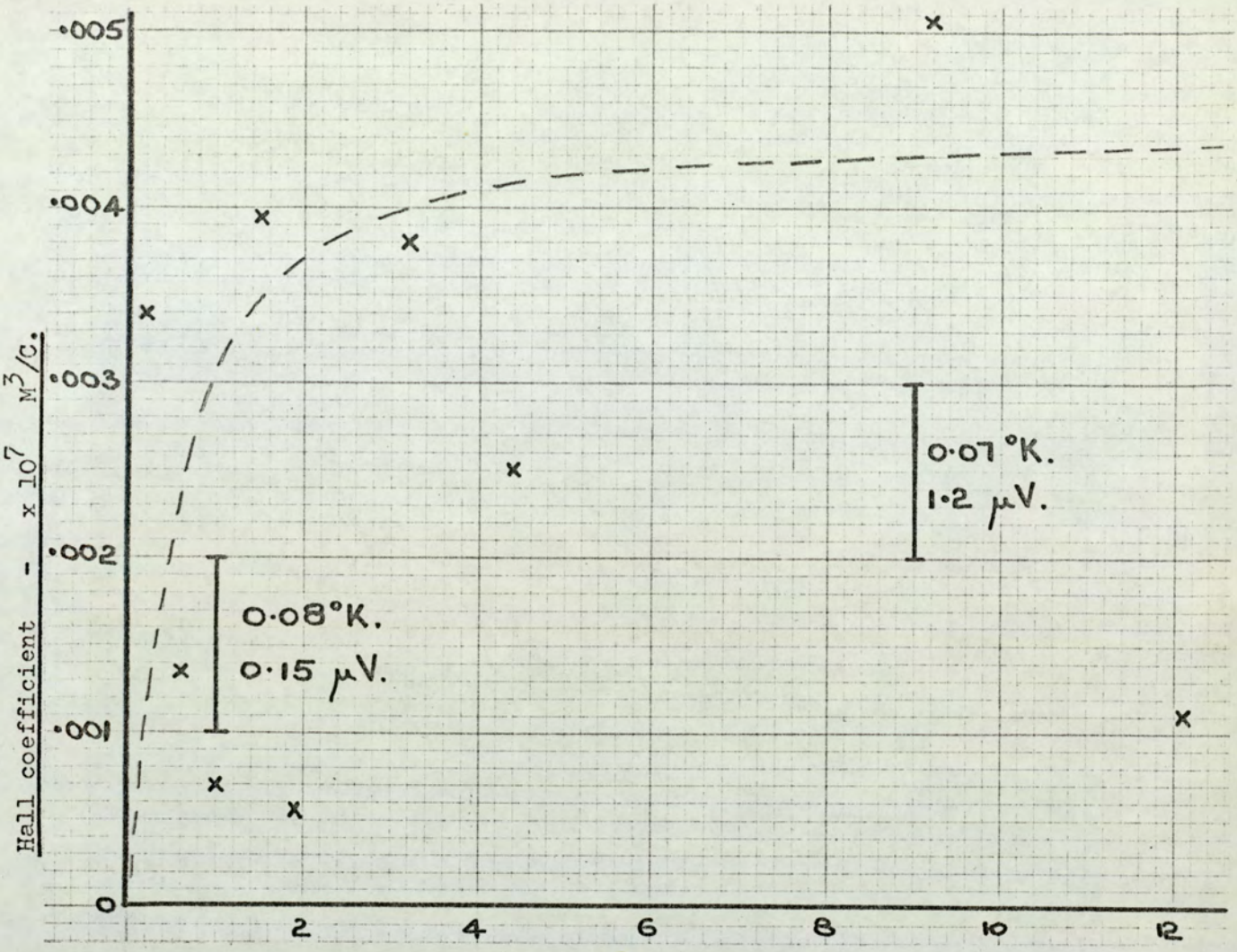

Fig. 144. Hall coefficient vs magnetic field at 609 Å close to the cross over temperature.

the low magnetic field curve, the remaining curves were observed to reduce in separation as the magnetic field was increased until a saturation value was obtained at the higher magnetic fields. The feature was observed on all curves subjected to a "field variation" run and illustrated a functional dependence of R_H on the applied magnetic field. It was noted that for all films an absolute coincidence of the curves occurred at the point of equal mobility of the carriers. The overall significance of this 'coincidence' feature will be discussed with reference to fig (144). The curve

represents the readings taken of Hall voltage against applied magnetic field for a film of 609 $\overset{o}{A}$ at 125°K, and its significance lies in the fact that it is the closest any set of 'field variation' runs came to falling on the actual cross over temperature. Bearing in mind that for the moment the actual form of functional dependence of R_H in the magnetic field has not been discussed, fig. 144 contains some important features despite its non-functional appearance. The ordinate is some 10^2 times more searching than those of the published Hall graphs. Because of the minutely small values of the computed Hall voltage the scatter in the points was thus not unreasonable. The results from which the R_H values were obtained consisted of a combination of Hall voltages, standing voltages and Ettinghausen voltages whose total magnitude was around 2000 measured units (units of 10^{-7} volt). The extracted Hall voltage, though only a few units, was never observed to fall astride the abscissa for any of the fields despite the closeness to the cross-over temperature. Such was the case for any of the sets of readings on any of the films, and contributed to the conclusion that the value of the cross-over temperature was totally field independent.

Having demonstrated the field-independence a further look at graph yielded insight into the electrical accuracy and thermal stability of the experimental arrangement. From the gradient of the curve of R_H against temperature for the 609 $\overset{o}{A}$ film (Fig. 119) it was possible to equate the magnitude of the variation either in the measured voltage or in the thermal drift which would cause a typical point to vary by one major graticule on the graph. It is noted that at 9 Kilogauss the variation arose through either a temperature change of 0.07°K or an inaccuracy in voltage reading of 1.2 μ Volts. The situation was even more acute at 1.0 Kilogauss in which the voltage sensitivity was 0.15 μ Volts per graticule.

The dashed curve represents a possible correct line taken from scaled readings away from the cross-over temperature. The total inaccuracy from both sources occuring simultaneously can be estimated. Either a 1 μVolt or a 10^{-1} ^{o}K variation would adequately resolve most of the scatter in the experimental values. In all cases the four voltages which together enable V_H to be evaluated are within the range 10^3 - 10^5 measured units and thus the accuracies of this specialist point may be extended to cover all readings.

The significance of the total field independence of the cross-over point of R_H may be interpreted from equation 6.5. The magnitude of the expression is sensitive only to the value of N, the number of carriers, and to the mobility ratio μ_e/μ_h. The possibility of the applied magnetic field modifying the mobility is very unlikely in that the effect would have to be identical for both carriers over the entire range of mobilities involved in the investigation. The alternative assumption is that it is in fact N which varies, as suggested by Azbel and Brandt. As the number of carriers must essentially remain non-zero at zero magnetic field the effect of the field is such that N increases by a quantity ΔN. Based on Azbel and Brandt's treatment for bulk materials ΔN is expected to bear a power law relationship to the magnetic field. The two carrier Hall expression may be written as:

$$R_H = \frac{1}{(N+\Delta N)e}\left[\frac{\mu_h - \mu_e}{\mu_h + \mu_e}\right] = \frac{F(\mu)}{N + AH^x} \quad \ldots (6.7)$$

where $F(\mu)$ is a function of the mobilities and is invarient at constant temperature. A and x are constants. As can be seen from the thin film results (e.g. fig. 137) the directional dependence of R_H in the magnetic field is in opposition

to that in either of the two bulk specimens (fig. 138). In bulk material an increase in field causes a reduction in the modulus of R_H whereas the reverse is the case in thin films. The two alternative effects were strongly evident and indicated a fundamental difference in the response to the field.

The quantitative evaluation of the constant x is of prime importance in that the mutual solution of the equations resulting in the individual mobilities and the number of carriers, depends on the value of N. This must be invariant in both the conductivity and Hall expressions and thus the value of ΔN must be capable of reduction to zero to enable the solution to be valid. The evaluation of x is however not direct. By differentiation of equation 6.7 at constant temperature one obtains with some re-arrangement:

$$\frac{1}{R_H^2}\left[\frac{\partial R_H}{\partial H}\right] = -AxH^{x-1} \quad \ldots\ldots (6.8)$$

The differential term was negative in the case of bulk material and therefore provided the product (Ax) is positive then we may write:

$$\log \frac{1}{R_H^2}\left[\frac{\partial R_H}{\partial H}\right] = \log Ax + (x-1)\log H \quad \ldots (6.9)$$

A plot of the left hand side of equation 6.9 against log H would result in a line of slope (x-1) provided x remained invariant. In the case of thin films the differential term was positive at all fields and thus the same relationship is valid as long as the product (Ax) is negative.

The ordinate for equation 6.9 was evaluated for the ribbon specimen using fig. 145 in which the Hall coefficient is presented against applied magnetic field at a selection of

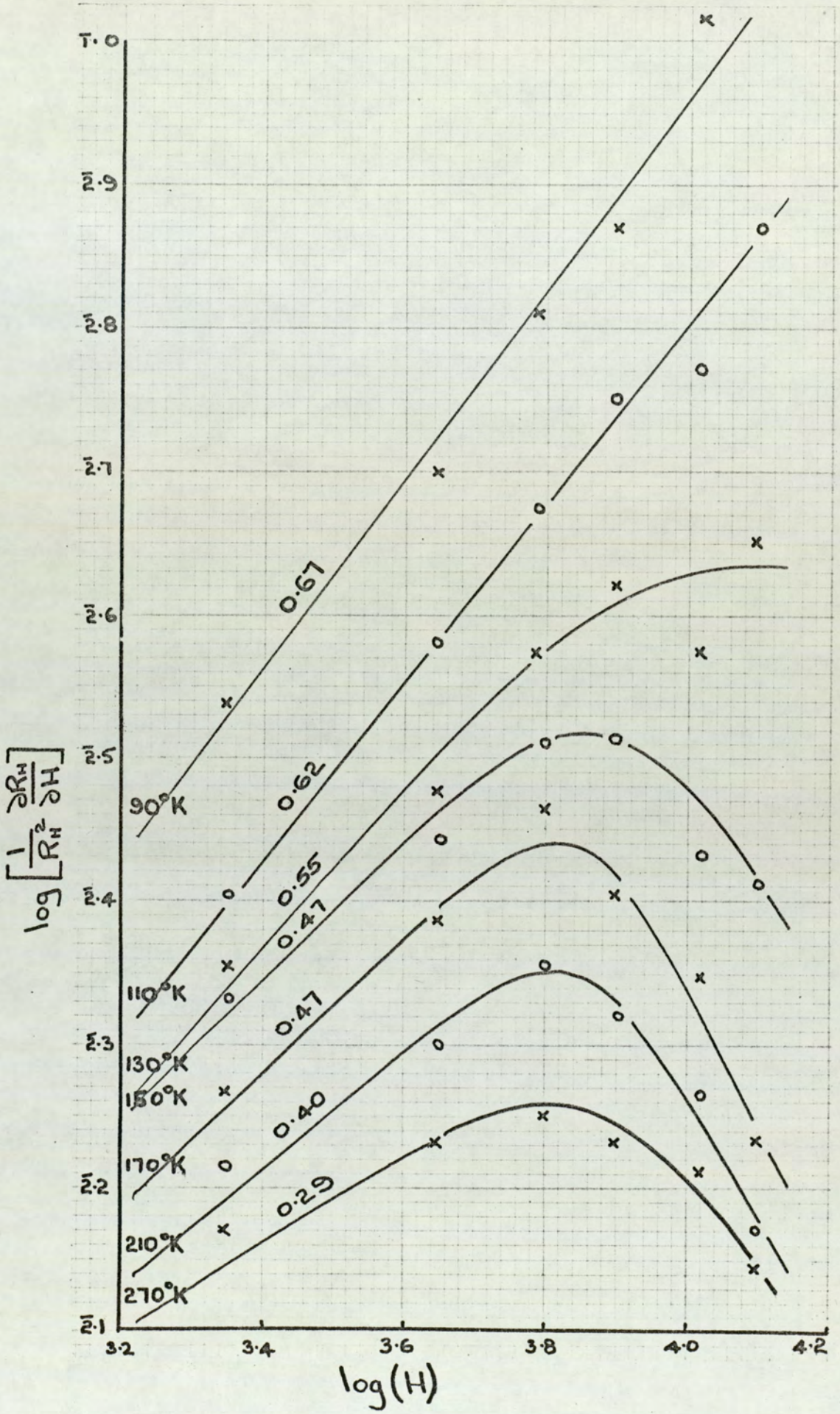

Fig. 145. Field variation analysis for the ribbon specimen.

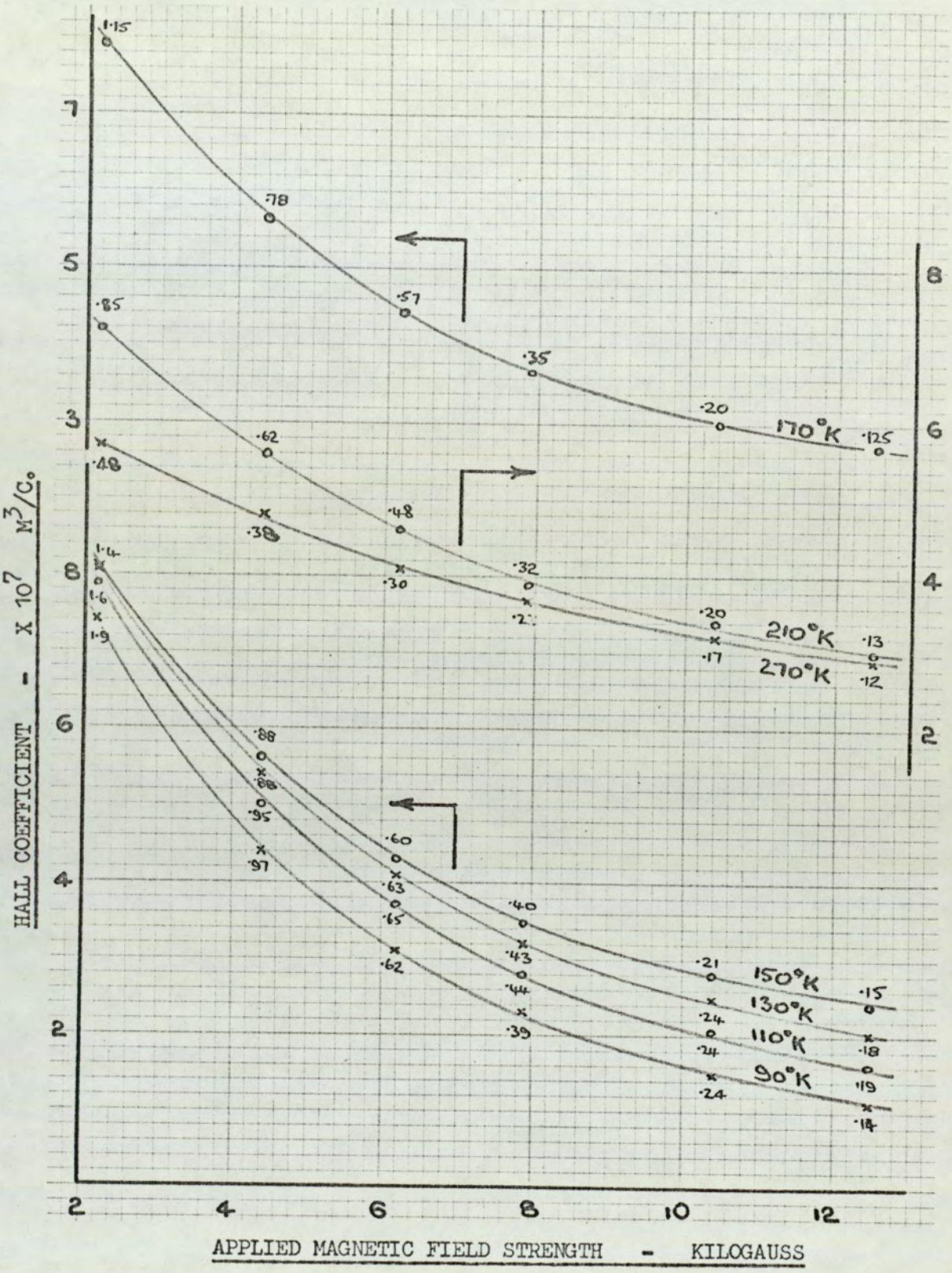

Fig. 146. The variation of the Hall coefficient with magnetic field at a selection of temperatures. Small figures represent the gradients at the points indicated.

temperatures. The gradient was measured at intervals along each line. Figure 146 was constructed in accordance with equation 6.9 from which the quantities (x-1) could be obtained. At low magnetic fields an average value of x of 1.50 was obtained in agreement with the predictions of Azbel and Brandt. The behaviour at higher fields is however less direct in that a change in x not only alters the gradient of the line directly but includes the perturbation caused by the change in the 'constant' term of (6.9). The apparent fall to a value of zero (x-1 = -1) is not real as log (Ax) would become infinitely negative thus invalidating the mathematics. A slight fall from the value of 1.5 must essentially occur, however, in order to produce the high field behaviour.

The value of x is seen to be temperature dependent, ranging from 1.67 at 90°K to 1.29 at 270°K. Fig. 147 shows that

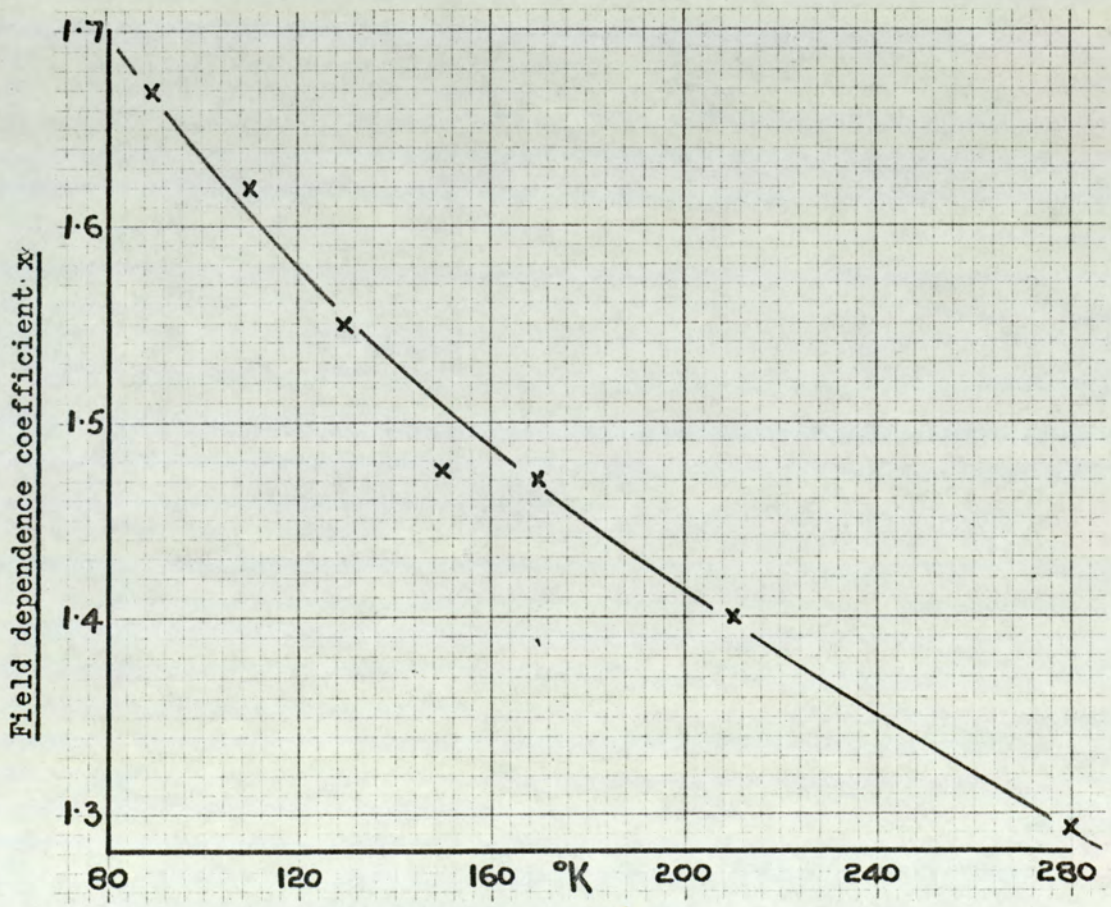

Fig.147. Temperature dependence of the field variation coefficient x for the ribbon specimen.

the variation is linear over the temperature range examined. In order to produce a corrected graph free from the perturbing influence of the changing number of carriers it is necessary to extrapolate the curves of fig. 138 to zero applied magnetic field. It can be shown with some re-arrangement of equation 6.7 for two sets of experimental values that the zero field Hall coefficient for bulk material is given by:

$$\underset{H\to 0}{R_H} = \frac{F(\mu)}{N} = \frac{R_1R_2(H_1^x - H_2^x)}{R_1H_1^x - R_2H_2^x} \quad \ldots . \quad (6.10)$$

where the coefficient x appropriate to the experimental temperature is taken from fig. 147. The corrected curve can be seen in fig. 138 in which the maxima in the curves was observed to be far less pronounced than a simple experiment would have indicated.

The response of R_H to a varying magnetic field is entirely different in the case of bismuth thin films. The prime feature is the rapid fall of R_H at low applied fields resulting in a value of $\partial R_H/\partial H$ which is of positive sign. Fig. 148 shows the variation of the Hall coefficient with magnetic field for a typical 'field variation' run taken from fig. 122 on a film of 744 ^{o}A. Again the true modulus effect is observed in that the profile is similar for either sign of R_H. The curves indicate a complete saturation of the Hall coefficient at fields above 5 Kilogauss and a fall to zero at zero magnetic field. Fig. 149 taken from fig. 125 at 927 ^{o}A confirmed the 'foregoing statements. The readings at 190 ^{o}K were undertaken at a larger number of magnetic fields and, as errors in field measurement are less significant in the saturation region the slight modulation of the line may arise from the Schubnikov-de Haas effect. In the

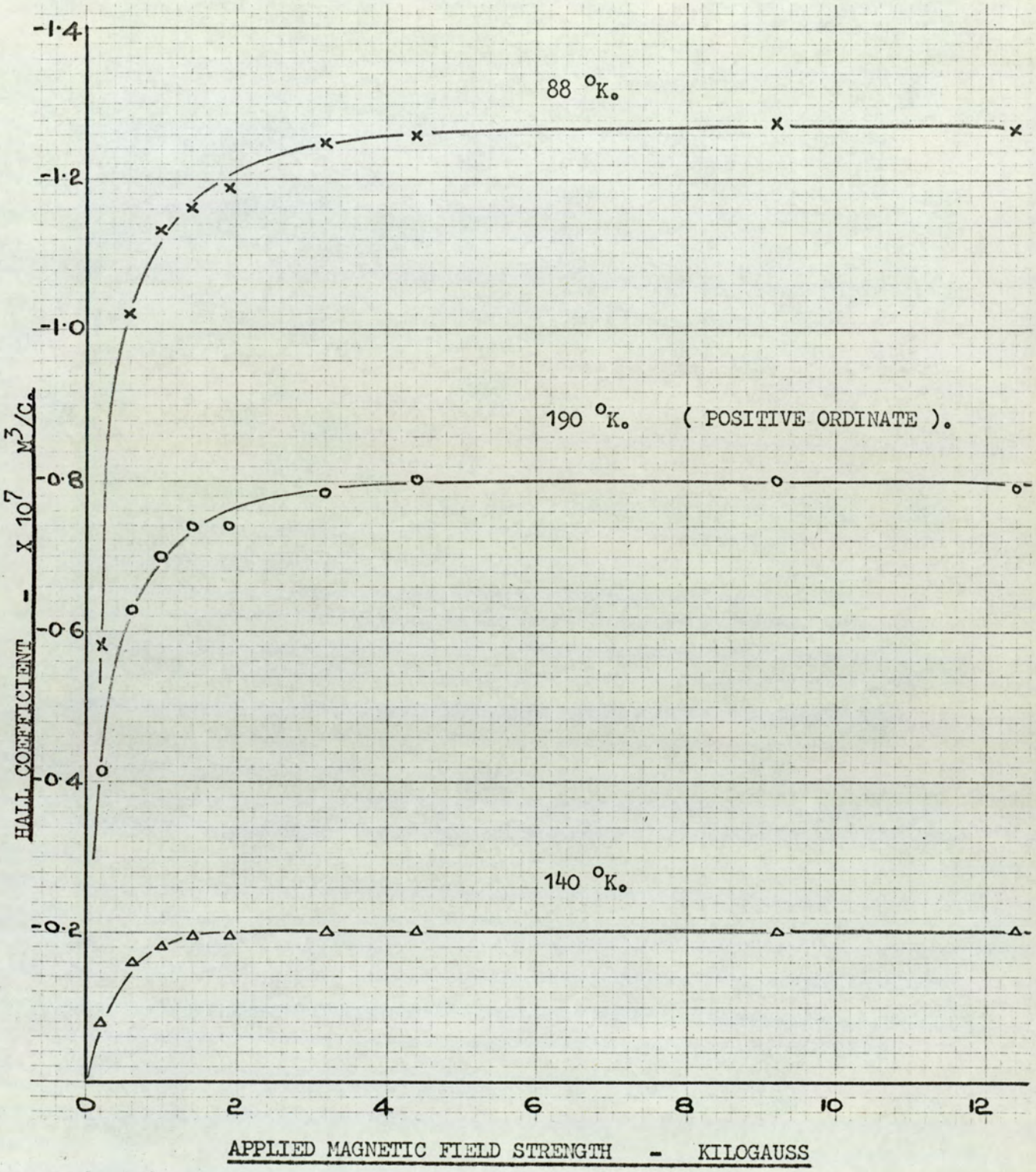

Fig. 148. The variation of the Hall coefficient with magnetic field at a selection of temperatures for a bismuth film of 744 Å.

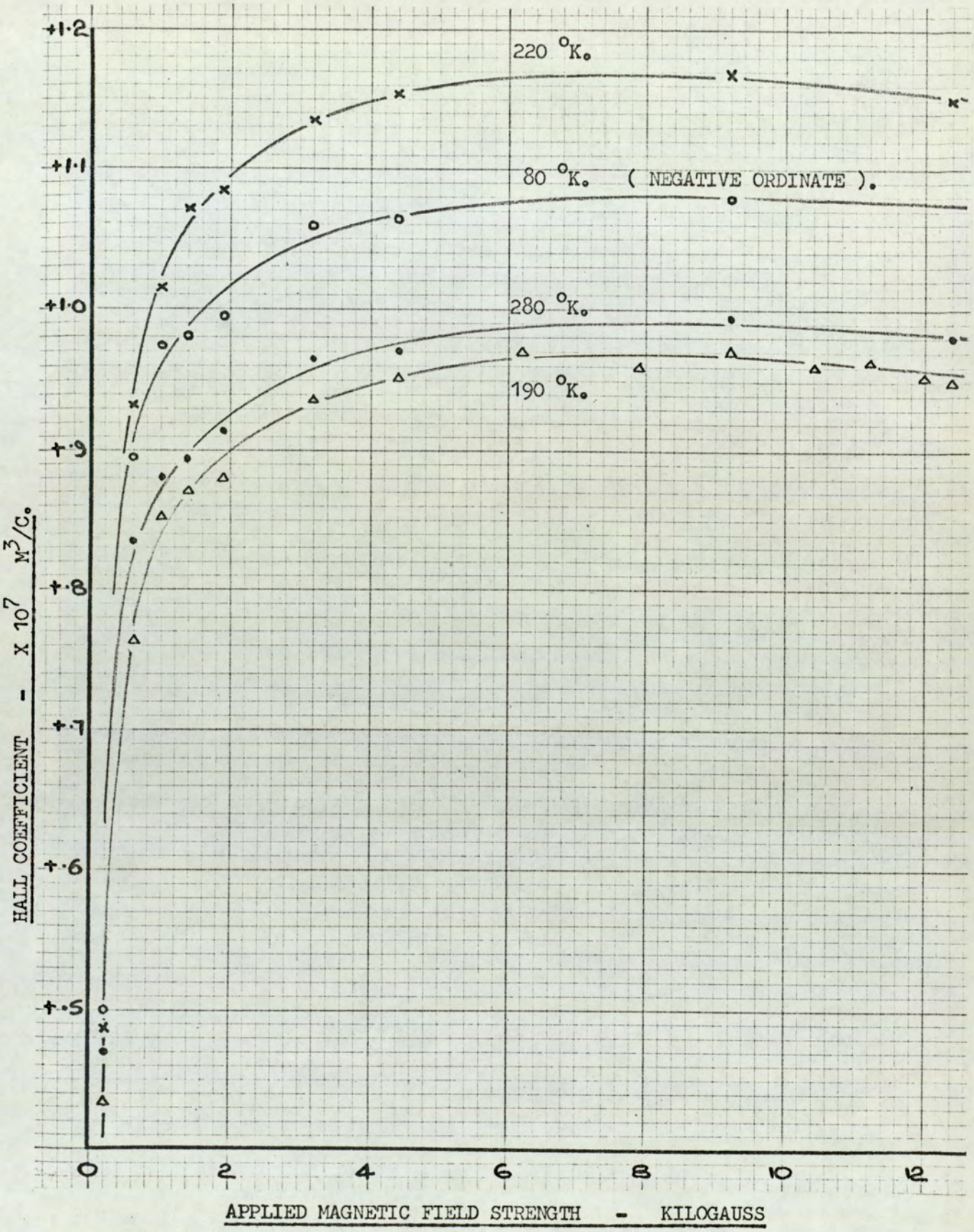

Fig. 149. The field variation of the Hall coefficient at a selection of temperatures for a bismuth film of 927 Å.

region of size quantisation, the energy levels in bismuth are quite discrete. Duggal [4] analysed the oscillatory behaviour of R_H in a magnetic field and found it to be periodic in higher values of H, as would be the case of Schubnikov-de Haas oscillations. It is notable that such effects which are usually associated with observations at liquid helium temperature may be studied at much higher temperatures by the use of semi-metal films.

The above features were observed for all films and led to an analysis to evaluate the coefficient x similar to that performed on the ribbon specimen. Figure 150 represents a typical analysis at 927 Å in which the power dependence was evaluated to be -0.55. A similar value of -0.52 was obtained at 4500 Å (fig. 151) although at these thicker films the saturation appeared to be incomplete. The points marked by a circle lay on the line generated by assuming a nominal power of $x = -\frac{1}{2}$ and it can be seen that the degree of correlation was high. For the thinner films, where there was a definite saturation the generated curve continued to increase with field. A value some 10 - 15% higher than the value obtained at 12.5 Kilogauss was reached asymptotically. In the solution of the equations to evaluate the number of carriers, the difference is not important in that the results were fairly insensitive to the value of the Hall coefficient. The main significance in the change of sign of the power dependence is that in order to remove the perturbing term, ΔN, the extrapolation must be produced to infinite magnetic field.

The exact significance of the fall to zero Hall coefficient at low magnetic fields is not fully understood. In the region of the saturated coefficient the value of the Hall voltage was directly proportional to the applied magnetic field strength for medium and high fields. The response of the Hall

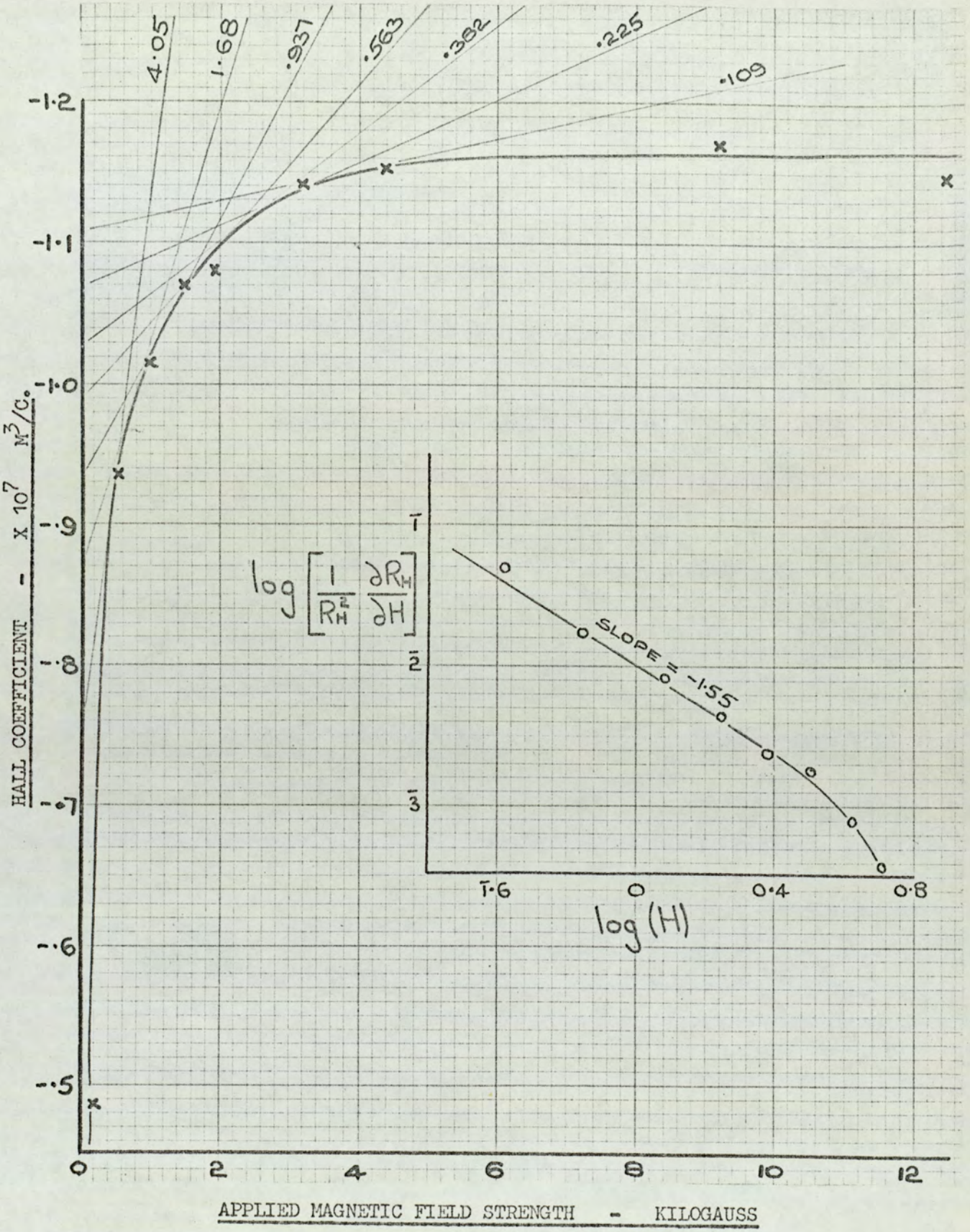

Fig. 150. Field variation of the Hall coefficient at 220 °K for a bismuth film of 927 Å. The inset shows a field variation analysis.

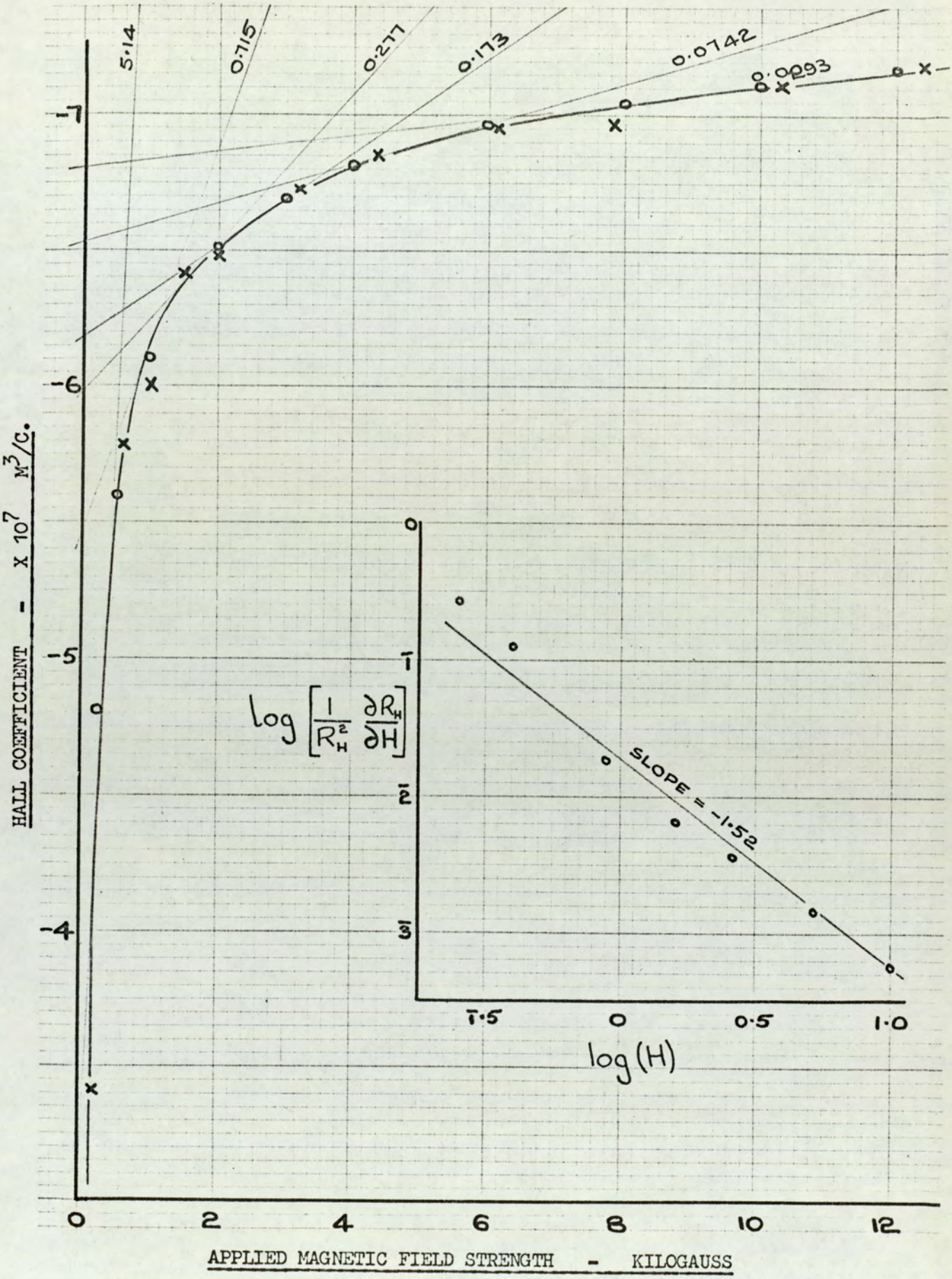

Fig. 151. Field variation of the Hall coefficient at 80 °K for a bismuth film of 4500 Å. The inset shows a field variation analysis.

coefficient to the applied field, as mentioned earlier, was such that it may be quantitatively attributed to a change in the number of carriers, the purpose of the present analysis being to eliminate this variable. It would be equally true to say however that in the thin film region the deflection of the carriers caused by the application of an external magnetic field was less than would be anticipated from the Lorentz equation i.e. a smaller Hall voltage was developed. The effect of surface scattering could contribute to this effect rather as a damping term, whose magnitude at a given temperature was not dependent on the applied field strength. At higher fields the larger value of the Hall voltage would cause this surface scattering effect to be less marked. An attempt to apply this rather idealised picture of a constant additive term to each individual Hall voltage giving rise to fig. 150 gave an interesting result. Modifying the equations of section 4.7 to read,

$$R_H = (V + \upsilon)\, Z_2$$

and by solving simultaneously for pairs of values of V and Z_2 a table was constructed showing the correction quantity, υ, and the corresponding coefficient R_H. (Each experimental point was paired in turn with the value at 4.4 Kilogauss).

Table 10. Corrected Hall coefficients

Magnetic field paired with 4.4 Kg.	υ (μV)	$R_H \times 10^7$
.22	16.6	1.189
.56	15.1	1.186
1.02	19.6	1.195
1.49	19.9	1.196
1.95	19.9	1.196
3.20	13.9	1.183
9.2	17.3	1.190

The degree of stability of the recalculated R_H values over the wide range of magnetic fields is readily seen. The additive voltage of around 18 μV could not possibly have arisen from experimental error, as confirmed by an appreciation of the zero point consistancy.

The results taken on the bulk specimen, fig. 139, are of interest in that the power dependence of ΔN was observed to change from +3/2 at temperatures above 200 ^{o}K to a distinct negative value at 80^{o}K. The transition at the lower temperatures was supposedly incomplete in that no quantitative analysis was possible. It could be that increased boundary scattering in the presence of a magnetic field contributed significantly to the change in dependence, even though the bulk resistivity results of fig. 80 do not show a size effect. The observation is of particular importance in that it dismisses the possibility of the negative sign of the power dependence in thin films being primarily due to crystallographic orientation, since the bulk specimen was randomly polycrystalline.

The direct comparison of the field dependence of R_H in the present analysis with results appearing in the literature is not ideal. Few authors have taken observations at fields below 2 Kilogauss, yet several have continued to 35 Kilogauss. Duggal[4] in an attempt to observe Schubnikov - de Haas oscillations in bismuth films produced curves whose monotonic portion showed an invariant value of R_H from 2 - 6 Kg. as in the present work, but did not refer specifically to the reduced values observable at his lower field of 1.5 Kg. In contrast, two reports by Colombani and Huet [9,109] show a field dependence above 5 Kg. in which the Hall coefficient falls steadily with increase in field strength (fig. 15 (ii).

The field dependence of the present polycrystalline bulk specimens was identical to that produced by Gitsu and Ivanov[39] for single crystals in which a curve similar to fig.145 was shown to hold up to 20 Kilogauss. The variation observed by Gitsu between two differing crystallographic axes was only slight.

In summary therefore it can be said that the thin film values of Hall coefficient against temperature at 12.5 Kilogauss result in a series of curves which are mutually consistant, in that additional variations caused by the magnetic field have been eliminated. As with the resistivity results the degree of consistancy between the films was indicated by comparison of the results at 735 Å and 744 Å. At all fields the correlation was high.

The discussion of the thin films results will be introduced by reference to the widely accepted Hall values on bulk single crystals of Abeles and Meiboom [28]. Table 11 shows their values for two crystallographic orientations at both 80°K and 300°K.

Table 11. Hall coefficient of bulk bismuth.

Temp.	$R_{\perp}$ x 10^7 MKS	$R_{\parallel}$ x 10^7 MKS
80°K	- 83.7	2.7
300°K	- 13.5	0.45

It can be readily appreciated from Table 11 that the value of the Hall coefficient of a randomly orientated bulk polycrystalline specimen would be dominated by the large negative value of the coefficient with the field perpendicular to the

trigonal axis. To a first approximation the experimental Hall coefficient will be given by:

$$R_H = \frac{1}{3}\left[2R_{\perp} + R_{11}\right] \quad \text{.....(6.11)}$$

Such a combination of values would result in a curve of Hall coefficient against temperature which would become rapidly more negative with decrease in temperature, indeed a curve whose profile is similar to that of the bulk polycrystalline specimen shown in fig.139.

From this bulk picture and a knowledge of the structure of thin bismuth films the monotonic change in R_H with thickness readily follows. It has been shown that a proportion of the high degree of preferred crystallite orientation occuring in the thinnest films is lost as the film thickness is increased. In considering the increasing orientation of successively thinner films, the decreased contribution to the measured coefficient of the large Hall component perpendicular to the trigonal axis caused the curve to become more positive. At a thickness of 4500 Å the displacement was such that the line was astride the abscissa. Further displacement by reduction in thickness caused the Hall coefficient at around 800 Å to be almost completely of positive sign. The effect of grain boundry scattering on the Hall coefficient of thin metal films is not always of extreme importance as discussed by Chopra and Bahl[51]. Under an equilibrium Hall field additional deflection of the carriers is suppressed. In a two carrier semi-metal system however, the bipolar flow of current even in the equilibrium state, means that additional scattering occurs at all times. The Hall voltage required to overcome the Lorentz force is thus reduced and in the thin film limit a reduction in the absolute value of

the Hall coefficient arises. The monotonic picture of the thickness dependence of R_H in thin bismuth films is thus on in which a reduction in thickness causes a gradual shift of the polycrystalline curve towards and across the abscissa. Further reduction in thickness however results in a decrease in the modulus of the Hall coefficient, and a return of the curve towards the abscissa. Dismissing in this section reference to quantum size effects, the above mentioned displacement and flattening of the Hall curves for a range of film thicknesses may be observed in fig. 140. The 'U' shape of the plot of Hall coefficient against thickness at 280°K taken from fig. 140 would in fact be identical to that produced by Colombani and Huet (109) (Fig. 16 ii) in which the curve crossed the abscissa at about 7000 Å. The tabulated result by Harris (45) shown in fig. 14(iv) agreed with this figure. Duggal (32) however observed that films grown epitaxially onto hot mica substrates did not revert to a negative sign even at 3μ due to a combination of high orientation and enlarged grains, as indicated in fig. 14(ii). The appearance of a mimima in the curves of the present work was in itself an indication of the high degree of preferred orientation. Over a range of temperatures the small positive coefficient with the field parallel to the trigonal axis was sufficient to mask the steeply increasing negative component.

The extensive analysis by Kioke (33) which gave detailed insight into resistivity and temperature coefficient of resistivity values at 300 °K further observed the Hall coefficient at 10 Kilogauss and found it to lie between 0.3 and 0.8 x 10^{-7} M^3/C as in fig.14(iii). At 7000 Å the coefficient became positive. It is notable in the literature that the diversity of published values of the Hall coefficient at 300 °K for bismuth films in the range 200 - 2000 Å rarely falls outside this small range. Jeppenson (110) for

example tabulated the variation from 200 - 1500 Å to be from $0.6 - 0.8 \times 10^{-7}$ M^3/C, in further agreement with the present work. Even the recrystallisation of bismuth films from the liquid phase as performed by Clawson [53] did not alter the Hall coefficient at 300°K, but the value became quite strongly positive at all temperatures, as shown in fig. 18. Arguements based on the increased preferred orientation due to recrystallisation, along the lines discussed above, would account for the behaviour observed by Clawson. (Clawson has incorrectly quoted the values of Abeles and Meiboom, those of Table 11 are correct).

The variation in sign of R_H caused by the presence of tetravalent impurities as outlined by Suzuki [42] (section 1.4.4.) was not considered to be responsible for the thickness dependent behaviour of the present investigation. It is felt that the effect of impurities would be such that a spread would arise at the temperatures at which the zero Hall voltage occurred, a feature which is not the case here. Furthermore, the specimens examined in the present work were all prepared from one batch of bismuth.

To summarise therefore it can be said that the value of the Hall coefficient in bismuth films was dependent on the strength of the applied magnetic field due to an effective increase in the number of carriers. The quantitative variation for bulk material and for thin films differ, but it was possible to eliminate the perturbing term. The variation of the Hall coefficient with thickness over a range of temperatures has been discussed in terms of the degree of preferred orientation and the crystallite size. Though only a monotonic variation of R_H has been indicated, a quantum size effect will later be shown to exist.

6.5. Magnetoresistance

It was suggested in the previous section that the small

effective number of carriers in bismuth gave rise to a Hall effect which was quite readily measurable. It further follows that the large mobilities of both the electrons and holes result in a magnetoresistance coefficient for bulk material which is again of a convenient magnitude for experimental investigations. Indeed, as reviewed by Fawcett [111], the abnormally high values of the magnetoresistance quoted by Kapitza are a direct significance of the low effective masses of the carriers and a long relaxation time. For an effective mass, m^*, of around 0.01 m, and in a field of a few kilogauss, the cyclotron radius in bismuth is of the order of 1000 $\mathring{A}$. It is likely, therfore, that the effect of grain boundary scattering would be of great importance.

The presence of a magnetoresistance effect in bulk material is not observed in many metals, as mentioned in chapter 2. For a single carrier system the equilibrium Hall field opposes the modification of the carrier paths with a result that no magnetoresistance is observed. In a two carrier system, however, the Hall field is unable to counteract the transverse flow of carriers. The bipolar flow results in additional scattering with subsequent increase in resistivity.

For an isotropic single crystal it was shown that the value of the magnetoresistance coefficient, B, obeyed an inverse square law relationship to the magnetic field,

$$B = \frac{\Delta\rho/\rho}{H^2} \qquad \ldots\ldots\ldots\ldots (6.12)$$

The high anisotropy in bismuth however must be considered a little more closely. Kapitza [34] studied the magnetoresistance coefficient in bismuth for various crystallographic orientations, principally with the magnetic field parallel and perpendicular to the trigonal axis and found the magnitude to be directional. The quadratic power dependence on the magnetic field was however observed

to be invariant. The observation was confirmed by Gitsu and Ivanov[39] who showed that the value of the coefficient with the magnetic field parallel to the trigonal axis exceeded those of the orthoganal case by some 40%, as shown in figure 10(ii). Kapitza's early work on a needle-like matrix of bismuth crystals grown by evaporation showed that the power law was considerably reduced in such specimens due to imperfections at the needle boundaries. In addition Ziman [112] has calculated that for bulk polycrystalline bismuth the power takes on a reduced value, possibly even approaching unity, because of the effect of the grain boundaries on the cyclotron orbits.

A perburbation of the trajectory taken by the carriers in the absence of a magnetic field must of necessity give rise to enhanced resistivity. The magnitude of the increased resistivity depends not only on the extent of the perturbation but on the basic length of the unperturbed free path. The longer this undistrubed path, the more severe will be the effect of the magnetic field. It is along these arguments that the large increase in magnetoresistance with reduction in temperature is explained. An increased magnetoresistance arises from either an increase in the zero field free path or a decrease in cyclotron radius.

The graph of the magnetoresistance ratio against temperature for the present bulk polycrystalline specimen is shown in figure 81, in which the exponential type of growth with reduction in temperature, and the response to the applied field, can be readily seen. At all fields a reduction in temperature from 280°K to 80°K increased the magnetoresistance ratio by a factor of 10^2. A log-log plot of the ratio against applied magnetic field for the bulk specimen is shown in figure 152, confirming a power law relationship. Because of the polycrystalline nature of the specimen the average value of the power was found to be 1.48 and was consistently held for the entire range

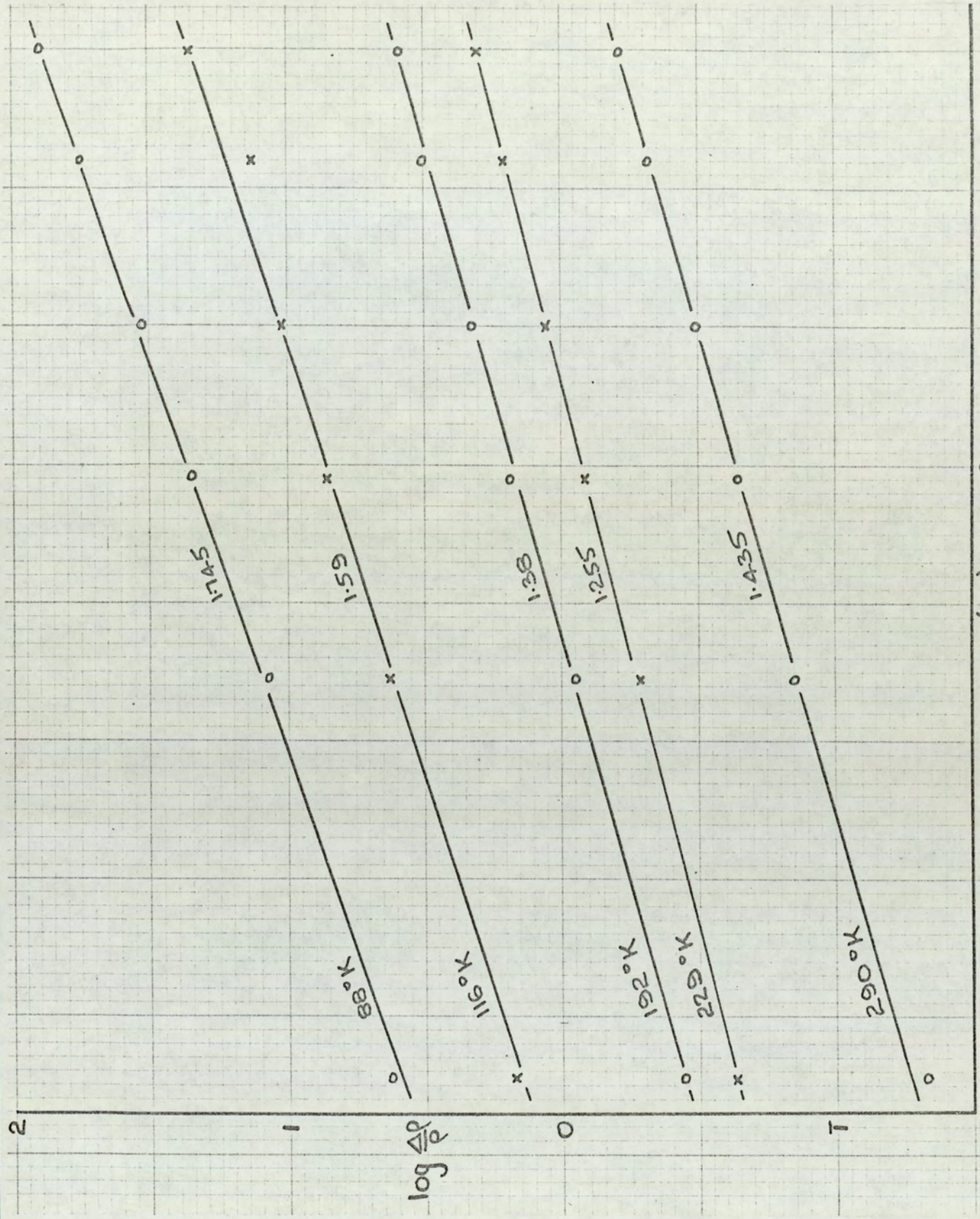

Fig. 152 Logarithmic plot of the Magnetoresistance ratio against applied magnetic field.

of temperatures and magnetic fields employed in the investigation. It is interesting to note though that the single crystal values of Abeles and Meiboom (see table 12) indicated a ratio of $\Delta\rho/\rho$ at 10 Kilogauss of 80 and 0.27 at 77°K and 290°K respectively. Superimposing these values on figure 81 indicate that the single crystal values are retained in the present polycrystalline specimen even though a change has occurred in the field dependence.

A lower magnetoresistance ratio occurred in measurements taken on the ribbon specimen, as in figure 82, though the exponential type of increase with reduction in temperature was still observed. A logarithmic plot of $\Delta\rho/\rho$ against applied field is given in figure 153 indicating a consistant power gradient of 1.42 over the entire range, in contrast to single crystal measurements of, for example, Friedman and Koenig (17), in which the quadratic dependence was always observed. In including these bulk values in the present investigation it must be noted that the magnetoresistance coefficient defined consistantly with the derivations of chapter 2 may only be used in the presence of a quadratic dependence.

The investigation of the magnetoresistance effect on the thin films of the present investigation required careful attention since the magnitude of the effect was extremely small. A reduction of around three orders of magnitude accompanied the change from bulk material to the thickest of the films investigated. At 4500 Å the degree by which the magnetoresistance ratio increased at the lower temperatures had subsided to the extent that the second order differential of the curve took on a negative value. The curve is shown in figure 83. The qualitative explanation for such a trend arises from the limitations imposed by the grain boundaries on the zero field mean free path, and will be discussed with reference to figure 154. The representation is highly simplified but contains

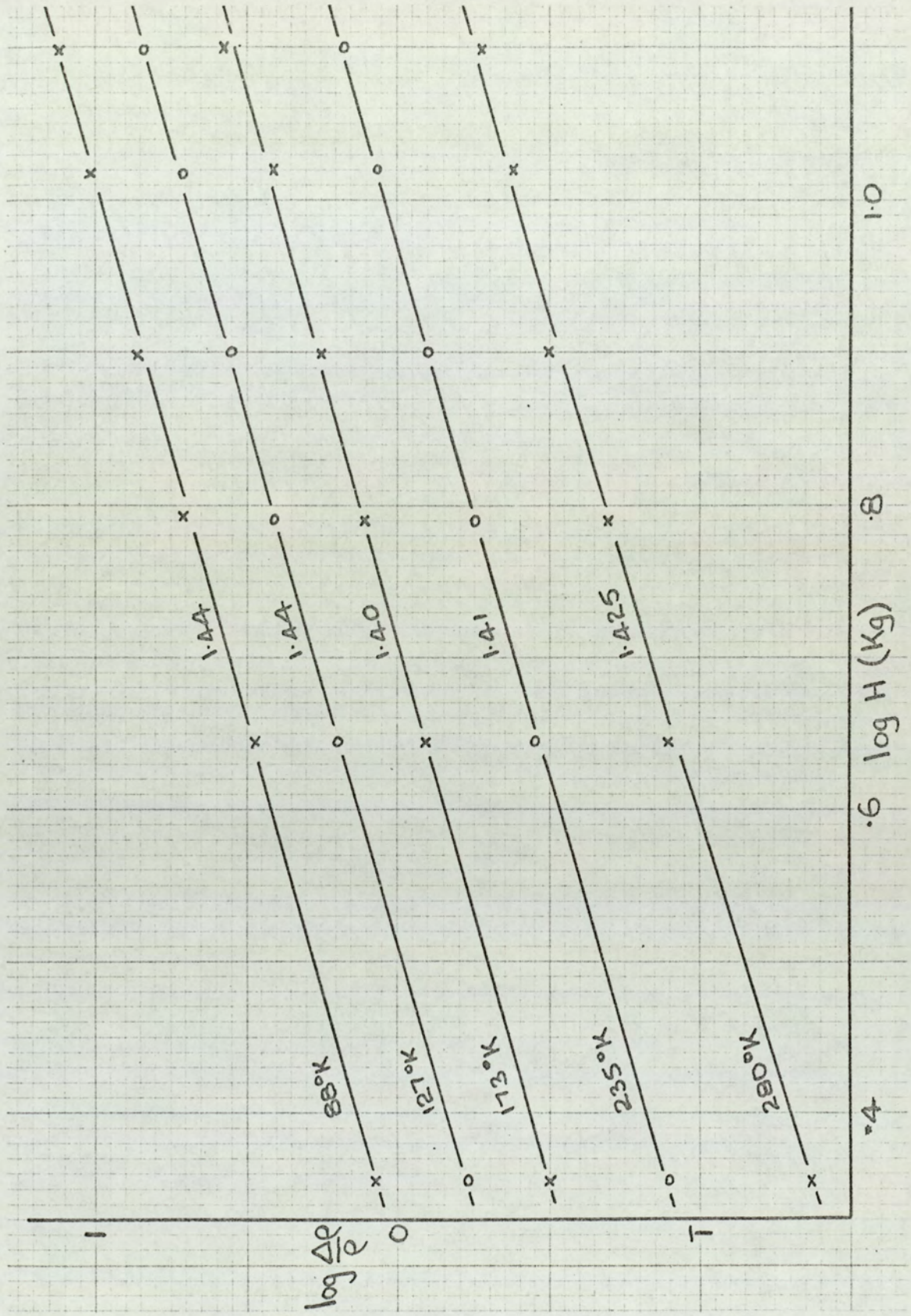

Fig. 153 Logarithmic plot of the Magnetoresistance ratio against applied magnetic field for the ribbon specimen.

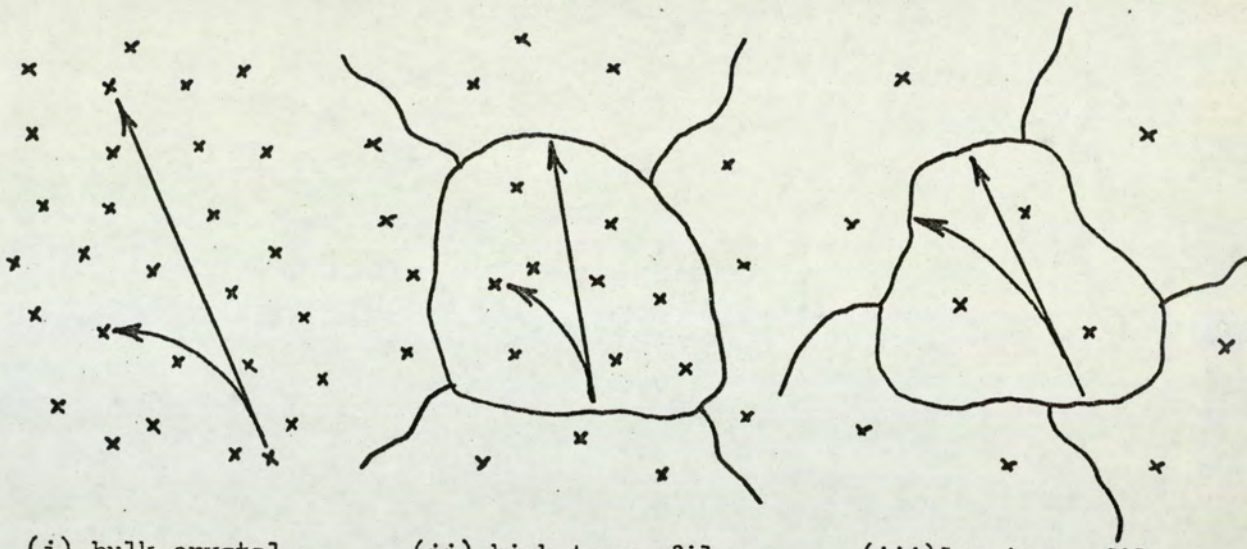

(i) bulk crystal. (ii) high temp. film. (iii) low temp. film.

$\Delta\rho/\rho$ large. $\Delta\rho/\rho$ small. $\Delta\rho/\rho \to 0$

Fig.154. Temperature and grain size variation of the magnetoresistance.

the salient features for a qualitative picture to be appreciated. As was concluded from the resistivity observations, the carrier paths are prematurely truncated by the grain boundaries, and corresponds to (i) and (ii). It is seen that a fall in the measured ratio would occur resulting mainly from the finite limit placed on the zero-field mean free paths. As grain size has a direct bearing in the above argument a thickness dependence of the magnetoresistance in the thin limit readily follows. A significant increase in the number of film surface boundary collisions is unlikely since the carriers bearing the bulk of the current are those whose trajectories are in the plane of the film. The orthogonally applied magnetic field will result in a deflection only within this plane.

Figure 84 shows the results taken at 2045 Å in which a maximum was observed in the magnetoresistance ratio curves at the lower temperatures. The effect of a further reduction in thickness can be followed through in figures 85 - 87. At 309 Å the curve was such that the boundary supression occurred at all temperatures. The magnitude of the effect at these thinner films was only $1 - 3 \times 10^{3}$, indicating that despite the large applied field, the

grain boundary collisions were predominant. Figure 154 (iii) illustrates that at low temperatures, in the presence of sparsely distributed scattering centres, the path length of the carriers is insensitive to the applied field. A magnetoresistance ratio approaching zero thus arises.

Observations of the magnetoresistance of bismuth films are not uncommon in the literature although few authors proceed to quote a coefficient. The effect of subsequent heat treatment of films is expected to produce a marked variation in the magnetoresistance effect due to the increase in the zero field mean free path. Kao's[2] observations on thick specimens indicated an order of magnitude fall in the effect below 2 - 3 μ whereas Lane [100] indicated a linear fall in value at thicknesses less than about 0.5 μ. The present results are in agreement with those of Ogrin[3] whose thin films displayed a similar grain size. The larger grains associated with sputtered films give rise to an increased magnetoresistance as observed in an alternative paper by Ogrin [113], and are similar to both the recrystallised films reported by Colombani and Huet[114] and to the single crystal films of Duggal and Rup[4]. The true effect of annealing of films is shown in figure 18, reporting the observations of Clawson [53] on films of 5 - 6000 $\mathring{A}$. A comparison of the 'as evaporated' results of figure 18 with those of the 4500 $\mathring{A}$ film of figure 83 shows a high degree of correlation. The anneal was observed to increase the magnetoresistance ratio by 1 - 2 orders of magnitude but probably more important was the strict adherence to the quadratic power law.

The quadratic power law observed by Clawson will be shown to hold for the films of the present investigation although the analysis had to be approached with some caution. Assuming for a moment that the power may be retained as a variable, equation 6.12

may be expressed as:

$$\log\left(\Delta\rho/\rho\right) = \log B + \quad x \log H \ldots\ldots\ldots (6.13)$$

A graphical plot to determine the power, x , will only be valid in the presence of an invariant coefficient, B. Figures 155, 156 and 157 illustrate the plot at a selection of temperatures for three films of differing thicknesses. Within the limits of experimental error the slope of the line equalled 2 from which the coefficient, B, could be evaluated using equation 6.12. The coefficient was not, however, constant as illustrated, for example in the corresponding B curves 110, 105 and 99. From a consideration of the relative magnitude of terms it can be demonstrated that the analysis is insensitive to variations in B of about 20%. It is concluded therefore that the magnetoresistance ratio is proportional to the square of the applied magnetic field, but that the coefficient is sensitive to the magnitude of the applied field.

As with the Hall coefficients a trend existed in all 'field variation' graphs towards a lower magnetoresistance coefficient at the lower magnetic fields. The phenomenon does tend to appear more pronounced at lower temperatures, as for example in figure 104, suggesting that the origin is associated with the boundary collisions of the carriers. It will be recalled that the Hall effect was discussed with reference to a variation in the number of carriers with magnetic field. For thin films the effective number of carriers increased as the field was reduced. As a consequence of the variation the question arises as its effect on the magnetoresistance ratio. Strictly the resistivities in the two modes of magnetic field should be compared only in the presence of equal numbers of carriers. The true analysis is complex in the presence of grain boundaries, but qualitatively would account for the

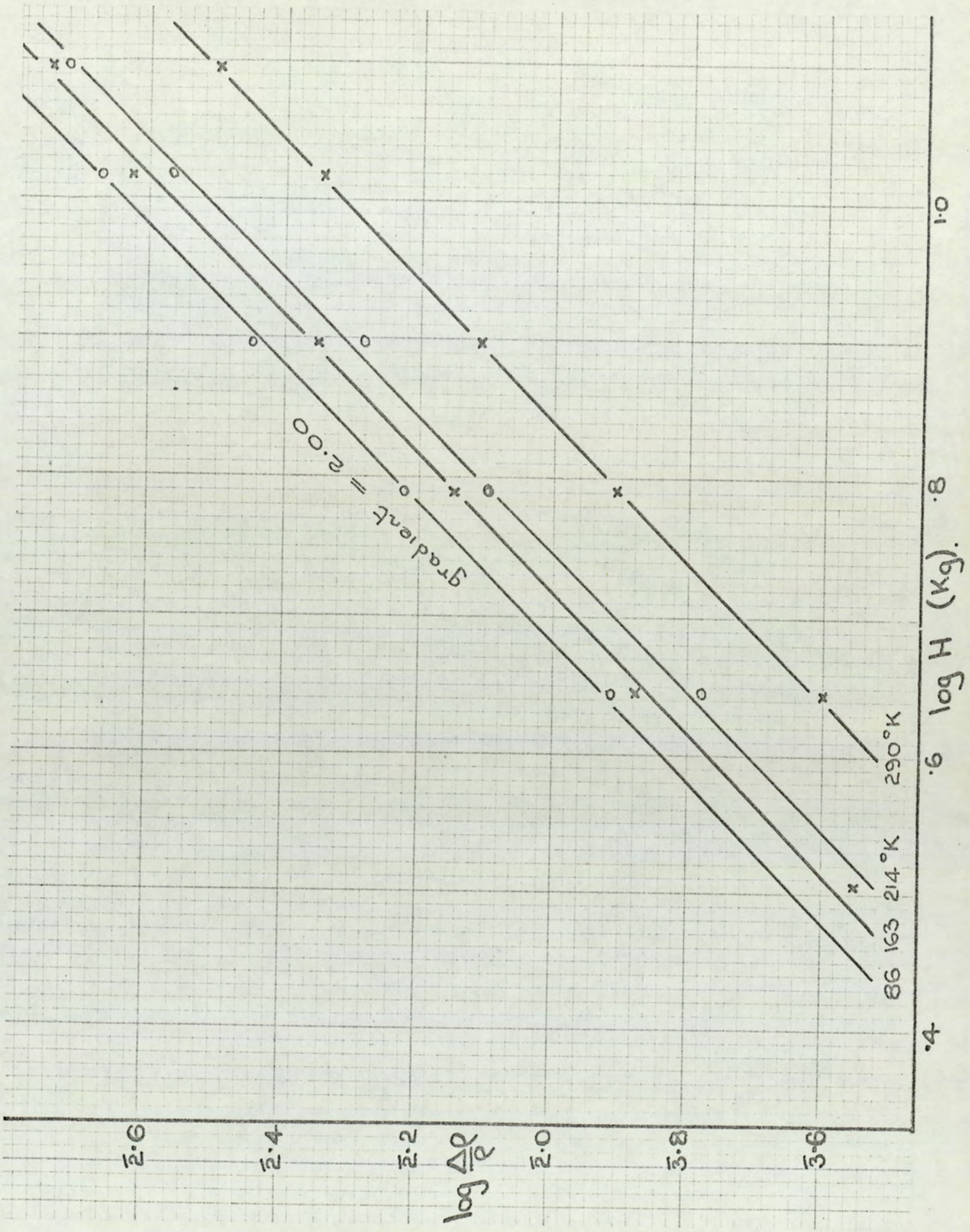

Fig. 155. Logarithmic plot of the Magnetoresistance ratio against applied magnetic field for a film of 4500 Å.

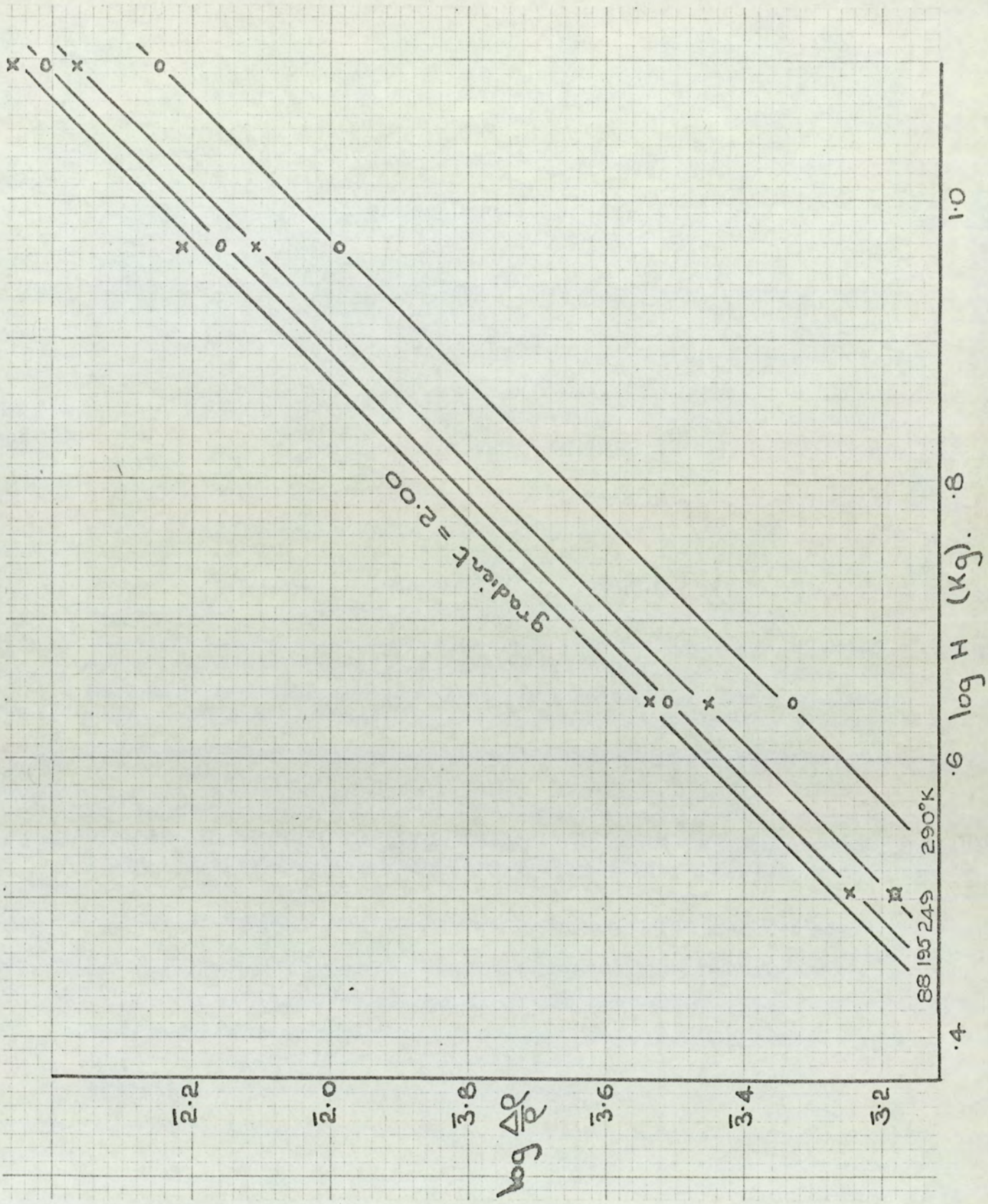

Fig. 156 Logarithmic plot of the Magnetoresistance ratio against applied magnetic field for a film of 1409 Å.

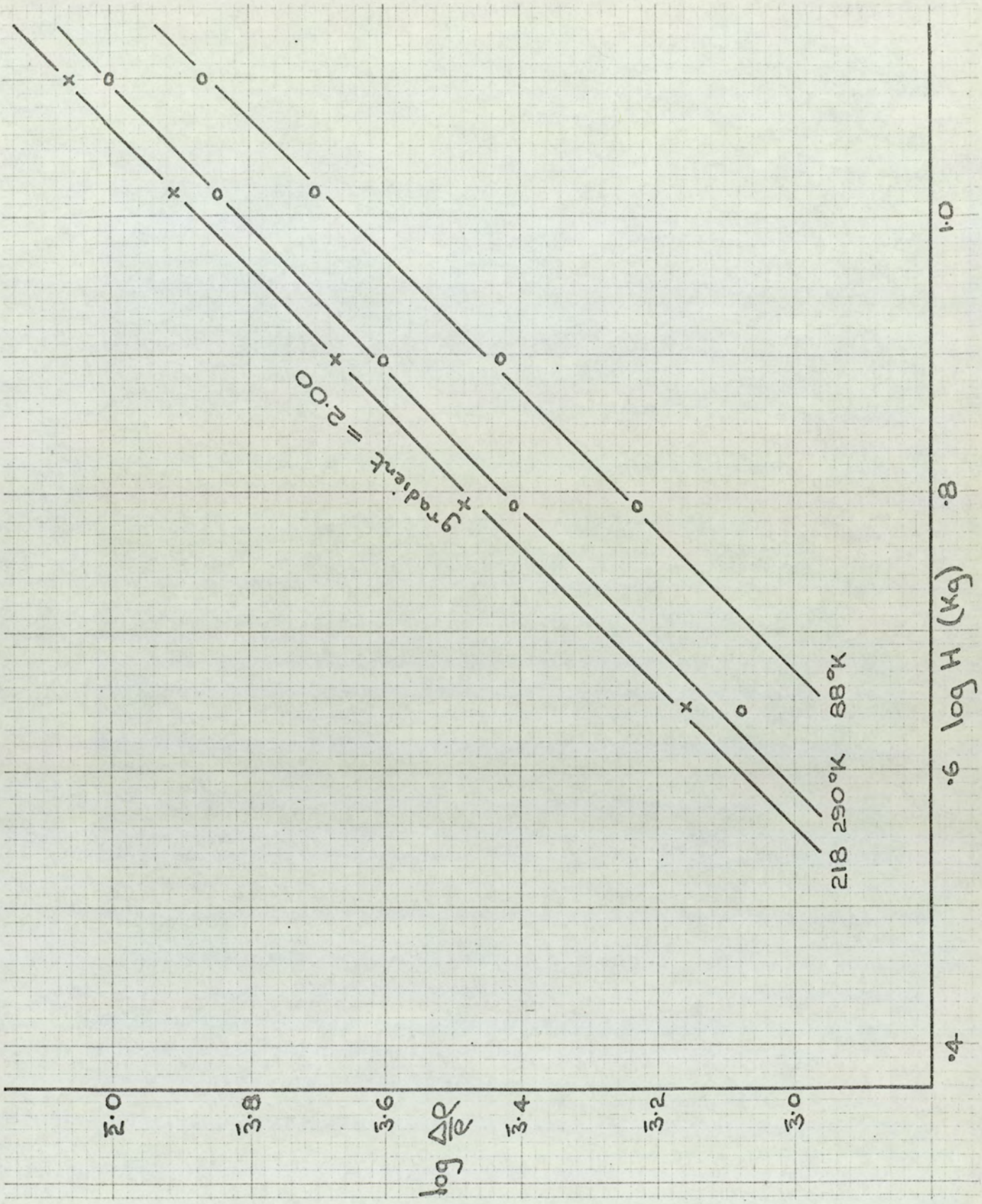

Fig. 157 Logarithmic plot of the Magnetoresistance ratio against applied magnetic field for a film of 862 Å.

apparent reduction in the coefficient B at low fields when calculated by the simple formulae. The essence of the approach is to replace the ratio ρ_H/ρ_o by ρ_H/ρ_o' where ρ_o' is the resistivity corresponding to the increased number of carriers. The simple computing of the former ratio involves division by a denominator which is too large for the appropriate magnetic field, thus supressing B.

Few references in the literature to the magnetoresistance of un-annealed bismuth films make comprehensive comparison difficult. An analysis similar to that of the present work in which results are quoted 'as evaporated' is that of Clawson[53]. Clawson's results are presented in figure 18 for films of 5 - 6000 Å. (The coefficient, B, in units of $(W/M^2)^{-2}$ is numerically equal to the magnetoresistance ratio in a field of 10 Kg.) Recalling the sensitivity of the coefficient to film thickness, and noting the onset of the low temperature supression in the present thickest film, the results of Clawson are a respectable extension of the present results at 4500 Å. The values have been summarised in Table 12.

Table 12. B-values at various thicknesses

Source	Thickness	B x 10^3 $(W/M^2)^{-2}$	
		77°K	290°K
Present	4500 Å	44	20
Clawson(evap)	6000 Å	190	40
Clawson (re-XL)	6000 Å	13,000	190
Abeles and Meiboom	BULK	80,000	270

In conclusion therefore it may be said that the temperature-induced exponential type increase in the magnetoresistance effect present

in the bulk bismuth is not featured in thin films. The change in behaviour arises from the finite limitation placed on the mean free path by the carrier scattering at the grain boundaries. In addition the magnitude of the effect is reduced by some three orders resulting from the fact that, in the presence of only a few scattering centres, the mean free path in a magnetic field cannot significantly differ from the zero field path. The films are observed to display a quadratic dependence on the magnetic field similar to the behaviour of single crystals, a feature which is in contrast to that observed in bulk polycrystalline specimens.

6.6 Simultaneous solution of the coefficients

The derivation of the galvomagnetic and resistivity coefficients in bismuth in terms of the numbers of carriers and the mobilities of the electrons and holes were given in chapter 2. The analysis was performed without introducing the difficulties of anisotropies and of specimens with finite boundaries. To a large extent the complete analysis of the problems of polycrystalline bismuth films would be highly restrictive and probably insoluble. This report shows, however, that from an experimental point of view the perturbation caused by the surface of the specimens and by the grain boundaries is a fundamental parameter governing the properties of films, and leads to the reproducability of physical properties. A film of a given thickness did not display the properties of bulk material but because of a related grain size these properties could be accurately predicted. The results obtained by the simultaneous solution of the coefficients are therefore those parameters which are unique to a particular film in the 'as evaporated' conditions and may be analysed and interpreted in this light.

The three equations of particular interest as derived in chapter 2 are:

$$\rho = \frac{1}{Ne(\mu_h + \mu_e)} \quad \ldots\ldots\ldots\ldots\ldots\ldots (6.14)$$

$$R_H = \frac{1}{Ne} \frac{(\mu_h - \mu_e)}{(\mu_h + \mu_e)} \quad \ldots\ldots\ldots\ldots (6.15)$$

$$B = \mu_h \mu_e \quad \ldots\ldots\ldots\ldots\ldots\ldots (6.16)$$

The variation in the number of carriers with magnetic field occuring in thin bismuth films was such that the equations were mutually consistant with particular regard to N when taken at high magnetic fields. The solutions quoted are thus those obtained from the coefficients at 12.5 Kilogauss. A simple re-arrangement of the coefficient equations enabled the values to be computed, the Algol program for which is given in Appendix III.

Fig. 158 shows the effective number of carriers as a function of temperature for a selection of the thicker films. The semi-conductor-type of rise in carrier density with increase in temperature is observed. The results are compared with the bulk single crystal values of Abeles and Meiboom and the curve of Ivanov[115]. With the exception of the anomolous results at 1100 $\overset{o}{A}$ the reduction in thickness caused a gradual increase in the effective number of carriers but retained a similar temperature dependence. It is noticeable from the presentation of results that, at 77^{o}K for example, the resistivity, magnetoresistance and Hall coefficients were respectively 40 times, 10^{-3} times and 10^{-2} times those of bulk material. Despite these ranging variations the spread in the carrier density was reasonably small. The curve for the present bulk polycrystalline specimen is observed to lie between the single crystal values and the present thick film values. This results from the observation that the Hall and magnetoresistance coefficients are below those of single crystals.

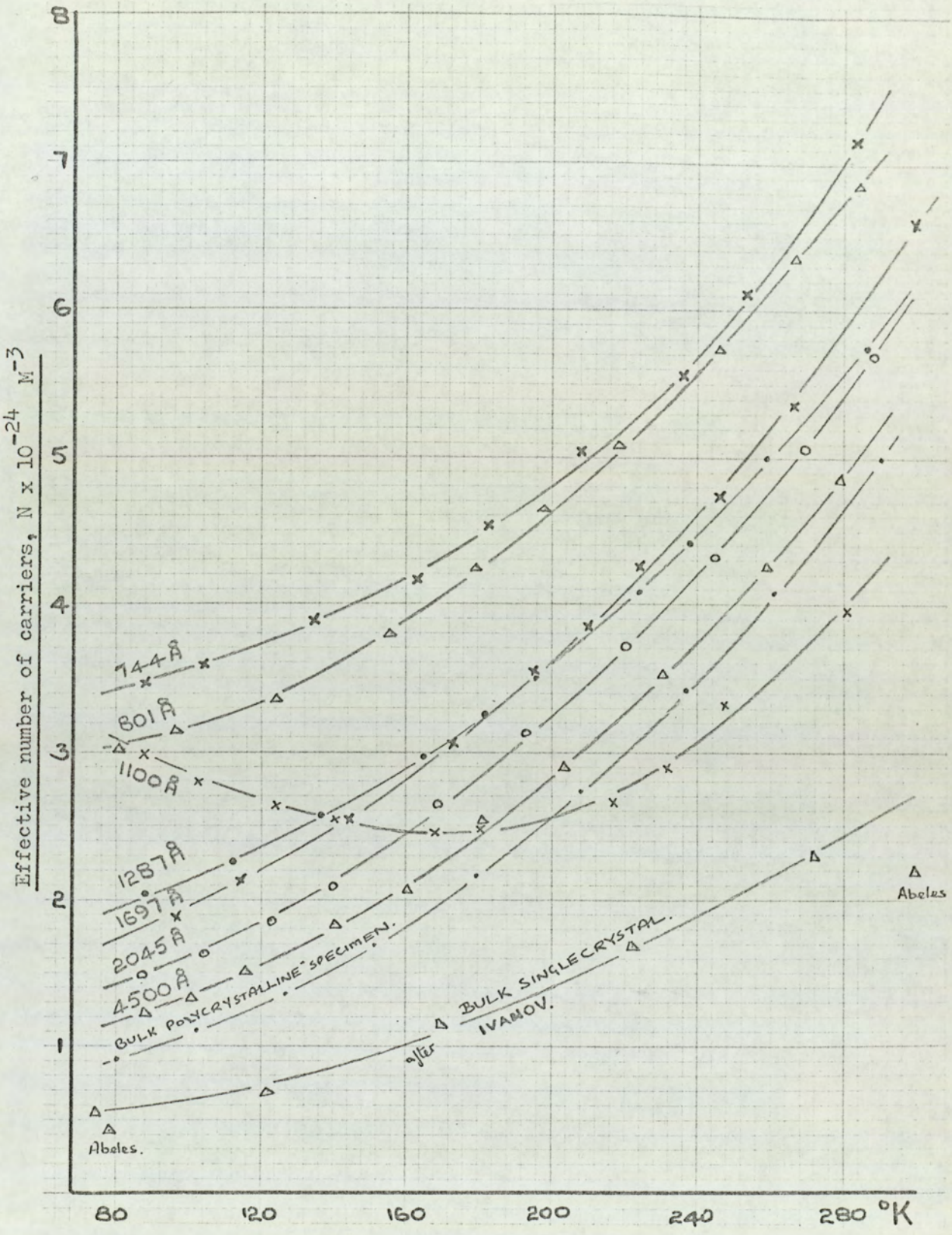

Fig. 158 Effective number of carriers vs. temperature for a selection of bismuth films.

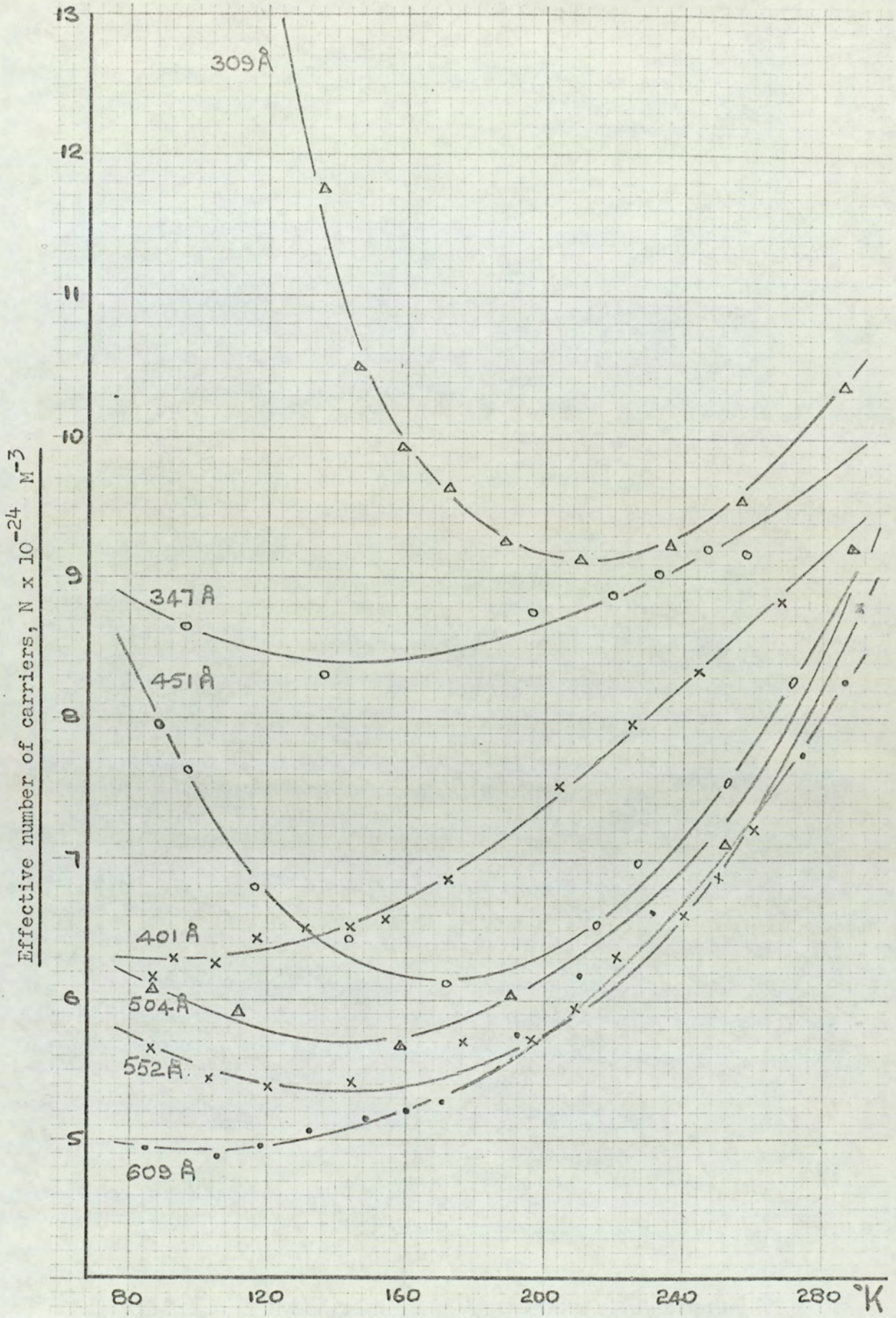

Fig. 159 Effective number of carriers vs. temperature for a selection of bismuth films

The range of thicknesses presented in figure 158 are those for which the structure of the films was more precise, and to which the simple theories were possibly applicable. For the thinner films the effect of the continuum of grain boundary scattering centres especially at low temperatures was considered to be beyond the limitations of the theory. For example, the sensitivity of the solution to the coefficient B meant that the small values obtained for the very thin film low temperature results severely affected the balance of the equations. Figure 159 illustrates the values obtained down to 309 Å from which the effect of the restrictive coefficients can be observed.

The effective mobilities of the carriers resulting from the solution of the coefficient are presented in figure 160. A major reduction in the effective mobilities occured as a result of the previously discussed decreased magnitude of the coefficients in the thin film region. The bulk single crystal results of Abeles and Meiboom are sketched in the upper portion of the graph (in units of the ordinate) and showed the change in mobility on entering the thin film region to be more pronounced for electrons than for holes. The successive decrease in mobility with reduction in thickness, a significance of the decreased magnetoresistance coefficient, can be seen in the curves. The change-over in majority carrier in all film s arises from the corresponding feature in the Hall effect, but the temperature dependence of the mobility is small - films of around 1000 Å display an almost invariant mobility with respect to change in temperature. The separation between the curves becomes successively reduced in the thinner films. Again the variation in mobility over the quoted range of thicknesses is much less than the changes which occur in the corresponding coefficients.

It is not proposed in this report to subject the analysis

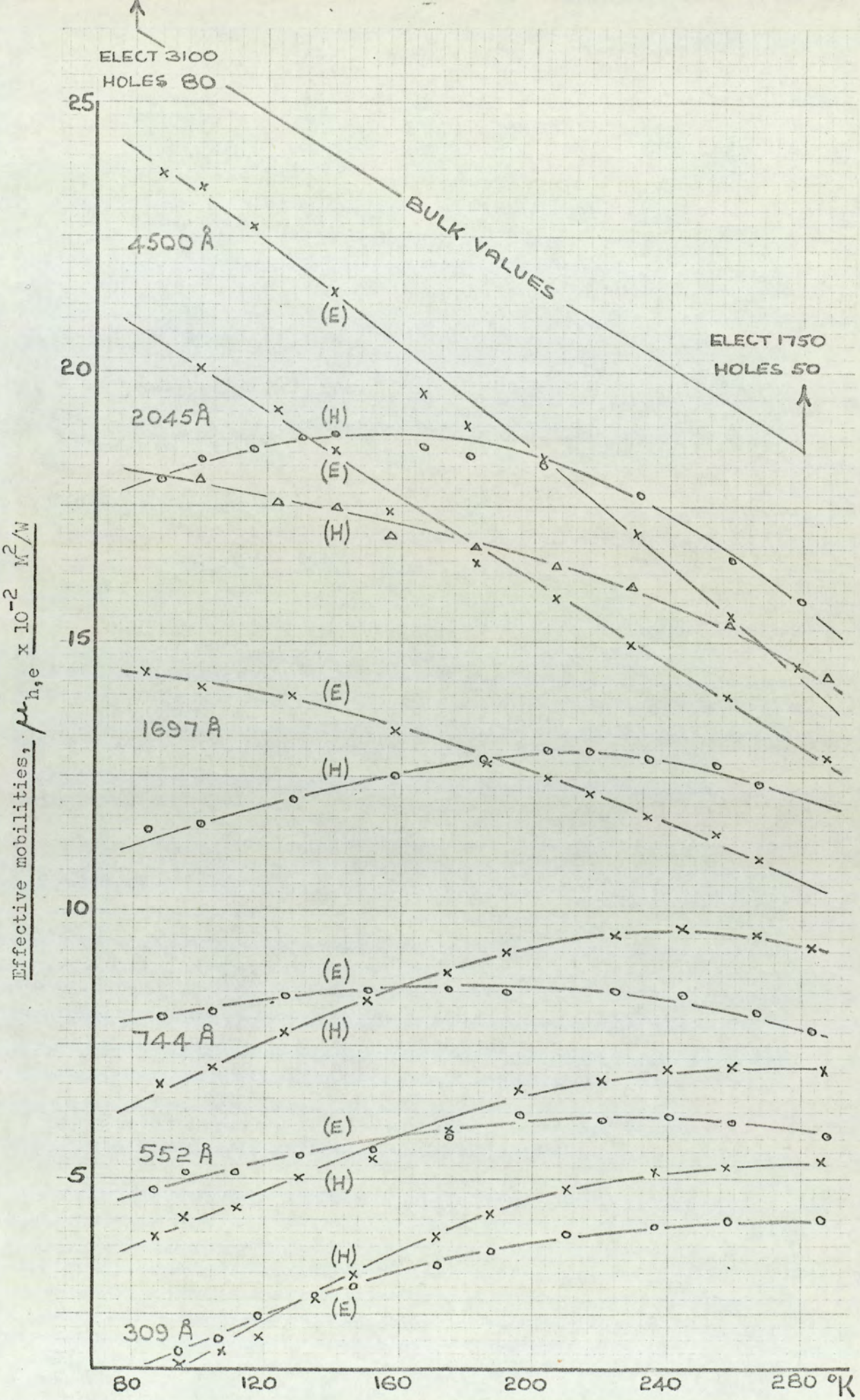

Fig. 160 Effective mobilities of electrons (E) and holes (H) vs temperature for a selection of bismuth films.

to deeper discussion as the derivation and method of solution has introduced a prime example of chicken-egg philosophy. The fall in mobilities with reduction in thickness is coupled directly with the low B-coefficient. The almost equal values of the mobilities in the thinner films are related to the near-zero values of the Hall coefficient explained in terms of bipolar flow. The changeover in majority carrier was attributed earlier to the degree of crystallite order. These arguments are circular and for this reason the earlier sections of chapter 6 have been discussed in terms of physical rather than mathematical reasoning. To use the present section as a basis for discussion would require independent values of N, μ_h or μ_e for thin bismuth films, values which are not available, and indeed which are difficult to obtain by other means in this temperature range.

The present analysis has, however, some justification. In presenting the coefficients ρ, R_H and B we have discussed three properties in reasonably unrelated units, of differing orders of magnitude, each set displaying individual features of special interest. It is only here that they are brought together to be reviewed as a complete picture. Notable is the smoothness, the almost monotonic nature of the change in N from one thickness to the next. It is thus possible to conclude for certainty that the microscopic effects, like the quantum oscillations of the following section, are real, and not, because of their small magnitude, due to experimental error.

6.7. Quantum size effect

6.7.1. Introduction

As discussed in chapter 2 the quantum size effect is defined as the dependence of the electrical properties of solids on their characteristic geometric dimensions. Although theoretically possible to be observed in most materials a limitation is imposed by the inability to prepare a specimen in a suitable state i.e. the required specimen

thickness in metals is below that for which the films become continuous. For the effect to occur the de Broglie wavelength of the carriers must be of the same order as the dimension of the film and thus the low effective mass and long relaxation time of bismuth contribute to the conclusion that it is a reasonable material for investigation. A further requirement, reviewed by Tavger and Demikhovskii [116], was the upper limit placed on the carrier concentration by the finite size of the specimen in order that only a few sub-bands would be populated. (Semi-metal films are known to be highly degenerate). It was shown from dimensional considerations [116] that for one sub-band to be populated the relationship $n \sim 1/d^3$, where d = film thickness, must be satisfied, a further feature for which it is advantageous to use bismuth. Under experimental conditions only a few sub-bands would be populated at 1000 Å, contrary to the behaviour of metals where large numbers would be populated even at 10 Å. Experimental limitations for determining, for example, the film thickness are such that even under ideal conditions a large amplitude and long period of oscillation would probably be needed to confirm the presence of a quantum size effect at all.

Thus the conditions in bismuth would appear to be such that, at least qualitatively, an oscillatory behaviour in the galvomagnetic properties could be attributed to the quantum size effect. It was demonstrated in chapter 2 that the effect of the thin dimension of the film was to split the electron energy spectrum into a series of discrete levels, each having a unique quantum number, n. Due to the lattice vibrations the discrete levels become smeared to form the series of sub-bands and has the effect of rounding the profile of an experimental curve. This does not materially modify the basic reasoning but merely makes the period a little uncertain. An increase in temperature is expected

to gradually mask the amplitude of the oscillation.

6.7.2. Literature review

The quantum size effect essentially arises from the galvomagnetic and resistivity properties, and pre-supposes the high degree of reliability and consistency in the bismuth films. It is for this reason that the review was not included in chapter 1. A selection of the four main experimental contributions from the literature are briefly recalled here.

The curves of Ogrin[113] are presented in figure 161(a). The oscillatory nature of the three measured quantities is readily observed, the effect of increasing temperature being to reduce the amplitude. From the profile of the present curves of resistivity against temperature one could conclude that the simple ratio ρ_T/ρ_{300} is not directly related to the slope of the ρ/T curve. The oscillatory nature of the magnetoresistance curve of Ogrin is marked although the curve for the mobility was derived solely from the one carrier approximation, $\mu = R_H/\rho$. Similarities between the curve of R_H and μ may result in part from the division by a non-oscillatory constant. At all thicknesses the magnetoresistance ratio is shown to be greater at the low temperatures than at 300°K contrary to the present and other investigations. The first maxima occured at 400 Å and the curves displayed a mean period of 400 - 500 Å.

Duggal[52], figure 161 (b), showed R_H to oscillate at 300°K and observed a mild modulation of the resistivity/thickness curve. A period in the resistivity ratio values similar to that of Ogrin was demonstrated but both of the 90°K curves exhibited a peak at 750 Å which was unexplained by Duggal.

Results bearing great similarity to the present work are presented in figure 161(c) as reproduced from a later paper by Ogrin[3] in which the rather unusual nature of the magnetoresistance curve at

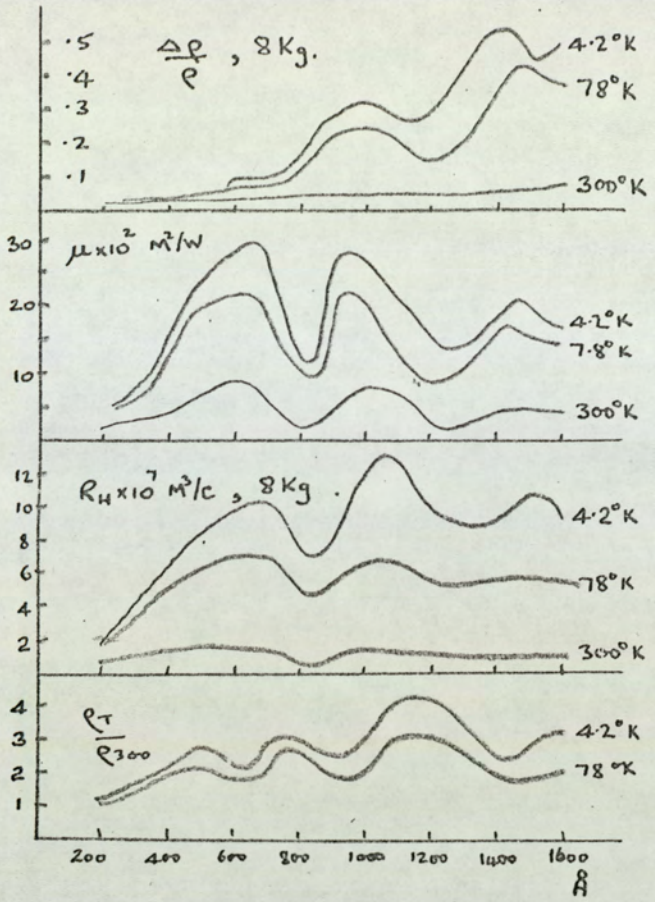

Fig. 161 (a).

Oscillatory galvomagnetic properties.

(after Ogrin).

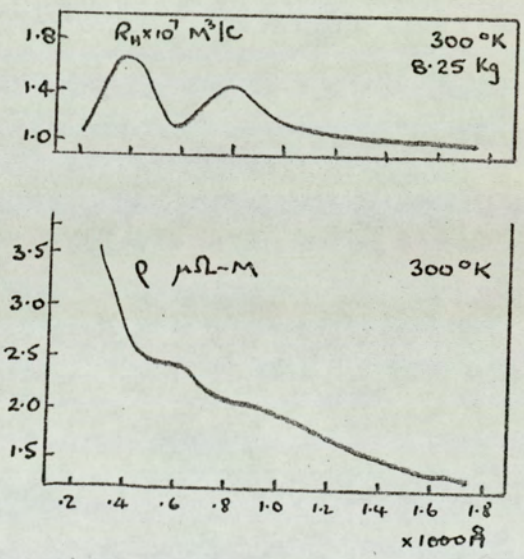

Fig. 161 (b).

Oscillatory galvomagnetic properties.

(after Duggal).

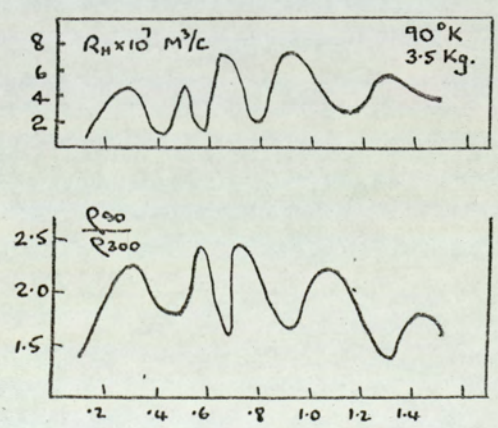

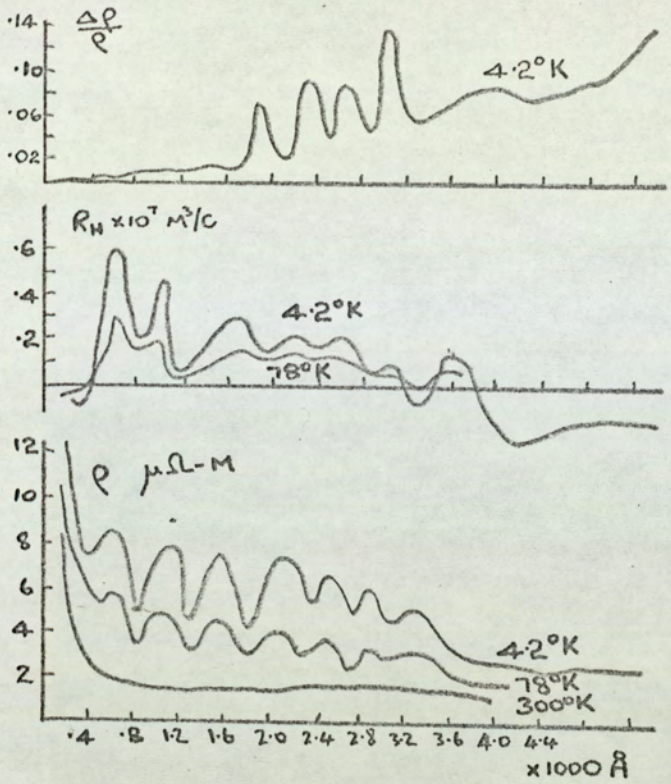

Fig. 161 (c).

Oscillatory galvomagnetic properties.

(after Ogrin).

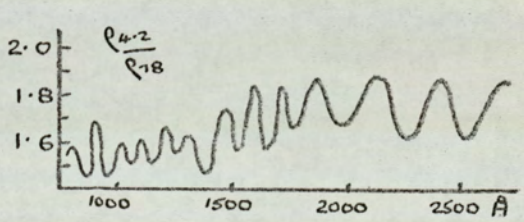

Fig. 161 (d).

Oscillatory galvomagnetic properties.

(after Fesenko).

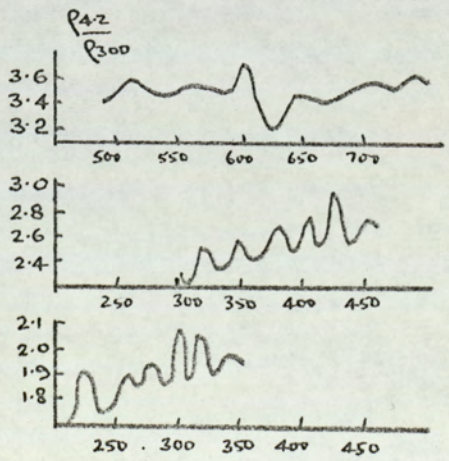

4.2°K is observed. The conclusion would be that up to the present comprehensive thickness limit of 1700 Å the magnetoresistance ratio, would be only slightly oscillatory at 78°K. The Hall coefficient curves reach a maximum monotonic positive value at approximately 800 Å as in the present work, but remain of positive ordinate for thicker films. The method of presentation of the resistivity values enables the three lines to be interpreted identically with the picture of an oscillatory low temperature asymptote as presented in section 6.3. and supports this rather unique approach. A period of 400 Å was observed.

A recent contribution, Fesenko[86], indicated a shorter period in the resistivity rates curves. For thicknesses in the range 1700 - 4000 Å a period of 250 Å was observed, falling to 100 Å at 1000 Å thickness. At lower thicknesses the high frequency period of 40 Å was attributed by Fresenko to the contribution due to holes.

6.7.3. Present results and discussion

An oscillatory behaviour in the present results has been observed in several of the measured parameters.

As presented in chapter 5, figure 143, the graph of the temperature coefficient of resistivity, at temperatures where boundary scattering was significant, displayed an oscillatory dependence on the film thickness. The amplitude of the oscillation was small, consistent with the observations of Ogrin or Duggal. A period of approximately 170 Å at the higher thicknesses was observed, falling slightly to 150 Å in the thin region. The exact interpretation of the coefficient as presented is that it is related to the value of the resistivity at a low temperature, say 77°K, but normalised to remove the effect of a linear displacement of the curve due to lattice imperfections. Thus in the normalised condition the oscillatory behaviour of the curve represents truly the modification to the low temperature value of the resistivity caused by the quantum size effect.

A selection of curves of the Hall coefficient against temperature were presented in figure 140 in which, at a chosen temperature, R_H was observed to vary in an oscillatory manner with respect to the film thickness. Figure 162 is a plot of the Hall coefficient against film thickness at temperatures of 88°K, 160°K and 280°K. Again the periodic profile is observed showing a series of principal minima at 230 Å spacing at thicknesses above 400 Å. A reduction in amplitude accompanied an increase in temperature, but an invariant period was retained. At 280°K many of the minor periods occuring at low temperature were absent and others reduced in magnitude.

The curve of magnetoresistance coefficient, B, against film thickness is shown in figure 163. A minor period of 100 Å existed up to 800 Å in thickness as modulation of a curve of a longer period.

Figure 164 is taken from the computed curves for the carrier densities and mobilities. Within the limits of the experiment the thickness variation of the carrier density would appear to be of a non-oscillatory form. The electron and hole mobilities are, however, oscillatory and naturally have a profile and period similar to that of the magnetoresistance coefficient.

The de Broglie wavelength in bismuth may be calculated from the relationship:

$$\lambda = \frac{h}{\sqrt{2m^* E}} \quad \ldots\ldots\ldots\ldots \quad (6.17)$$

where m^* = carrier effective mass

E = Fermi energy.

Equation 6.17 can be equated to the expression for the Eigen values of the Schrödinger equation in the case of bismuth because of the unsignificant departure of the carrier energies from that of the Fermi energy in the presence of a low carrier population.

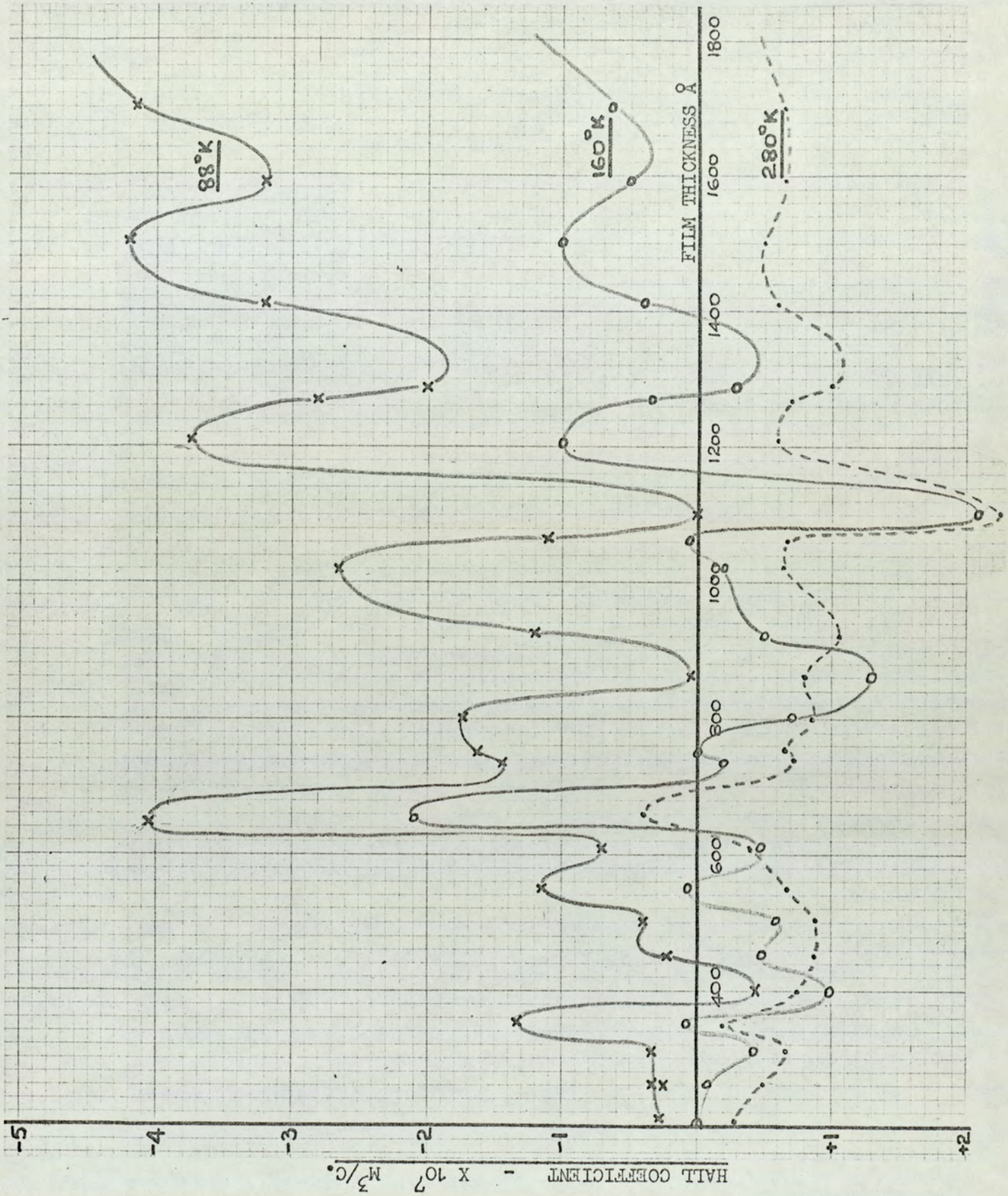

Fig. 162. Hall coefficient against film thickness at a selection of temperatures.

Fig. 163. Magnetoresistance coefficient at 80°K. against film thickness

Fig. 164. Carrier density and mobilities at 80° K. against film thickness

The resultant expression is simply:

$$\frac{\lambda}{2} = \frac{a}{n} \qquad \ldots\ldots\ldots\ldots\ldots\ldots\ldots\ldots (6.18)$$

i.e. the de Broglie wavelength for a particular type of carrier is twice the period of the quantum oscillations.

The discussion of the experimental results is undertaken with some caution. A recent report by Cottey [117] reviewed the limited significance of the oscillatory behaviour of the galvomagnetic properties in a material as complex as bismuth, when related to the simple theory of the quantum size effect.

The variation in carrier density with film thickness was shown in the present investigation to be almost monotonic, resulting in the conclusion that the oscillatory behaviour in the curves was attributed to the carrier mobilities. The difference in order between the de Broglie wavelengths of electrons and holes did, however, mean that the periods of oscillation from the two sources would differ by the same sort of value.

The principal maxima in the curve of carrier mobility against thickness can be observed at 400, 820 and 1240 $\mathring{A}$ indicating a de Broglie wavelength for electrons of approximately 800 $\mathring{A}$. The wavelength of 200 $\mathring{A}$ appropriate to the higher frequency component of the oscillation resulted from the contribution due to holes. As naturally follows the features are repeated in the magnetoresistance coefficient curves but the amplitude due to holes was observed to reduce with increase in film thickness.

The period of oscillation for electrons of 400 $\mathring{A}$ may be re-substituted into the Eigen value equation to obtain values for the Fermi energy. Assuming an electron effective mass in bismuth of 0.01 m_o the Fermi energy was computed to be 0.022 eV, and corresponds exactly to the value obtained by Weiner [20]. A

diversity of values of both E_F and m^* make more detailed comparison difficult. For the same Fermi energy a reduction in oscillatory period of a factor of four results in a hole effective mass of 0.160 m_o, and lies between the values of Kao[21] for m_h^* for cyclotron resonance experiments with the applied magnetic field parallel and perpendicular to the trigonal axis. The sensitivity of the carrier effective masses to the crystallite orientation is tabulated by Kao[21]. The effect of an increased disorientation with increase in film thickness causes additional components of the carrier effective masses orthogonal to the trigonal axis to be introduced, i.e. a reduction in m_e^* and an increase in m_h^*. The result is an increase in hole - and decrease in electron de Broglie wavelengths and adds to the general untidiness of the quantum oscillation curves at greater thicknesses. The possibility is not excluded that the envelope of magnetoresistance oscillations of Ogrin (Fig. 161(c)) at thicknesses between 2000 Å and 4000 Å resulted from the beating of the electron and hole de Broglie waver.

The Hall coefficient oscillatory curves loose the majority of the hole contributions to their profile at room temperature, the major period then becoming more pronounced. The prime maxima occuring at 340, 680 and 1020 Å are coincident with the irregularities in the current density curve. The two oscillatory frequencies are difficult to separate. A possible expanation lies in the fact that, in the absence of an oscillatory carrier density, the modulation of the R_H curves is dependant only on the magnitude of the ratio μ_e/μ_h. The consistancy in phase of the two mobilities was precise but the relative ratio of the amplitudes can be seen to be slightly variant. It is possible that the profile of the R_H curve is modified by this source. The periods are however still present in that seven maxima are observed in the inclusive interval 350 - 1250 Å.

The compounding of the mobilities in the resistivity formula may also be modified in a similar way to the R_H curves. The distinctive periodicities are again blended into one but the total number of maxima is consistant, and a distinct region of elevated values in the region 800 - 1200 Å occurs corresponding to the depression in the magnetoresistance values.

The present observations thus display maxima for electrons at intervals of approximately 400 Å, a period which is in agreement with the simple theory of the quantum size effect and values quoted in the literature. Furthermore an oscillation of smaller amplitude and higher frequency occurs at the lower temperatures arising from the contribution due to holes. This period is approximately 200 Å. A more searching problem is, however, that of the interpretation of the results. Sandomirskii's derivation included a prediction that a change in band gap would occur with reduction in film thickness and that below about 400 Å the spacing would be such that the overlap would disappear. An associated increase in resistivity would be expected from this source although its appearance would be inconclusive due to the possibility of a similar observation arising solely out of the thinness of the film - island structure etc. In practice the increase is not observed in the present resistivity results down to 211 Å in thickness, a point which is also noted by Tavger and Demikhovskii[116].

An important feature hitherto not reported in the literature is the influence of the crystallite structure of the evaporated films on the quantum size effect. It has been demonstrated in chapter 4 that the crystallite size of evaporated bismuth films is a function of the film thickness. In the presence of specular reflection from the film boundaries so that only the normal momentum vector is reversed the possibility arises of the formation of the standing

waves, not in the thickness of the film, but within the length of the grains themselves, consistent with the idea of the "super-lattice" discussed in chapter 2. It has been shown in the present resistivity theory that the carriers responsible for the greater portion of the film current are those travelling nearly parallel to the surface. The quantising dimension may equally well be the mean grain boundary spacing and not the film surface separation. The picture then becomes one identical to that of a rectangular wave guide and the interpretation of the conduction minima readily follow. The mathematics is equally valid except that the period arises from the difference in grain size between films whose thicknesses differ by 400 $\mathring{A}$. Reference to the linearity of figure 59 indicates that the difference in grain size is also 400 $\mathring{A}$. The period is thus unchanged. The present results and those of Komnik[118] are from polycrystalline films, those of Ogrin and Duggal consist of larger crystals.

At the present stage the picture is not clear. It may be concluded that effects do occur which are consistent with the manifestation of a quantum size effect, and numerically of the right order. Uncertainties in the film structure and the failure of the films to approach the ideals of the simple theory leave many unanswered questions. Cottey[117] has suggested that an alternative and more accurate approach would be to use only one film and to observe the effect of resonant absorbtion of electromagnetic radiation in the infra-red region. The problem has, however, yet to be fully analysed before the full potential of the large galvomagnetic properties of thin bismuth films can be applied to micro-electronics.

CHAPTER 7

Concluding Remarks

7.1 General Conclusions

Many reports have appeared in the literature regarding the galvomagnetic coefficients in bismuth films but these have in many instances been presented for different specimens. A comprehensive study of the properties of thin bismuth films in the 'as evaporated' condition, taken over the whole matrix of thickness, temperature and magnetic field, has not previously been published. It was the purpose of the present investigation to undertake such a study and to analyse the effect of those parameters which led to a modification of the properties of the films.

Thin bismuth films have been prepared under controlled conditions and their physical parameters of thickness and grain size have been carefully measured. The resistivity, Hall coefficient and magnetoresistance effects have been investigated over a wide range of temperature and applied magnetic fields. The complexities and uncertainties of a complete mathematical analysis have been avoided. The coefficients have been discussed in physical terms, a knowledge of which has been gained from a critical appreciation of the literature. The simultaneous solution of the equations to find the carrier density and mobilities resulting in a set of curves which varied smoothly with film thickness. This continuity indicated a consistency in the coefficients and led to a justifiable presentation of evidence for a quantum size effect.

The following sub-sections present a summary of the main conclusions reached in the discussion of the galvomagnetic effects in thin bismuth films.

7.1.1. Resistivity

The resistivity of thin bismuth films has been presented, and seen to display values in excess of those of bulk material due to the polycrstalline nature of the specimens. The semi-conductor type behaviour resulted in a negative temperature coefficient of resistivity, the contribution from lattice scattering being independent of film thickness. At temperatures below about 160°K, carrier collisions with the film and grain boundaries became significant causing an increase in the measured resistivity. The two regions of the curve tended towards a set of asymptotic axes, the gradient of the lower temperature one being an oscillatory function of the film thickness.

The values of the resistivity of the thinnest films displayed a saturation value at 77°K consistent with the observations of Friedman and Koenig on bulk material at 4.2°K. The saturation was attributed by Friedman and Koenig to the shape of the constant energy surfaces and occurs even in the presence of a specular reflection coefficient at the film and grain boundaries.

The resistivity results of the present polycrystalline bulk specimen were similar to the single crystal values of Abeles and Meiboom, the grain size being such that a size effect was not observed.

7.1.2. Hall coefficient

The effect of the anisotropy in bismuth has its largest influence in the magnitude of the Hall effect. In bulk polycrystalline material the positive Hall coefficient with the applied magnetic field parallel to the trigonal axis was dominated by the large negative coefficient in the orthogonal case. The effect of the increased degree of crystallite orientation in thin films, however, caused the coefficient curve to be displaced across the abscissa to positive values at the higher temperatures. At about 800 Å the curve was almost entirely of positive sign. The magnitude of the positive coefficient

decreased in the thinnest films due to the effects of the bipolar current.

The effective number of carriers, N, in bismuth was observed to be a function of the applied magnetic field, the relationship being such that a fall in field caused an apparent increase in N. A power law relationship was derived showing a power of -½, contrary to the behaviour of bulk material in which a value of + 3/2 was obtained. On removal of the perturbing term, Δ N, a consistent set of curves for R_H against temperature were obtained independent of the applied magnetic field. The values of R_H were shown to be an oscillatory function of the film thickness, consistent with the existance of a quantum size effect.

7.1.3. Magnetoresistance coefficient

The magnetoresistance of bulk polycrystalline bismuth was shown to increase exponentially with reduction in temperature, the magnitude of the effect being similar to that in single crystals. However, the quadratic dependence of the magnetoresistance ratio, $\Delta\rho/\rho$, on the applied magnetic field did not hold for such specimens. A power of approximately 3/2 was demonstrated, consistent with the prediction of Ziman and attributed to the effect of the grain boundaries on the cyclotron orbits.

The magnetoresistance coefficient in thin bismuth films was reduced by several orders of magnitude from the bulk values, because of the limitations placed on the carrier free path by the grain and surface boundaries. The exponential type increase was not observed at 4500 Å, the low temperature values showing a tendancy towards a saturation limit. The films did however show a quadratic dependence on the applied magnetic field.

A reduction in thickness further supressed the low temperature value until at 300 Å the slope of the coefficient/ temperature curve

was positive at all temperatures. The finite limit of the carrier path in the presence of both small grains and low temperatures accounted for the very small value of the magnetoresistance coefficient under these conditions.

The apparently reduced coefficient at low fields was believed to have its origin in the variation of the carrier density in the presence of an applied field.

7.1.4. Quantum size effect

The resistivity, Hall coefficient, magnetoresistance and carrier mobility have been presented as functions of the film thickness. An oscillatory nature in the resulting curves has been observed and is a manifestation of a quantum size effect. The period of oscillation was observed to be independent of temperature, although its amplitude decreased with increase in temperature due to a thermal smearing of the quantised energy levels.

From the monotonic variation of the carrier density with film thickness it was concluded that the variations in the carrier mobilities contributed primarily to the profile of the coefficient curves. A period for electrons of 400 $\mathring{A}$ was demonstrated. The resultant de Broglie wavelength of 800 $\mathring{A}$ was consistent with the predictions of the elementary theory. A higher frequency modulation to the curve was attributed to the contribution due to holes having a de Broglie wavelength of 200 $\mathring{A}$. These values resulted in a Fermi energy of 0.022 eV. The interaction of the parameters N, μ_e and μ_h made the resolutions of the oscillations more difficult to analyse in the case of the Hall coefficient and resistivity although the main features were displayed.

7.2. Suggestions for further work

At the onset of the present programme of research it was hoped to proceed from a general background knowledge of thin film

technology to this final report as the resistivity and galvomagnetic properties of the bismuth films in as comprehensive a manner as possible. The major unanswered question was the deeper significance of crystallite size as a fundamental parameter governing the electrical properties of bismuth films, and its particular relationship to the quantum size effect.

As mentioned in section 7.1.4 the study of the quantum size effect is far from complete and in fact its further study by this method was concluded by Cottey to be of limited significance. The overall picture from the galvomagnetic properties could show a multifold improvement, however, by the investigation of a series of bismuth films whose consecutive thicknesses differ by a much smaller interval, say 10 $\mathring{A}$. The present analysis has verified the consistency in the galvomagnetic coefficients obtained by the use of applied magnetic fields of 10 kilogauss, and the possibility of a reduction in the number of temperature points between 77 and 300 ^{o}K to about 5 or 6. By these means a programme of research of similar length could reasonably deal with the uncertainty in the electron and hole quantum periodicity.

An experimental arrangement by which the films could be evaporated, examined and thermally annealed under ultra-high vacuum conditions would reduce the variability in performance due to differential oxidisation. In particular the use of a super-conducting solenoid is recommended, in which the evaporation takes place along the solenoid axis. The film normal would then be in the direction of the applied magnetic field. The use of the pressure contact assembly developed in the present investigation would make the system reliable. Suitably heated, the variation in the properties under various stages of anneal could be measured and related to the observations of the quantum size effect. A development of the techniques of the Scanning Electron Microscope would assist in the closer correlation between the grain size and film thickness.

APPENDIX 1

A typical temperature variation run as taken on a film of 1270 Å

DATE: 14.2.69; FIIM NO: 48; RUN NO: 69;

FILM CURRENT: 1.500 mA; MAGNETIC FIELD STRENGTH : 9.2 Kg.

CONSTANT Z1 = 0.001583 CONSTANT Z2 = -0.000848/9.2 Kg.

B.S.T.	T/C	°K	Heater mA.	i	+ ve Field		zero	- ve Field		$\frac{\Delta\rho}{\rho} \times 10^3$	B x 10^3 $(W/M^2)^{-2}$	ρ $\mu\Omega$-M	$R_H \times 10^7$ M^3/C
					V_H	V_R	V_R	V_R	V_H				
11.45	-5.307	87.5	0	-	- 8144	8723	8627	8724	+49192	11.15	13.17	13.67	-2.643
				+	+ 8244	8741	8640	8731	-49100				
12.00	-5.240	91.5	30	+	+ 7644	8562	8463	8552	-47303	11.14	13.16	13.39	-2.536
				-	- 7563	8546	8451	8545	+47516				
12.15	-5.072	100.5	50	-	- 5900	8171	8075	8159	+43442	11.15	13.17	12.77	-2.267
				+	+ 5969	8154	8064	8154	-43042				
12.30	-4.856	111.0	70	+	+ 3590	7668	7576	7657	-37590	11.42	13.49	11.98	-1.896
				-	- 3071	7647	7562	7650	+37990				
12.45	-4.607	123.0	90	-	- 86	7107	7023	7100	+32286	11.50	13.59	11.11	-1.490
				+	+ 783	7090	7010	7092	-31483				
1.00	-4.322	135.0	110	+	- 1783	6562	6486	6560	-24840	11.56	13.66	10.27	-1.062
				-	+ 3000	6566	6490	6564	+26000				
1.15	-4.070	146.0	130	-	+ 5900	6180	6105	6169	+21900	11.49	13.58	9.65	-0.738
				+	- 4310	6153	6084	6156	-20309				
1.30	-3.625	162.5	150	+	- 6849	5603	5536	5598	-13849	11.79	13.93	8.76	-0.316
				-	+ 9100	5602	5536	5602	+15800				

APPENDIX 1. Contd.

B.S.T.	T/C	°K	Heater mA.	i	+ ve Field		zero	- ve Field		$\frac{\Delta\rho}{\rho} \times 10^3$	B x 10^3 $(W/M^2)^{-2}$	ρ $\mu\Omega$-M	$R_H \times 10^7$ M^3/C
					V_H	V_R	V_R	V_R	V_H				
1.45	-3.289	175.0	170	-	+11100	5205	5144	5201	+11800	11.58	13.68	8.13	-0.039
				+	- 8500	5191	5131	5191	- 9500				
2.00	-2.920	187.5	190	+	-10000	4852	4790	4842	- 6200	11.80	13.94	7.58	+0.188
				-	+12957	4838	4784	4842	+ 8586				
2.15	-2.656	196.5	210	-	+14096	4619	4567	4619	+ 6960	11.34	13.40	7.23	+0.316
				+	-11000	4615	4562	4612	- 4425				
2.30	-2.378	205.0	230	+	-10939	4390	4339	4387	- 2118	11.34	13.40	6.88	+0.421
				-	+14738	4396	4347	4386	+ 5316				
2.45	-2.169	211.5	250	-	+14738	4248	4201	4248	+ 3796	11.02	13.12	6.64	+0.492
				+	-11187	4242	4194	4237	- 787				
3.00	-1.850	221.5	270	+	-11187	4048	4004	4045	+ 694	10.80	12.76	6.34	+0.563
				-	+14856	4052	4008	4052	+ 2326				
3.15	-1.512	231.5	290	-	+14960	3886	3845	3886	+ 1160	10.68	12.62	6.08	+0.622
				+	-11000	3879	3836	3875	+ 2204				
3.30	-1.234	239.5	310	+	-10661	3739	3697	3733	+ 3361	10.61	12.54	5.85	+0.662
				-	+14821	3739	3700	3740	+ 102				
3.45	-0.780	252.0	330	-	+14821	3553	3516	3552	- 734	10.25	12.11	5.56	+0.698
				+	-10129	3542	3505	3539	+ 4584				
4.00	-0.440	261.5	350	+	- 9700	3402	3366	3398	+ 5270	10.01	11.83	5.34	+0.708
				-	+14391	3413	3379	3412	- 1357				
4.15	+0.043	274.0	370	-	+14156	3234	3203	3232	- 1941	9.31	11.00	5.06	+0.717
				+	- 9245	3216	3186	3215	+ 5745				
--	+0.700	291.0	0	+	- 9272	2830	2807	2831	+ 4768	8.28	9.79	4.44	+0.648
				-	+ 9244	2830	2807	2831	- 4844				

APPENDIX 1. Contd.

A typical field variation run as taken on a film of 1100 Å

DATE: 20. 5. 69; FILM NO: 41; RUN NO: 52;

FILM CURRENT: 1.500 mA; FILM TEMPERATURE: 171.5 °K

CONSTANT Z1 = 0.002145 CONSTANT Z2 = -0.0011/ Kg.

Applied Magnetic Field Kg.	i	+ ve Field		zero	- ve Field		$\frac{\Delta\rho}{\rho} \times 10^3$	B x 10^3 $(W/M^2)^{-2}$	ρ $\mu\Omega$-M	$R_H \times 10^7$ $M^3/C.$
		V_H	V_R	V_R	V_R	V_H				
12.5	-	-32666	8063	7999	8063	-84666	8.000	5.120	17.16	+2.244
	+	+34035	8065	8001	8065	+84035				
9.4	+	+39835	8035	7996	8032	+77735	4.534	5.350	17.15	+2.285
	-	-40135	8028	7993	8028	-78735				
4.4	-	-52200	8035	8028	8035	-65659	0.871	4.499	17.22	+2.241
	+	+52459	8039	8032	8039	+65059				
1.95	+	+54917				+62417				+2.115
	-	-55417				-62917				
1.49	-	-56227				-61886				+2.030
	+	+56057				+61400				
1.02	+	+56903				+60500				+2.016
	-	-57116				-61000				
0.49	-	-57933				-59833				+1.730
	+	+57809				+59433				
0.22	+	+58427		8012		+58846			17.18	+0.998
	-	-58886		8010		-59265				

APPENDIX 11

Algol programme for primary computation.

```
28/08/70          COMPILED BY XALE MK.  48

'BEGIN' 'COMMENT' CRUICKSHANK BLSTF254, SOLUTION OF THE
  GALVOMAGNETIC VOLTAGES IN BISMUTH FILMS,PRIMARY COMPUTATION;
'REAL''ARRAY' V[1:10];
'INTEGER' J,RUNNO,Q,FILMNO,I;
'REAL' FIELD,VR,VM,VH,Z1,Z2,RHO,RH,MC;

      FILMNO:=READ;     RUNNO:=READ;
          Z1:=READ;         Z2:=READ;
AGAIN: FIELD:=READ;
REPEAT:    I:=READ;
'FOR' J:=1 'STEP' 1 'UNTIL' 10 'DO'
       V[J]:=READ;
VR:=(V[3]+V[8])*0.5;
VM:=(V[2]+V[4]+V[7]+V[9]-2*(V[3]+V[8]))*0.25;
VM:=2*VM/(V[3]+V[8]);
VH:=(V[1]+V[10]-V[5]-V[6])*0.25*I;
MC:=VM/FIELD/FIELD*100000;
RHO:=Z1*VR;
RH:=Z2*VH/FIELD;
WRITETEXT('('FILM%NUMBER')');PRINT(FILMNO,2,0);SPACE(14);
WRITETEXT('('RUN%NUMBER')');PRINT(RUNNO,2,0);NEWLINE(3);
WRITETEXT('('%%%%VH%%%%%%VM%%%%%%VR%%%%%%VM%%%%%%VH')');
NEWLINE(2);
'FOR'J:=1'STEP'1'UNTIL'5'DO'
       PRINT(V[J],6,0);NEWLINE(2);
'FOR'J:=6'STEP'1'UNTIL'10'DO'
       PRINT(V[J],6,0);NEWLINE(2);
WRITETEXT('('MAGNETORESISTANCE%RATIO%EQUALS'('6S')'')');
       PRINT(VM*1000,3,3);WRITETEXT('('X%10↑-3')');NEWLINE(2);
WRITETEXT('('MAGNETORESISTANCE%COEFFICIENT%EQUALS')');
       PRINT(MC,3,3);WRITETEXT('('X%10↑-3%TESLA↑-2')');NEWLINE(2);
WRITETEXT('('RESISTIVITY%EQUALS'('18S')'')');
          PRINT(RHO,3,3);WRITETEXT('('MICRO%OHM%M')');NEWLINE(2);
WRITETEXT('('HALL%COEFFICIENT%EQUALS'('13S')'')');
       PRINT(RH,3,3);WRITETEXT('('X%10↑-7%CU%M/C')');NEWLINE(6);
Q:=READ;
'IF' Q=99 'THEN''GOTO' AGAIN 'ELSE''IF' Q=999 'THEN'
   'GOTO' FINISH 'ELSE''GOTO' REPEAT;
FINISH:'END';
```

FILM NUMBER 48 RUN NUMBER 69

VH	VM	VR	VM	VH
-8144	8723	8627	8724	49192
8244	8741	8640	8731	-49100

MAGNETORESISTANCE RATIO EQUALS 11.148 X 10↑-3

MAGNETORESISTANCE COEFFICIENT EQUALS 13.172 X 10↑-3 TESLA↑-2

RESISTIVITY EQUALS 13.667 MICRO OHM M

HALL COEFFICIENT EQUALS -2.643 X 10↑-7 CU M/C

APPENDIX III

Algol programme for secondary computation

```
29/09/70          COMPILED BY XALE MK.  48

'BEGIN''COMMENT' CRUICKSHANK BLST#254,SOLUTION OF THE
 GALVOMAGNETIC COEFF. IN BISMUTH FILMS,SECONDARY COMPUTATION;
'REAL' RHO,RH,MR,ROOT,N,MUH,MUE;
'INTEGER' FILMNO,RUNNO;
      FILMNO:=READ;      RUNNO:=READ;
AGAIN:RHO:=READ;'IF'RHO=999'THEN''GOTO'FINISH;
        RH:=READ;
        MR:=READ;
      ROOT:=SQRT(RH*RH+0.4*MR*RHO*RHO);
         N:=62.5/ROOT;
       MUH:=5*(ROOT+RH)/RHO;
       MUE:=5*(ROOT-RH)/RHO;
WRITETEXT('('FILM%NUMBER')');PRINT(FILMNO,2,0);SPACE(14);
WRITETEXT('('RUN%NUMBER')');PRINT(RUNNO,2,0);NEWLINE(2);
WRITETEXT('('RHO%=')');PRINT(RHO,2,3);
WRITETEXT('('%%%%%%%%RH%=')');PRINT(RH,2,2);
WRITETEXT('('%%%%%%%%MR%=')');PRINT(MR,2,2);NEWLINE(3);
WRITETEXT('('NUMBER%OF%CARRIERS%EQUALS'('6S')'')');
      PRINT(N,3,2);WRITETEXT('('X%10↑24%M↑-3')');NEWLINE(2);
WRITETEXT('('HOLE%MOBILITY%EQUALS'('11S')'')');
      PRINT(MUH,3,2);WRITETEXT('('X%10↑-2%M↑2/W')');NEWLINE(2);
WRITETEXT('('ELECTRON%MOBILITY%EQUALS'('7S')'')');
      PRINT(MUE,3,2);WRITETEXT('('X%10↑-2%M↑2/W')');NEWLINE(6);
'GOTO' AGAIN;
FINISH;'END';
```

FILM NUMBER 28 RUN NUMBER 24

RHO = 5,830 RH = 0.10 MR = 34.29

NUMBER OF CARRIERS EQUALS	2.89	X 10↑24 M↑-3
HOLE MOBILITY EQUALS	18.60	X 10↑-2 M↑2/W
ELECTRON MOBILITY EQUALS	18.43	X 10↑-2 M↑2/W

REFERENCES

1)	Wright D.A.	Electron Engng. 31. 659 (1959)
2)	Kao Y-H	J. phys. Soc. Japan 21 (Supp).678(1966)
3)	Ogrin Y.F., Luttskii V.N., and Sheftal R.M.	Radio Engng. 12. 699 (1967)
4)	Duggal V.P. and Rup R.	Phys. Lett. 24a 160 (1967)
5)	Ivanov G.A. and Papov A.M.	Soviet Phys. solid St. 5. 1040 (1963)
6)	Fritsche L., Marquard K. and Wolf F.	Z. Naturforschg. 20 a. 640 (1965)
7)	Colombani A. and Huet P	Comptes rendus 256, 2357 (1963)
8)	Colombani A. and Huet P	Comptes rendus 255. 3179 (1962)
9)	Colombani A. and Huet P	Comptes rendus 254. 1988. (1962)
10)	Borovik E.S.	Bull. Acad. Sci (USSR) 19.383 (1955)
11)	Barrett C.S.	Australian J. Phys. 13. 209 (1960)
12)	Guinier A.	"X-ray crystallographic technology", Hilger and Watts Ltd. 1952.
13)	Boyle W.S. and Smith G.E.	Progress in Semiconductors 7.3(1964)
14)	Jones H.	Proc. Roy. Soc. A147. 396 (1934); A155. 653 (1936)
15)	Mott N.F. and Jones H.	"The theory of the properties of metals and alloys", Clarendon Press, 1936.
16)	Jain A.N. and Koenig S.H	Phys. Rev. 127. 442 (1962)
17)	Friedman A.N. and Koenig S.H.	I.B.M. J.Res. Dev. 4. 158. (1960)
18)	Boyle W.S. and Brailsford A.D.	Phys. Rev. 120. 1943 (1960)
19)	Brandt N.B., Dubrovskaya A.E. and Kytin G.A.	Soviety Phys. J.E.T.P. 10. 405 (1960)
20)	Weiner D.	Phys. Rev. 125. 1226 (1962)
21)	Kao Y-H	Phys. Rev. 129. 1122 (1963)
22)	Aubrey J.E.	J. Phys. Chem. Solids 19. 321 (1961)
23)	Galt J.K., Yager W.A. and Merritt F.R.	Phys. Rev. 114. 1396 (1959)
24)	Gallo C.F., Chandrasekhar B.S. and Sutter P.H.	J. appl. Phys. 34. 144 (1962)

25)	Hapase M.G., Tare V.B. and Biswas A.B.	Acta Met. 15. 131 (1967)
26)	Goldsmid H.J	Adv. Phys. 14. 273 (1965)
27)	Focke A.B. and Hill J.R.	Phys. Rev. 50. 179 (1936)
28)	Abeles B. and Meiboom S.	Phys. Rev. 101. 544 (1956)
29)	Brandt N.B., Svistova E.A. and Tabieva G.K.	Soviet Phys. J.E.T.P. 6.17 (1966)
30)	Friedman A.N., Hall J.J. and Koenig S.H.	Bull. Am. Phys. Soc.II 4.168 (1959)
31)	Price P.J.	I.B.M. J.Res. Dev. 4. 152 (1960)
32)	Duggal V.P., Rup R. and Tripathi P.	Appl. Phys. Lett. 9. 293 (1966)
33)	Kioke R. and Kurokawa H.	Japan. J. appl.Phys. 5. 503 (1966)
34)	Kapitza P.	Proc. Roy. Soc. 119A. 401 (1928)
35)	de Haas W. and Schubunikov L.	Leid.Comm. 207. 236 (1930)
36)	Kohler M.	Ann. der Phys. 32. 211 (1938)
37)	Justi E.	Zeit. F. Phys. 41 563 (1940)
38)	Grenier C.G., Reynolds J.M. and Sybert J.R.	Phys.Rev. 132. 58 (1963)
39)	Gitsu D.V. and Ivanov G.A.	Soviet Phys. solid S_t. 3.1323 (1960)
40)	Huet P. and Colombani A.	Comptes rendus 244. 1626 (1957)
41)	Jain A.L.	Phys. Rev. 114. 1518 (1959)
42)	Suzuki M. and Kikuchi S.	J. Phys. Soc.Japan 17.1900 (1962)
43)	Leverton W.F. and Dekker A.J.	Phys. Rev. 81.156 (1951)
44)	Heaps C.W.	Phys. Rev. 30. 61 (1927)
45)	Harris L. and Piper J.	J. opt. Soc.Am. 53.1271 (1963)
46)	Ogrin Y.F., Lutskii V.N. and Arifova M.V.	Soviet Phys. J.E.T.P. 26. 714 (1968)
47)	Colombani A. and Huet P.	"Structure and properties of thin films", Wiley, 1962.
48)	Neuman M.R. and Ko W.H.	J. appl. Phys. 37. 3327 (1966)
49)	Ivanov G.A. and Popov A.M.	Soviet Phys. solid St. 5. 1040 (1962)
50)	Pippard A.B. and Chambers R.G.	Proc. Roy.Soc. A64. 955 (1952)

51)	Chopra K.L. and Bahl S.K.	J. appl.Phys. 38.3607 (1967)
52)	Duggal V.P. and Rup R.	J. appl.Phys. 40.492 (1969)
53)	Clawson A.R.	Solid St. Electronics 8.967 (1965)
54)	Frenkel J.	Zeit. F. Phys. 26. 117 (1924)
55)	McCarrol B. and Ehrlich G.	"Condensation and Evaporation of solids", Gordon and Breach, N.Y.,1962.
56)	Lewis B.	2nd Conf. on thin films, Inst.Phys. (1968)
57)	Chapman B.N. and Campbell D.S.	2nd Conf. on thin films,Inst.Phys.(1968)
58)	Pashley D.W.	Adv.Phys. 14.327 (1965)
59)	Pashley D.W., Strowell M.J. and Jacobs M.H.	Phil.Mag. 10.127 (1964)
60)	Chopra K.L. and Randlett M.R.	Appl.Phys.Lett. 11.202(1967)
61)	Chopra K.L. and Randlett M.R.	J. appl.Phys. 39. 1874 (1968)
62)	Chopra K.L.	J. appl. Phys. 37.2249 (1967)
63)	Jorgenson G.V. and Wehner G.K.	10th Natl. Vac.Symp.(Am.Vac.Soc.)p.388
64)	Chopra K.L.	2nd.Conf.on thin films,Inst.Phys.(1968)
66)	Stewart A.D. and Thompson M.W.	J. Matl.Sci. 4.56 (1969)
67)	Hopkins B.J. and Dobson P.J.	2nd Conf. on thin films, Inst.Phys.(1968)
68)	McLaren E.H. and Murdock E.G.	Canadian J.Phys.41.95 (1963)
69)	Wojtczak L.	Phys.Status Solidi 23.163 (1967)
70)	Palatnik L.S. and Kommik Y.F.	Soviet Phys. Doklady 3.196 (1958)
71)	Palatnik L.S. and Gladkikh Gladkikh N.T.	Soviet Phys.solid St. 4.143 (1962)
72)	Komnik Y.F.	Soviet Phys. solid S_t. 6.2309 (1965)
73)	Palatnik L.S. and Kosevich V.M.	Fiz.Met.Met. 15.371 (1963)
74)	Palatnik L.S. and Komnik Y.F.	Fiz.Met.Met. 10.632 (1960)
75)	Kooy C. and Nievwenhvizen J.M.	Proc.Int.Symp.on thin Films, Gottingen, 1966.
76)	Belous M.V. and Wayman C.M.	J. appl.Phys. 38.5119 (1967)
77)	Namba Y.	Japan J. appl.Phys. 7.783 (1968)
78)	Wilson A.H.	"The Theory of Metals", Camb.Univ.Press, (1953)

79) Keesom A. and van den Ende B. Comm.Leiden 203d (1930)

80) Wilson A.H. "The Theory of Metals", Camb.Univ. Press, 1953.

81) Fuchs K. Proc. Camb. Phil.Soc. 34.100 (1938)

82) Sondheimer E.H. Adv. Phys. 1.1 (1952)

83) Cottey A .A. Thin solid Films 1.297 (1967)

84) Brandt N.B., Svistova E.A. and Kashirskii Y.G. Soviet Phys. J.E.T.P. 9. 136 (1969)

85) Sandomirskii V.B. Soviet Phys. J.E.T.P. 25.101 (1967)

86) Fesenko E.P. Soviet Phys. solid St. 11.9 (1970)

87) Haller F.B. Rev. scient.Instrum 35.1356 (1964)

88) Archer-Hall J.A. Private communication.

89) Kohl W.H. "Materials Technology for Electron Tubes", Reinhold Publ.1951

90) "Etchineering" Trade name, Microponent Developments Ltd. Birmingham.

91) "Nichrome" Trade name, British Driver Harris Ltd.

92) van der Pauw L.J. Philips Res.Rep.13. 1 (1958)

93) Cady W.G. "Piezoelectricity", Dover, 1964.

94) Lawson W.H. J. scient.Instrum.44.917 (1967)

95) Edgecombe J. J. Vac. sci.Tech.3.28 (1965)

96) Tolansky S. "Multiple beam interferometry" Clarenden Press, 1949.

97) Koehler W.F. J. Opt. Soc. Amer. 43. 738 (1953)

98) Shultz L.G. J. Opt. Soc. Amer. 41. 261 (1951)

99) Scott G.D., McLauchlan T.A. and Sennett R.S. J. appl. Phys. 21. 843 (1950)

100) Lane C.T. Phys. Rev. 48. 193 (1935)

101) Holland L. "Vacuum deposition of thin films" Chapman & Hall, 1963.

102) Forrest A.M. and Hallett A.C. 9th Inst.conf.Low temp.Phys. p.740 (1964)

103) Bate R.T., Drobish W.E. and Einspruch N.G. Phys.Rev. 149. 485 (1966)

104) Uozumi K. Japan J. appl.Phys. 7. 1012 (1968)

105) Mott N.F. — Trans. Faraday Soc. 43. 429 (1947)

106) Cabrera N. and Mott N.F. — Rep. Prog. Phys. 12. 163 (1949)

107) Ham F.S. and Mattis D. — I.B.M. J. Res.Dev. 4.143 (1960)

108) Azbel M.Y. and Brandt N.B. — Soviet Phys. J.E.T.P. Lett.48. 1206 (1969)

109) Colombani A. and Huet P. — Cromptes rendus 244. 1344 (1957)

110) Jeppensen M.A., Flagg S.R. and Rancourt J.D. — J. appl.Phys. 31.860 (1963)

111) Fawcett E. — Adv.Phys. 13. 139 (1964)

112) Ziman J.M. — Phil.Mag. 3. 117 (1958)

113) Ogrin Y.F., Lutskii V.N and Elinson M.I. — J.E.T.P. letters 3.71 (1966)

114) Colombani A., and Huet P. — Compter rendus. 256.406 (1963)

115) Ivanov G.A. — Soviet Phys. solid St. 6. 720 (1964)

116) Tavger B.A. and Demikhovskii V.Y. — Soviet Phys. Uspekhi 11.644 (1969)

117) Cottey A.A. — "Intraband spectroscopy of the quantum size effect". The author is indebted to A.A.C. for an advance copy of this report.

118) Komnik Y.F. and Bukhshtab E.I. — Soviety Phys. J.E.T.P. 27. 34 (1968)

Acknowledgements

This research was carried out at the University of Aston in Birmingham during the tenure of a Research Studentship. I am indebted to the Science Research Council for the provision of an award in support of the study.

I offer my gratitude to Dr. W.E.J. Neal in appreciation of his encouragement, advice and supervision of the research programme.

I should also like to thank Professor S.E. Hunt, Head of Department of Physics for his continual interest in the work, and acknowledge the contribution from members of the Academic and Technical Staff. In particular I should like to credit Mr. W.E. Cooper for his experimental assistance and for many of the excellent sketches, and Mr. D. Hill of the Department of Building for his photographic work.

Finally, I record my appreciation of Mrs. R. Finch for typing this thesis.